JSCSEN 77(10)1483–1685(2012)

ISSN 1820-7421 (Online)

Journal of the Serbian Chemical Society

Electronic Version

Society 115th Anniversary 1897 - 2012

VOLUME 77

No 11

BELGRADE 2012

Available on line at

www.shd.org.rs/JSCS/

The full search of JSCS is available through

DOAJ DIRECTORY OF OPEN ACCESS JOURNALS

www.doaj.org

Штампање ове свеске је суфинансирао ЛУКОИЛ Србија АД

Publication of this issue is financially co-supported by LUKOIL Srbija AD

Journal of the Serbian Chemical Society
JSCS-info@shd.org.rs • www.shd.org.rs/JSCS

J. Serb. Chem. Soc. Vol. 77, No. 11 (2012)

CONTENTS

R. Ranković, S. Stojadinović, M. Sarvan, B. Kasalica, M. Krmar, J. Radić-Perić and *M. Perić*: A multidisciplinary study on magnesium (Review) 1483

Organic Chemistry

Z. Ferjančić, R. Matović and *R. N. Saičić*: Synthetic studies towards D-modified paclitaxel analogues 1529

L. I. Socea, T. V. Apostol, G. Şaramet, Ş. F. Bărbuceanu, C. Draghici and *M. Dinu*: Synthesis and root growth activity of some new acetylhydrazinecarbothioamides and 1,2,4-triazoles substituted with the 5*H*-dibenzo[*a*,*d*][7]annulene moiety 1541

H. M. Patel: Synthesis, characterization and dyeing behaviour of heterocyclic acid dyes and mordant acid dyes on wool and silk fabrics 1551

H. H. Jardosh and *M. P. Patel*: Lanthanum triflate-triggered synthesis of tetrahydroquinazolinone derivatives of *N*-allylquinolone and their biological assessment 1561

Biochemistry and Biotechnology

J. B. Zvezdanović, D. Z. Marković, D. J. Cvetković and *J. S. Stanojević*: UV-induced change in the antioxidant activity of quercetin toward benzophenone-initiated lipid peroxidation 1571

Inorganic Chemistry

M. Lashanizadegan and *M. Sarkheil*: Solvent-dependent synthesis and mono-hydrolysis of the di-Schiff base of (±)*trans*-1,2-cyclohexanediamine and 2-pyridinecarboxaldehyde in Cu(II), Co(II) and Zn(II) complexes 1589

W. Trakarnpruk, A. Wannatem and *J. Kongpeth*: Polyoxometalate catalysts in the oxidation of cyclooctane by hydrogen peroxide (Short communication) 1599

Electrochemistry

A. Janković, S. Eraković, A. Dindune, Dj. Veljović, T. Stevanović, Dj. Janaćković and *V. Mišković-Stanković*: Electrochemical impedance spectroscopy of a silver-doped hydroxyapatite coating in simulated body fluid used as a corrosive agent 1609

Analytical Chemistry

L. A. Pavun, J. M. Dimitrić Marković, P. T. Đurđević, M. D. Jelikić-Stankov, D. B. Đikanović, A. R. Ćirić and *D. L. Malešev*: Development and validation of a fluorometric method for the determination of hesperidin in human plasma and pharmaceutical forms 1625

A. Lolić, T. Tripković, R. Baošić, S. Nikolić-Mandić and *B. Stanimirović*: Development of a flow injection method with amperometric detection for the indirect determination of copper in drinking water samples 1641

M. Natić, D. Dabić, D. Milojković-Opsenica, B. Dojčinović, G. Roglić, D. Manojlović and *Ž. Tešić*: Development and validation of a simple thin-layer chromatographic method for the analysis of *p*-chlorophenol in treated wastewater 1649

Environmental

K. Trivunac, Z. Sekulić and *S. Stevanović*: Zinc removal from wastewater by a complexation–microfiltration process 1661

S. Maletić, S. Rončević, B. Dalmacija, J. Agbaba, M. Watson, A. Tubić and *S. Ugarčina Perović*: Characterisation of weathered petroleum hydrocarbons during a landfarming bioremediation study 1671

Published by the Serbian Chemical Society
Karnegijeva 4/III, 11000 Belgrade, Serbia
Printed by the Faculty of Technology and Metallurgy
Karnegijeva 4, P.O. Box 35-03, 11120 Belgrade, Serbia

Journal of the Serbian Chemical Society
JSCS-info@shd.org.rs • www.shd.org.rs/JSCS
J. Serb. Chem. Soc. 77 (11) 1483–1528 (2012)
JSCS–4367
UDC 546.46:66.087.3+533.9:519.6+54
Review

REVIEW

A multidisciplinary study on magnesium

RADOMIR RANKOVIĆ[1#], STEVAN STOJADINOVIĆ[2], MIRJANA SARVAN[2], BEĆKO KASALICA[2], MARIJA KRMAR[1], JELENA RADIĆ-PERIĆ[1#] and MILJENKO PERIĆ[1*#]

[1]Faculty of Physical Chemistry, University of Belgrade, Studentski trg 12–16, P.O. Box 47, 11158 Belgrade Serbia and [2]Faculty of Physics, University of Belgrade, Studentski trg 12–16, 11158 Belgrade Serbia

(Received 12 September, revised 10 October 2012)

Abstract: During plasma electrolytic oxidation of a magnesium alloy (96 % Mg, 3 % Al and 1 % Zn), a luminescence spectrum in the wave number range between 19950 and 20400 cm^{-1} was obtained. The broad peak with a clearly pronounced structure was assigned to the v′–v″ = 0 sequence of the $B^1\Sigma^+ \rightarrow X^1\Sigma^+$ electronic transition of MgO. Quantum-mechanical perturbative approach was applied to extract the form of the potential energy curves for the electronic states involved in the observed spectrum, from the positions of the spectral bands. These potential curves, combined with the results of quantum-chemical calculations of the electric transition moment, were employed in subsequent variational calculations to obtain the Franck–Condon factors and transition moments for the observed vibrational transitions. Comparing the results of these calculations with the measured intensity distribution within the spectrum, the relative population of the upper electronic state vibration levels was derived. This enabled the plasma temperature to be estimated. Additionally, the temperature was determined by analysis of the recorded $A^2\Sigma^+$ (v′ = 0) – $X^2\Pi$ (v″ = 0) emission spectrum of OH. The composition of the plasma containing magnesium, oxygen, and hydrogen under the assumption of a local thermal equilibrium was calculated in the temperature range up to 12000 K and for pressures of 10^5, 10^6, 10^7, and 10^8 Pa, in order to explain the appearance of the observed spectral features and to contribute to the elucidation of processes occurring during the electrolytic oxidation of Mg.

Keywords: magnesium alloy; plasma electrolytic oxidation; galvanoluminescence; $B^1\Sigma^+ \rightarrow X^1\Sigma^+$ electronic transition of MgO; perturbative and variational quantum-mechanical methods; *ab initio* quantum-chemical calculations; computation of plasma composition.

* Corresponding author. E-mail: peric@ffh.bg.ac.rs
# Serbian Chemical Society member.
doi: 10.2298/JSC120912105R

CONTENTS

1. INTRODUCTION
2. PHYSICS CHEMISTRY, MATERIAL SCIENCE
3. SPECTROSCOPY
   3.1. Transitions
   3.2. Vibrational structure of spectra
   3.3. Rotational structure of electronic transitions
   3.4. Spectral systems of MgO
4. QUANTUM CHEMISTRY
   4.1. MgO
5. QUANTUM MECHANICS
   5.1. Perturbative approach
   5.2. Variational approach
6. DETERMINATION OF PLASMA COMPOSITION
7. PLASMA ELECTROLYTIC OXIDATION
8. EXPERIMENTAL
9. RESULTS AND DISCUSSION
   9.1. Luminescence of the $B^1\Sigma^+$–$X^1\Sigma^+$ system of MgO during PEO of Mg
   9.2. $B^1\Sigma^+$–$X^1\Sigma^+$ spectrum of MgO
   9.3. Computation of F–C factors and vibrational transition moments
   9.4. Estimation of population of vibrational levels and determination of plasma temperature
   9.5. Estimation of plasma temperature based on the use of OH bands
   9.6. Calculation of plasma composition
10. CONCLUSIONS

1. INTRODUCTION

The usual form of a review paper is such that the author picks up some research field, sometimes a particular method, and reports briefly about all the systems which have been investigated in/with it. In the other words, he writes nothing about everything (but “everything” only for those who are working in the same field, or using the same method). In the present review, we take the opposite point of view. We consider a particular element, magnesium, even only a molecule that involves it, MgO, eventually solely a spectral band sequence of this molecule, and show all that we were able and/or forced to do on it in order to make an infinitesimal progress in our knowledge of some particular properties of this element. Figuratively speaking again, we write everything about nothing.

2. PHYSICS CHEMISTRY, MATERIAL SCIENCE

Magnesium is one of the most abundant elements on the Earth, but also, as is nowadays believed, in the whole universe[1–3] (see Supplement A). Elemental

magnesium is a fairly strong, silvery-white, light-weight (two thirds the density of aluminium) alkaline earth metal. It is highly reactive and thus not found naturally on Earth. However, when once produced, it is coated with a thin layer of oxide (passivation), which partly masks this reactivity. It is mainly obtained by electrolysis of magnesium salts extracted from brine. Magnesium is highly flammable when molten or in powder or ribbon form. It burns in air with a characteristic brilliant white light, which includes strong ultraviolet radiation. The flame temperature of Mg and Mg alloys can reach over 3000 °C. Once ignited, it is difficult to extinguish, being able to burn in nitrogen (forming magnesium nitride), carbon dioxide (forming magnesium oxide) and water (forming magnesium oxide). Commercially, the main use for the metal is as an alloying agent to make aluminium–magnesium alloys, called "magna(e)lium". These alloys are useful for their relative lightness and strength. An important application field of magnesium is electronic devices. Owing to its low weight, and good mechanical and electrical properties, magnesium is widely used for the manufacture of automotive and truck components, mobile phones, laptop and tablet computers, cameras, and other electronic components. Due to important interactions between phosphate and magnesium ions, magnesium is essential to the basic nucleic acid chemistry of life, and thus to all cells of all known living organisms. Over 300 enzymes require the presence of magnesium ions for their catalytic action. Plants have an additional use for magnesium in that chlorophylls are magnesium-centred porphyrins. Magnesium compounds are typically white crystals. Most are soluble in water. They, primarily magnesium oxide (MgO), are used as refractory materials in furnace linings for the production of iron, steel, non-ferrous metals, glass and cement, and also in the agricultural, chemical, and construction industries.

3. SPECTROSCOPY

3.1. Transitions

The intensity of the transition between two molecular states described by the wave functions Ψ'' and Ψ' is proportional to the square of the transition moment (TM) defined as:[4,5]

$$R^{',''} = \int \Psi'^{*} A \Psi'' \mathrm{d}\tau \tag{1}$$

where A is the operator that determines the mechanism of the transition. In the most important case of "optical" transitions, considered here, A is the (vector) dipole operator, $\vec{\mu}$, defined by:

$$\vec{\mu} = \sum_i q_i \vec{r}_i \tag{2}$$

where q_i is the charge and $\vec{r}_i$ is the radius vector of the i-th particle. The sum runs over all charged particles (electrons and nuclei). The proportionally factor

between the intensity of an transition and the square of the TM involves, beside natural constants and statistical weights, in the case of absorption, the energy difference, ΔE, between the levels in question, and at emission ΔE^4. Assuming the general case, when the two energy levels in question belong to different electronic (e), vibrational (v), rotational (r), and spin states, Eq. (1) can be written as:

$$\vec{R}^{\prime,\prime\prime} = \int\int\int\int \Psi^{\prime *}(\mathrm{e,v,r,s})\vec{\mu}\Psi^{\prime\prime}(\mathrm{e,v,r,s})\mathrm{d}\tau_\mathrm{e}\mathrm{d}\tau_\mathrm{v}\mathrm{d}\tau_\mathrm{r}\mathrm{d}\tau_\mathrm{s} \tag{3}$$

The total wave functions, Ψ'' and Ψ', are usually (in the framework of the non-relativistic, Born–Oppenheimer (B–O), rigid rotator/infinitesimal vibrator approximations) assumed as products of the partial wave functions describing individual degrees of freedom, *i.e*. in the form:

$$\Psi(\mathrm{e,v,r,s}) = \psi_\mathrm{e}\psi_\mathrm{v}\psi_\mathrm{r}\psi_\mathrm{s} \tag{4}$$

If only "allowed" transitions are of interest, the spin variables can be excluded from consideration since in this case transitions are only possible when both states in question have the same spin function. The problem now is that the rotation functions are defined in a space-fixed coordinate system, while the electronic and vibrational functions are naturally expressed in a moving coordinate system tied to the molecule. Thus, one has to start with the expression for the components of TM, μ_F ($F = X, Y, Z$), along the axes of the space-fixed frame:

$$R_F^{\prime,\prime\prime} = \int\int\int \psi_\mathrm{r}^{*\prime}\psi_\mathrm{v}^{*\prime}\psi_\mathrm{e}^{*\prime}\mu_F\psi_\mathrm{e}^{\prime\prime}\psi_\mathrm{v}^{\prime\prime}\psi_\mathrm{r}^{\prime\prime}\mathrm{d}\tau_\mathrm{e}\mathrm{d}\tau_\mathrm{v}\mathrm{d}\tau_\mathrm{r} \tag{5}$$

and then transform some of the quantities to the molecule-fixed frame, x, y, z. The components of the dipole operator transform as:

$$\mu_F = \sum_g \lambda_{Fg}\mu_g \tag{6}$$

where $g = x$, y or z, and λ_{Fg} are the elements of the transformation matrix that involves sin and cos functions of two eulerian angles ϕ and θ. Since (only) the rotation functions depend on the eulerian angles (and only on them), Eq. (5) can be transformed into:

$$R_F^{\prime,\prime\prime} = \sum_g \int \psi_\mathrm{r}^{*\prime}\lambda_{Fg}\psi_\mathrm{r}^{\prime\prime}\mathrm{d}\tau_\mathrm{r}\left[\int \psi_\mathrm{v}^{*\prime}\left(\int \psi_\mathrm{e}^{*\prime}\mu_g\psi_\mathrm{e}^{\prime\prime}\mathrm{d}\tau_\mathrm{e}\right)\psi_\mathrm{v}^{\prime\prime}\mathrm{d}\tau_\mathrm{v}\right] \tag{7}$$

The expression in parentheses:

$$\int \psi_\mathrm{e}^{*\prime}\mu_g\psi_\mathrm{e}^{\prime\prime}\mathrm{d}\tau_\mathrm{e} \equiv R_g^{\prime,\prime\prime} \tag{8}$$

is the g-component of the "electric transition moment" (actually, in this context it would be more logical to call this quantity the electronic TM, to stress that the integration is carried out only with respect to the electronic coordinates; however, most authors prefer the term "electric", to distinguish this quantity from, *e.g*., the

magnetic TM). The electric TM represents a generalization of the usual electric dipole moment (obtained from Eq. (8) when $\Psi_{e'} = \Psi_{e''}$) and, unlike the latter, it can, even in diatomic molecules, have both parallel and perpendicular components with respect to the molecular axis. This quantity is a function of the bond length, r (*i.e.*, of the vibrational coordinate), and can thus be represented by a Taylor expansion:

$$R_g^{',''} = \left(R_g^{',''}\right)_{r=r_e} + \left(\frac{\mathrm{d}R_g^{',''}}{\mathrm{d}r}\right)_{r=r_e} \left(r - r_e\right) + \ldots \tag{9}$$

where r_e is the equilibrium bond length. Inserting Eq. (9) into Eq. (7), one obtains:

$$R_F^{',''} = \sum_g \int \psi_{r'}^* \lambda_{Fg} \psi_{r''} \mathrm{d}\tau_r \times$$
$$\times \left[\left(R_g^{',''}\right)_{r=r_e} \int \psi_{v'}^* \psi_{v''} \mathrm{d}\tau_v + \left(\frac{\mathrm{d}R_g^{',''}}{\mathrm{d}r}\right)_{r=r_e} \int \psi_{v'}^* \left(r - r_e\right) \psi_{v''} \mathrm{d}\tau_v + \ldots \right] \tag{10}$$

With help of Formula (10), all the selection rules for optical transitions in diatomic molecules can be discussed. Since electronic transitions are dealt with in the present study, pure rotation and vibration–rotation transitions are discussed very briefly.

i) Pure rotation spectra, $e' = e'' \equiv e$, v' = v'' ≡ v, $r' \neq r''$. In this case, $\int \psi_v^* \psi_v \mathrm{d}\tau_v = 1$, and in the harmonic approximation $\int \psi_v^* \left(r - r_e\right) \psi_v \mathrm{d}\tau_v = 0$. The electric TM becomes then the dipole moment of the molecule that, due to axial symmetry of diatomic molecules, always lies along the internuclear axis (z). Equation (10) reduces then to:

$$R_F^{',''} = \left(R_z^e\right)_{r=r_e} \sum_g \int \psi_{r'}^* \lambda_{Fg} \psi_{r''} \mathrm{d}\tau_r \tag{11}$$

A rotation spectrum can thus appear only if the molecule considered has a non-vanishing dipole moment. Such are heteronuclear, but not homonuclear diatomics. The situation concerning the transition rules is not changed even if one goes beyond the harmonic approximation; for a homonuclear diatomic molecule $\mathrm{d}R_g^e / \mathrm{d}r$, as well as all higher derivatives equal zero. A pure rotation spectrum consists of a number of nearly equidistant lines with the spacing in the order of magnitude of typically 10 cm^{-1}, which form a molecular band.

ii) Vibration–rotation spectra, $e' = e'' \equiv e$, v' ≠ v''. In this case, $\int \psi_{v'}^* \psi_{v''} \mathrm{d}\tau_v = 0$, and Eq. (10) reduces to:

$$R_F^{',''} = \left(\frac{\mathrm{d}R_Z^{\mathrm{e}}}{\mathrm{d}r} \right)_{r=r_{\mathrm{e}}} \sum_g \int \psi_{\mathrm{r}'}^* \lambda_{Fg} \psi_{\mathrm{r}''} \mathrm{d}\tau_{\mathrm{r}} \int \psi_{\mathrm{v}'}^* \left(r - r_{\mathrm{e}} \right) \psi_{\mathrm{v}''} d\tau_{\mathrm{v}} + \ldots \qquad (12)$$

Since Expression (12) equals zero when there is no change in the dipole moment with variation of the bond length, only heteronuclear diatomics can have a vibration–rotation spectra. In the harmonic approximation, the second integral implies the selection rule v′ – v″ = ±1. In higher approximations, "overtones" are possible, corresponding to the selection rule v′ – v″ = ±2, ±3, … but they are normally of low intensity. The rotation selection rules are determined by the first integral, and they are the same as for pure rotational transitions. Each vibrational transition is accompanied by a number of rotational ones. Owing the above selection rules for vibrational transitions, a vibration–rotation spectrum is usually similar to a pure rotational one, the most prominent difference being that the former appears in the near and the latter in the far infrared region.

iii) Electronic transitions, $e' \neq e''$. In the first Franck–Condon (F–C) approximation, the second term in the square parentheses on the right-hand side of Eq. (10) can be neglected:

$$R_F^{',''} \cong \left(R_g^{',''} \right)_{r=r_0} \sum_g \int \psi_{\mathrm{r}'}^* \lambda_{Fg} \psi_{\mathrm{r}''} \mathrm{d}\tau_{\mathrm{r}} \int \psi_{\mathrm{v}'}^* \psi_{\mathrm{v}''} d\tau_{\mathrm{v}} \qquad (13)$$

Instead of the dipole moment, as in Eqs. (11) and (12), one now has the electric TM (see. Eq. (8)), which also in homonuclear diatomics can be non-zero. It will be non-vanishing if the product of the irreducible representations of the electronic wave functions equals the irreducible representation of the *x*-, *y*-, or *z*-components of the dipole operator. In the case of heteronuclear diatomics, the *z*-component of this operator belongs to the Σ^+, and *x*- and *y*-components build together a basis for the Π irreducible representation of the point group $C_{\infty v}$. This results in the selection rule $\Delta\Lambda = 0, \pm 1$, where $\Lambda = 0$ (Σ^+ or Σ^- electronic state), 1 (Π state), 2 (Δ state), *etc.*, is the projection of the electronic angular momentum along the internuclear axis. An additional selection rule is that the transitions $\Sigma^+ \leftrightarrow \Sigma^+$ and $\Sigma^- \leftrightarrow \Sigma^-$ are allowed, while the transitions $\Sigma^+ \leftrightarrow \Sigma^-$ are forbidden. In the case of homonuclear diatomics, the *z*-component of this operator belongs to a Σ_u^+, and the *x*- and *y*-components to a Π_u irreducible representation of the point group $D_{\infty \mathrm{h}}$. This yields the additional selection rule that an electronic transition is allowed only if one of the combining states has *g* and the other *u* symmetry. All the mentioned selection rules (as well as $\Delta S = 0$, where *S* is the total electronic spin of the molecule) are valid within the framework of the non-relativistic and B–O approximation.

The square of the second integral in Eq. (13), representing the overlap of the vibrational wave functions of the combining state:

$$FC \equiv \left[\int \psi_{v'}^{*} \psi_{v''} \mathrm{d}\tau_{v} \right]^{2} \quad (14)$$

is called the Franck–Condon factor (FCF). Unlike the case of pure vibration(––rotation) spectra, it is not subject to any selection rules. Very often, the electronic spectra are recorded using instruments of relatively low resolution, such that it is not possible to clearly identify the rotational structure of bands but only the positions of their maxima ("heads"). The magnitudes of the FCFs determine the intensity distribution within a band system, which consists of transitions between different vibrational levels of two electronic states. The most prominent features in spectral systems are band progressions (characterized in absorption by a fixed vibrational quantum number v″ of the lower electronic state, and variable quantum number v′ in the excited state, and fixed v′ and variable v″ in emission) and sequences (v′ – v″ = const.). If the equilibrium bond lengths and vibrational frequencies are similar in both electronic states, the most intense band in an experimentally recorded spectrum corresponds to the transition v′ – v″ = 0. A long progression with the maximum at a quite large value of $|v' - v''|$ indicates that the equilibrium bond lengths in the combining electronic states are appreciably different. Electronic spectra appear in the visible and ultraviolet region. While the band heads in a progression are separated from one another by several hundreds to a few thousand cm^{-1} (corresponding to the wave numbers of the vibrational frequencies), the separation of the bands in a sequence is usually between several tens and several hundreds cm^{-1}, reflecting the difference in the values of vibrational frequencies in the two electronic states in question.

The F–C approximation is thus mathematically based on the assumption that the electric transition moment is a constant quantity. In terms of naive quantum mechanics or classical physics, if one considers, for example, absorption, it can be interpreted such that the electronic transition occurs so quickly that the nuclei remain after the jump from the lower into upper state in the same position where they were at the beginning of the electron jump. This picture is quite compatible with that lying behind the B–O approximation. More sophisticatedly speaking, the transition is most probable to a vibrational level the wave function of which has the largest overlap with that of the starting vibrational level ("vertical" transition).

Going beyond the F–C approximation, the dependence of the electric TM on the internuclear distance, as indicated by the second term on the right-hand side of Eq. (10), has to be taken into account. In a diatomic molecule, this only quantitatively influences the transition probabilities and can make the transition not strictly "vertical". However, in the case of a polyatomic species, the consequences of the incorporation of this term into the treatment can be dramatic; it can happen, namely, that the value of the electric TM at the equilibrium geometry vanishes, but not its (first) derivative with respect to a particular non-to-

tally symmetric vibrational coordinate (the unique vibrational coordinate in diatomics is totally symmetric). In this case, a transition forbidden in the F–C approximation becomes "vibronically induced".

The intensity of the spectral band appearing as a consequence of the emission transition between the vibrational level v′ of the electronic state e′ and the vibrational level v″ of the electronic e″ is determined by the formula:

$$I_{e'v',e''v''} \propto N_{v'}\left(E_{v'e'} - E_{e''v''}\right)^4 \left|\vec{R}^{e'v',e''v''}\right|^2 e^{-\frac{E_{v'e'}-E_{e''v''}}{kT}} \equiv$$
$$\equiv N_{v'}\left(E_{v'e'} - E_{e''v''}\right)^4 (TM)_{e'v',e''v''} e^{-\frac{E_{v'e'}-E_{e''v''}}{kT}} \quad (15)$$

where $E_{v'e'}$ and $E_{v''e''}$ are the energies of these two states, $R^{e'v',e''v''}$ is the vibrational transition moment, $N_{v'}$ is the number of molecules in the upper state, k is the Boltzmann constant and T temperature. The notation $(TM)_{e'v',e''v''} = \left|R^{e'v',e''v''}\right|^2$ for the square of the vibrational TM is introduced. Since the energy differences between all transitions to be handled in the present study, namely the members of the v′ – v″ = 0 sequence, (0–0), (1–1),… are negligibly small compared to the energy of the electronic transition, the quantity $E_{v'e'} - E_{v''e''}$ can be, in this context, handled as constant and then the number of the molecules in the upper state is:

$$N_{v'} \propto \frac{I_{e'v',e''v''}}{(TM)_{e'v',e''v''}} \quad (16)$$

In the F–C approximation, it is assumed that the electric TM is constant, and in this case the formula (16) reduces to

$$N_{v'} \propto \frac{I_{e'v',e''v''}}{(FCF)_{e'v',e''v''}} \quad (17)$$

where $(FCF)_{e'v',e''v''}$ is the F–C factor for the transition considered.

Assuming a local thermal equilibrium of the system, the ratio of the number of molecules $N_{e'v'}$ in the vibrational state v′ and in the lowest vibrational state v′ = 0 of the same electronic species, $N_{e'0}$, is determined by:

$$\frac{N_{e'v'}}{N_{e'0}} = e^{-\frac{E_{e'v'}-E_{e'0}}{kT}} \quad (18)$$

i.e.,:

$$\ln\left(\frac{N_{e'v'}}{N_{e'0}}\right) = -\frac{E_{e'v'} - E_{e'0}}{kT} \quad (19)$$

Combining the Formulae (16), (17) and (19), for the sequence v′ = v″, one obtains:

$$\ln\left[\frac{\frac{I_{e'v,e''v}}{(TM)_{e'v',e''v''}}}{\frac{I_{e'0,e''0}}{(TM)_{e'0,v'0}}}\right]=-\left(\frac{E_{e'v'}-E_{e'0}}{k}\right)\frac{1}{T} \quad (20)$$

and

$$\ln\left[\frac{\frac{I_{e'v,e''v}}{(FCF)_{e'v,e''v}}}{\frac{I_{e'0,e''0}}{(FCF)_{e'0,e''0}}}\right]=-\left(\frac{E_{e'v'}-E_{e'0}}{k}\right)\frac{1}{T} \quad (21)$$

The Formulae (20) and/or (21) will be used later to determine the plasma temperature.

3.2. Vibrational structure of spectra

Experimentally derived vibrational energy levels of an electronic state are usually represented by the formula:[4]

$$E_v \equiv T_e hc + G(v)hc = \\ = T_e hc + hc\omega_e\left(v+\frac{1}{2}\right) - hc\omega_e x_e\left(v+\frac{1}{2}\right)^2 + hc\omega_e y_e\left(v+\frac{1}{2}\right)^3 + \ldots \quad (22)$$

where $G(v)$ are the corresponding term values (in cm^{-1}). In Eq. (22), T_e is the electronic term value; for the ground electronic state $T_e = 0$. Herzberg[4] called (as many people working in molecular spectroscopy and/or quantum chemistry have done) the quantity ω_e (as well as ω) the "vibrational frequency measured in cm^{-1}". The subscript "e" in ω_e stands for "equilibrium". The sense of this notation is the following: in the case of a harmonic oscillator, ω is a clearly defined quantity determined only by the values for the force constant and reduced mass; on the other hand, the quantity ω_e is just an empirical parameter appearing in experimentally derived formulae, such as Eq. (22). It would equal ω only if the correction terms (quadratic, cubic, *etc*.) in Eq. (22) were neglected. This is slightly misleading (see, *e.g*., recent papers in the present journal[6,7]), because the frequency, such as in the expressions $E = h\nu$ and $E = \hbar\omega$, has dimension s^{-1} (the former, ν, is the linear and the latter, ω, the angular frequency, $\omega = 2\pi\nu$). Herzberg's ω is actually the wave number, and formulae of the type (22) will be written in this paper as:

$$E_{\mathrm{v}} \equiv T_{\mathrm{e}}hc + G(\mathrm{v})hc = \\ = T_{\mathrm{e}}hc + \left(\mathrm{v}+\frac{1}{2}\right)\tilde{\nu}hc - \left(\mathrm{v}+\frac{1}{2}\right)^2(\omega_{\mathrm{e}}x_{\mathrm{e}})hc + \left(\mathrm{v}+\frac{1}{2}\right)^3(\omega_{\mathrm{e}}y_{\mathrm{e}})hc + \ldots \quad (23)$$

where:

$$\tilde{\nu} \equiv \frac{1}{\lambda} = \frac{\nu}{c} = \frac{\omega}{2\pi c} \quad (24)$$

In Eq. (24), $\tilde{\nu}$ is the wave number (in cm^{-1}; to repeat, equal to Herzberg's ω_{e}), and λ it the wavelength, usually expressed in nm. However, the notations $\omega_{\mathrm{e}}x_{\mathrm{e}}$ and $\omega_{\mathrm{e}}y_{\mathrm{e}}$ will be retained for the experimentally determined anharmonicity parameters expressed in cm^{-1}, and the parentheses indicate that these formal products will be handled as single quantities. Note that the first cor-rection term in Eq. (22) appears with a minus sign. This choice was made because the energy distance between successive vibrational levels almost always decreases with increasing quantum number v, such that the quantity $\omega_{\mathrm{e}}x_{\mathrm{e}}$ is positive. On the other hand, the contribution of higher correction terms, such as $\omega_{\mathrm{e}}y_{\mathrm{e}}$, often negligible, can be either positive or negative.

3.3. Rotational structure of electronic transitions

If it is assumed that only the nuclei contribute to the moment of inertia of a diatomic molecule, that the molecule is in an $^1\Sigma^{\pm}$ electronic state and that it is a rigid rotator, then the rotation functions are spherical harmonics. In this case, the rotation energy levels are given by the formula:

$$E(J) = \frac{\hbar^2}{2I}J(J+1) = \frac{\hbar^2}{2\mu r_{\mathrm{e}}^2}J(J+1) \equiv BJ(J+1)hc \quad (25)$$

where

$$B \equiv \frac{\hbar^2}{2\mu r_{\mathrm{e}}^2 hc} = \frac{h}{8\pi^2 c\mu r_{\mathrm{e}}^2} \quad (26)$$

is the rotational constant, expressed in cm^{-1}, and the quantum number J takes the values 0, 1, 2,... Each energy level (except for $J = 0$ is $2J + 1$ degenerate, because the corresponding wave functions also depend on the value of the quantum number M, measuring the projection of the angular momentum on a space-fixed axis (Z). The projection of the angular momentum on the molecular axis equals zero. The selection rule for rotational transitions is $J' - J'' = 0, \pm 1$, with the restriction that the transition $J = 0 \leftrightarrow J = 0$ is forbidden.

However, the presence of electrons implies that the moment of inertia about the nuclear axis is not exactly zero, so that a diatomic molecule (if I_A is not

neglected) should be handled as a prolate symmetric top rather than as a linear molecule. The energy formula (25) is then replaced by:

$$E(J) = \left[BJ\left(J+1\right) + \left(A-B\right)\Lambda^2 \right] hc \tag{27}$$

where $A \equiv \hbar^2/(2I_A hc) = h/(8\pi^2 c I_A)$, and Λ is the quantum number for the projection of the electronic angular momentum on the internuclear axis. For a given Λ, the quantum number J takes the values $J = \Lambda, \Lambda+1, \Lambda+2,\ldots$

The presence of the electron spin introduces coupling between electronic orbital, rotational and electronic spin degrees of freedom. There are several coupling schemes, known as the Hund's coupling cases.[4] The most widely applied are: case (a), covering the cases when the spin–orbit interaction is so strong that the projection, Σ, of the total electron spin on the molecule axis and consequently, the quantity $\Omega \equiv \Lambda + \Sigma$ is nearly conserved. In this case the "nearly good" quantum number Ω takes over the role of Λ from Eq. (27), *i.e.*, it represents the projection of J on the molecular axis and thus for a given Ω, the quantum number J takes the values $J = \Omega, \Omega+1,\ldots$; the other extreme represents a very weak spin–orbit coupling (Hund's case (b)). In this case, the electron spin is almost totally decoupled from the internuclear axis. The quantum numbers Σ and Ω are then not at all good, but instead N, representing the total angular momentum apart from spin, becomes a nearly good quantum number. Its projection on the internuclear axis is Λ.

The appearance of nearly good quantum numbers implies additional not strictly rigorous but useful (for classification of experimentally observed features) selection rules. In Hund's case (a), this is $\Delta\Sigma = 0$, and in case (b) $\Delta N = 0, \pm 1$ (again with the restriction that $\Delta N = 0$ does not occur in Σ–Σ electronic transitions). The only rigorous selection rule for rotational transitions is $\Delta J = 0, \pm 1$. However, even this rule ceases to be rigorous if the molecular nuclei have a non-vanishing spin. In such a case, the only rigorous selection rule is $\Delta F = 0, \pm 1$, where F is the quantum number for the total angular momentum involving also nuclear spins. However, because of the very weak coupling between the total angular momentum apart from nuclear spin and the nuclear spin, the selection rule $\Delta J = 0, \pm 1$ remains very strong.

Now, the simplest case of the rotational structure of an electronic transition is considered, namely, when both electronic states are of $^1\Sigma$ symmetry, and when the effects of anharmonicity can be neglected,. The selection rule for rotational transitions is then $J' = J'' + 1$ ("R branch") and $J' = J'' - 1$ ("P branch"). Let us take $J' = J$, then for the R branch, $J' = J'' + 1 = J + 1$, and the term values are:

$$\begin{aligned} \tilde{\nu} &= \tilde{\nu}_0 + F'\left(J'\right) - F''\left(J''\right) = \tilde{\nu}_0 + B'\left(J+1\right)\left(J+2\right) - B''J\left(J+1\right) = \\ &= \tilde{\nu}_0 + 2B' + \left(3B' - B''\right)J + \left(B' - B''\right)J^2 \end{aligned} \tag{28}$$

where $\tilde{\nu}_0$ is a constant for the given electronic–vibrational transition, the "band origin". For the P branch, $J' = J'' - 1 = J - 1$, and the term values are thus:

$$\begin{aligned}\tilde{\nu} &= \tilde{\nu}_0 + F'(J') - F''(J'') = \tilde{\nu}_0 + B'(J-1)J - B''J(J+1) = \\ &= \tilde{\nu}_0 - (B'+B'')J + (B'-B'')J^2\end{aligned} \tag{29}$$

When $B' < B''$, the contribution of the quadratic term in J in Eq. (28) is negative, while the contribution of the linear term is positive (B' and B'' cannot differ very much from one another). At small J values, the linear term dominates but the difference in the contribution of the linear and quadratic terms becomes continuously smaller with increasing J; at a certain J value, $J = J_h$, they equalize, and after that the quadratic term becomes dominant. Around the $J = J_\mathrm{h}$ value (vertex of the parabola), the rotational lines are crowded and build a "band head". The band head appears at a wave number $\tilde{\nu}_\mathrm{h}$ higher than that of the band origin, *i.e.*, at the "violet side" with respect to $\tilde{\nu}_0$. The band is said to be "shaded" ("degraded") towards the red (*i.e.*, towards longer wave lengths). Conversely, when $B' > B''$ (this will be the situation for the case handled below), there is a band head in the P-branch on the red side with respect to the band origin, and this band is violet degraded. The position of the band head is found when the condition $\mathrm{d}\tilde{\nu}/\mathrm{d}J = 0$ is fulfilled. In the case when $B' > B''$, differentiating Eq. (29), one obtains:

$$J_\mathrm{h} = \frac{(B'+B'')}{2(B'-B'')} \tag{30}$$

Replacing in Eq. (29) J with J_h given by Eq. (30), one obtains for the term difference between the band head and the band origin (in the present case, there is no spectral line at the band origin, because the transition $J = 0 \leftrightarrow J = 0$ is forbidden):

$$\tilde{\nu}_\mathrm{h} - \tilde{\nu}_0 = -\frac{(B'+B'')^2}{4(B'-B'')} \tag{31}$$

In electronic transitions that do not involve two Σ species, in addition to the P and R branches, there is also a Q branch corresponding to the selection rule $\Delta J = 0$. The term values are:

$$\begin{aligned}\tilde{\nu} &= \tilde{\nu}_0 + F'(J') - F''(J'') = \\ &= \tilde{\nu}_0 + B'J(J+1) - B''J(J+1) = \tilde{\nu}_0 + (B'-B'')J(J+1)\end{aligned} \tag{32}$$

In electronic transitions between orbitally (Π, Δ, ...) and spin (doublet, triplet,...) degenerate species, there are several P, Q, and R sub-branches (sub-bands).

When the energies of rotational levels are determined by Eq. (25), each rotational level is $2J + 1$ degenerate. Since the rotational energy is in generally much smaller than the thermal energy, $\sim kT$, in usual spectroscopic experiments,

the lowest-lying (J = 0) non-degenerate rotational level is, because of continuously increasing statistical weight with increasing J, less populated than some of the higher levels. Consequently, the maximum within a band consisting of rotational lines that correspond to the selection rule $J' - J'' = \pm 1$ is not at the "band origin" (the line that involves J' = 0 or J'' = 0) but instead at those J values for which an optimal compromise between two opposite tendencies, namely, an increase in the statistical weight and a decrease in the Boltzmann factor, $\exp\left|-E(J)/kT\right|$, is reached.

3.4. Spectral systems of MgO

When one starts with the (molecular) spectroscopic aspects of a problem, the first step is to look into two monographs. The first one is by Herzberg [4,9,10] – it actually consists of four volumes (the fourth one written in collaboration with Huber), plus a small additional book containing the heart of the first three monumental ones.[11] There is probably no other example in the scientific literature that the books written in the fifties of the preceding century that have lost almost nothing of their actuality. One only has to look at experimental papers published after that time and to complete in this way the information collected in Herzberg's books. Herzberg did it himself in the seventies and in his book (with Huber)[10] one can find all relevant data on diatomic molecules published until the end of 1975. Herzberg's (HH) books have become such a standard source of information on molecular spectra that many authors of new studies do not cite explicitly the authors of old experimental works but they simply quote them as "Herzberg and the references therein". This praxis will be followed in the present review. The other unavoidable book is that by Pearse and Gaydon (PG).[12] Its fourth (to our knowledge the last) edition was printed in 1976, *i.e.*, nearly at the same time as the Huber–Herzberg's compilation of data on diatomics. This edition contains the data published until the end of 1974. While the three volumes by HH also involve the complete theory underlying molecular spectra and numerical values for all possible molecular parameters, such as vibrational frequencies, anharmonicity and rotational constants, internuclear distances, *etc*. (this is reflected in the title of the series: "Molecular Spectra and Molecular Structure"), the book by PG (as the title, "The Identification of Molecular Spectra" says), only involves the results of direct spectral measurements, *i.e.*, the positions of band heads and their relative intensities. Thus, the books by HH and PG are in a sense complementary to each other: *e.g.*, in the HH books, one finds the transition energies in wave numbers, while they are collected by PG in wavelengths (this causes some difficulties when the results from these books are compared with one another; the numbers in HH's books correspond to vacuum and the band positions collected in PG to air, and thus the exact wavelength corresponding to a HH wave number cannot be obtained by simply inverting the last quantity). Those who still believe that it is possible to divide research into experi-

mental and theoretical would say that the HH's books are aimed at theoreticians and that by PG at experimentalists.

Selected data for MgO, taken from HH,[10] are presented in Supplement B. HH constructed this table based on about 50 studies published from 1943 to 1975. All spectra observed until 1975 involved eight singlet and four triplet electronic states.

In the book by PG,[12] there are data about five spectral systems of MgO, namely of a strong green, a weaker red and three ultra-violet systems.

The red system appears in the wavelength range 690–470 nm and is assigned to the $B^1\Sigma^+$–$A^1\Pi$ electronic transition. The data in the PG monograph are taken from Mahanti and Lagerqvist and Uhler.[13–15] The spectrum was found to appear in the core of the magnesium arc in air, and in burning magnesium ribbon. Single-headed bands are degraded to the violet.

The information about the green system, assigned to the $B^1\Sigma^+$–$X^1\Sigma^+$ transition, was taken from Mahanti[13] and Lagerqvist.[16] This spectrum appears not only in a Mg arc in air, burning Mg ribbon, in flames, shock tubes and in the King furnace, but also in sun-spots. The spectral system is dominated by a very marked (0,0) sequence and the bands are degraded to the violet. The data for this system from the PG book are collected in Table I. The measured band position was used to calculate the vibrational term values in the $X^1\Sigma^+$ and $B^1\Sigma^+$ electronic states and to construct the corresponding Desladres table. In Table I, are also presented the term values computed by means of Eq. (23) using the vibrational frequencies and anharmonicity constants given in the literature.[10]

The information about violet systems of MgO, appearing between 396 and 364 nm, was based on several studies.[17–21] Two systems of red-degraded bands, $C^1\Sigma^-$–$A^1\Pi$ and $D^1\Sigma^-$–$A^1\Pi$, and a violet-degraded $^3\Delta$–$^3\Pi$ system were detected. In addition, Singh [22–24] reported on three other red-degraded ultra-violet systems appearing at 265.2 ($E^1\Sigma^+$–$X^1\Sigma^+$), 263.7 nm ($F^1\Pi$–$X^1\Sigma^+$) and 255.6 nm ($G^1\Pi$–$X^1\Sigma^+$). A violet-degraded band, assigned to $G^1\Pi$–$A^1\Pi$, was also detected at 275.01 nm.

Newer experimental studies, including optical spectroscopy, laser–magnet resonance, laser-induced fluorescence, two-colour resonance-enhanced two-photon ionization studies and vibrationally resolved photoelectron spectroscopy [25–37] have been cited in a recent theoretical study by Maatouk *et al.*[38]

Comparing the data collected by HH and PG, it could be stated that HH included in their book the $A^2\Sigma^+$–$X^2\Sigma$ systems in the (infra-red) region at about 1900 nm, which was only indirectly mentioned by PG. The reason might be that the first reference used by HH[39] appeared between the third and fourth editions of PG's book, and the second one[40] even later. Interestingly, neither HH nor PG cited the important study by Ghosh *et al.*[41] PG did not cite the paper by Lagerqvist and Uhler[42] and not even that by Pešić,[43] a former coworker of Gaydon. On

the other hand, HH included in their book the results obtained by Antić-Jovanović *et al*. at the Faculty of Physical Chemistry in Belgrade.[44,45] Later, the results of the calculation of *FCF*s for the $B^1\Sigma^+$–$X^1\Sigma^+$ transition by Prasad and Prasad[46] will also be used.

TABLE I. Term values for bands of the green system, $B^2\Sigma^+$–$X^2\Sigma^+$ of MgO. The band heads (subscript h) are taken from ref. 12, and the band origins (subscript o) are computed by means of the formulae from ref. 10. The numbers without parentheses represent the original wavelengths in nm. Numbers in parentheses, without asterisks, in the central field of the table are the corresponding wave numbers (in cm^{-1}) obtained without an air–vacuum correction (*i.e.*, they are inverse values of the corresponding wavelengths). Based on them, the term values ($G_{v''}$, $T_{v'}$ and $G_{v'}$, subscript h) were calculated. The numbers in the central field given in parentheses with asterisks were obtained as differences of the derived term values

$T_{v'}$		$(19971)_h$	$(20753)_h$	$(21552)_h$	$(22320)_h$	$(23103)_h$	$(23877)_h$	–	–
$G_{v'}$		$(0)_h$	$(782)_h$	$(1581)_h$	$(2349)_h$	$(3132)_h$	$(3906)_h$	–	–
$T_{v'}$		20004_o	20818_o	21623_o	22418_o	23205_o	23981_o	24748_o	25506_o
$G_{v'}$		0_o	815_o	1620_o	2415_o	3201_o	3978_o	4745_o	5502_o
$G_{v''}$	v″	v′							
		0	1	2	3	4	5	6	7
$(0)_h$	0	500.73	481.85						
		(19971)	(20753)						
0_o		(19971)*	(20753)*						
		20004	20818						
$(762)_h$	1	520.60	499.67	481.01					
		(19209)	(20013)	(20790)					
775_o		(19209)*	(19991)*	(20790)*					
		19229	20043	20848					
$(1493)_h$	2		519.20	498.59	480.15				
			(19260)	(20057)	(20827)				
1539_o			(19260)*	(20059)*	(20827)*				
			19279	20084	20879				
$(2237)_h$	3			517.74	497.45				
				(19315)	(20103)				
2293_o				(19315)*	(20083)*				
				19330	20125				
$(2950)_h$	4				516.25	496.21			
					(19370)	(20153)			
3037_o					(19370)*	(20153)*			
					19381	20168			
$(3673)_h$	5					514.68	494.95		
						(19430)	(20204)		
3770_o						(19430)*	(20204)*		
						19435	20211		

TABLE I. Continued

$G_{v''}$	v″	v′							
		0	1	2	3	4	5	6	7
4493_o	6							493.53 (20262) 20255	
5205_o	7								492.39 (20309) 20301

4. QUANTUM CHEMISTRY

At the beginning of nineties (of the previous century), the pope (actually, one of several) of quantum chemistry, W. Kutzelnigg, once said: "Twenty years ago, theoretical chemists claimed that they had calculated electronic transition energies with an uncertainty of 0.1 eV. They claim now that in these twenty years tremendous progress was achieved in their research field. However, if one asks them what the uncertainty in calculating electronic transition energies is today, they would say, 0.1 eV".

Working within the framework of his dissertation on several low-lying electronic states of HCN, the senior-coauthor of this review used in 1975 two atomic orbital (AO) basis sets. The smaller one consisted of 25 gaussians. It was found to be not flexible enough, and all the final calculations were performed with a "large" basis involving 27 AOs. The configuration-interaction (CI) space included roughly 20000 Slater determinants, about 2000 of them being selected for explicit calculations.[47] Ten years later, he tried to improve the results employing 50 gaussians, the CI space was chosen to consist of roughly 500000 determinants, and the secular problem actually solved was of dimensions up to 10000.[48] However, the new calculations did not bring anything substantially new. In favour of that speaks also the fact that the old study was cited (up to several years ago) 40 times, and the newer one only 16 times (indeed, it was accompanied by two additional papers, but the total number of citations for all three of them was comparable to that of the old paper). This tendency seems to continue. In the *ab initio* study discussed below, published in 2010,[38] solely the oxygen atom was described by 145 gaussians but the error margin remained at first sight the same as before. However, the reader should not come to the premature conclusion that nothing worthy has been realized in quantum chemistry since the seventies of the last century. First, in seventies, the usual error margin was 0.1–0.2 eV[49] and nowadays it is around 0.05 eV for the systems handled in this paragraph. That does not look spectacular, but recall that 0.2 eV corresponds to the difference between yellow and red (or yellow and green) colour, while 0.05 eV is only half a way between yellow and orange. Furthermore, molecules such as MgO and AlO do not belong to the easiest ones for *ab initio* computations.

We do not insist that the title of this section is quite appropriate. It is only justified if one accepts the more historical than logical concept that molecules "belong" to chemistry, while atoms are a subject of physics. "Quantum chemistry" in its *ab initio* variant, commented above, is actually a kind of applied quantum mechanics. It would be more sensible to use the term quantum chemistry for investigations such a those carried out, *e.g.*, by Gutman *et al.*[50–59] However, in this case, a serious alternative to the name "quantum chemistry" would be "mathematical chemistry" or even something like "applied (mathematical) topology". This shows how difficult it is nowadays to classify scientific fields, particularly in terms of traditional categories.

4.1. MgO

The most extensive theoretical *ab initio* study on the MgO molecule was recently reported by Maatouk *et al.*[38] and the following discussion will rely on it. The preceding theoretical studies[30,60–72] performed on singlet and triplet electronic states will just be mentioned here. In them, equilibrium geometries, vibrational frequencies, excitation energies, transition moments and spin–orbit constants were determined for a number of electronic states lying up to 50000 cm^{-1} above the ground state. It was found that the ground state $X^1\Sigma^+$ represents an open-shell system because of the dominant Mg^+O^- form, and that the ionic–covalent interactions give rise to numerous avoided crossings between the potential energy curves.

Maatouk *et al.*[38] carried out the electronic structure calculations using the MOLPRO program suite.[73] The potential energy curves, electric TMs, and spin––orbit matrix elements were computed for a large number of singlet, doublet, and quintet electronic states by means of the complete active self-consistent field (CASSCF)[74] approach followed by the internally contracted multireference configuration interaction (MRCI) method,[75,76] with the cc-pV5Z AO basis sets.[77,78] Here, primarily, the results for the $X^1\Sigma^+$ and $B^1\Sigma^+$ electronic states (and the neighbouring species) will be considered, being involved in the transition that will be discussed below.

In the ground electronic state, $X^1\Sigma^+$, and not far from the equilibrium geometry (F–C region), the MgO molecule has two dominating electronic configurations, …$5\sigma^2$ $6\sigma^1$ $2\pi^4$ $7\sigma^1$ and …$5\sigma^2$ $6\sigma^2$ $2\pi^4$. At large Mg–O distances, the latter one predominates. In the F–C region, the lowest-lying excited electronic states of MgO are $a^3\Pi$ and $A^1\Pi$, both of them corresponding to the …$5\sigma^2$ $6\sigma^2$ $2\pi^3$ $7\sigma^1$ electronic configuration, and embedded only 0.2–0.4 eV above the ground state. The following two excited states are $b^3\Sigma^+$ and $B^1\Sigma^+$, the first of which has …$5\sigma^2$ $6\sigma^1$ $2\pi^4$ $7\sigma^1$ as the dominant configuration. The $B^1\Sigma^+$ state, with a vertical energy of about 2.5 eV ($T_e \approx 20000$ cm^{-1}), has in the F–C region, the same main electronic configurations as in the ground state. Consequently, the equilibrium bond lengths and vibrational frequencies are similar in the $B^1\Sigma^+$ and $X^1\Sigma^+$ states

but these spectroscopic parameters are quite different from their counterparts in the other electronic species mentioned. Upon enlarging bond length, the $B^1\Sigma^+$ electronic state is continuously more dominated by the configurations …$5\sigma^2$ $6\sigma^2$ $2\pi^4$ and …$5\sigma^2$ $6\sigma^2$ $2\pi^2$ $6\sigma^2$, and thus at these geometries it differs considerably from the $X^1\Sigma^+$ state. Consequently, the electric TM between these two species shows a strong dependence on the bond length, as seen in Fig. 5 of Ref. 38. The other electronic states of MgO lie in the F–C region at considerably higher energies (> 3.5 eV).

The results of the *ab initio* study by Maatouk *et al.* are compared with the corresponding experimental findings in Table II. It is not our intension to analyse it; the only goal is to present the reader with the state of the art of modern *ab initio* computations. Just a small comment: look at the numbers 3558.50124 and 785.262621 cm^{-1} equivalent to the electronic transition energy and vibrational frequency, as given in the literature.[36] In our opinion, these are examples of senseless "accuracy" – even the natural width of spectral lines is much larger than the margin error quoted.

TABLE II. Comparison of *ab initio* results[38] with the corresponding experimental findings

State	T_e cm^{-1}	$(T_e)_{exp}$ cm^{-1}	$\tilde{\nu}$ cm^{-1}	$\tilde{\nu}_{exp}$ cm^{-1}	$\omega_e x_e$ cm^{-1}	$(\omega_e x_e)_{exp}$ cm^{-1}	r_e Å	$(r_e)_{exp}$ Å
$3^3\Delta$	52321		340.8		1.85		2.367	
$3^3\Sigma^-$	51748		337.5		2.03		2.356	
$2^1\Sigma^-$							∞	
$4^1\Pi$	44987.9		891.8		1.31		2.172	
$1^5\Pi$	41390.0		141.2		5.42		2.577	
$G^1\Pi$	40364.1	40259.8[a]	621.4		2.59		1.869	1.834[a]
$2^1\Delta$	39173.6		601.3		85.71		2.650	
$E^1\Sigma^+$	39113.1	37722[a]	698.1	705[a]	10.95	4.18[b]	1.837	1.829[a]
		37719[b]		714.2[b]				1.83[b]
$3^3\Pi$	38050.9	39967[l]	880.5		59.25		1.921	
$F^1\Pi$	37322.6	37922[a]	699.2	696[a]	5.12	4.5[c]	1.786	1.772[a]
		37919[c]		705[c]	6.9[d]			1.766[c]
				711[d]				1.77[d]
$2\ ^3\Sigma^-$	31520.3		798.4		28.95		1.991	
$e^3\Sigma^-$	30076	31250[a]					∞	∞[a]
$C^1\Sigma^-$	29516.1	30080.6[a]	626.9	632.4[a]	4.19	5.2[a]	1.886	1.873[a]
$D^1\Delta$	29228.2	29851.6[a]	625.1	632.5[a]	4.27	5.3[a]	1.886	1.8718[a]
		29835.4[e]		631.6[e]		5.2[e]		1.8606[e]
$d^3\Delta$	28930.5	29300[a]	653.5	650[a]	4.34	4.9[e]	1.875	1.87[a]
		29466.2[e]		655.2[e]				1.8710[e]
$2^3\Pi$	28218.4		283.4		1.61		2.799	
$c^3\Sigma^+$	27703.0	28300[a]	642.4		4.60		1.880	
$B^1\Sigma^+$	19332.7	19984.0[a,f,j]	808.2	824.08[a]	3.79	4.76[a]	1.753	1.737[a]
		19982.6[g]						
$b^3\Sigma^+$	7726.6		673.7		4.37		1.807	

TABLE II. Continued

State	T_e cm^{-1}	$(T_e)_{exp}$ cm^{-1}	$\tilde{\nu}$ cm^{-1}	$\tilde{\nu}_{exp}$ cm^{-1}	$\omega_e x_e$ cm^{-1}	$(\omega_e x_e)_{exp}$ cm^{-1}	r_e Å	$(r_e)_{exp}$ Å
$A^1\Pi$	3078.5	3563.3[a,f]	654.3	664.4[a]	4.03	3.91[a]	1.879	1.864[a]
		3561.9[g]		664.3929[h]		3.9293[h]		1.864325[h]
		3563.8377[h]		664.3[i]		3.8[i]		1.8636[i]
		3560.1[i]		664.4765[j]		3.9264[j]		
		3563[j]		664.4360[k]		3.92853[k]		
		3558.50124[k]						
$a^3\Pi$	1645.4	2400[a]	644.8	650[a]	5.3		1.885	1.87[a]
		2492.5[l]		691.1[l]		4.0 [l]		1.8687[i]
		2623[g]		648[g]		3.9 [g]		
		2620.6[i]		648.3[m]		3.9 [m]		
		2618.9453[k]		650.2[i]		4.2 [i]		
				650.18028[k]		4.2 [k]		
$X^1\Sigma^+$	0	0	769.0	785.06[a,f]	4.45	5.18[a,f]	1.766	1.749[a]
		0		785.2183[j]		5.1327[j]		
		0		785.14[g]		5.07[g]		
		0		785.262621[k]		5.12379[k]		

[a]Ref. 10 and references therein; [b]ref. 35; [c]ref. 34; [d]ref. 37; [e]ref. 27; [f]ref. 42; [g]ref. 25; [h]ref. 29; [i]ref. 28; [j]ref. 32; [k]ref. 36; [l]ref. 33; [m]ref. 26

5. QUANTUM MECHANICS

5.1. Perturbative approach

The experimentally derived formulae (23) were either used directly or *via* Deslandres Tables constructed based on them for the assignment of the bands observed in our spectra (see, *e.g.*, Table I). However, for the determination of plasma temperatures, the FCFs and/or vibrational TMs are also required. In order to calculate these quantities, the vibrational Schrödinger Equation for the two electronic states in question has to be solved and the so-obtained wave functions used to compute the required quantities. In order to avoid explicit *ab initio* calculations of the potential curves for the electronic states in question, a way must first be found to extract the potential energy functions which, combined with the corresponding kinetic energy operator, give the energy eigenvalues as close as possible to those presented by formulae (23). This problem was solved by using quantum-mechanical perturbative and variational approaches.

The vibrational Hamiltonian in the form:

$$H = H^0 + V' \tag{33}$$

was assumed where:

$$H^0 = -\frac{\hbar^2}{2\mu}\frac{\mathrm{d}^2}{\mathrm{d}x^2} + \frac{1}{2}k^x x^2 \equiv \frac{1}{2}\left(-\frac{d^2}{d\xi^2} + \frac{1}{2}\xi^2\right)\hbar\omega \tag{34}$$

and

$$V' = k_3^x x^3 + k_4^x x^4 \equiv \left(k_3 \xi^3 + k_4 \xi^4\right)\hbar\omega \tag{35}$$

where $x \equiv (r - r_e)$ is the difference between the instantaneous bond length, r, and its equilibrium value, r_e, and μ is the reduced mass. The dimensionless coordinate ξ, $\xi \equiv (\sqrt{\alpha})x$, where $\alpha \equiv (\mu\omega)/\hbar$, and $\omega = \sqrt{k/\mu}$ is the harmonic vibrational frequency (in s^{-1}), was introduced. k_3 and k_4 are the dimensionless cubic and quartic force constants, respectively, defined as:

$$k_3 \equiv \frac{1}{\alpha^{3/2}\hbar\omega} k_3^x \equiv \frac{\hbar^{1/2}}{\mu^{3/2}\omega^{5/2}} k_3^x, \quad k_4 \equiv \frac{1}{\alpha^2\hbar\omega} k_3^r \equiv \frac{\hbar}{\mu^2\omega^3} k_3^x \tag{36}$$

It is assumed that $|k_3| \gg |k_4|$, precisely that $|k_4|$ is at least by one order of magnitude smaller than $|k_3|$.

The eigenvalues of the zeroth-order, H^0, given by Eq. (34) are:

$$E_v^{(0)} = \left(v + \frac{1}{2}\right)\hbar\omega \tag{37}$$

and the corresponding wave functions are:

$$\psi_v^{(0)}(\xi) = N_v H_v(\xi) e^{-\frac{1}{2}\xi^2} \equiv |v\rangle \tag{38}$$

where N_v is the normalization factor and H_v is the Hermite polynomial. Applying the Rayleigh–Schrödinger perturbative approach (see, *e.g.*, ref. 79), the energy up to fourth order is obtained:

$$E_v = E_v^{(0)} + E_v^{(1)} + E_v^{(2)} + E_v^{(3)} + E_v^{(4)} \tag{39}$$

The corrections caused by the term $k_3^r r^3 \equiv k_3 \xi^3 \hbar\omega$ are (for details see Supplement C):

$$\begin{aligned} E_{v,3}^{(2)} &= -\frac{15}{4}\left(v + \frac{1}{2}\right)^2 k_3^2 \hbar\omega - \frac{7}{16} k_3^2 \hbar\omega \\ E_{v,3}^{(4)} &= -\frac{705}{16}\left(v + \frac{1}{2}\right)^3 k_3^4 \hbar\omega - \frac{1155}{64}\left(v + \frac{1}{2}\right) k_3^4 \hbar\omega \\ E_{v,3}^{(1)} &= E_{v,3}^{(3)} = 0 \end{aligned} \tag{40}$$

Since it is assumed that the energy contribution of the term $k_4^r r^4 \equiv k_4 \xi^4 \hbar\omega$ is much smaller than that of $k_3^r r^3 \equiv k_3 \xi^3 \hbar\omega$, it was found sensible to derive in this case only the results up to the second-order perturbation theory:

$$E_{\mathrm{v},4}^{(1)} = \frac{3}{2}\left(\mathrm{v}+\frac{1}{2}\right)^2 k_4\hbar\omega + \frac{3}{8}k_4\hbar\omega$$
$$E_{\mathrm{v},4}^{(2)} = -\frac{17}{4}\left(\mathrm{v}+\frac{1}{2}\right)^3 k_4^2\hbar\omega - \frac{67}{16}\left(\mathrm{v}+\frac{1}{2}\right)k_4^2\hbar\omega \quad (41)$$

The next terms, $E_{\mathrm{v},3}^{(6)}, E_{\mathrm{v},4}^{(3)}$ would introduce the expressions proportional to $(\mathrm{v} + 1/2)^4$ and small corrections of the terms $(\mathrm{v} + 1/2)^p$ with $p \leq 3$, *etc*. (Actually, the one-dimensional oscillator is such a classical test-system in quantum mechanics that it is very probable that the formulae (40) and (41) have been derived many times before. However, we found it easier to rederive them than to find a source where they are presented). Thus, in the present approximation:

$$\begin{aligned}\frac{E}{\hbar\omega} &= \left(-\frac{7}{16}k + \frac{3}{8}k\right) + \left(\mathrm{v}+\frac{1}{2}\right)\left(1 - \frac{1155}{64}k - \frac{67}{16}k\right) + \\ &+ \left(\mathrm{v}+\frac{1}{2}\right)\left(-\frac{15}{4}k + \frac{3}{2}k\right) + \left(\mathrm{v}+\frac{1}{2}\right)\left(-\frac{705}{16}k - \frac{17}{4}k\right) \cong \\ &\cong \left(\mathrm{v}+\frac{1}{2}\right) - \left(\mathrm{v}+\frac{1}{2}\right)\left(\frac{15}{4}k - \frac{3}{2}k\right) + \left(\mathrm{v}+\frac{1}{2}\right)\left(-\frac{705}{16}k - \frac{17}{4}k\right)\end{aligned} \quad (42)$$

We can now establish the relation between the parameters determining the form of our vibrational Hamiltonian and the experimentally derived parameters $\tilde{\nu}$ (= Herzberg's ω_e), $\omega_\mathrm{e}x_\mathrm{e}$, $\omega_\mathrm{e}y_\mathrm{e}$, *etc*. The quadratic force constant from Eq. (34) is determined as:

$$k^x = \mu\omega^2 = 4\mu\pi^2c^2\tilde{\nu}^2 \quad (43)$$

To simplify the discussion, it is assumed now that the perturbation only contains the cubic term, and the perturbative energy formula is considered up to the second-order. The cubic force constants, k_3^x and/or k_3, are found by comparing the second term on the right-hand side of Eq. (23) with the second term on the right-hand side of Eq. (42) when $k_4 = 0$. It follows that:

$$k_3^x = \frac{2}{\sqrt{15}}\frac{\mu^{3/2}\omega^2}{\hbar}\sqrt{(\omega_\mathrm{e}x_\mathrm{e})hc} \quad (44)$$

It is convenient to replace the expressions (43) and (44) by the more practical working formulae:

$$\left[k_2(\mathrm{au})\right] = 3.7833\times10^{-8}\mu_r\left[\tilde{\nu}(\mathrm{cm}^{-1})\right]^2 \quad (45)$$
$$\left[k_3(\mathrm{au})\right] = 1.7810\times10^{-9}\mu_r^{3/2}\left[\tilde{\nu}\left(\mathrm{cm}^{-1}\right)\right]^2\left[\omega_\mathrm{e}x_\mathrm{e}\left(\mathrm{cm}^{-1}\right)\right]$$

The force constants are now expressed in atomic units ($m_e \equiv 1$, $|e| \equiv 1$, $\hbar \equiv 1$), μ is assumed in relative atomic mass units ($\mu(^{12}C) \equiv 12$).

5.2. Variational approach

In variational calculations of eigenvalues and eigenfunctions of an anharmonic oscillator, as well as of the FCFs and TMs for particular combinations of vibrational levels of two electronic states, the following procedure is applied. One of the electronic states, *a* (typically the ground state), is chosen as the reference one and the basis functions (being the eigenfunctions of a suitably chosen harmonic oscillator) are centred with respect to its equilibrium bond length, r_e. If the potential energy curve is computed *ab initio*, it is fitted to the polynomial:

$$V_a = a_2 (r - r_e)^2 + a_3 (r - r_e)^3 + a_4 (r - r_e)^4 + \ldots \tag{47}$$

The Hamiltonian is then supposed in the form:

$$\begin{aligned} H_a = T + V_a = &-\frac{\hbar^2}{2\mu}\frac{d^2}{dr^2} + \frac{1}{2}k^r (r - r_e)^2 + \\ &+\left(a_2 - \frac{1}{2}k^r\right)(r - r_e)^2 + a_3 (r - r_e)^3 + a_4 (r - r_e)^4 + \ldots \end{aligned} \tag{48}$$

The eigenfunctions of the operator:

$$H^0 = -\frac{\hbar^2}{2\mu}\frac{d^2}{dr^2} + \frac{1}{2}k^r (r - r_e)^2 \tag{49}$$

are used as the basis.

Note that in Eq. (48), the quadratic part of the potential energy (47) is divided into two terms. The reason is that the eigenfunctions of a harmonic oscillator of the type (49) with a_2 instead of k^r could lead to a slower convergence of the results, particularly when the same basis functions for the description of other electronic states are employed (as will be done); if these states have equilibrium geometry significantly different from that of the reference state, it is to expect that more diffuse basis functions than the eigenfunctions of H^0 would be appropriate. Note also that the particular choice of k^r (except the mentioned one, namely, speed of convergence) has no other effect on the results of calculations. The potential energy curve of the other state, *b*, is fitted by polynomial series in the same variable as the reference state:

$$V_b = b_0 + b_1 (r - r_e) + b_2 (r - r_e)^2 + b_3 (r - r_e)^3 + b_4 (r - r_e)^4 + \ldots \tag{50}$$

where r_e is (as before) the equilibrium bond length in the ground electronic state. In this case, one also has a constant and a linear term in $(r - r_e)$, because the two states in question have different equilibrium bond lengths and their minima are separated in energy. The Hamiltonian for the *b* state is: $H_b = T + V_b$. Of course,

instead of *ab initio* computed potentials, their experimentally derived counterparts could be used. As already stated, the corresponding Schrödinger equation is solved variationally. The variable $(r - r_e) \equiv x$ is replaced by its dimensionless counterpart, ξ, and the matrix elements are derived with the help of the formulae (C1–C4) from Supplement C (note that the matrix elements of the operator H^0, Eq. (49), are simply $H_{ij}^0 = (v+1/2)\hbar\omega\delta_{ij}$). To ensure convergent results for say 20 energy levels, not more than 30–40 basis functions are required. The eigenfunctions for the v″-th level of the electronic state *a* and the v′-th level of the state b are obtained in the form:

$$\left|\psi_{v''}\right\rangle = \sum_i c_i^{v''} \left|\psi_i^{(0)}\right\rangle, \; \left|\psi_{v'}\right\rangle = \sum_j d_j^{v'} \left|\psi_j^{(0)}\right\rangle \tag{51}$$

where $\left|\psi_i^{(0)}\right\rangle$ and $\left|\psi_j^{(0)}\right\rangle$ are the eigenfunctions of the operator (49), and $c_i^{v''}$ and $d_j^{v'}$ are the respective expansion coefficients. The advantage of the choice of the same basis for both states now becomes clear. The FCF for the two vibrational states in question is simply:

$$\left(FCF\right)_{v'v''} = \left[\sum_j d_j^{v'} \left\langle \psi_j^{(0)} \middle| \sum_i c_i^{v''} \middle| \psi_i^{(0)} \right\rangle\right]^2 = \left[\sum_i d_i^{v'} c_i^{v''}\right]^2 \tag{52}$$

When the bond-length dependence of the electric TM is taken into account, it is fitted to the form:

$$R^{e',e''} = \sum_k R'_k \left(r - r_e\right)^k \equiv \sum_k R'_k \, x^k \equiv \sum_k R'_k \, \alpha^{-\frac{k}{2}} \xi^k \equiv \sum_k R_k \xi^k \tag{53}$$

($R_k \equiv \alpha^{-k/2} R'_k$) and the vibrational TM is computed as:

$$\begin{aligned} R^{e'v',e''v''} &= \sum_j d_j^{v'} \left\langle \psi_j^{(0)} \middle| \sum_k R_k \xi^k \sum_i c_i^{v''} \middle| \psi_i^{(0)} \right\rangle = \\ &= \sum_i \sum_j \sum_k d_j^{v'} R_k c_i^{v''} \left\langle \psi_j^{(0)} \middle| \xi^k \middle| \psi_i^{(0)} \right\rangle \end{aligned} \tag{54}$$

A general disadvantage of the presented variational approach is that it is not able to describe properly the vibrational states lying close to the dissociation limit; at $x \to \infty$, each polynomial tends to $+\infty$ or to $-\infty$, while the potential curve for a real bound state, asymptotically tends to a horizontal line. However, in the present study, only low-lying vibrational levels are considered and this drawback of the method does not play any role.

6. DETERMINATION OF PLASMA COMPOSITION

In one of the next sections, the results of the calculation of the equilibrium composition of plasmas containing Mg, O and H are presented. These calculations were performed by means of a self-written computer program following the approach developed by White *et. al.*[80] This method is described in Supplement D – in this section, only the key points are presented.

For the determination of the equilibrium composition of a gas mixture, the only quantity needed is the molal standard (Gibbs) free energy function G^0. The Gibbs energy of a mixture of n chemical species containing x_i moles of the i-th species can be expressed as:

$$G(X) = \sum_{i=1}^{n} x_i f_i \tag{55}$$

$X = \{x_1, x_2, ..., x_n\}$ $X = \{x_1, x_2, \ldots, x_n\}$ is a set of mol numbers, and f_i is the chemical potential of the i-th species, given by:

$$f_i = G_i^0 + RT \ln p_i = G_i^0 + RT \ln\left(\frac{x_i}{\bar{x}} P\right) \equiv \left(c_i + \ln \frac{x_i}{\bar{x}}\right) \tag{56}$$

In Eq. (56), the notation:

$$c_i = G_i^0 + RT \ln p \tag{57}$$

$$\bar{x} = \sum_{j=1}^{n} x_i \tag{58}$$

is introduced, where T is the temperature and p is the total pressure of the system. Thus, Eq. (55) can be rewritten in the form:

$$G(X) = \sum_{i=1}^{n} x_i \left(c_i + \ln \frac{x_i}{\bar{x}}\right) \tag{59}$$

Let it be supposed that one starts with a mixture of atoms of m elements and that the number of atoms of the element j is proportional to b_j. The determination of the equilibrium composition is equivalent to finding the set of non-negative values of x_i which minimize (59) and satisfy two conditions: *i*) the mass balance constraint:

$$\sum_{i=1}^{n} x_i a_{ij} = b_j, \quad (j = 1, 2, ..., m) \tag{60}$$

where a_{ij} is the number of atoms of element j in the chemical species (atom, molecule or ion) i and *ii*) the charge balance condition,[81]

$$\sum_{i=1}^{n} x_i a_i = 0 \tag{61}$$

where a_i is the charge number of species i. The summation in Eq. (61) formally runs over all chemical species, but this sum actually only involves the contributions from atomic and molecular ions and electrons. It is convenient to write Eqs. (60) and (61) as a single system:

$$\sum_{i=1}^{n} x_i a_{ij} = b_j, \quad (j = 1,\ 2,\ ...,\ m+1) \tag{62}$$

where $b_{m+1} = 0$ and $a_{i,m+1} = a_i$. Starting with any positive set of values $X^{(0)} = \{x_1^{(0)}, x_2^{(0)}, \ldots, x_n^{(0)}\}$ that satisfies the conditions (62), and form the expression analogous to (59), one obtains the optimal coefficients $X = \{x_1, x_2, \ldots, x_n\}$ that lead to the condition $\partial G(X) / \partial x_i = 0$ for all x_i, by applying the iterative approach described in Supplement D.

This algorithm has been used in numerous calculations of plasma composition.[81–96] The free energy data are taken from JANAF Thermochemical Tables,[97] or computed using derived partition functions based on previous quantum chemical calculations of molecular structure parameters.[6,7,98–100]

7. PLASMA ELECTROLYTIC OXIDATION

Plasma electrolytic oxidation (PEO) is high-voltage anodizing process employed to produce relatively thick oxide coatings on valve metals, such as magnesium, aluminium and titanium, with the incorporation of species originating both from the substrate and electrolyte. During anodization, two types of oxide films can grow, barrier and porous oxide ones.[101] The type of an oxide film is primarily determined by the type of electrolyte and by the anodizing conditions. The thickness of compact barrier oxide films is limited to several hundreds nm due to the dielectric breakdown initiated during film growth. Anodization of metals above the breakdown voltage is followed by an intense generation of sparks.[102] Thick and hard oxide coatings formed by the anodic-spark deposition method can range from tens to hundreds of microns. They consist of a thin barrier layer adjacent to the metal, followed by an intermediate layer with relatively low porosity, and an outer layer containing large pores, cracks and channels. Porous oxide films are formed in electrolytes that partially dissolve oxide films.[103] Such films consist of two regions: an outer one of thick porous-type oxide and a thin compact inner region lying adjacent to the metal. The thickness of the porous oxide films can grow to hundreds of microns.

Anodization of metals is accompanied by the emission of a weak electromagnetic radiation, mostly in the visible region of the spectrum.[104–109] This process is termed galvanoluminescence (GL) or electroluminescence.[110] GL has

been investigated by many authors but explanations of the nature and the mechanism of GL are still not completely resolved, because of the complex environment and the many experimental parameters that determine the intensity and spectral distribution of GL. During the past several years, a group from the Faculty of Physics of the University of Belgrade have conducted a number of investigations of the GL during the anodization of aluminium and showed that the nature and GL intensity depend on the type of the electrolyte (organic or inorganic), surface pre-treatment and anodizing conditions.[111–118]

There are two main reasons for investigating GL: The first one is that it (combined with other kinds of measurements) yields information about the system considered, particularly about the microstructure of the oxide films formed in the anodization process. The second reason is that the discharge built during this process is a convenient medium for the occurrence of a number of spectral lines and bands and thus, it can serve as a source of new spectroscopic information.

Surface pre-treatment of samples (surface preparation and annealing) has a significant influence on GL obtained in inorganic electrolytes. In fact, the pre-treatment of samples governs the concentration of "flaws" in oxide films, which are related to the GL mechanism.[111–113,116] "Flaws" is a general term for micro-fissures, cracks, local regions of different compositions and impurities, *etc*. The annealing temperature of the samples is another pre-treatment factor that affects the GL intensity. Higher annealing temperatures result in higher GL intensities. Annealing at different temperatures has various influences on the state of the surface of a sample, the number of defects, crystal grains and their orientation, in other words, on the concentration of "flaws". The GL of oxide films formed by anodization of aluminium samples annealed at temperatures above 500 °C showed that the sudden rise in the formation of gamma crystalline regions caused by aluminium annealing is strongly related to the appearance of GL and its intensity.[114,115,118] An analysis based on literature data on simple molecular species involving the Al atom, as well as those atoms whose presence was possible under given experimental conditions (hydrogen, oxygen, *etc*.), showed that the sources of GL are the molecules AlH, AlO, Al_2 and AlH_2, related to the formation of islands of gamma alumina crystals at annealing temperatures above 500 °C. In the case of organic electrolytes, GL is agitated by collision of electrons, injected into the oxide film at the electrolyte–oxide interface and accelerated by the high electric field (nearly 10^7 V cm^{-1}), with luminescence centres (carboxylate ions) inside the oxide film.[106,107]

Anodization of metals above the breakdown voltage leads to formation of a plasma, as indicated by the presence of microdischarges on the metal surface, accompanied by gas evolution.[109,110] Various processes, including chemical, electrochemical, thermodynamical and plasma-chemical reactions, occur at the discharge sites, due to the increased local temperature (10^3 to 10^4 K) and pres-

sure (up to ~10^2 MPa) that modify the structure, composition and morphology of oxide coatings.

Given the liquid environment, optical emission spectroscopy (OES) is the best available technique for PEO plasma characterization. The main difficulty in the application of OES for PEO characterization comes from space and time inhomogeneity of the microdischarges appearing randomly across the anode surface. The first step in the application of OES for PEO is the identification of the atomic and ionic lines in the visible and near UV spectral region.[120–130] Relative line intensity measurements of species originating in the substrate or in the electrolyte were used for the determination of the electron temperature.[121,123,124,126,128,132] The spectral line shape analysis of hydrogen Balmer lines were used for an estimation of the electron density.[122,123,126–128] The molecular vibrational temperature was determined from the luminescence of AlO[129] and MgO.[131]

8. EXPERIMENTAL

In the experiment to be described,[131] samples of a magnesium alloy (96 % Mg, 3 % Al, and 1% Zn (Goodfellow) with dimensions 25 mm×5 mm×0.25 mm were used as the working electrodes. They were sealed with insulation resin leaving only an active surface with an area of 1.5 cm^2. Before the anodization, the samples were degreased in acetone, ethanol and distilled water, using an ultrasonic cleaner, and dried in a warm-air stream. The magnesium alloy was anodized in an aqueous solution containing 4 g L^{-1} $Na_2SiO_3 \cdot 5H_2O$ and 4 g L^{-1} KOH. The electrolyte was prepared using double distilled and deionised water and *p.a.* grade chemical compounds. During anodization, the current density was set to 150 mA cm^{-2}.

A schematic diagram of the experimental setup used for the luminescence measurements is shown in Fig. 1. The anodization occurred in an electrolytic cell with flat glass windows.[107] Two platinum wires (5 cm long, 1 mm in diameter) were used as cathodes. The power supply was a self-made DC power unit providing voltages of 0–600 V and a current of 0–500 mA. During the anodization, the electrolyte was circulated through the chamber-reservoir system, and a control temperature sensor was situated immediately by the sample. The temperature of the electrolyte was kept fixed at 20±1 °C.

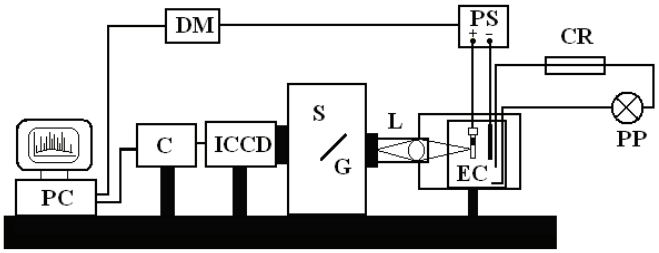

Fig. 1. Schematic diagram of the experimental setup used for the luminescence measurements: EC – electrolytic cell; PS – power supply; PP – peristatical pump; CR – chamber-reservoir system; L – achromatic lens; S – spectrograph Hilger; G – diffraction grating (1200 grooves mm^{-1}); ICCD – intensified charge coupled device; C – controller ST-133; DM – digital multimeter HP 34970A; PC – personal computer.

The spectral luminescence was taken on a spectrometer system based on an intensified charge coupled device (ICCD). The optical detection system consisted of a large-aperture achromatic lens, a Hilger spectrometer with diffraction grating of 1200 grooves mm^{-1} (wavelength range of 43 nm), and a very sensitive PI–MAX ICCD thermoelectrically cooled camera (–40 °C) with a high quantum efficiency (Princeton Instruments). The system was used with several grating positions with an overlapping wavelength range of 5 nm. The image of anode surface was projected with unity magnification to the entrance slit of the spectrometer. The optical detection system was calibrated using a light emitting diodes based light source.[133] The spectra were adjusted to the spectral response of the measuring system. The anodization voltage and the electrolyte temperature were recorded by a 20-channel digital PC-controlled multimeter HP 34970A (DM).

9. RESULTS AND DISCUSSION

9.1. Luminescence of the $B^1\Sigma^+$–$X^1\Sigma^+$ system of MgO during PEO of Mg

In recent years, several research groups were focused on the investigation of PEO as a surface-protective treatment for magnesium and its alloys.[134–138] Despite numerous studies on metals, primarily on Al, in which OES was used for the characterization of PEO, there are only few such papers on Mg.[128,130,131,139,140] Herein, the results of our recent study on this species are presented.[131]

In the initial phase of anodization of the magnesium alloy, the voltage increased linearly with time to about 220 V, resulting in a constant rate of increase of the oxide film thickness. Simultaneously, a weak anodic luminescence was observed. This stage of anodization was followed by a deflection from linearity in the voltage curve, starting from the so-called breakdown voltage. During this phase of the process, a large number of sparks appeared, randomly distributed over the surface. Sparking luminescence combined with the anodic one and the total luminescence intensity increased. After the breakdown, the oxide surface became laced with a number of cracks, pores and channels (Fig. 2).

A number of emission spectral atomic and ionic lines were recorded in the wavelength range from 370 to 850 nm (*i.e.*, from 11800 to 27000 cm^{-1}). The species that were identified[141] (K, Na, Mg, H_α and O) originated from both the magnesium electrode and the electrolyte. We refrained from using these lines for the determination of plasma parameters, such as temperature and electron density: The spectral resolution was relatively low, so that some of the lines were overlapped, the strong alkali metal lines were at least partly self-absorbed and finally, the sensitivity of the measurements depended on the wavelength, making comparison of lines appearing in different spectral regions difficult.

9.2. $B^1\Sigma^+$–$X^1\Sigma^+$ *Spectrum of MgO*

Now, focus was directed on the wave number range between 19950 and 20400 cm^{-1}. A number of spectra at different time delays with respect to the beginning of the PEO process were recorded. A typical spectrum is presented in

Fig. 3. It appears as a broad peak with clearly pronounced structure. The most intense sub-peak is at 19976 cm^{-1}, and the other sub-peaks are blue-shifted with respect to it. While the overall intensity of the broad peak presented in Fig. 3 significantly varied with time, the relative intensities of the sub-peaks within it showed quite small variations. The below used results for relative intensity of the local peaks were obtained by averaging over about 30 recorded spectra. The positions of the sub-peaks are presented in column Exp. 5 of Table III. They were assigned, as will be shown below, to the $v' - v'' = 0$ band sequence of the $B^1\Sigma^+ - X^1\Sigma^+$ emission transition of MgO.

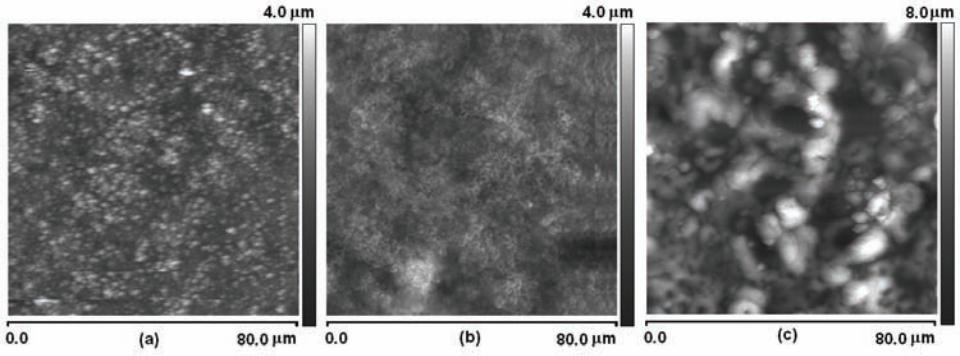

Fig. 2. Atomic force microscopy image of the oxide coating on the magnesium alloy formed after breakdown (anodization time 5 min).[131]

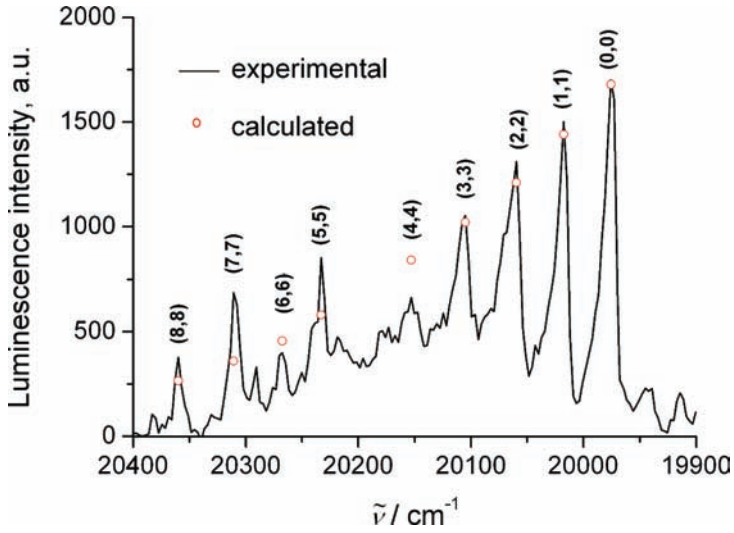

Fig. 3. Luminescence spectrum between 19950 and 20400 cm^{-1} obtained after subtracting the anodic luminescence contribution.[131] The peaks are assigned to (v', v'') bands of the $B^1\Sigma^+ - X^1\Sigma^+$ system of MgO. The circles denote the intensities of the peaks as obtained in the simulation procedure described in the text.

TABLE III. Positions (in cm^{-1}) of the v′ – v″ = 0 band heads ($\tilde{\nu}_h$) and origins ($\tilde{\nu}_0$) of the $B^1\Sigma^+$–$X^1\Sigma^+$ spectral system of MgO. In parentheses are given the term values relative to the position of the 0–0 band[131]

Para-meter	Exp. 1[41] $\tilde{\nu}_h$	Exp. 2[16] $\tilde{\nu}_h$	Exp. 3[43] $\tilde{\nu}_h$	Exp. 4[12] $\tilde{\nu}_h$	Exp. 5[131] $\tilde{\nu}_h$	Fit 1[41] $\tilde{\nu}_h$	Fit 2[43] $\tilde{\nu}_h$	Fit 3[43] $\tilde{\nu}_0$	Fit 4[10] $\tilde{\nu}_0$	Fit 5[131] $\tilde{\nu}_0$
T_e						19950		19983.97	19984.0	
$\tilde{\nu}'$						754		796.08	824.08	
$(\omega_e,x_e)'$						3.06		4.44	4.76	
$\tilde{\nu}''$						722		758.38	785.06	
$(\omega_e,x_e)''$						5.96		4.84	5.18	
0–0	19966 (0)	19965 (0)	19967 (0)	19971 (0)	19976 (0)	19967 (0)	19966 (0)	20003 (0)	20004 (0)	20004 (0)
1–1	20007 (41)	20007 (42)	20008 (41)	20013 (42)	20018 (42)	20005 (38)	20008 (41)	20041 (38)	20044 (40)	20044 (40)
2–2	20049 (83)	20051 (86)	20049 (82)	20057 (86)	20060 (84)	20049 (82)	20049 (83)	20081 (78)	20084 (81)	20084 (81)
3–3	20093 (127)	20097 (132)	20092 (125)	20103 (132)	20106 (130)	20098 (131)	20092 (125)	20121 (118)	20126 (122)	20127 (123)
4–4	20146 (180)		20137 (170)	20153 (182)	20153 (177)	20153 (186)	20134 (168)	20162 (159)	20168 (164)	20171 (167)
5–5	20200 (234)			20204 (233)	20231 (255)	20215 (248)		20203 (200)	20211 (208)	20216 (213)
6–6	20257 (291)			20262 (291)	20268 (292)	20281 (314)		20245 (243)	20255 (252)	20265 (261)
7–7	20304 (338)			20309 (338)	20310 (334)	20354 (387)		20289 (286)	20300 (297)	20316 (312)
8–8	20347 (381)				20360 (384)	20433 (466)		20333 (330)	20346 (342)	20372 (368)
9–9	20388 (422)					20517 (550)		20377 (374)	20393 (389)	20434 (430)

A brief analysis of previous experimental studies on the *B*–*X* spectral system of MgO is here presented. In several studies, the rotational constants for the $X^1\Sigma^+$ and $B^1\Sigma^+$ states were precisely determined (Table II). It was found that they are very similar in both electronic states, with that for the upper state being slightly larger. The similarity of the equilibrium bond lengths and vibrational frequencies, as well as the fact that the *B*–*X* system involves the $^1\Sigma$ species, determines the general structure of the spectrum. It is dominated by the v′ – v″ = 0 band sequence and the bands have *P* and *R* branches. The position of the P band heads ($\tilde{\nu}_h$) with respect to the band origins ($\tilde{\nu}_0$) can be estimated by means of the Formula (31) with B'' = 0.5743 cm^{-1} and B' = 0.5822 cm^{-1};[10] one obtains $\tilde{\nu}_h - \tilde{\nu}_0 \cong 40\ cm^{-1}$. This large difference reflects the similarity of the rotational constants for the $X^1\Sigma^+$ and $B^1\Sigma^+$ states. The positions of the band heads and band origins for the v′ – v″ = 0 sequence, as measured or fitted by various authors, are given in Table III.

The vibrational structure of the blue–green band system was investigated by Ghosh *et al*.[41] The authors recorded about thirty violet-degraded emission bands in the wave number region between 19000 and 21000 cm^{-1} and assigned them to the sequences $v' - v'' = 0, \pm 1$, with the vibrational quantum number *v* up to ten. In the second column of Table III (Exp. 1), the experimental results for the heads of the $v' - v'' = 0$ bands are presented. In all previous studies, the positions of the $B^1\Sigma^+$–$X^1\Sigma^+$ bands were fitted by various formulas of the type Eq. (23), quadratic in the vibrational quantum numbers. The parameters $T_e, \tilde{\nu}$ and $\omega_e x_e$ given by Ghosh *et al*. as well as the term values computed using them are presented in the seventh column of Table III (Fit 1). Comparison of the numbers in columns Exp. 1 and Fit 1 shows that only the position of the bands up to 4–4 are reliably reproduced by Formula (23).

The same band system was later investigated by Mahanti,[13] Lagerqvist and Uhler[16,42] and Pešić.[19,43] The experimental results of Lagerqvist[16] and Pešić [43] are shown in columns Exp. 2 and Exp. 3, respectively. The band positions adopted by PG,[12] taken from the studies of Mahanti[13] and Lagerqvist,[16] are presented in column Exp. 4. Pešić[43] adopted from Lagerquist and Uhler[42] the parameters $T_e, \tilde{\nu}$, and $\omega_e x_e$ for the positions of the band origins, corrected them to take into account the difference between the positions of the band origins and band heads and obtained by means of Formula (3) the term values collected in column Fit 2. They agreed well with his own experimental results from column Exp. 3. However, when the original parameters by Lagerquist and Uhler (given at the top of column Fit 3) were used to calculate the origins of the bands with $v' = v'' \geq 5$, as shown in column Fit 3, the agreement with the corresponding experimental data from columns Exp. 1 and Exp. 4 (the numbers in parentheses) becomes poor.

The most reliable parameters for the values of the vibrational term are those presented in the HH book,[10] column Fit 4, because they (in contrast to those used by Ghosh *et al*. and Pešić) involved the correct vibrational frequencies. However, even they do not describe accurately the positions of $v' = v'' \geq 4$ bands. Thus, no hitherto applied formula quadratic in the vibrational quantum number v has given good reproduction of the measured band positions for higher v values. This is easy to explain: The differences in the wave numbers of the successive bands observed (column Exp. 4) are 42, 44, 46, 50, 51, 58 and 47 cm^{-1}, and they nearly follow quadratic dependence only for first few terms. This will be born in mind in the following discussion.

Bearing in mind the restrictions caused by specific features of our experiment, the results of the study,[131] column Exp. 5 of Table IV, were found to agree reasonably with previous more precise gas-phase spectral measurements. Namely, the accuracy of the measured band heads was estimated to be roughly ±5 cm^{-1}. Furthermore, the position of the bands depended to a certain extent on the matrix conditions, and it was not possible to resolve the features corresponding to

isotopic species ^{24}MgO, ^{25}MgO, and ^{26}MgO, the last two each present in relative fractions of about 0.10.

TABLE IV. Franck–Condon factors (first row for each quantum number v″), and squared vibrational moments (third row) for transitions between vibrational levels of the $X^2\Sigma^+$ and $B^2\Sigma^+$ electronic states of MgO (our study[131]). Second row: results of previous studies

v″	v′						
	0	1	2	3	4	5	6
0	.9826	.0170	.0004				
	.983[a]	.017[a]	.000[a]				
	1.421	.0089	.0003[b]				
			.0002				
1	.0173	.9464	.0351	.0011			
	.017[a]	.948[a]	.033[a]	.001[a]			
	.0480	1.344	.0375[b]	.0001			
			.0180				
2		.0364	.9067	.0544	.0024		
		.035[a]	.911 [a] .901 [b]	.053 [a] .0576 [b]	.0018 [b]		
		.0969			.0011		
			1.263	.0274			
3		.0002	.0573	.8632	.0751	.0042	
		.000[a]	.053[a]	.881[a]	.0804[b]	.0033[b]	
		.0017	.0606[b]	.857[b]	.0371	.0019	
			.1471	1.179			
4			.0005	.0801	.8154	.0972	.0067
			.0010[b]	.061[a]	.806[b]	.105[b]	.0029
			.0039	.0827[b]	1.090	.0472	
				.1981			
5				.0011	.1049	.7626	.1212
				.0075	.108[b]	.752[b]	.0577
					.2494	.9963	
6					.0022	.1317	.7041
					.0035[b]	.135[b]	.8974
					.0130	.3005	

[a]Ref. 46; [b]ref. 25

9.3. Computation of F–C factors and vibrational transition moments

FCFs and vibrational TMs for the $B^1\Sigma^+$–$X^1\Sigma^+$ system of MgO were calculated by means of the approaches described in Section 5, "Quantum mechanics". The potential energy part of the Hamiltonian was assumed in the form of polynomials of the third order in the coordinate $x \equiv (r - r_e)$. In this paragraph, the potential energy and the bond length are expressed in atomic units; thus the energy is given in hartree (1 hartree = 27.211 eV) and the bond length in bohr (1 bohr = 0.529177 Å). The force constants k_2 and k_3 were determined by means of

Formulae (45) and (46), employing the molecular parameters from Ref. 10 (*i.e.*, those appearing in the table presented in Supplement B), giving:

$$V\left(X\ ^1\Sigma^+\right) = 0.111991x^2 - 0.07426x^3,$$
$$V\left(B\ ^1\Sigma^+\right) = 0.0910532 + 0.12331\left(x + 0.0225\right)^2 - 0.07844\left(x + 0.0225\right)^3 \quad (63)$$

where $\Delta r_e = -0.0225$ bohr is the difference between the equilibrium bond lengths in the excited and ground electronic state. Thus, both potentials in Eq. (63) are given with respect to the equilibrium bond lengths in the ground state. The form of the electric moment for the transition between the $B^1\Sigma^+$ and $X^1\Sigma^+$ states was estimated based on Fig. 4 of the *ab initio* study:[38]

$$R_{e',e''}\left(\text{au}\right) = -1.2 + 0.7x \quad (64)$$

The Schrödinger equation (63) with the potentials was solved variationally, as described above.

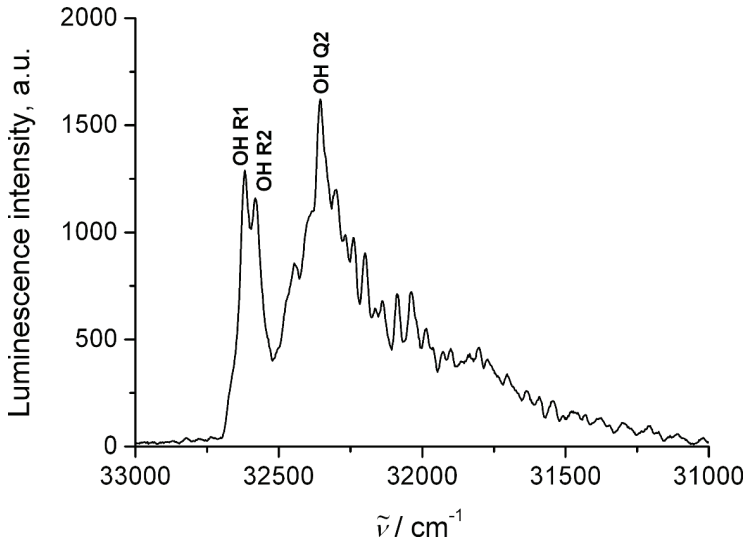

Fig. 4. $A^2\Sigma^+$ (v′ = 0)–$X^2\Pi$ (v″ = 0) luminescence spectrum of OH between 31000 and 33000 cm^{-1}.[131]

The results for the band origins are presented in the last column of Table IV (Fit 5). For low vibrational quantum numbers (up to v′ = v″ = 3), they coincide with the numbers in the column Fit. 4, generated by employing Formulae (23) with the same set of molecular parameters. The agreement becomes continuously poorer with increasing v′ = v″ ≥ 4, reflecting the restricted reliability of the second-order perturbative approach used to determine the force constants which appear in the Formulae (63). The computed FCFs and squared vibrational TMs for

levels up to v = 6 are given in Table IV. The FCFs computed by Prasad and Prasad[46] and those quoted by Ikeda *et al.*[25] are given in column F–C_{exp}. The agreement between these three sets of results, particularly for larger FCFs, is very good. This indirectly indicates that also the computed vibrational TMs are reliable. The ratio (TM^2/FCF) decreases uniformly with increasing vibrational quantum number within the v′ – v″ = 0 sequence, reflecting the decrease of the absolute value of the electric TM with increasing bond length (see Fig. 5a).

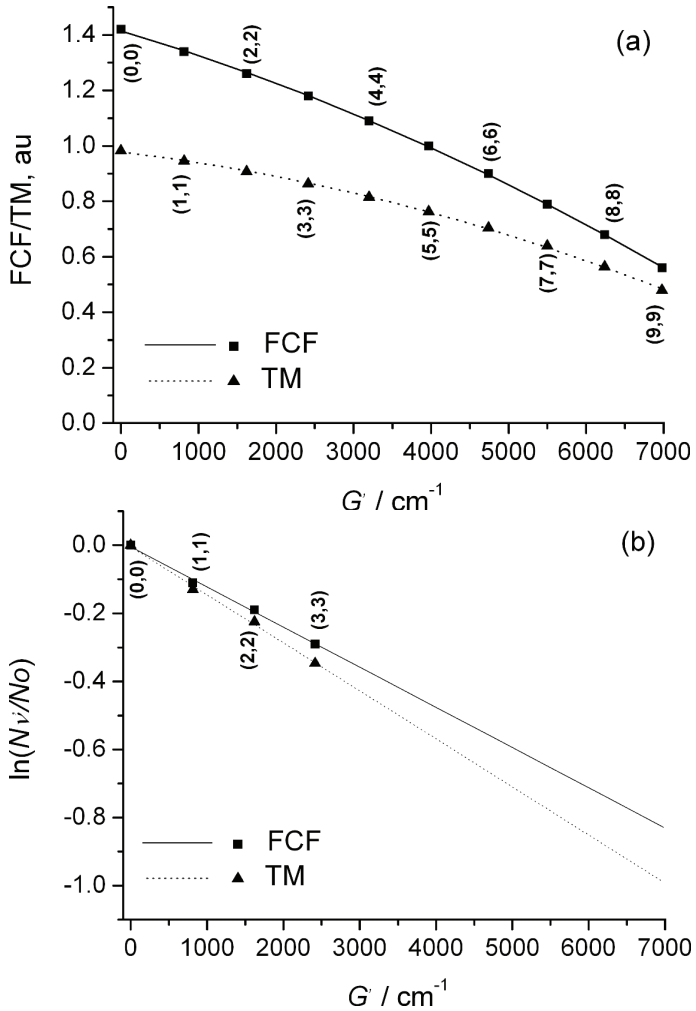

Fig. 5. a) Calculated Franck–Condon factors (*FCF*) and squared vibrational transition moments (TM) for the v′ = v″ band sequence of the $B^1\Sigma^+$–$X^1\Sigma^+$ system of MgO, as functions of vibrational quantum number, *i.e.*, of the vibrational term values of the $B^1\Sigma^+$ electronic state; b) logarithm of the relative population of the v′ = 0, 1, 2, and 3 vibrational levels as function of the corresponding term values.[131]

9.4. Estimation of the population of vibrational levels and determination of plasma temperature

The relative population, $N_{v'}$, of the vibrational levels in the $B^1\Sigma^+$ electronic state was estimated by means of the procedure described in Section 3, "Spectroscopy". It was obtained for the levels v′ from 0 to 3 as the ratio of the measured intensity of the peaks corresponding to the (0–0), (1–1), (2–2), and (3–3) transitions and the corresponding (squared) vibrational TMs. The values for ln ($N_{v'}/N_{v'=0}$) as function of the vibrational term values (G')/quantum numbers of the $B^1\Sigma^+$ electronic state are displayed in Fig. 4b. The nearly linear dependence of ln ($N_{v'}/N_{v'=0}$) on the G' leads to the conclusion quasi-equilibrium conditions existed, at least for vibrational motions. The slope of the straight line, $-1/kT$, determines the plasma temperature of $T \approx 11500$ K. When the TMs are replaced by the corresponding FCFs, $T \approx 9800$ K is obtained. The difference between these two temperature values shows that it is important to account for the variation of the electronic transition moment with the bond length. Taking into account the limited accuracy of the present experimental results (the accuracy of measured intensities was roughly estimated to be 10 %), as well as of the *ab initio* computed electric transition-moment function, it was considered justified to conclude that the temperature of the plasma was $T = 11000\pm2000$ K. This value is not very different from that obtained in a study on AlO ($T = 8000\pm2000$ K).[129] Assuming $T = 11000$ K and using the vibrational TMs for v′ = v″ = 0–8, the complete v′ – – v″ = 0 band sequence of the $B^1\Sigma^+$–$X^1\Sigma^+$ system of MgO is simulated in Fig. 3. In spite of some discrepancies between the experimental and simulated results, the general agreement could be considered satisfactory.

9.5. Estimation of the plasma temperature based on the use of OH bands

We additionally determined the plasma temperature by means of the $A^2\Sigma^+$–$X^2\Pi$ (v′ = v″ = 0) emission spectrum of OH, employing the approach of de Izarra.[142] Four groups of unresolved rotational lines were recorded with the maxima at 32364, 32484, 32597 and 32622 cm^{-1}, corresponding to the Q_2, Q_1, R_2, and R_1 band heads, respectively (Fig. 5). Using Tables 2–5 from Ref. 142, the temperature was estimated to be 3500±500 K.

9.6. Calculation of the plasma composition

At first sight the difference between the temperature estimated by means of the intensity distribution within the MgO band system and that derived from the unresolved rotational spectrum of OH should be a clear indication for the absence of a local thermal equilibrium (LTE) in the plasma. In the first case, one is namely dealing with the vibrational and in the second case, with the rotational temperature, and the possibility that these two motion modes are not in equilibrium with each other must be taken into account. However, there are also other pos-

sible explanations. Let it be noted that temperatures similar to those of the present study were reported by several authors.[121,122,143,144] Based on experimental results, Klapkiv[143,144] proposed a model of the discharge plasma consisting of a central core (containing electrons, ionic and atomic species) with the temperature at roughly 7000 K, surrounded by lower-temperature regions involving various compounds formed in chemical reactions between the species originating both in the substrate and the electrolyte. Arrabal *et al.*[139] and Hussein *at al.*[128,140] estimated a plasma temperature of 7000 K. Dunleavy *et al.*[122] determined the temperature of the peripheral zone to be about 3500 K by comparing the intensities of the H_α and H_β Balmer lines, while the use of Mg^+ and Si^+ lines yielded T = 16000±3500 K for the plasma core temperature. Employing these data, as well as those for the electron density, they concluded that the LTE conditions were fulfilled in the plasma core, while the colder peripheral region was found to be in partial LTE.

Now, the consequences of the assumption of the LTE for all degrees of freedom under the present experimental conditions will be investigated. Employing the method described in Section 6, the composition of a plasma containing Mg, O and H, at temperatures up to T = 12000 K and for pressures of 10^5, 10^6, 10^7 and 10^8 Pa, was calculated. Pressures in such a wide region were considered because it was argued that in systems similar to the present one they might be up to ≈10^2 MPa.[145] Since the amounts of Mg, O and H in the investigated plasma were unknown, the computations were performed at Mg:O:H ratios of 1:1:1, 1:1:0, 0:1:1, and 0:1:2 in order to estimate the influence of a particular choice on the conclusions which could be reached on the basis of the results. The free energy data for 26 atomic/ionic/molecular species involving Mg, O and H (plus electrons) collected in JANAF tables[97] were extended by an extrapolation procedure from 6000 to 12000 K. Some of the results are presented in Figs. 6 and 7.

The results for a pressure of 10^5 Pa (*i.e.*, nearly 1 atm) and at Mg:O:H = = 1:1:1 are presented in Fig. 6. At T = 11000 K, 90 % of magnesium is in form of Mg^+ and 10 % appears as Mg, while the partial pressure of MgO is about $1/10^5$ of the total pressure. Slightly below T = 9000 K, the partial pressures of Mg and Mg^+ become equal, and at lower temperatures atomic Mg is the dominating form of magnesium. The most abundant form of magnesium in the temperature region below T = 3000 K is MgOH. The concentration of OH reaches a maximum in the temperature region between 3000 and 4000 K. Increasing the total pressure favours the building (*i.e.*, suppresses dissociation) of MgO, and suppresses the ionization process $Mg \rightarrow Mg^+ + e^-$. Consequently, at a total pressure of 10^6 Pa (Fig. 6b of ref. 131), the partial pressures of Mg and Mg^+ are nearly equal at 11000 K, and roughly 0.1 % of the magnesium is in form of MgO. At $p = 10^7$ Pa (Fig 6c in ref. 131) and T = 11000 K, about 2 % of the magnesium is in form of MgO. Finally, at $p = 10^8$ Pa (Fig. 7) and T = 11000 K, the partial pressure of MgO ex-

ceeds that of Mg^+, becoming only four times lower than that of the most abundant magnesium species, atomic Mg.

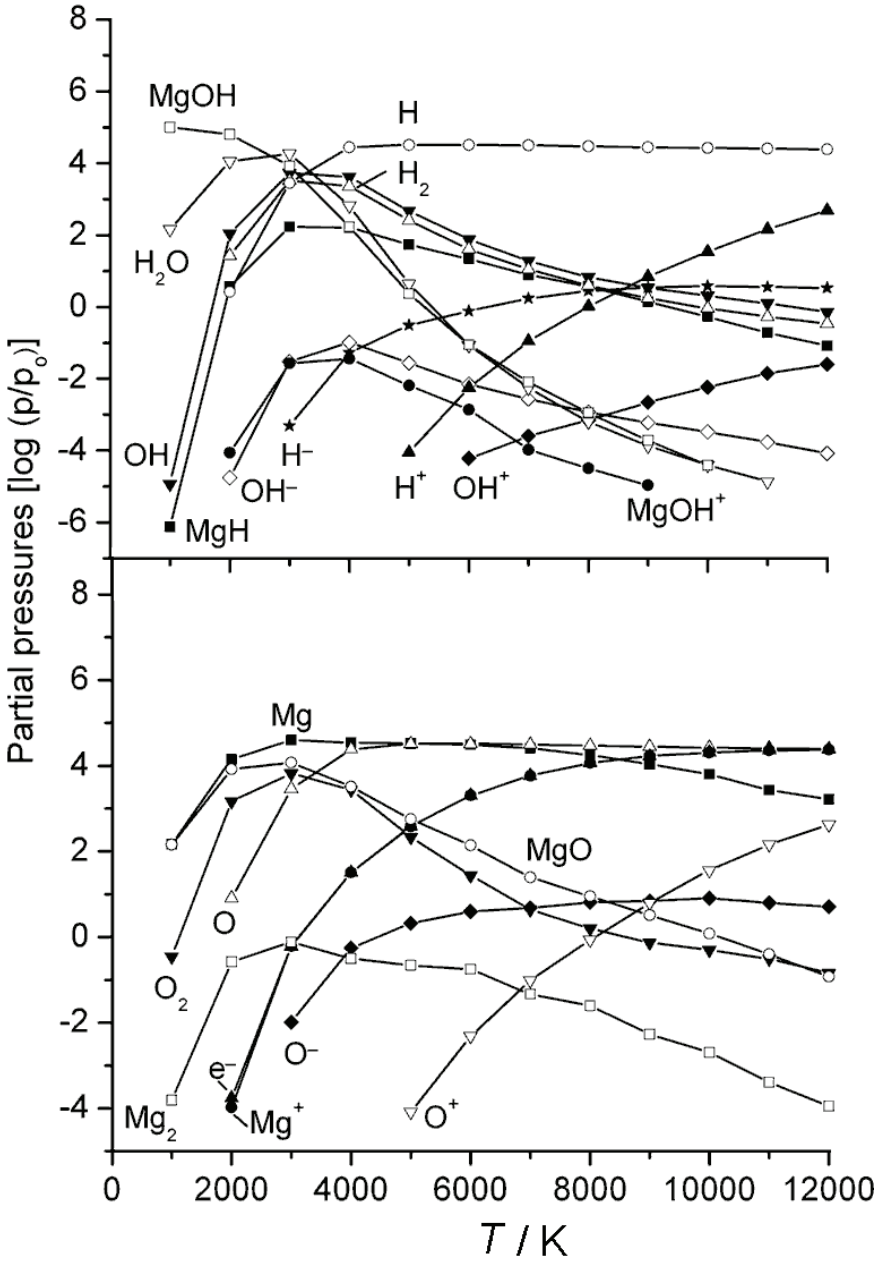

Fig. 6. Equilibrium composition of the plasma containing a mixture of magnesium, oxygen, and hydrogen in the mole ratio 1:1:1 at $p = 10^5$ Pa.[131]

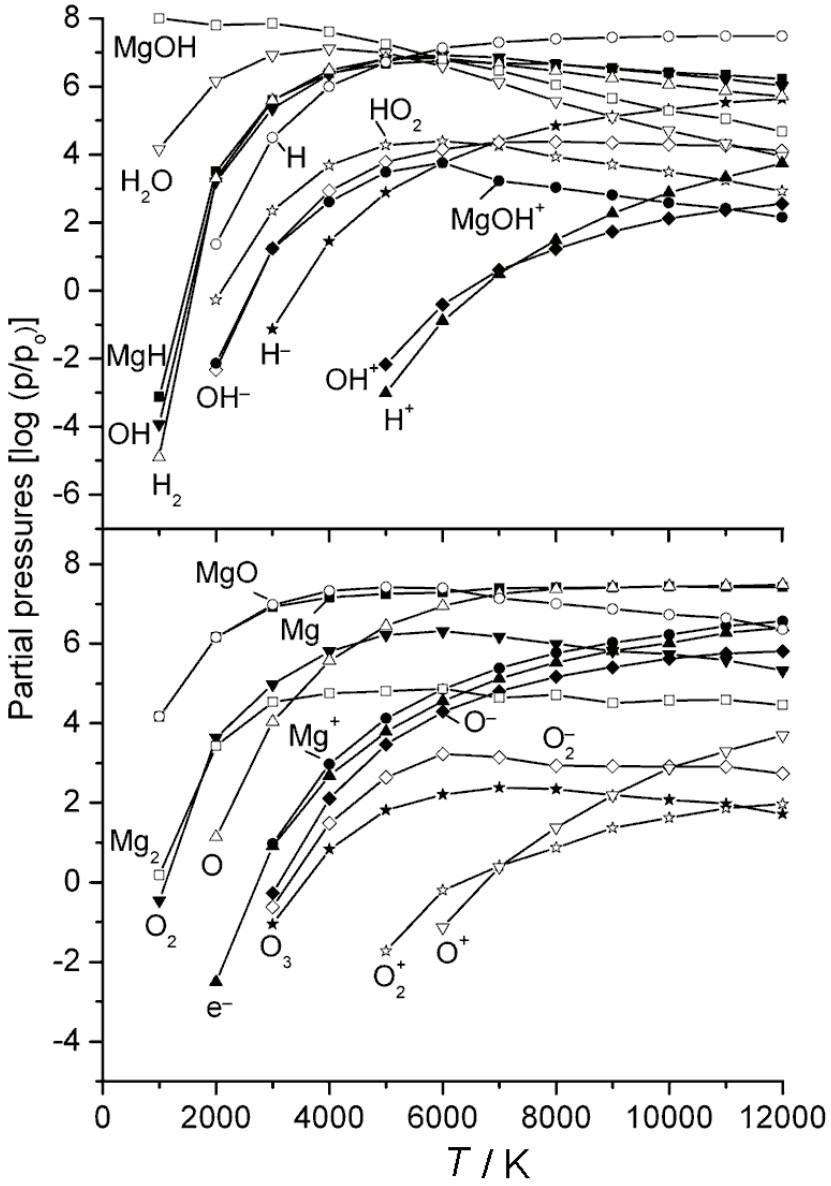

Fig. 7. Equilibrium composition of plasma containing a mixture of magnesium, oxygen, and hydrogen in the mole ratio 1:1:1 at $p = 10^8$ Pa.[131]

Now an attempt will be made to interpret our experimental results in the light of the calculated plasma compositions.[131] The first question concerns the reliability of the value of T = 11000 K, based on the intensity distribution within the $B^1\Sigma^+$–$X^1\Sigma^+$ band system of MgO. Is it possible to obtain this molecular spec-

trum at such a high temperature? First, it should be noted that in LTE, the population of the $B^1\Sigma^+$ electronic state of MgO would be about 7 % with respect to that of the ground state at T = 11000 K. Thus, it would be large enough to cause the appearance of an emission spectrum if the MgO molecules were present in a sufficient concentration at this temperature. The results of the above calculations of the plasma composition show that this is the case when the pressure in the plasma core is higher than the normal one. This is illustrated in Fig. 8, in which the temperature dependence of the function $p_{MgO}\times\exp(-E/kT)$ is shown, where $E \approx 20000\ \mathrm{cm}^{-1}\times hc$, being the excitation energy for the $B^1\Sigma^+$ electronic state, and p_{MgO} is the partial pressure of MgO at different pressures. Two sets of results are presented; the first (full lines) correspond to a plasma with the global composition Mg:O:H = 1:1:1, and the second one (dotted lines) to a plasma without hydrogen, *i.e.*, with the global composition Mg:O:H = 1:1:0. Note that the distributions $p_{MgO}\times\exp(-E/kT) = f(T)$ are practically same in both cases (except for a systematic shift of the dotted lines towards larger values) at each particular pressure. This shows that the relative amounts of Mg, O and H, assumed in calculations do not critically influence the general conclusions that could be drawn.

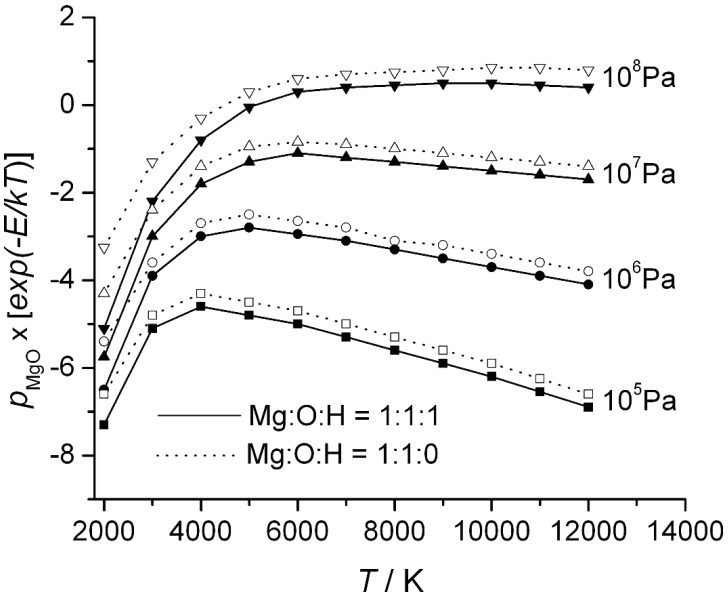

Fig. 8. Temperature dependence of $p_{MgO}\times\exp(-E/kT)$, where E is the excitation energy for the $B^1\Sigma^+$ electronic state, at various pressures for the global plasma composition Mg:O:H = 1:1:1 (full lines) and Mg:O:H = 1:1:0 (dotted lines).[131]

How reliable is the lower temperature value ($T \approx 3500$ K), based on the measured OH spectrum? Let the problem be sharpened: suppose that it is certain that an LTE exists and that the approaches for estimating the temperature T = 3500 K

from the OH band and T = 11000 K from the MgO bands are completely exact. Does this necessarily mean that there are only these two temperatures characterizing the plasma? Is it not possible that there is a relatively large region of the plasma where the temperature is, say, 5000 K, but the OH and MgO spectra are not obtained from this region because the temperature is too high for existence of OH molecules and too low for excitation of the MgO molecules? In order to answer this question, the function $p_{OH}\times\exp(-E/kT) = f(T)$ is shown in Fig. 9 (at the moment, we concentrate solely on OH; an analogous analysis could be applied to MgO), where $E \approx 32600$ cm$^{-1}\times hc$ is the excitation energy for the $A^2\Sigma^+$ electronic state and p_{OH} is the partial pressure of OH. Due to near cancellation of the effect of decrease in p_{OH} and increase in $\exp(-E/kT)$ with increasing T, there is almost no dependence of $p_{OH}\times\exp(-E/kT)$ on T in the temperature region between 4000 and 12000 K, independently of the pressure and global plasma compositions considered. The intensity of the OH bands should be even higher if the temperature in the region where the OH molecules exist were higher than the estimated T = 3500 K. Two conclusions can be drawn: the OH molecules are formed and exist only in the peripheral, colder plasma region; the temperature gradient between the peripheral region and the plasma core is very high, having as a consequence a very narrow plasma region with intermediate temperatures. The second conclusion supports the Klapkiv model,[143,144] and is in accordance with the results by

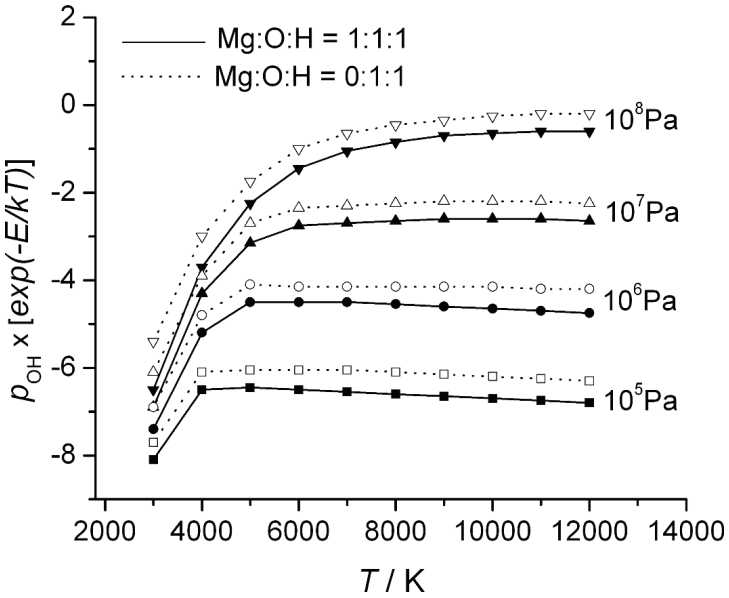

Fig. 9. Temperature dependence of $p_{OH}\times\exp(-E/kT)$, where E is the excitation energy for the $A^2\Sigma^+$ electronic state of OH, at various pressures for the global plasma composition Mg:O:H = 1:1:1 (full lines) and Mg:O:H = 0:1:1 (dotted lines).[131]

Dunleavy *et al.*[122] who obtained, using a completely different method, a low-region temperature identical to that of the present study.

10. CONCLUSIONS

The research described in the present review began in the field of material science. The starting goal was to investigate the behaviour of metal alloys in the process of plasma electrolytic oxidation. Special electronics, optics, microscopy and crystallography were needed to enquire the morphology of the material, particularly of the thin oxide films produced. In order to obtain information about the processes which occurred, with the aim to become able to monitor them, luminescence spectra were recorded. Their identification led into the field of atomic and molecular spectroscopy. The understanding, and in certain cases even assignment of molecular features recorded, would not have been possible without the use of results of quantum-chemical calculations. On the other hand, it turned out that the systems in question could serve as a source of new spectroscopic information. For an estimation of important parameters, such as temperature and electron number density, various plasma diagnostics methods had to be applied. The results of measurements of molecular spectra were combined with quantum-mechanical calculations for an estimation of the plasma parameters when the standard approaches failed. In order to understand the appearance of the spectra, and the features of the system they originate from, the compositions of the plasmas in question were calculated. This required the use of methods of classical and statistical thermodynamics. The message of the present review is just to show how many different scientific fields encompass an, at first glance, simple research problem.

SUPPLEMENTARY MATERIAL

Supplements A–D are available electronically from http://www.shd.org.rs/JSCS/, or from the corresponding author on request.

Acknowledgements. We thank the Ministry of Education, Science and Technological Development of the Republic of Serbia for financial support (Contract No. 172040).

И З В О Д

ЈЕДНА МУЛТИДИСЦИПЛИНАРНА СТУДИЈА НА МАГНЕЗИЈУМУ

РАДОМИР РАНКОВИЋ[1], СТЕВАН СТОЈАДИНОВИЋ[2], МИРЈАНА САРВАН[2], БЕЋКО КАСАЛИЦА[2], МАРИЈА КРМАР[1], ЈЕЛЕНА РАДИЋ-ПЕРИЋ[1] и МИЉЕНКО ПЕРИЋ[1]

[1]Факултет за физичку хемију Универзитета у Београду и [2]Физички факултет Универзитета у Београду

У току плазмене електролитичке оксидације једне легуре магнезијума (96% Mg, 3% Al и 1% Zn) добили смо галванолуминисцентни спектар у области таласних бројева између 19950 и 20400 cm^{-1}. Широки пик са јасно израженом структуром приписан је v − v = 0 секвенцији електронског прелаза $B^1\Sigma^+ \rightarrow X^1\Sigma^+$ молекула MgO. Применом квантномеханичке теорије пертурбације, из положаја спектралних трака изведена је

форма кривих потенцијане енергије за оба електронска стања. Ове потенцијалске криве, комбиноване са квантнохемијски израчунатим електричним моментом прелаза, коришћене су у варијационом рачунању Франк–Кондонових фактора и момената прелаза за опажене вибрационе прелазе. Поређењем резултата ових рачуна са измереном расподелом интензитета у спектру извели смо релативну запоседнутост вибрационих нивоа горњег електронског стања. То је омогућило процену температуре плазме. Температура је додатно одређена на основу снимљеног емисионог спектра $A^2\Sigma^+$ (v = 0)–$X^2\Pi$ (v = 0) радикала OH. Под претпоставком постојања локалне термодинамичке равнотеже израчунат је састав плазме која садржи магнезијум, кисеоник и водоник, у области темепратуре до 12000 K за притиске од 10^5, 10^6, 10^7, and 10^8 Pa, да би се објаснила појава регистрованог спектра и допринело расветљавању процеса који се догађају за време електролитичке оксидације Mg.

(Примљено 12. септембра, ревидирано 10. октобра 2012)

REFERENCES

1. W. F. McDonough, *The Composition of the Earth*, in *Earthquake Thermodynamics and Phase Transformations in the Earth's Interior*, R. Teisseyre, E. Majewski, Eds., Academic Press, San Diego, CA, 2001
2. J. W. Morgan, E. Anders, *Proc. Nat. Acad. Sci. U.S.A.* **77** (1980) 6973
3. A. P. Dickin, *In situ Cosmogenic Isotopes, Radiogenic Isotope Geology*, Cambridge University Press, Cambridge, UK, 2005
4. G. Herzberg, *Molecular Spectra and Molecular Structure I. Spectra of Diatomic Molecules*, Van Nostrand, New York, 1955
5. M. Perić, in *Electron – A Hundred Years from Discovery*, Sveska prva, Milan Kurepa, Ed., Zavod za udžbenike i nastavna sredstva, Belgrade, 1997, p. 311 (in Serbian)
6. M. Senćanski, J. Radić-Perić, M. Perić, *J. Serb. Chem. Soc.* **76** (2011) 539
7. M. Senćanski, Lj. Stojanović, S. Jerosimić, J. Radić-Perić, M. Perić, *J. Serb. Chem. Soc.* **76** (2011) 557
8. G. Herzberg, *Molecular Spectra and Molecular Structure II. Infrared and Raman Spectra of Polyatomic Molecules*, Van Nostrand, New York, 1945
9. G. Herzberg, *Molecular Spectra and Molecular Structure III. Electronic Spectra of Polyatomic Molecules*, Van Nostrand, New York, 1967
10. K. P. Huber, G. Herzberg, *Molecular Spectra and Molecular Structure IV. Constants of Diatomic Molecules*, Van Nostrand, New York, 1979
11. G. Herzberg, *The Spectra and Structure of Simple Free Radicals*, Cornel University Press, Ithaca and London, 1971
12. R. W. B. Pearse, A. G. Gaydon, *The Identification of Molecular Spectra*, Chapman and Hall, London, 1976
13. P. C. Mahanty, *Phys. Rev.* **42** (1932) 609
14. P. C. Mahanty, *Indian J. Phys.* **9** (1935) 455
15. A. Lagerqvist, U. Uhler, *Nature* **164** (1949) 665
16. A. Lagerqvist, *Ark. Mat. Astron. Fys.* **A29**, No. 25 (1943) 1
17. L. Brewer, R. F. Porter, *J. Chem. Phys.* **22** (1954) 1867
18. D. Pešić, A. G. Gaydon, *Proc. Phys. Soc.* **73** (1959) 244
19. D. Pešić, *Proc. Phys. Soc.* **76** (1960) 844
20. L. Brewer, S. Trajmar , R. A. Berg, *Astrophys. J.* **135** (1962) 955
21. S. Trajmar, G. E. Ewing, *Astrophys. J.* **142** (1965) 77

22. M. Singh, *J. Phys., B* **4** (1971) 565
23. M. Singh, *J. Phys., B* **6** (1973) 1339
24. M. Singh, *J. Phys., B* **6** (1973) 1917
25. T. Ikeda, N. B. Wong, D. O. Harris, R. W. Field, *J. Mol. Spectrosc*. **68** (1977) 452
26. B. Bourguignon, J.C. McCombie, J. Rostas, *Chem. Phys. Lett*. **113** (1985) 323
27. B. Bourguignon, J. Rostas, *J. Mol. Spectrosc*. **146** (1991) 437
28. P. C. F. Ip, K. J. Cross, R. W. Field, J. Rostas, B. Bourguignon, J. McCombie, *J. Mol. Spectrosc*. **146** (1991) 409
29. E. Kagi, T. Hirano, S. Takano, K. Kawaguchi, *J. Mol. Spectrosc*. **168** (1994) 109
30. P. Mürtz, H. Thümmel, C. Pfelzer, W. Urban, *Mol. Phys*. **86** (1995) 513
31. J. H. Kim, X. Li, L. S. Wang, H. L. de Clercq, C. A. Fancher, O. C. Thomas, K. H. Bowen, *J. Phys. Chem., A* **105** (2001) 5709
32. J. W. Daily, C. Dreyer, A. Abbud-Madrid, M. C. Branch, *J. Mol. Spectrosc*. **214** (2002) 111
33. D. Bellert, K. L. Burns, N.-T. Van-Oanh, J. Wang, W. H. Breckenridge, *Chem. Phys. Lett*. **381** (2003) 381
34. D. Bellert, K. L. Burns, N.-T. Van-Oanh, J. Wang, W. H. Breckenridge, *Chem. Phys. Lett*. **381** (2003) 725
35. J. Wang, N.-T. Van-Oanh, D. Bellert, W. H. Breckenridge, M.-A. Gaveau, E. Gloaguen, B. Soep, J.-M. Mestdagh, *Chem. Phys. Lett*. **392** (2004) 62
36. E. Kagi, K. Kawaguchi, *J. Mol. Struct*. **795** (2006) 179
37. J. Wang, W. H. Breckenridge, *J. Chem. Phys*. **124** (2006) 124308
38. A. Maatouk, A. Ben Houria, O. Yazidi, N. Jaidane, M. Hochlaf, *J. Chem. Phys*. **133** (2010) 144302
39. L.-B. Knight, Jr., W. Weltner, Jr., *J. Chem. Phys*. **55** (1971) 5066
40. S. Rosenwaks, R. E. Steele, H. P. Broida, *J. Chem. Phys*. **63** (1975) 1963
41. P. N. Ghosh, P. C. Mahanty, B. C. Mukkerjee, *Phys. Rev*. **35** (1930) 1491
42. A. Lagerqvist, U. Uhler, *Ark. Fys*. **1** (1949) 459
43. D. S. Pešić, *Proc. Phys. Soc*. **83** (1964) 885
44. A. Antić-Jovanović, D. S. Pešić, V. Bojović, *J. Mol. Spectrosc*. **60** (1976) 416
45. A. Antić-Jovanović, V. Bojović, D. S. Pešić, *J. Phys., B* **9** (1976) L575
46. S. S. Prasad, K. Prasad, *Proc. Phys. Soc*. **80** (1962) 311
47. M. Perić, S. D. Peyerimhoff, R. J. Buenker, *Can. J. Chem*. **20** (1077) 3664
48. M. Perić, H. Dohmann, S. D. Peyerimhoff, R. J. Buenker, *Z. Phys. D* **5** (1987) 65
49. M. Perić, *Bull. Soc. Chim. Beograd* **44** (1979) 465
50. S. Radenković, I. Gutman, *J. Serb. Chem. Soc.* **74** (2009) 155
51. J. Đurđević, I. Gutman, R. Ponec, *J. Serb. Chem. Soc.* **74** (2009) 549
52. I. Gutman, J. Đurđević, *J. Serb. Chem. Soc.* **74** (2009) 765
53. B. Furtula, I. Gutman, S. Jeremić, S. Radenković, *J. Serb. Chem. Soc.* **75** (2010) 83
54. S. Jeremić, S. Radenković, I. Gutman, *J. Serb. Chem. Soc.* **75** (2010) 943
55. D. Vukičević, J. Đurđević, I. Gutman, *J. Serb. Chem. Soc.* **75** (2010) 1093
56. S. Marković, J. Đurđević, S. Jeremić, I. Gutman, *J. Serb. Chem. Soc.* **75** (2010) 1241
57. I. Gutman, B. Furtula, A. T. Balaban, *J. Serb. Chem.* **76** (2011) 733
58. I. Gutman, A. T. Balaban, *J. Serb. Chem. Soc.* **76** (2011) 1505
59. M. Marković, J. Đurđević, I. Gutman, *J. Serb. Chem. Soc.* **77** (2012) 751
60. J. Schamps, H. Lefebvre-Brion, *J. Chem. Phys*. **56** (1972) 573
61. S. R. Langhoff, C. W. Bauschlicher, Jr., H. Partridge, *J. Chem. Phys*. **84** (1986) 4474

62. H. Thümmel, R. Klotz, S. D. Peyerimhoff, *Chem. Phys*. **129** (1989) 417
63. A. F. Jalbout, *J. Mol. Struct*. **618** (2002) 85
64. C. W. Bauschlicher, Jr., D. M. Silver, D. R. Yarkony, *J. Chem. Phys*. **73** (1980) 2867
65. C. W. Bauschlicher, Jr., B. H. Lengsfield III, M. Silver, D. R. Yarkony, *J. Chem. Phys*. **74** (1981) 2379
66. C. W. Bauschlicher, Jr., S. R. Langhoff, H. Partridge, *J. Chem. Phys*. **101** (1994) 2644
67. C. W. Bauschlicher, H. Partridge, *Chem. Phys. Lett*. **342** (2001) 441
68. D. R. Yarkony, *J. Chem. Phys*. **89** (1988) 7324
69. R. N. Diffenderfer, D. R. Yarkony, *J. Phys. Chem*. **86** (1982) 5098
70. R. N. Diffenderfer, D. R. Yarkony, P. J. Dagdigian, *J. Quant. Spectrosc. Radiat. Transf*. **29** (1983) 329
71. B. Huron, J. P. Malrieu, P. Rancurel, *Chem. Phys*. **3** (1974) 277
72. H. Thümmel, R. Klotz, S. D. Peyerimhoff, *Chem. Phys*. **135** (1989) 229
73. *MOLPRO, version 2008.1, a package of* ab initio *programs*, http://www.molpro.net
74. P. J. Knowles, H.-J. Werner, *Chem. Phys. Lett*. **115** (1985) 259
75. H. J. Werner, P. J. Knowles, *J. Chem. Phys*. **89** (1988) 5803
76. J. Knowles, H.-J. Werner, *Chem. Phys. Lett*. **145** (1988) 514
77. T. H. Dunning, Jr., *J. Chem. Phys*. **90** (1989) 1007
78. D. Feller, *J. Comp. Chem*. **17** (1996) 1571
79. M. Perić, in *Structure and Spectra of Molecules*, M. Gašić, Ed., SASA, Belgrade. 2009 (in Serbian)
80. W. B. White, S. M. Johnson, G. B. Dantzig, *J. Chem. Phys*. **28** (1958) 751
81. J. Radić-Perić, M. Perić, *Spectrochim. Acta, B* **35** (1980) 297
82. J. Radić-Perić, *Spectrochim. Acta, B* **38** (1980) 1021
83. J. Radić-Perić, *Bull. Soc. Chim. Beograd* **49** (1984) 185
84. J. Radić-Perić, *Bull. Soc. Chim. Beograd* **49** (1984) 429
85. J. Radić-Perić, M. Perić, *J. Serb. Chem. Soc*. **50** (1985) 535
86. J. Radić-Perić, *Computers Chem*. **14** (1990) 343
87. J. Radić-Perić, *J. Anal. At. Spectrom*. **7** (1992) 235
88. J. Radić-Perić, J. High Temp. Chem. Processes **2** (1993)115
89. J. Radić-Perić, A. Lađević, *J. Serb. Chem. Soc*. **59** (1993) 491
90. J. Radić-Perić, A. Lađević, *VDI Berichte* **1166** (1995) 487.
91. J. Radić-Perić, M. Markićević, *J. Serb. Chem. Soc*. **65** (2000) 181
92. J. Radić-Perić, N. Pekas, *J. Serb. Chem. Soc*. **66** (2001) 181.
93. J. Radić-Perić, N. Pantelić, *J. Therm. Anal. Cal*. **72** (2003) 35
94. J. Radić-Perić, A. Dašić, *J. Therm. Anal. Cal*. **79** (2005) 59
95. J. Radić-Perić, *Mat. Sci. Forum* **494** (2005) 303
96. J. Radić-Perić, *Mat. Sci. Forum* **518** (2006) 349
97. *JANAF Thermochemical Tables*, Nat. Stand. Ref. Data Ser., US Nat. Bur. Stand. Vol. 27 (1971); *NIST–JANAF Thermochemical Tables, J. Phys. Chem. Ref. Data*, 4th ed., M. W. Chase Jr., Ed., 1999
98. J. Radić-Perić, M. Perić, *Z. Naturforsch.* **42a** (1987) 103
99. J. Radić-Perić, *J. Math. Chem*. **8** (1991) 269
100. M. Perić, J. Radić-Perić, *J. Serb. Chem. Soc*. **60** (1995) 987
101. J. W. Diglee, T. C. Downie, C. W. Goulding, *Chem. Rev*. **69** (1969) 365
102. M. Petković, S. Stojadinović, R. Vasilić, I. Belča, Z. Nedić, B. Kasalica, U. B. Mioč, *Appl. Surf. Sci*. **257** (2011) 9555

103. A. Despic, V. Parkhutik, *Mod. Aspect Electroc*. **20** (1989) 401
104. S. Stojadinovic, Lj. Zekovic, I. Belca, B. Kasalica, D. Nikolic, *Electrochem. Commun*. **6** (2004) 708
105. S. Stojadinovic, I. Belca, B. Kasalica, Lj. Zekovic, M. Tadic, *Electrochem. Commun*. **8** (2006) 1621
106. S. Stojadinovic, M. Tadic, I. Belca, B. Kasalica, Lj. Zekovic, *Electrochim. Acta* **52** (2007) 7166
107. S. Stojadinovic, I. Belca, M. Tadic, B. Kasalica, Z. Nedic, Lj. Zekovic, *J. Electroanal. Chem*. **619–620** (2008) 125
108. S. Stojadinović, R. Vasilić, M. Petković, I. Belča, B. Kasalica, M. Perić, Lj. Zeković, *Electrochim. Acta* **59** (2012) 354
109. S. Stojadinović, R. Vasilić, M. Petković, I. Belča, B. Kasalica, M. Perić, Lj. Zeković, *Electrochim. Acta* **79** (2012) 133
110. S. Ikonopisov, *Electrochim. Acta* **20** (1975) 783
111. S. Stojadinovic, Lj. Zekovic, I. Belca, B. Kasalica, *Electrochem. Commun*. **6** (2004) 427
112. S. Stojadinovic, I. Belca, Lj. Zekovic, B. Kasalica, D. Nikolic, *Electrochem. Commun*. **6** (2004) 1016
113. B. Kasalica, S. Stojadinovic, Lj. Zekovic, I. Belca, D. Nikolic, *Electrochem. Commun*. **6** (2005) 735
114. B. Kasalica, I. Belca, S. Stojadinovic, M. Sarvan, M. Peric, Lj. Zekovic, *J. Phys. Chem., C* **111** (2007) 12315
115. M. Sarvan**,** S. Stojadinovic, B. Kasalica, I. Belca, Lj. Zekovic, *Electrochim. Acta* **53** (2008) 2183
116. S. Stojadinovic, R. Vasilic, I. Belca, M. Tadic, B. Kasalica, Lj. Zekovic, *Appl. Surf. Sci*. **255** (2008) 2845
117. S. Stojadinovic, R. Vasilic, M. Petkovic, Z. Nedic, B. Kasalica, I. Belca, Lj. Zekovic, *Electrochim. Acta* **55** (2010) 3857
118. M. Sarvan, M. Perić, Lj. Zeković, S. Stojadinović, I. Belča, M. Petković, B. Kasalica, *Spectrochim. Acta A* **81** (2011) 672
119. S. Stojadinovic, R. Vasilic, I. Belca, M. Petkovic, B. Kasalica, Z. Nedic, Lj. Zekovic, *Corros. Sci*. **52** (2010) 3258
120. M. Petković, S. Stojadinović, R. Vasilić, Lj. Zeković, *Appl. Surf. Sci*. 257 (2011) 10590
121. M. D. Klapkiv, H. M. Nykyforchyn, V. M. Posuvailo, *Mater. Sci*. **30** (1994) 333
122. C. S. Dunleavy, I. O. Golosnoy, J. A. Curran, T. W. Clyne, *Surf. Coat. Technol*. **203** (2009) 3410
123. J. Jovović, S. Stojadinović, N. M. Šišović, N. Konjević, *J. Quant. Spectrosc. Radiat. Transfer* **113** (2012) 1928
124. R. O. Hussein, X. Nie, D. O. Northwood, A. Yerokhin, A. Matthews, *J. Phys., D* **43** (2010) 105203
125. S. Stojadinović, J. Jovović, M. Petković, R. Vasilić, N. Konjević, *Surf. Coat. Technol*. **205** (2011) 5406
126. J. Jovović, S. Stojadinović, N. M. Šišović, N. Konjević, *Surf. Coat. Technol*. **206** (2011) 24
127. S. Stojadinović, R. Vasilić, M. Petković, Lj. Zeković, *Surf. Coat. Technol*. **206** (2011) 575
128. R. O. Hussein, P. Zhang, X. Nie, Y. Xia, D. O. Northwood, *Surf. Coat. Technol*. **206** (2011) 1990

129. S. Stojadinović. M. Perić, M. Petković, R. Vasilić, B. Kasalica, I. Belča, J. Radić-Perić, *Electrochim. Acta* **56** (2011) 10122
130. S. Stojadinović, R. Vasilić, M. Petković, I. Belča, B. Kasalica, M. Perić, Lj. Zeković, *Electrochim. Acta* **59** (2012) 354
131. S. Stojadinović, M. Perić, J. Radić-Perić, R. Vasilić, M. Petković, Lj. Zeković, *Surf. Coat. Technol*. **206** (2012) 2905
132. R. O. Hussein, X. Nie, D. O. Northwood, *Mater. Phys. Chem.* **134** (2012) 484
133. B. V. Kasalica, I. D. Belca, S. Đ. Stojadinovic, Lj. D. Zekovic, D. Nikolic, *Appl. Spectrosc*. **60** (2006) 1090
134. H. Chen, G. H. Lv, G. L. Zhang, H. Pang, X. Q. Wang, H. J. Lee, S. Z. Yang, *Surf. Coat. Technol*. **205** (2010) S32
135. J. Cai, F. Caoa, L. Chang, J. Zheng, J. Zhang, C. Cao, *Appl. Surf. Sci*. **257** (2011) 3804
136. L. Zhao, C. Cui, Q. Wang, S. Bu, *Corr. Sci*. **52** (2010) 2228
137. A. Bai, *Surf. Coat. Technol*. **204** (2010)1856
138. J. Liang, P. Bala Srinivasan, C. Blawert, W. Dietzel, *Electrochim. Acta* **55** (2010) 6802
139. R. Arrabal, E, Matykina, T. Hashimoto, P. Skeldon, G. E. Thompson, *Surf. Coat. Technol*. **203** (2009) 2207
140. R. O. Hussein, P. Zhang, D. O. Northwood, X. Nie, *Corros. Mater*. **36** (2011) 38
141. Yu. Ralchenko, A.E. Kramida, J. Reader and NIST ASD Team (2011), NIST Atomic Spectra Database (ver. 4.l.0) [Online], National Institute of Standards and Technology, Gaithersburg, MD
142. C. de Izarra C, *J. Phys. D*: *Appl. Phys*. **33** (2000) 1697
143. M. Klapkiv, *Mater. Sci*. **31** (1995) 394
144. M. Klapkiv, *Mater. Sci*. **35** (1999) 279
145. A. L. Yerokhin, X. Nie, A. Leyland, A. Matthews, S. J. Dowey, *Surf. Coat. Technol.* **122** (1999) 73.

Journal of the Serbian Chemical Society
JSCS@tmf.bg.ac.rs • www.shd.org.rs/JSCS
J. Serb. Chem. Soc. 77 (11) S202–S208 (2012) *Supplementary material*

SUPPLEMENTARY MATERIAL TO

A multidisciplinary study on magnesium

RADOMIR RANKOVIĆ[1], STEVAN STOJADINOVIĆ[2], MIRJANA SARVAN[2], BEĆKO KASALICA[2], MARIJA KRMAR[1], JELENA RADIĆ-PERIĆ[1] and MILJENKO PERIĆ[1]*

[1]*Faculty of Physical Chemistry, University of Belgrade, Studentski trg 12–16, P.O. Box 47, 11158 Belgrade Serbia and* [2]*Faculty of Physics, University of Belgrade, Studentski trg 12–16, 11158 Belgrade Serbia*

J. Serb. Chem. Soc. 77 (11) (2012) 1483–1528

SUPPLEMENT A

Astrophysics, geophysics, geochemistry

The Earth is built by three major and distinctly different units: the core, the mantle-crust system (silicate Earth) and the atmosphere–hydrosphere system, being the products of planetary differentiation and having very different composition.[1,2] While the composition of the crust and the atmosphere–hydrosphere system can be determined by usual experimental methods, information about the Earth's mantel and, particularly, core has been gathered more or less indirectly. One of the key tools thereby is the (logical) assumption, partly verified by measurements, that the global composition of the Earth cannot be much different from that of the other objects with the common origin, *i.e.*, of those belonging to the Solar system. The most easily accessible objects of such an art are meteorids, because around 15,000 tonnes of them enter the Earth's atmosphere each year. (One should make distinction between "meteorid", "meteor", and "meteorite". Meteoroids are sand- to boulder-sized particles of debris in the Solar system. The visible path of a meteoroid (when it begins to heat up and break apart) that enters the Earth's atmosphere is called a meteor. If a meteoroid reaches the ground and survives impact, then it is called a meteorite). There are several types of meteorids/meteorites, including stony, carbonaceous chondrites and iron–nickel ones. Magnesium is an important constituent of a number of meteorid types.

The investigations on the Earth's composition have lead to the following conclusions. The radius of the core is about 1/2 that of the Earth's, and thus its volume is about 1/8 of the Earth's. However, the mass of the core is roughly 1/3 of the Earth's mass, because the core is about 90 % of an Fe–Ni (heavy-metal)

* Corresponding author. E-mail: peric@ffh.bg.ac.rs

alloy (with a dominating contribution of iron, 85 % against 5 % Ni). The main constituents of the mantle and crust are silicates containing primarily magnesium, iron, aluminium and calcium. The most abundant element in this part of the Earth is O (44 %), followed by Mg (22.8 %), Si (21 %), Fe (6.3 %), and Al (2.35 %).[1]

Beside being an important constituent of the Earth, Mg has been used for dating of different astrophysical and geological events and processes. It has three stable isotopes: ^{24}Mg, ^{25}Mg and ^{26}Mg. All are present in significant amounts. About 79 % of Mg is ^{24}Mg. ^{24}Mg is produced in stars larger than 3 solar masses by fusing helium and neon in the alpha process at temperatures above 600 mega-kelvins. Its large abundance in the universe (it is believed to be the ninth most frequent element) is connected with the fact that its nucleus is a multiple of an α particle. ^{26}Mg has found application in isotopic geology as a radiogenic daughter product of ^{26}Al, which has a half-life of 717,000 years.[3]

SUPPLEMENT B

TABLE S-I. A part of the table with molecular constants for $^{24}Mg^{16}O$ given by HH[4]

State	T_e / cm^{-1}	ω_e / cm^{-1}	$\omega_e x_e$ / cm^{-1}	r_e / Å	Observed transitions	ν_{00} / cm^{-1}
$G\,^1\Pi$	[40259.8]	–	–	[1.834]	$G\rightarrow A$	$36365._4$
					$G\rightarrow X$	$39868._6$
$F\,^1\Pi$	(37922)	[696]	–	$[1.772_8]$	$F\rightarrow X$	37879.1
$E\,^1\Sigma^+$	(37722)	[705]	–	[1.829]	$E\rightarrow A$	34180
					$E\rightarrow X$	$37683._5$
$C\,^1\Sigma^-$	30080.6	632.4	5.2	$[1.872_9]$	$C\rightarrow A$	26500.94
$e\,^3\Sigma^-$	–	–	–	–	$(e\leftarrow a)$	–
$D\,^1\Delta$	29851.6	632.5	5.3	1.871_8	$D\rightarrow A$	26272.04
$d\,^3\Delta_i$	(29300)	(650)		(1.8_7)	$(d\leftrightarrow a)$	26867
$c\,^3\Sigma^+$	(28300)				$(c\leftarrow a)$	25900
$B\,^1\Sigma^+$	19984.0	824.0_8	4.7_6	1.737_1	$B\rightarrow A$	16500.2_9
					$B\rightarrow X$	20003.5_7
$A\,^1\Pi$	3563.3	664.4_4	3.91	1.864_0	–	–
$a\,^3\Pi_i$	(2400)	(650)		(1.8_7)	–	–
$X\,^1\Sigma^+$	0	785.0_6	5.1_8	1.749_0	–	–

SUPPLEMENT C

Perturbative treatment of a one-dimensional anharmonic oscillator

In the perturbative and variation approaches to the Schrödinger equation of an one-dimensional anharmonic oscillator, used in the present study, the matrix elements ξ, ξ^2, ξ^3 and ξ^4 in the basis consisting of eigenfunctions, Eq. (12) in the parent paper. The only non-vanishing matrix elements are:

$$\langle \mathrm{v}+1|\xi|\mathrm{v}\rangle = \sqrt{\frac{\mathrm{v}+1}{2}} \qquad \text{(C.1)}$$

$$\langle \mathrm{v}|\xi^2|\mathrm{v}\rangle = \left(\mathrm{v}+\frac{1}{2}\right), \quad \langle \mathrm{v}+2|\xi^2|\mathrm{v}\rangle = \frac{\sqrt{(\mathrm{v}+1)(\mathrm{v}+2)}}{2} \tag{C.2}$$

$$\langle \mathrm{v}+1|\xi^3|\mathrm{v}\rangle = \frac{3\sqrt{(\mathrm{v}+1)^3}}{\sqrt{8}}, \quad \langle \mathrm{v}+3|\xi^3|\mathrm{v}\rangle = \frac{\sqrt{(\mathrm{v}+1)(\mathrm{v}+2)(\mathrm{v}+3)}}{\sqrt{8}} \tag{C.3}$$

and

$$\langle \mathrm{v}|\xi^4|\mathrm{v}\rangle = \frac{3}{4}\left(2\mathrm{v}^2+2\mathrm{v}+1\right), \quad \langle \mathrm{v}+2|\xi^4|\mathrm{v}\rangle = \left(\mathrm{v}+\frac{3}{2}\right)\sqrt{(\mathrm{v}+2)(\mathrm{v}+1)}, \quad \langle \mathrm{v}+4|\xi^4|\mathrm{v}\rangle = \frac{\sqrt{(\mathrm{v}+4)(\mathrm{v}+3)(\mathrm{v}+2)(\mathrm{v}+1)}}{4} \tag{C.4}$$

Applying the Rayleigh–Schrödinger perturbative approach, one obtains for the energy up to fourth order the formulae:

$$E_{\mathrm{v}}^{(1)} = \left\langle \psi_{\mathrm{v}}^{(0)} \middle| V' \middle| \psi_{\mathrm{v}}^{(0)} \right\rangle \equiv V'_{\mathrm{vv}},$$

$$E_{\mathrm{v}}^{(2)} = \sum_{i\neq \mathrm{v}} \frac{|V'_{i\mathrm{v}}|^2}{E_{\mathrm{v}}^{(0)} - E_i^{(0)}}, \tag{C.5}$$

$$E_{\mathrm{v}}^{(3)} = \sum_{i\neq \mathrm{v}}\sum_{k\neq \mathrm{v}} \frac{V'_{\mathrm{v}i}V'_{ik}V'_{k\mathrm{v}}}{\left(E_{\mathrm{v}}^{(0)} - E_i^{(0)}\right)\left(E_{\mathrm{v}}^{(0)} - E_k^{(0)}\right)} - V'_{\mathrm{vv}} \sum_{i\neq \mathrm{v}} \frac{|V'_{i\mathrm{v}}|^2}{\left(E_{\mathrm{v}}^{(0)} - E_i^{(0)}\right)},$$

and

$$E_{\mathrm{v}}^{(4)} = \sum_{i\neq \mathrm{v}}\sum_{j\neq \mathrm{v}}\sum_{k\neq \mathrm{v}} \frac{V_{\mathrm{v}i}^{(1)}V_{ij}^{(1)}V_{jk}^{(1)}V_{k\mathrm{v}}^{(1)}}{\left[E_{\mathrm{v}}^{(0)} - E_i^{(0)}\right]\left[E_{\mathrm{v}}^{(0)} - E_j^{(0)}\right]\left[E_{\mathrm{v}}^{(0)} - E_k^{(0)}\right]} -$$

$$-2V_{\mathrm{vv}}^{(1)} \sum_{i\neq \mathrm{v}}\sum_{k\neq \mathrm{v}} \frac{V_{\mathrm{v}i}^{(1)}V_{ik}^{(1)}V_{k\mathrm{v}}^{(1)}}{\left[E_{\mathrm{v}}^{(0)} - E_i^{(0)}\right]^2\left[E_{\mathrm{v}}^{(0)} - E_k^{(0)}\right]} + \tag{C.6}$$

$$+\left[V_{\mathrm{vv}}^{(1)}\right]^2 \sum_{i\neq \mathrm{v}} \frac{\left|V_{i\mathrm{v}}^{(1)}\right|^2}{\left[E_{\mathrm{v}}^{(0)} - E_i^{(0)}\right]^3} - \sum_{i\neq \mathrm{v}}\sum_{k\neq \mathrm{v}} \frac{\left|V_{i\mathrm{v}}^{(1)}\right|^2\left|V_{k\mathrm{v}}^{(1)}\right|^2}{\left[E_{\mathrm{v}}^{(0)} - E_i^{(0)}\right]\left[E_{\mathrm{v}}^{(0)} - E_k^{(0)}\right]^2}$$

where:

$$V'_{iv} \equiv \left\langle \psi_i^{(0)} \middle| V' \middle| \psi_v^{(0)} \right\rangle \tag{C.7}$$

In the case of a one-dimensional anharmonic oscillator, the cubic term in Eq. (35) from the parent paper, involving ξ^3, does not contribute to the first- and the third-order energy correction. The fourth-order energy contribution of this term is,

$$E_{v,3}^{(4)} = \sum_{i\neq v}\sum_{j\neq v}\sum_{k\neq v} \frac{V_{vi}^{(1)}V_{ij}^{(1)}V_{jk}^{(1)}V_{kv}^{(1)}}{\left[E_v^{(0)}-E_i^{(0)}\right]\left[E_v^{(0)}-E_j^{(0)}\right]\left[E_v^{(0)}-E_k^{(0)}\right]} - E_v^{(2)}\sum_{j\neq v}\frac{\left|V_{jv}^{(1)}\right|^2}{\left[E_v^{(0)}-E_j^{(0)}\right]^2} \tag{C.8}$$

Using the above presented expressions, one obtains the formulae (40–42) in the parent paper.

SUPPLEMENT D

Details of the method for the calculation of the plasma composition

We start with any positive set of values $X^{(0)} = \{x_1^{(0)}, x_2^{(0)},\ldots, x_n^{(0)}\}$ that satisfies the conditions (62) and forms an expression analogous to Eq. (59) in the parent paper:

$$G\left[X^{(0)}\right] = \sum_{i=1}^{n} x_i^{(0)}\left[c_i + \ln\frac{x_i^{(0)}}{\bar{x}^{(0)}}\right] \tag{D.1}$$

with:

$$\bar{x}^{(0)} = \sum_{i=1}^{n} x_i^{(0)} \tag{D.2}$$

Of course, (S.1) will be a poor approximation to Eq. (59) from the parent paper. Thus, now a new set of coefficients, $X^{(1)} = \{x_1^{(1)}, x_2^{(1)}, \ldots x_n^{(1)}\}$, must be searched for that gives the function:

$$G\left[X^{(1)}\right] = \sum_{i=1}^{n} x_i^{(1)}\left[c_i + \ln\frac{x_i^{(1)}}{\bar{x}^{(1)}}\right] \tag{D.3}$$

with

$$\bar{x}^{(1)} = \sum_{i=1}^{n} x_i^{(1)} \tag{D.4}$$

to be a better approximation to Eq. (59) in the parent paper. Let $\Delta_i \equiv x_i^{(1)} - x_i^{(0)}$ and $\bar{\Delta} = \bar{x}_i^{(1)} - x^{(0)}$. We expand the function $G\left|X^{(1)}\right|$ assuming $X^{(1)} = \{x_1^{(1)}, x_2^{(1)},\ldots, x_n^{(1)}\}$, to be variables in a second-order Taylor series about $X^{(0)}$:

$$\begin{aligned}
Q\left[X^{(1)}\right] &= \left\{G\left[X^{(1)}\right]\right\}_{X^{(1)}=X^{(0)}} + \sum_{i=1}^{n}\left\{\frac{\partial G\left[X^{(1)}\right]}{\partial x_i^{(0)}}\right\}_{X^{(1)}=X^{(0)}} \Delta_i + \\
&+ \frac{1}{2}\sum_{i=1}^{n}\sum_{k=1}^{n}\left\{\frac{\partial^2 G\left[X^{(1)}\right]}{\partial x_i^{(0)}\partial x_i^{(0)}}\right\}_{X^{(1)}=X^{(0)}} \Delta_i\Delta_k = \\
&= G\left[X^{(0)}\right] + \sum_{i=1}^{n}\left[c_i + \ln\frac{x_i^{(0)}}{\bar{x}^{(0)}}\right]\Delta_i + \frac{1}{2}\sum_{i=1}^{n}\Delta_i\left[\frac{\Delta_i}{x_i^{(0)}} - \frac{\bar{\Delta}}{\bar{x}^{(0)}}\right] = \\
&\equiv G\left[X^{(0)}\right] + \sum_{i=1}^{n}\left[c_i + \ln\frac{x_i^{(0)}}{\bar{x}^{(0)}}\right]\left[x_i^{(1)} - x_i^{(0)}\right] + \\
&+ \frac{1}{2}\sum_{i=1}^{n}\left[x_i^{(1)} - x_i^{(0)}\right]\left[\frac{x_i^{(1)} - x_i^{(0)}}{x_i^{(0)}} - \frac{\bar{x}^{(1)} - \bar{x}^{(0)}}{\bar{x}^{(0)}}\right].
\end{aligned} \tag{D.5}$$

(This equation (in a somewhat different notation) is erroneously typed in the original paper.[70])

Knowing that the optimal coefficients $X = \{x_1, x_2, \ldots x_n\}$ lead to the condition $\partial G(X) / \partial x_i = 0$ for all x_i, the derivatives of the function $Q\left|X^{(1)}\right|$ are set to zero. However, this cannot be done directly because the variables $X^{(1)} = \{x_1^{(1)}, x_2^{(1)},\ldots, x_n^{(1)}\}$ [unlike the zero-th-order coefficients $X^{(0)} = \{x_1^{(0)}, x_2^{(0)},\ldots, x_n^{(0)}\}$] do not automatically satisfy the conditions (62) in the parent paper. Thus, the fulfilment of these conditions must be ensured. This can be realised by applying the method of Lagrange multipliers. The function $Q\left|X^{(1)}\right|$ is replaced by:

$$H\left[X^{(1)}\right] = Q\left[X^{(1)}\right] - \sum_{k=1}^{m+1}\pi_k\left[a_{ik}x_i^{(1)} - b_k\right] \tag{D.6}$$

where π_k are yet undetermined Lagrange multipliers. The conditions $\partial H\left|X^{(1)}\right| / \partial x_i^{(0)} = 0$ lead to a set of equations:

$$\frac{\partial H\left[X^{(1)}\right]}{\partial x_i^{(1)}} = \left[c_i + \ln\frac{x_i^{(0)}}{\bar{x}^{(0)}}\right] + \left[\frac{x_i^{(1)}}{x_i^{(0)}} - \frac{\bar{x}^{(1)}}{\bar{x}^{(0)}}\right] - \sum_{k=1}^{m+1}\pi_k a_{ik} = 0, \quad i = 1,\ 2,...,\ n \tag{D.7}$$

Equation (D.7) and:

$$\sum_{k=1}^{n} x_i^{(1)} a_{ik} = b_k\,, \quad k = 1,\ 2,...,\ m+1 \tag{D.8}$$

represent (when $\bar{x}^{(1)}$ is substituted by the right-hand side of Eq. (D.4)) a system of $n+m+1$ linear equations, the solutions of which are the new generation of coefficients, $X^{(1)} = \{x_1^{(1)}, x_2^{(1)},\ldots, x_n^{(1)}\}$, and the Lagrange multipliers $\pi_1, \pi_2,\ldots, \pi_{m+1}$. The coefficients $X^{(1)} = \{x_1^{(1)}, x_2^{(1)},\ldots, x_n^{(1)}\}$ are employed to obtain (D.3). A new function:

$$G\left[X^{(2)}\right] = \sum_{i=1}^{n} x_i^{(2)}\left[c_i + \ln\frac{x_i^{(2)}}{\bar{x}^{(2)}}\right] \tag{D.9}$$

is supposed, where now the new coefficients $X^{(2)} = \{x_1^{(2)}, x_2^{(2)},\ldots, x_n^{(2)}\}$ are handled as variables, and this function is expanded in a Taylor series about $X^{(1)}$. The procedure is repeated until convergence is achieved.

It was shown[80] that the mathematical problem can be reduced to the solution of a system of $m + 2$ (*i.e.*, in the original work to $m + 1$, because White *et al*. did not consider the constraint (61) in the parent paper) equations. Thus, the size of the system of linear equations to be solved can be reduced (practically) to the number of elements in question. From Eq. (D.7), it follows, namely:

$$x_i^{(1)} = -x_i^{(0)} f_i\left[X^{(0)}\right] + \frac{x_i^{(0)}}{\bar{x}^{(0)}}\bar{x}^{(1)} + x_i^{(0)}\sum_{k=1}^{m+1}\pi_k a_{ik} \tag{D.10}$$

where:

$$f_i\left[X^{(0)}\right] \equiv \left[c_i + \ln\frac{x_i^{(0)}}{\bar{x}^{(0)}}\right] \tag{D.11}$$

Summing over i in Eq. (D.11), when Eq. (62) from the parent paper is taken into account, gives:

$$\sum_{k=1}^{m+1}\pi_k b_k = \sum_{i=1}^{n} x_i^{(0)} f_i\left[X^{(0)}\right] \tag{D.12}$$

Inserting Eq. (D.10) into Eq. (D.8), and using the condition (62) from the parent paper, one obtains:

$$\sum_{k=1}^{m+1} r_{ik}\pi_k + b_k u = \sum_{i=1}^{n} a_{ij} x_i^{(0)} f_i\left[X^{(0)} \right], \quad k = 1,\ 2,...,\ m+1 \tag{D.13}$$

where:

$$r_{jk} = r_{kj} \equiv \sum_{i=1}^{n} \left(a_{ij} a_{ik} \right) x_i^{(0)} \tag{D.14}$$

and

$$u \equiv \frac{\overline{x}^{(1)}}{\overline{x}^{(0)}} - 1 \tag{D.15}$$

Eqs. (D.13) and (D.15) taken together represent a system of m + 2 linear equations in the unknowns $\pi_1, \pi_2, ..., \pi_{m+1}$ and u. After solving them, we can calculate the coefficients $x_1^{(1)}$, $x_2^{(1)}$,…, $x_n^{(1)}$ by means of Eq. (D.10). White *et al.*[5] also showed how to ensure non-negative values of the coefficients $X(p)$ = $\{x_1^{(p)}, x_2^{(p)},\ldots, x_n^{(p)}\}$ in each cycle, and proposed a very simple way for computing the concentrations of species present in traces.

REFERENCES

1. W. F. McDonough, *The Composition of the Earth, in Earthquake Thermodynamics and Phase Transformations in the Earth's Interior*, R. Teisseyre, E. Majewski, Eds., Academic Press, San Diego, CA, 2001
2. J. W. Morgan, E. Anders, *Proc. Nat. Acad. Sci. U.S.A.* **77** (1980) 6973
3. A. P. Dickin, In situ *Cosmogenic Isotopes, Radiogenic Isotope Geology*, Cambridge University Press, Cambridge, UK, 2005
4. K. P. Huber, G. Herzberg, *Molecular Spectra and Molecular Structure IV. Constants of Diatomic Molecules*, Van Nostrand Reinhold, New York, 1979
5. W. B. White, S. M. Johnson, G. B. Dantzig, *J. Chem. Phys.* **28** (1958) 751.

Journal of the Serbian Chemical Society
JSCS-info@shd.org.rs • www.shd.org.rs/JSCS
J. Serb. Chem. Soc. 77 (11) 1529–1539 (2012)
JSCS–4368
UDC 582.476:5.4.73.05+547.513+
66.095.25:615.277
Original scientific paper

Synthetic studies towards D-modified paclitaxel analogues

ZORANA FERJANČIĆ[1]*, RADOMIR MATOVIĆ[2] and RADOMIR N. SAIČIĆ[1]**

[1]Faculty of Chemistry, University of Belgrade, Studentski trg 16, P. O. Box 158, 11000 Belgrade, Serbia and [2]ICTM – Center for Chemistry, Njegoševa 12, 11000 Belgrade, Serbia

(Received, 26 June 2012)

Abstract: A synthetic sequence has been developed for the preparation of 9,10-di-*O*-diacetyl-4-desmethylene-4*β*-(3-butenyl)-4*α*-hydroxy-5-*O*-mesyltaxicin I--1,2-carbonate **3**, an intermediate in an attempted synthesis of a cyclobutane paclitaxel analogue. A series of reactions of **3** were investigated, including the protection of the sterically hindered C-4*α*-hydroxy group and the oxidative cleavage of the terminal double bond. Cyclization of **13** to the cyclobutane-containing intermediate failed due to the unexpected instability of the dimethylsilane protecting group under basic conditions.

Keywords: taxoids; taxanes antitumor agents; radical allylation; silyl protecting groups.

INTRODUCTION

Over the past 25 years, structure–activity relationships (SAR) studies on the antitumor agent paclitaxel have been thoroughly conducted, identifying the major sites involved in its microtubules stabilizing activity.[1] Among these numerous studies, considerable research efforts were directed toward the understanding of the role of the oxetane D-ring in the cytotoxic activity of paclitaxel.[2] The contribution of this ring to the biological activity of paclitaxel is not clear and two hypotheses have been proposed as explanations.[2d,f] The inflexible oxetane ring may force the molecule to adopt a biologically active conformation through its rigidifying effect on the taxane skeleton,[2e,k] or the oxetane oxygen atom might be involved in the stabilizing dipolar or hydrogen bonding interactions with the tubulin protein.[2b,c,h]

In the course of our studies on D-modified 7-deoxypaclitaxel analogues,[2l,n,3] we wished to synthesize analogue **1** in which the oxetane ring would be replaced by cyclobutane, according to the retrosynthetic plan presented in Scheme 1. Analogue **1**, as compared with paclitaxel, possesses a conformationally rigid four-

Corresponding authors: E-mail: *zferjan@chem.bg.ac.rs; **rsaicic@chem.bg.ac.rs
doi: 10.2298/JSC120626094F

membered D-ring without the electronegative oxygen atom in it. This modification should allow us to determine whether the oxetane ring exerts its influence to the biological activity of taxoids through conformational or electronic effects.

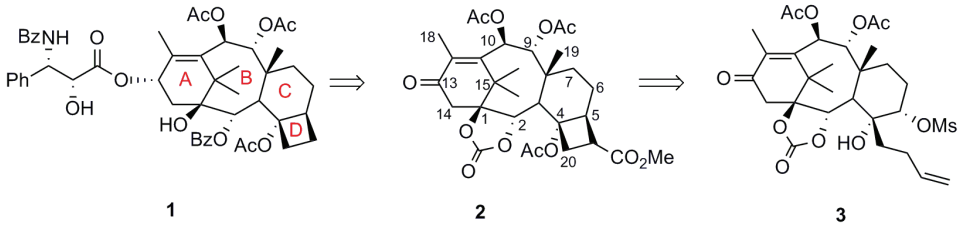

Scheme 1. Retrosynthetic analysis of cyclobutane paclitaxel analogue **1**.

RESULTS AND DISCUSSION

As the starting material for the preparation of analogue **1**, we chose triol **4**, one of the intermediates in our synthesis of 7-deoxy-C,D-*seco*-paclitaxel from taxine B (Scheme 2).[2l,n] Mesylation of the free C-20 and C-5 hydroxyl groups afforded **5** in good yield. Exposure of **5** to the action of the Hunig's base in refluxing toluene furnished epoxymesylate **6**, which was converted to bromohydrin **7** by Lewis acid induced nucleophilic opening of the 4(20)-epoxide. Finally, alcohol **3** was obtained by a free radical allylation of compound **7** with allyltributyltin, using AIBN as initiator. This protocol for elongation of the C-4*β* alkyl chain had already been successfully applied in our synthesis of the C,D-spirolactone analogue of paclitaxel.[2o] It is interesting to note that radical allylation of com-

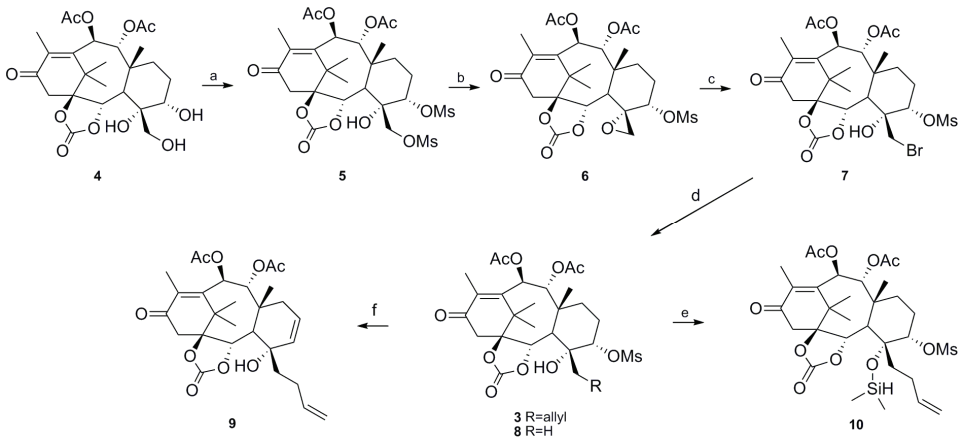

Scheme 2. Conversion of triol **4** into the DMS-protected alcohol **10**. Reagents, conditions and yields: a) MsCl, pyridine, rt, 72 h, 70 %; b) DIPEA, $PhCH_3$, 120 °C, 3 h, 87 %; c) Bu_4NBr, $BF_3{\cdot}OEt_2$, DCM, rt, 15 min, 84 %; d) allyltributyltin, AIBN, PhH, reflux, 3 h, **3** 57 % and **8** 15 %; e) DMSCl, imidazole, DMF, 55 °C, 67 % f) MOMCl, NaI, DIPEA, DME, 86 °C, 26 %.

pound **7** requires the use of a large amount of the initiator: when the standard reaction conditions (catalytic quantities of AIBN) were applied, only the starting material was isolated. However, performing the reaction with 3–4.5 equivalents of the initiator allowed us to obtain alcohol **3** in 57 % yield. Use of such a large amount of the initiator resulted in the formation of side product **8** (15 % yield), probably by reduction of the intermediary C-20 radical with AIBN.

All attempts to protect the tertiary hydroxyl group in **8** were unsuccessful, undoubtedly a direct result of a considerable steric hindrance. For example, treatment of **8** with TMSCl/imidazole in DMF, NaH/MeI in THF or lithium hexamethyldisilazide/methyl chloroformate in THF[2c] led only to the recovery of starting material. Attempted acetylation under forcing conditions with excess Ac_2O/ /DMAP[2i] in toluene at 60 °C also failed to provide the desired product. Interestingly, application of reaction conditions for the protection of tertiary alcohol as a methoxymethyl (MOM) ether (MOMCl, NaI, DMF, *N*,*N*-diisopropylethylamine, reflux)[4] caused only the elimination of C-5 mesylate and the formation of compound **9**. Finally, we found that treatment of **3** with chlorodimethylsilane and imidazole in DMF at 55 °C afforded the dimethylsilane (DMS) protected compound **10** in 67 % yield. Chlorodimethylsilane is a small and reactive reagent and it has already been successively used as a "specific" protecting group for the C-1 tertiary hydroxyl group of taxoids.[5]

We next turned our attention to the oxidative cleavage of the terminal double bond in the silyl ether **10** (Scheme 3). Some preliminary experiments indicated that during the reaction of **10** with a mixture of osmium tetraoxide and sodium periodate in THF/water, oxidation of the DMS protecting group also occurred, resulting in the formation of **11**. The ^{1}H-NMR spectrum exhibited two singlets for the methyls from the DMS group (instead of two doublets) and the absence of the DMS hydrogen atom. The desired transformation could be accomplished by ozonolysis: exposure of **10** to the action of ozone, followed by treatment with dimethyl sulfide to furnish aldehyde **12**. Oxidation of aldehyde **12** with oxone[6] in DMF and subsequent esterification of the carboxylic acid afforded compound **13** in 61 % yield (over two steps). The crucial ring-closure step in the synthesis – formation of the cyclobutane ring – was planned to be effected by the treatment of methyl ester **13** with potassium hexamethyldisilazide in THF at low temperature. However, these conditions proved conducive to the loss of the DMS protecting group and cyclization of thus obtained C-4 alcohol into lactone **14**. The outcome of this reaction was quite unexpected bearing in mind previous work from Chen,[5b] in which the DMS protecting group was unaffected under similar reaction conditions. Alternatively, lactone **14** could also be obtained directly from alcohol **3** by the action of OsO_4 and $NaIO_4$ followed by oxidation of the intermediary hemiacetal with Jones reagent.[2o] Finally, according to the previously observed elimination of the C-5 mesylate in alcohol **3**, we tried to form a

$\Delta^{5,6}$ double bond in **14**. The presence of a 5,6-double bond in the analogue with a C,D-spirolactone moiety could induce a conformational change of the C-ring which positiones the essential C-2, C-13 and C-4 ester groups in the appropriate spatial orientation for the improved biological activity of this type of taxoids.[1b,c] We have previously shown that the C,D-spirolactone paclitaxel analogue was the first D-ring-modified analogue to show significant cytotoxicity, as a result of a different mechanism of action in comparison with paclitaxel, involving mTOR inhibition-dependent autophagy instead of G_2/M cell cycle arrest-dependent apoptosis.[2o] Therefore, elimination of C-5 mesylate in **14** was attempted with several bases (*N*,*N*-diisopropylethylamine, DBU): unfortunately, these experiments led only to the recovery of starting material. Treatment of **14** with a nucleophile, such as the thiophenoxide anion, resulted in the formation of a complex mixture of polar products. The difference in reactivity between compounds **3** and **14** suggests that neighboring free C-4 hydroxyl group in **3** activates the C-5 mesylate toward elimination by intramolecular hydrogen bonding.

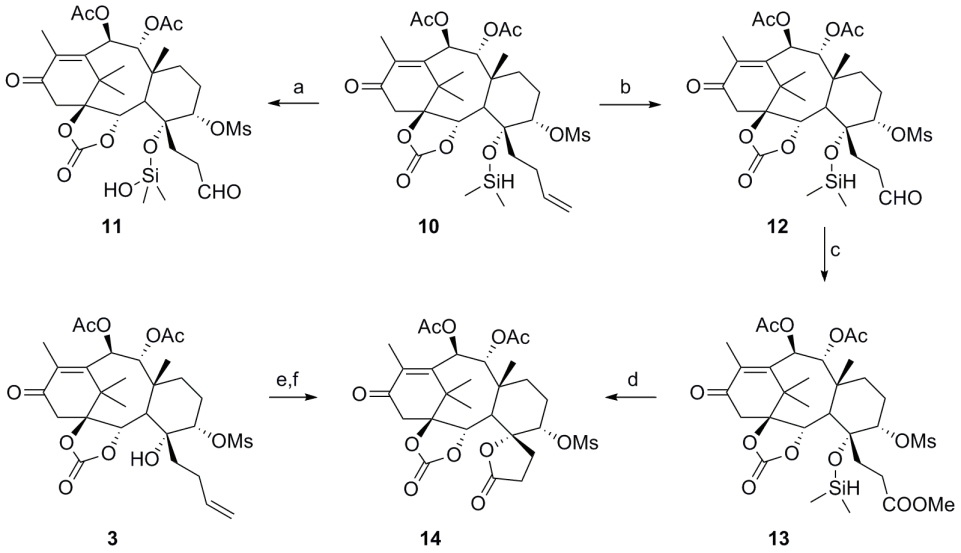

Scheme 3. Preparation of intermediate **13** and conversion of **3** and **13** into **14**. Reagents and conditions: a) OsO_4, $NaIO_4$, THF, H_2O, rt, 3 h, 42 %; b) O_3, DCM, –80 °C, then Me_2S, 18 h, 58 %; c) oxone, DMF, rt, 1 h, then CH_2N_2, THF, 0 °C, 1 h, 61 %; d) KHMDS, THF, –78 °C, 30 min, 77 %; e) OsO_4, $NaIO_4$, THF, H_2O, rt, 1 h; f) Jones reagent, acetone, 0 °C, 49 % from **3**.

EXPERIMENTAL

General experimental. All chromatographic separations[7] were performed on silica, 10-18, 60A, ICN Biomedicals. Standard techniques were used for the purification of the reagents and solvents.[8] The NMR spectra were recorded on a Varian Gemini 200 (^{1}H-NMR at 200

MHz, ^{13}C-NMR at 50 MHz, for samples in deuterated chloroform), and on a Bruker Avance III 500 (^{1}H-NMR at 500 MHz, ^{13}C-NMR at 125 MHz). The chemical shifts are expressed in ppm (δ) using tetramethylsilane as an internal standard and the coupling constants (J) are in Hz. The IR spectra were recorded on a Nicolet 6700 FT instrument and are expressed in cm^{-1}. The mass spectra were obtained on Agilent Technologies 6210 TOF LC/MS instrument (LC: series 1200).

*Compound **5***. To a solution of **4** (65 mg; 0.13 mmol) in pyridine (4 mL) at 0° C was added mesyl chloride (222 mg; 1.95 mmol; 15 eq). The reaction mixture was stirred at 0° C for 15 min and then allowed to warm to rt. After 24 h, a second batch of mesyl chloride (222 mg) was added and stirring of the reaction mixture was continued for 24 h. The reaction mixture was diluted with CH_2Cl_2 and the resulting solution was washed successively with ice-cold 2.5% HCl, aq. $NaHCO_3$ and water and dried over anh. $MgSO_4$. After removal of the solvent under reduced pressure, the residue was purified by dry flash chromatography (eluent: benzene/ethyl acetate = 1/1) to give **5** (60 mg, 70%) as a colorless film. IR (film, cm^{-1}): 3489, 2998, 2937, 1812, 1750, 1686, 1412, 1354, 1237, 1175, 1026; ^{1}H-NMR (200 MHz; $CDCl_3$, δ / / ppm): 6.04 (1H, *d*, *J* = 10.3 Hz), 5.63 (1H, *d*, *J* = 10.0 Hz), 4.92 (1H, *bs*), 4.89 (1H, *d*, *J* = 3.7 Hz), 4.62 (1H, *d*, *J* = 11.4 Hz), 4.48 (1H, *d*, *J* = 11.4 Hz), 3.99 (1H, *s*), 3.90 (1H, *d*, *J* = 19.4 Hz), 3.15 (3H, *s*), 3.00 (3H, *s*), 2.91 (1H, *d*, *J* = 3.67 Hz), 2.86 (1H, *d*, *J* = 19.1 Hz), 2.26 (3H, *s*), 2.11 (3H, *s*), 2.10–1.60 (4H, *m*), 2.05 (3H, *s*), 1.67 (3H, *s*), 1.34 (3H, *s*), 0.97 (3H, *s*); ^{13}C--NMR (50 MHz, $CDCl_3$, δ / ppm): 197.04 (C), 170.17 (C), 169.19 (C), 152.41 (C), 149.83 (C), 143.35 (C), 88.90 (C), 79.58 (CH), 79.13 (CH), 75.00 (CH), 73.70 (C), 72.58 (CH), 68.52 (CH_2), 43.74 (CH), 43.24 (C), 41.44 (C), 40.80 (CH_2), 38.73 (CH_3), 37.27 (CH_3), 32.68 (CH_3), 24.78 (2×CH_2), 20.59 (CH_3), 20.50 (CH_3), 19.92 (CH_3), 18.95 (CH_3), 13.68 (CH_3); HRMS (ESI-TOF high acc) calcd. for $C_{27}H_{39}O_{15}S_2$ (MH^+) 667.1725, found 667.1727.

*Compound **6***. A solution of **5** (134 mg; 0.20 mmol) and DIPEA (181 mg; 1.4 mmol; 7 eq) in anhydrous toluene (21 mL) was heated to reflux with stirring for 3 h. The solvent was removed under reduced pressure and the residue was purified by dry flash chromatography (eluent: benzene/ethyl acetate = 1/1) to give compound **6** (100 mg; 87%) as a colorless film. IR (film, cm^{-1}): 2994, 2939, 1815, 1746, 1688, 1435, 1371, 1236, 1175, 1036; ^{1}H-NMR (200 MHz; $CDCl_3$, δ / ppm): 6.09 (1H, *d*, *J* = 10.3 Hz), 5.72 (1H, *d*, *J* = 10.3 Hz), 4.75 (1H, *d*, *J* = = 4.4 Hz), 4.20 (1H, *bs*), 3.45 (1H, *d*, *J* = 4.0 Hz), 3.23 (1H, *d*, *J* = 4.4 Hz), 3.11 (1H, *d*, *J* = = 19.4 Hz), 3.04 (3H, *s*), 2.94 (1H, *d*, *J* = 19.4 Hz), 2.73 (1H, *d*, *J* = 4.0 Hz), 2.31 (3H, *s*), 2.13 (3H, *s*), 2.13–1.60 (4H, *m*), 2.05 (3H, *s*), 1.63 (3H, *s*), 1.33 (3H, *s*), 1.08 (3H, *s*); ^{13}C-NMR (50 MHz, $CDCl_3$, δ / ppm): 196.20 (C), 170.02 (C), 169.33 (C), 152.12 (C), 150.10 (C), 143.98 (C), 87.78 (C), 85.54 (CH), 77.96 (CH), 74.85 (CH), 72.43 (CH), 59.36 (C), 51.76 (CH_2), 44.30 (C), 41.44 (C), 40.88 (CH_2), 38.69 (CH_3), 37.93 (CH), 32.59 (CH_3), 26.98 (CH_2), 25.33 (CH_2), 20.67 (CH_3), 20.50 (CH_3), 19.92 (CH_3), 17.52 (CH_3), 14.29 (CH_3); HRMS (ESI-TOF high acc) calcd. for $C_{26}H_{35}O_{12}S$ (MH^+) 571.1844, found 571.1834.

*Compound **7***. To a solution of **6** (280 mg, 0.49 mmol) and Bu_4NBr (630 mg, 1.96 mmol, 4 eq) in CH_2Cl_2 (25 mL) was added BF_3•Et_2O (139 mg, 0.98 mmol, 2 eq) dropwise at rt under an argon atmosphere. The reaction mixture was stirred for 15 min and diluted with CH_2Cl_2, washed successively with water and brine, dried over anhydrous $MgSO_4$ and concentrated under reduced pressure. Purification by dry-flash chromatography (eluent:benzene/ethyl acetate = 7/3) gave compound **7** (255 mg, 80%) as white powder. m.p. 256 °C with decomposition. IR (film, cm^{-1}): 3467, 2928, 1812, 1750, 1686, 1360, 1233, 1173, 1027; ^{1}H-NMR (200 MHz; $CDCl_3$, δ / ppm): 6.04 (1H, *d*, *J* = 10.2 Hz), 5.63 (1H, *d*, *J* = 10.2 Hz), 5.03 (1H, *bs*), 4.83 (1H, *d*, *J* = 4.7 Hz), 4.16 (1H, *d*, *J* = 11.7 Hz), 3.87 (1H, *d*, *J* = 19.3 Hz), 3.79 (1H, *d*, *J* =

= 12.0 Hz), 3.11 (1H, *s*), 3.07 (1H, *d*, *J* = 4.4 Hz), 3.00 (3H, *s*), 2.86 (1H, *d*, *J* = 19.3 Hz), 2.27 (3H, *s*), 2.12 (3H, *s*), 2.12–1.60 (4H, *m*), 2.06 (3H, *s*), 1.67 (3H, *s*), 1.34 (3H, *s*), 1.02 (3H, *s*); ^{13}C-NMR (50 MHz, $CDCl_3$, δ / ppm): 196.95 (C), 170.29 (C), 169.20 (C), 152.12 (C), 149.59 (C), 143.49 (C), 88.82 (C), 80.52 (CH), 79.33 (CH), 75.09 (CH), 73.27 (C), 72.54 (CH), 43.83 (CH), 43.44 (C), 41.48 (C), 40.84 (CH_2), 38.67 (CH_3), 38.33 (CH_2), 32.77 (CH_3), 25.00 (2×CH_2), 20.68 (CH_3), 20.63 (CH_3), 20.05 (CH_3), 19.43 (CH_3), 13.78 (CH_3); HRMS (ESI-TOF high acc) calcd. for $C_{26}H_{36}BrO_{12}S$ (MH^+) 651.1105, found 651.1094.

*Compound **3***. A deaerated solution of **7** (220 mg, 0.34 mmol), allyltributyltin (1.68 g, 5.08 mmol, 15 eq) and AIBN (83 mg, 0.51 mmol, 1.5 eq) in benzene (44 mL) was stirred at 80 °C under an argon atmosphere. After 1 h, AIBN (83 mg) was added and stirring and heating of the reaction mixture were continued for 1 h. After removal of the solvent under reduced pressure, the residue was purified by dry-flash chromatography (eluent: benzene/ethyl acetate = 8/2) to give compound **3** (120 mg, 57%) and compound **8** (29 mg, 15%) as a colorless films. Compound **3**: IR (film, cm^{-1}): 3542, 3439, 2946, 1812, 1750, 1684, 1349, 1234, 1172, 1034; ^{1}H-NMR (500 MHz, $CDCl_3$, δ / ppm): 6.04 (1H, *d*, *J* = 10.5 Hz, H-10), 5.86–5.78 (1H, *m*, H-22), 5.62 (1H, *d*, *J* = 10.5 Hz, H-9), 5.11 (1H, broad *dd*, *J* = 1.0 and 17.0 Hz, H-23), 5.06 (1H, *dd*, *J* = 1.0 and 10.0 Hz, H-23), 4.88 (1H, *d*, *J* = 4.5 Hz, H-2), 4.79 (1H, *bs*, H-5), 3.79 (1H, *d*, *J* = = 19.0 Hz, H-14), 2.97 (3H, *s*, Ms), 2.90 (1H, *s*, OH), 2.84 (1H, *d*, *J* = 19.0 Hz, H-14), 2.78 (1H, *d*, *J* = 4.5 Hz, H-3), 2.32–2.23 (1H, *m*, H-21), 2.26 (3H, *s*, H-18), 2.23––2.13 (2H, *m*, H-20 and H-21), 2.11 (3H, *s*, Ac), 2.05 (3H, *s*, Ac), 2.06–1.98 (1H, *m*, H-6), 1.91–1.85 (1H, *m*, H-6), 1.78–1.68 (3H, *m*, H-20 and 2×H-7), 1.67 (3H, *s*, H-16 or H-17), 1.33 (3H, *s*, H-16 or H-17), 1.03 (3H, *s*, H-19); ^{13}C-NMR (125 MHz, $CDCl_3$, δ / ppm): 197.18 (C, C-13), 170.45 (C, Ac), 169.38 (C, Ac), 152.53 (C, CO), 149.71 (C, C-11), 143.45 (C, C-12), 137.66 (CH, C-22), 116.60 (CH_2, C-23), 89.38 (C, C-1), 81.74 (CH, C-5), 80.41 (CH, C-2), 75.70 (C, C-4), 75.60 (CH, C-9), 72.88 (CH, C-10), 45.23 (CH, C-3), 43.82 (C, C-8), 41.50 (C, C-15), 41.16 (CH_2, C-14), 38.82 (CH_3, Ms), 35.34 (CH_2, C-20), 33.02 (CH_3, C-16 or C-17), 28.24 (CH_2, C-21), 25.52 (CH_2, C-6), 25.44 (CH_2, C-7), 20.90 (CH_3, Ac), 20.81 (CH_3, Ac), 20.27 (CH_3, C-16 or C-17), 19.18 (CH_3, C-19), 13.99 (CH_3, C-18). HRMS (ESI-TOF high acc) calcd. for $C_{29}H_{41}O_{12}S$ (MH^+): 613.2313, found: 613.2318. Compound **8**: IR (film, cm^{-1}): 3500, 2965, 1811, 1750, 1685, 1348, 1237, 1171, 1026; ^{1}H-NMR (500 MHz, $CDCl_3$, δ / ppm): 6.04 (1H, *d*, *J* = 10.5 Hz, H-10), 5.63 (1H, *d*, *J* = 10.5 Hz, H-9), 4.88 (1H, *d*, *J* = 4.5 Hz, H-2), 4.57–4.55 (1H, *m*, H-5), 3.78 (1H, *d*, *J* = 19.5 Hz, H-14), 2.98 (3H, *s*, Ms), 2.85 (1H, *d*, *J* = = 19.0 Hz, H-14), 2.79 (1H, *d*, *J* = 4.5 Hz, H-3), 2.27 (3H, *s*, H-18), 2.11 (3H, *s*, Ac), 2.05 (3H, *s*, Ac), 2.05–2.00 (1H, *m*, H-6), 1.92–1.85 (1H, *m*, H-6), 1.76–1.69 (3H, *m*, 2×H-7), 1.68 (3H, *s*, H-16 or H-17), 1.57 (3H, *s*, H-20), 1.34 (3H, *s*, H-16 or H-17), 1.03 (3H, *s*, H-19); ^{13}C--NMR (125 MHz, $CDCl_3$, δ / ppm): 197.00 (C, C-13), 170.28 (C, Ac), 169.21 (C, Ac), 152.42 (C, CO), 149.52 (C, C-11), 143.40 (C, C-12), 89.21 (C, C-1), 84.93 (CH, C-5), 80.23 (CH, C-2), 75.43 (CH, C-9), 73.38 (C, C-4), 72.68 (CH, C-10), 44.11 (CH, C-3), 43.57 (C, C-8), 41.33 (C, C-15), 40.89 (CH_2, C-14), 38.69 (CH_3, Ms), 32.82 (CH_3, C-16 or C-17), 26.42 (CH_3, C-20), 25.46 (CH_2, C-6), 25.25 (CH_2, C-7), 20.72 (CH_3, Ac), 20.64 (CH_3, Ac), 20.08 (CH_3, C-16 or C-17), 18.57 (CH_3, C-19), 13.83 (CH_3, C-18). HRMS (ESI-TOF high acc) calcd. for $C_{26}H_{37}O_{12}S$ (MH^+): 573.2000, found: 573.1992.

*Compound **9***. A mixture of sodium iodide (12.5 mg, 0.084 mmol) and MOMCl (8.4 mg, 0.104 mmol) in DME (0.2 mL) was stirred for 10 min at rt. Then a solution of **3** (6.4 mg, 0.010 mmol) and DIPEA (14.8 mg, 0.114 mmol) in DME (0.5 mL) was stirred for 20 min at rt and overnight under reflux. A second portion of sodium iodide (25 mg,), MOMCl (17 mg) and DIPEA (30 mg) were added and stirring of the reaction mixture was continued for additional

24 h. The reaction mixture was quenched with saturated $NaHCO_3$ and water and extracted twice with methylene chloride. The combined extracts were washed with brine, dried over $MgSO_4$ and concentrated under reduced pressure. The residue was purified by column chromatography (eluent: benzene/ethyl acetate = 6/4) to give compound **9** (1.4 mg, 26%) as a colorless film. ^{1}H-NMR (200 MHz; $CDCl_3$, δ / ppm): 6.02 (1H, *d*, *J* = 10.4 Hz), 5.89–5.66 (2H, *m*), 5.70 (1H, *d*, *J* = 10.0 Hz), 5.60–5.52 (1H, *m*), 5.12–4.97 (2H, *m*), 4.92 (1H, *d*, *J* = 6.6 Hz), 3.75 (1H, *d*, *J* = 19.1 Hz), 2.83 (1H, *d*, *J* = 19.5 Hz), 2.40–1.92 (6H, *m*), 2.33 (1H, *d*, *J* = = 6.3 Hz), 2.10 (3H, *s*), 2.08 (3H, *s*), 2.06 (3H, *s*), 1.67 (3H, *s*), 1.31 (3H, *s*), 1.03 (3H, *s*).

*Compound **10***. To a solution of **3** (150 mg, 0.245 mmol) and imidazole (166 mg, 2.45 mmol, 10 eq) in DMF (1.2 mL) was added chlorodimethylsilane (231 mg, 2.45 mmol, 10 eq) dropwise at 0 °C, under an argon atmosphere. The reaction mixture was stirred at 0 °C for 15 min, and then at 55 °C for 1 h. After this period of time, imidazole (166 mg) and chlorodimethylsilane (231 mg) were added and the reaction was stirred at 55 °C for another hour. The reaction mixture was diluted with CH_2Cl_2, washed with water, dried over anhydrous $MgSO_4$ and concentrated under reduced pressure. Purification by dry-flash chromatography (eluent: benzene/ethyl acetate = 7/3) gave compound **10** (110 mg, 67 %) as a colorless film. IR (film, cm^{-1}): 2964, 1811, 1750, 1685, 1342, 1233, 1173, 1027; ^{1}H-NMR (500 MHz, $CDCl_3$, δ / ppm): 6.02 (1H, *d*, *J* = 10.0 Hz, H-10), 5.77–5.69 (1H, *m*, H-22), 5.62 (1H, *d*, *J* = 10.0 Hz, H-9), 5.05 (1H, broad *dd*, *J* = 1.5 and 17.0 Hz, H-23), 5.02 (1H, *dd*, *J* = 1.0 and 10.5 Hz, H-23), 4.87––4.85 (2H, *m*, H-5 and Si-H), 4.82 (1H, *d*, *J* = 4.5 Hz, H-2), 3.75 (1H, *d*, *J* = 19.0 Hz, H-14), 3.02 (3H, *s*, Ms), 2.80 (1H, *d*, *J* = 19.0 Hz, H-14), 2.72 (1H, *d*, *J* = 4.5 Hz, H-3), 2.29–2.24 (2H, *m*, H-21 and H-20), 2.29 (3H, *s*, H-18), 2.22–2.10 (2H, *m*, H-6 and H-21), 2.10 (3H, *s*, Ac), 2.05 (3H, *s*, Ac), 2.03–1.99 (1H, *m*, H-20), 1.78–1.73 (3H, *m*, H-6 and 2×H-7), 1.66 (3H, *s*, H-16 or H-17), 1.33 (3H, *s*, H-16 or H-17), 1.09 (3H, *s*, H-19), 0.32 (3H, *d*, *J* = 3.0 Hz, Si-CH_3), 0.29 (3H, *d*, *J* = 2.5 Hz, Si-CH_3); ^{13}C-NMR (125 MHz, $CDCl_3$, δ / ppm): 196.99 (C, C-13), 170.44 (C, Ac), 169.42 (C, Ac), 152.78 (C, CO), 150.63 (C, C-11), 142.90 (C, C-12), 136.91 (CH, C-22), 116.03 (CH_2, C-23), 88.83 (C, C-1), 81.13 (CH, C-5), 79.89 (C, C-4), 79.78 (CH, C-2), 75.92 (CH, C-9), 73.20 (CH, C-10), 45.53 (CH, C-3), 44.75 (C, C-8), 41.50 (C, C-15), 41.29 (CH_2, C-14), 39.99 (CH_3, Ms), 35.69 (CH_2, C-20), 33.20 (CH_3, C-16 or C-17), 28.76 (CH_2, C-21), 25.37 (CH_2, C-7), 25.16 (CH_2, C-6), 20.94 (CH_3, Ac), 20.86 (CH_3, Ac), 20.27 (CH_3, C-16 or C-17), 19.64 (CH_3, C-19), 13.80 (CH_3, C-18) 1.04 (CH_3, DMS), 0.95 (CH_3, DMS). HRMS (ESI-TOF high acc) calcd. for $C_{31}H_{47}O_{12}SSi$ (MH^+): 671.2552, found: 671.2530.

*Compound **11***. OsO_4 (30 μL of a 2.5% solution in *t*-BuOH) was added to a solution of **10** (9.6 mg, 0.015 mmol) in a mixture of THF (0.6 mL) and water (0.3 mL), followed by the addition of $NaIO_4$ (16 mg, 0.075 mmol; 5 eq). The reaction mixture was stirred for 1 h at rt, then sodium dithionite (50 mg) was added and stirring was continued for 20 min. The reaction mixture was diluted with CH_2Cl_2, washed with aq. $Na_2S_2O_3$ and water, dried over anhydrous $MgSO_4$ and concentrated under reduced pressure. The crude product was roughly purified by dry-flash chromatography (eluent: petrol ether/ethyl acetate = 1/1) affording **11** (4.3 mg; 42 %) as a colorless film. ^{1}H-NMR (200 MHz, $CDCl_3$, δ / ppm): 9.81 (1H, *s*), 6.00 (1H, *d*, *J* = 10.0 Hz), 5.63 (1H, *d*, *J* = 10.0 Hz), 4.83 (1H, *d*, *J* = 5.0 Hz), 4.82 (1H, *bs*), 3.73 (1H, *d*, *J* = 19.2 Hz), 3.10 (3H, *s*, Ms), 2.84 (1H, *d*, *J* = 19.2 Hz), 2.99–2.67 (2H, *m*), 2.66 (1H, *d*, *J* = 4.6 Hz), 2.49–2.35 (1H, *m*), 2.26 (3H, *s*, H-18), 2.25–2.11 (2H, *m*), 2.11 (3H, *s*, Ac), 2.06 (3H, *s*, Ac), 1.90–1.66 (3H, *m*), 1.68 (3H, *s*), 1.35 (3H, *s*), 1.13 (3H, *s*), 0.26 (3H, *s*), 0.23 (3H, *s*).

*Compound **12***. Into a cold (–80 °C) solution of **10** (45 mg, 0.067 mmol) in CH_2Cl_2 was bubbled ozone gas until the solution became light blue. Excess ozone was purged from the

reaction by bubbling argon through the cold reaction mixture for 10 min, followed by the addition of dimethyl sulfide (0.2 mL). The reaction mixture was stirred at room temperature overnight and concentrated under reduced pressure. Purification of the residue by column chromatography (eluent: benzene/ethyl acetate = 7/3) gave compound **12** (27 mg, 58 %) as a colorless film. IR (film, cm^{-1}): 2965, 1810, 1750, 1685, 1341, 1233, 1174, 1031; ^{1}H-NMR (500 MHz, $CDCl_3$, δ / ppm): 9.80 (1H, *s*, CHO), 6.01 (1H, *d*, *J* = 10.5 Hz, H-10), 5.63 (1H, *d*, *J* = 10.0 Hz, H-9), 4.87 (1H, *d*, *J* = 4.5 Hz, H-2), 4.82 (1H, *m*, Si-H), 4.73 (1H, *bd*, *J* = 2.5 Hz, H-5), 3.67 (1H, *d*, *J* = 19.0 Hz, H-14), 3.04 (3H, *s*, Ms), 2.82 (1H, *d*, *J* = 19.0 Hz, H-14), 2.80–2.75 (2H, *m*, 2×H-21), 2.75 (1H, *d*, *J* = 5.0 Hz, H-3), 2.46–2.39 (1H, *m*, H-20), 2.29 (3H, *s*, H-18), 2.25–2.22 (2H, *m*, H-6 and H-20), 2.11 (3H, *s*, Ac), 2.05 (3H, *s*, Ac), 1.90–1.83 (1H, *m*, H-6), 1.76–1.74 (2H, *m*, 2×H-7), 1.67 (3H, *s*, H-16 or H-17), 1.33 (3H, *s*, H-16 or H-17), 1.10 (3H, *s*, H-19), 0.31 (3H, *d*, *J* = 3.0 Hz, Si-CH_3), 0.30 (3H, *d*, *J* = 3.5 Hz, Si-CH_3). ^{13}C--NMR (125 MHz, $CDCl_3$, δ / ppm): 199.99 (C, CHO), 196.54 (C, C-13), 170.15 (C, Ac), 169.17 (C, Ac), 152.29 (C, CO), 150.44 (C, C-11), 142.53 (C, C-12), 88.66 (C, C-1), 81.14 (CH, C-5), 79.45 (C, C-4), 79.19 (CH, C-2), 75.56 (CH, C-9), 72.88 (CH, C-10), 45.30 (CH, C-3), 44.39 (C, C-8), 41.20 (C, C-15), 40.99 (CH_2, C-14), 39.81 (CH_3, Ms), 39.75 (CH_2, C-21), 32.93 (CH_3, C-16 or C-17), 28.46 (CH_2, C-20), 25.24 (CH_2, C-7), 24.77 (CH_2, C-6), 20.65 (CH_3, Ac), 20.56 (CH_3, Ac), 19.99 (CH_3, C-16 or C-17), 19.05 (CH_3, C-19), 13.53 (CH_3, C-18), 0.83 (CH_3, DMS), 0.65 (CH_3, DMS). HRMS (ESI-TOF high acc) calcd. for $C_{30}H_{45}O_{13}SSi$ (MH^+): 673.2345, found: 673.2335.

*Compound **13***. To a solution of **12** (22 mg, 0.032 mmol) in DMF (0.6 mL) oxone (60 mg, 0.098 mmol, 3 eq) was added in one portion and the reaction was stirred at rt for 2 h. The reaction mixture was diluted with ethyl acetate, washed with water, dried over anhydrous $MgSO_4$ and concentrated under reduced pressure. The residue was dissolved in THF at 0 °C and ethereal solution of diazomethane was slowly added. The reaction mixture was stirred at 0 °C for 1 h and concentrated under reduced pressure. Purification by column chromatography (eluent: benzene/ethyl acetate = 7/3) gave compound **13** (14 mg, 61%) as a colorless film. IR (film, cm^{-1}): 2959, 1809, 1743, 1682, 1373, 1339, 1234, 1174, 1024; ^{1}H-NMR (500 MHz, $CDCl_3$, δ / ppm): 6.01 (1H, *d*, *J* = 10.0 Hz, H-10), 5.63 (1H, *d*, *J* = 10.0 Hz, H-9), 4.85–4.82 (2H, *m*, H-2 and Si-H), 4.76 (1H, *bd*, *J* = 2.0 Hz, H-5), 3.70 (3H, *s*, CO_2Me), 3.68 (1H, *d*, *J* = = 19.0 Hz, H-14), 3.04 (3H, *s*, Ms), 2.82 (1H, *d*, *J* = 19.5 Hz, H-14), 2.74 (1H, *d*, *J* = 4.5 Hz, H-3), 2.57–2.52 (2H, *m*, 2×H-21), 2.49–2.44 (1H, *m*, H-20), 2.29 (3H, *s*, H-18), 2.29–2.24 (2H, *m*, H-6 and H-20), 2.11 (3H, *s*, Ac), 2.06 (3H, *s*, Ac), 1.92–1.85 (1H, *m*, H-6), 1.76–1.72 (2H, *m*, 2×H-7), 1.67 (3H, *s*, H-16 or H-17), 1.33 (3H, *s*, H-16 or H-17), 1.12 (3H, *s*, H-19), 0.33 (3H, *d*, *J* = 2.5 Hz, Si-CH_3), 0.30 (3H, *d*, *J* = 2.5 Hz, Si-CH_3); ^{13}C-NMR (125 MHz, $CDCl_3$, δ / ppm): 196.66 (C, C-13), 172.93 (C, CO_2Me), 170.21 (C, Ac), 169.25 (C, Ac), 152.37 (C, CO), 150.49 (C, C-11), 142.62 (C, C-12), 88.65 (C, C-1), 80.99 (CH, C-5), 79.48 (C, C-4), 79.26 (CH, C-2), 75.60 (CH, C-9), 72.94 (CH, C-10), 52.01 (CH_3, CO_2Me), 45.33 (CH, C-3), 44.43 (C, C-8), 41.23 (C, C-15), 41.01 (CH_2, C-14), 39.87 (CH_3, Ms), 33.00 (CH_3, C-16 or C-17), 31.82 (CH_2, C-20), 29.83 (CH_2, C-21), 25.27 (CH_2, C-7), 24.83 (CH_2, C-6), 20.74 (CH_3, Ac), 20.65 (CH_3, Ac), 20.05 (CH_3, C-16 or C-17), 19.19 (CH_3, C-19), 13.59 (CH_3, C-18) 0.82 (CH_3, DMS), 0.66 (CH_3, DMS). HRMS (ESI-TOF high acc) calcd. for $C_{31}H_{46}O_{14}SSiNa$ (MNa^+): 725.2270, found: 725.2259.

*Compound **14***. OsO_4 (20 μL of a 2.5% solution in *t*-BuOH) was added to a solution of **3** (7 mg, 0.0011 mmol) in a mixture of THF (0.6 mL) and water (0.3 mL), followed by the addition of $NaIO_4$ (12.1 mg, 0.057 mmol; 5 eq). The reaction mixture was stirred for 1 h at rt, then sodium dithionite (40 mg) was added and stirring was continued for 20 min. The reaction

mixture was diluted with CH_2Cl_2, washed with aq. $Na_2S_2O_3$ and water, dried over anhydrous $MgSO_4$ and concentrated under reduced pressure. The crude product was roughly purified by dry-flash chromatography (eluent: petrol ether/ethyl acetate = 1/1) affording hemiacetal (3.7 mg) that was used in the next step. Jones reagent (25 μL, 0.009 mmol; 1.5 eq) was added to a solution of hemiacetal (3.7 mg, 0.006 mmol) in acetone (0.5 mL) at 0 °C, and the resulting mixture was stirred for 15 min, when isopropanol (100 μL) was added. The reaction mixture was diluted with CH_2Cl_2, washed with brine, dried over anhydrous $MgSO_4$ and concentrated under reduced pressure. Purification by coloumn chromatography (eluent: benzene/ethyl acetate = 1/2) gave compound **14** (3.5 mg, 49% over two steps) as a colorless film. IR (film, cm^{-1}): 2993, 2937, 1816, 1746, 1685, 1370, 1353, 1233, 1174, 1024; ^{1}H NMR (500 MHz, $CDCl_3$, δ / ppm): 6.06 (1H, *d*, *J* = 10.5 Hz, H-10), 5.67 (1H, *d*, *J* = 10.0 Hz, H-9), 4.85 (1H, *bd*, *J* = 5.0 Hz, H-2), 4.67 (1H, *bt*, *J* = 2.5 Hz, H-5), 3.54 (1H, *d*, *J* = 19.5 Hz, H-14), 3.06 (1H, *d*, *J* = 5.0 Hz, H-3), 3.01 (3H, *s*, Ms), 2.94 (1H, *dd*, *J* = 19.5 Hz, H-14), 2.82–2.74 (1H, *m*, H-21), 2.67–2.58 (2H, *m*, H-20 and H-21), 2.27 (3H, *s*, H-18), 2.14–2.10 (1H, *m*, H-6), 2.12 (3H, *s*, Ac), 2.06 (3H, *s*, Ac), 1.97–1.91 (2H, *m*, H-6 and H-20), 1.81 (1H, *ddd*, *J* = 2.5, 4.0 and 14.0 Hz, H-7), 1.74 (1H, *dd*, *J* = 3.5 and 13.5 Hz, H-7), 1.68 (3H, *s*, H-16 or H-17), 1.35 (3H, *s*, H-16 or H-17), 1.003 (3H, *s*, H-19); ^{13}C-NMR (125 MHz, $CDCl_3$, δ / ppm): 196.44 (C, C-13), 173.12 (C, C-22), 170.07 (C, Ac), 169.17 (C, Ac), 151.45 (C, CO), 149.82 (C, C-11), 143.32 (C, C-12), 88.65 (C, C-1 or C-4), 85.16 (C, C-1 or C-4), 81.66 (CH, C-5), 78.63 (CH, C-2), 74.59 (CH, C-9), 72.49 (CH, C-10), 43.89 (C, C-8), 41.60 (C, C-15), 41.51 (CH, C-3), 40.53 (CH_2, C-14), 39.10 (CH_3, Ms), 32.79 (CH_3, C-16 or C-17), 28.99 (CH_2, C-20), 27.41 (CH_2, C-21), 24.84 (2×CH_2, C-6 and C-7), 20.71 (CH_3, Ac), 20.58 (CH_3, Ac), 20.07 (CH_3, C-16 or C-17), 18.38 (CH_3, C-19), 13.86 (CH_3, C-18). HRMS (ESI-TOF high acc) calcd. for $C_{28}H_{37}O_{13}S$ (MH^+): 613.1949, found: 613.1922.

CONCLUSIONS

In conclusion, triol **4**, a versatile starting compound in the synthesis of several taxane analogues, was converted into ester **13** – an advanced intermediate in the attempted synthesis of cyclobutane taxane analogue **1**. However, the cyclization failed, due to the unexpected instability of the DMS protecting group in **13** under basic conditions. In addition, useful information was acquired on the reactivity of the obtained taxoid intermediates, as well as on the dimethylsilane (DMS) protecting group. Observation that alcohol **3** has the propensity for elimination of C_5 mesylate and the formation of the $\Delta^{5,6}$ double bond provides a possibility for a future investigation of 5,6-dehydro-C,D-spirolactone analogues. The synthesis and biological evaluation of a novel taxane analogue with a C,D-spirolactone moiety would be of considerable interest, bearing in mind the fact that this type of taxoids show mechanistically different cytotoxic action as compared to paclitaxel.

Acknowledgments. Financial support of the Ministry of Education, Science and Technological Development of the Republic of Serbia is acknowledged (Project No. 172027).

ИЗВОД

СИНТЕТИЧКЕ СТУДИЈЕ АНАЛОГА ПАКЛИТАКСЕЛА СА МОДИФИКОВАНИМ D-ПРСТЕНОМ

ЗОРАНА ФЕРЈАНЧИЋ[1], РАДОМИР МАТОВИЋ[2] и РАДОМИР Н. САИЧИЋ[1]

[1]Хемијски факултет Универзитета у Београду, Студентски трг 12–16, п. пр. 158, 11000 Београд и [2]ИХТМ – Центар за хемију, Његошева 12, 11000 Београд

Развијена је синтетичка секвенца за добијање 9,10-ди-*O*-ацетил-4-десметилен-4*β*--(3-бутенил)-4*α*-хидрокси-5-О-мезилтаксицин I-1,2-карбоната (**3**), интермедијера у покушаној синтези циклобутанског аналога паклитаксела. Испитивана је могућност даље хемијске трансформације једињења **3**, као што је заштита стерно изразито заштићене С-4*α* хидроксилне групе и оксидативна фрагментација терминалне двоструке везе. Циклизација једињења **13** није дала жељени резултат – интермедијер са циклобутановим прстеном, што је последица неочекиване нестабилности DMS-заштитне групе у базним реакционим условима.

(Примљено 26. јуна 2012)

REFERENCES

1. For reviews on taxoid chemistry and SAR studies, see: a) D. G. I. Kingston, P. G. Jagtap, H. Yuan, L. Samala, *Prog. Chem. Org. Nat. Prod.* **84** (2002) 53; b) F. Gueritte, *Curr. Pharm. Des.* **7** (2001) 933; c) D. G. I. Kingston, *J. Nat. Prod.* **63** (2000) 726; d) *The Chemistry and Pharmacology of Taxol and its Derivatives*, in *Pharmacochemistry Library*, Vol. 22, V. Farina, Ed., Elsevier, Amsterdam, 1995; e) D. Guenard, F. Gueritte-Voegelin, P. Potier, *Acc. Chem. Res.* **26** (1993) 160
2. a) G. Samaranayake, N. F. Magri, C. Jitraugsri, D. G. I. Kingston, *J. Org. Chem*. **56** (1991) 5114; b) R. Marder-Karsenti, J. Dubois, L. Bricard, D. Guenard, F. Gueritte-Voegelein, *J. Org. Chem.* **62** (1997) 6631; c) A. L. Gunatilaka, F. D. Ramdayal, M. H. Sarragiotto, D. G. I. Kingston, D. L. Sackett, E. Hamel, *J. Org. Chem*. **64** (1999) 2694; d) T. C. Boge, M. Hepperle, D. G. Vander Velde, C. W. Gunn, G. L. Grunewald, G. I. Georg, *Bioorg. Med. Chem. Lett.* **9** (1999) 3041; e) J. Dubois, S. Thoret, F. Gueritte, D. Guenard, *Tetrahedron Lett*. **41** (2000) 3331; f) M. Wang, B. Cornett, J. Nettles, D. C. Liotta, J. P. Snyder, *J. Org. Chem.* **65** (2000) 1059; g) L. Barboni, A. Datta, D. Dutta, G. I. Georg, D. G. Vander Velde, R. H. Himes, M. Wang, J. P. Snyder, *J. Org. Chem.* **66** (2001) 3321; h) L. Merckle, J. Dubois, E. Place, S. Thoret, F. Gueritte, D. Guenard, C. Poupat, A. Ahond, P. Potier, *J. Org. Chem.* **66** (2001) 5058; i) P. H. Beusker, H. Veldhuis, J. Brinkhorst, D. G. H. Hetterscheid, N. Feichter, A. Bugaut, H. W. Scheeren, *Eur. J. Org. Chem.* (2003) 689; j) V. Deka, J. Dubois, S. Thoret, F. Gueritte, D. Guenard, *Org. Lett.* **5** (2003) 5031; k) L. Barboni, G. Giarlo, M. Ricciutelli, R. Ballini, G. I. Georg, D. G. Vander Velde, R. H. Himes, M. Wang, A. Lakdawala, J. P. Snyder, *Org. Lett.* **6** (2004) 461; l) Z. Ferjancic, R. Matovic, Z. Cekovic, J. P. Snyder, R. N. Saicic, *Tetrahedron Lett*. **46** (2005) 5049; m) S. Thoret, F. Gueritte, D. Guenard, J. Dubois, *Org. Lett.* **8** (2006) 2301; n) Z. Ferjancic, R. Matovic, Z. Cekovic, Y. Jiang, J. P. Snyder, V. Trajkovic, R. N. Saicic, *Tetrahedron*, **62** (2006) 8503; o) M. Trmcic, R. Matovic, G. Tovilovic, B. Ristic, V. Trajkovic, Z. Ferjancic, R. N. Saicic, *Org. Biomol. Chem.* **10** (2012) 4933
3. Z. Ferjancic, R. Matovic, Z. Cekovic, R. N. Saicic, *J. Serb. Chem. Soc*. **71** (2006) 705

4. K. Narasaka, T. Sakakura, T. Uchimaru, D. Guedin-Vuong, *J. Am. Chem. Soc.* **106** (1984) 2954
5. a) S.-H. Chen, J. F. Kadow, V. Farina, C. R. Fairchild, K. A. Johnston, *J. Org. Chem.* **59** (1994) 6156; b) S.-H. Chen, *Tetrahedron Lett.* **37** (1996) 3935; c) T. Doi, S. Fuse, S. Miyamoto, K. Nakai, D. Sasuga, T. Takahashi, *Chem. Asian J.* **1** (2006) 370; d) M. E. Ondari, K. D. Walker, *J. Org. Chem.* **74** (2009) 2186
6. B. R. Travis, M. Sivakumar, G. Olatunji Hollist, B. Borhan, *Org. Lett.* **5** (2003) 1031
7. For a description of the technique of dry-flash chromatography, see: a) L. M. Harwood, *Aldrichim. Acta* **18** (1985) 25; b) A. I. Vogel, A. R. Tatchell, B. S. Furnis, A. J. Hannaford, P. W. G. Smith, *Vogel's Textbook of Practical Organic Chemistry*, 5th ed., Longman, London, 1989, p. 220; c) An account which includes some improvements of the separation technique: D. S. Pedersen, C. Rosenbohm, *Synthesis* (2001) 2431
8. D. D. Perrin, W. L. F. Armarego, *Purification of Laboratory Chemicals*, 3rd ed., Pergamon Press, Oxford, 1988.

Journal of the Serbian Chemical Society
JSCS-info@shd.org.rs • www.shd.org.rs/JSCS
J. Serb. Chem. Soc. *77* (11) 1541–1549 (2012)
JSCS–4369
UDC 547.497.1+547.79:611.018.1+615.9
Original scientific paper

Synthesis and root growth activity of some new acetylhydrazinecarbothioamides and 1,2,4-triazoles substituted with the 5*H*-dibenzo[*a*,*d*][7]annulene moiety

LAURA I. SOCEA[1]*, THEODORA V. APOSTOL[1], GABRIEL ŞARAMET[1], ŞTEFANIA F. BĂRBUCEANU[1], CONSTANTIN DRAGHICI[2] and MIHAELA DINU[1]

[1]*Carol Davila University of Medicine and Pharmacy, Faculty of Pharmacy, Organic Chemistry Department, Traian Vuia Street 6, 020956, Bucharest, Romania and* [2]*C. D. Neniţescu Institute of Organic Chemistry, Romanian Academy, Splaiul Independenţei 202B, 060023, Bucharest, Romania*

(Received 20 January, revised 20 June 2012)

Abstract: New hydrazinecarbothioamides **5a**–**d** bearing 5*H*-dibenzo[*a*,*d*][7]annulene moiety were synthesized using classical procedures. ^{1}H-NMR analysis indicated the existence of two conformational isomers, a major axial (about 75 %) and a minor equatorial one (25 %), which are interconvertible by middle ring inversion. Cyclization of compounds **5a**–**d** in NaOH solution produced the corresponding 4*H*-1,2,4-triazole-3-thiols (**6a**–**d**) that proved to be pure axial isomers. All the new compounds were extensively characterized by elemental analysis, IR, UV, ^{1}H-NMR and ^{13}C-NMR spectroscopy and were biologically investigated using phytobiological tests.

Keywords: carbothioamide; 1,2,4-triazole; 5*H*-dibenzo[*a*,*d*][7]annulene; plant growth regulation activity.

INTRODUCTION

The 5*H*-dibenzo[*a*,*d*][7]annulene ring is present in the structure of many compounds used in therapeutics as antibacterial, anticonvulsive, anticholinergic, myorelaxant, antihistaminic, antifungal, carbonic anhydrase inhibitors, anti-inflammatory, analgesic, anti-arrhythmia, antiparasitic agents, but mostly they are used as antidepressant drugs.[1–4]

Hydrazinecarbothioamides are compounds with various pharmacological activities: anti-inflammatory, antimicrobial, tuberculostatic, anticonvulsive and antiviral.[5–8]

The synthesis of compounds containing the 1,2,4-triazole ring in their structure has attracted widespread attention, mainly in connection with their wide range of pharmacological properties. It is well documented that 1,2,4-triazole

* Corresponding author. E-mail: laurasocea@gmail.com
doi: 10.2298/JSC120120068S

derivatives possess antimicrobial, antifungal, tuberculostatic, analgesic and carbonic anhydrase inhibitor activities.[9–13]

Motivated by these facts and as a continuation of previous work,[2,14–18] the synthesis, characterization and action on vegetal cell division of new hydrazinecarbothioamides and 1,2,4-triazole derivatives containing the 5*H*-dibenzo[*a*,*d*]-[7]annulene moiety are presented herein.

The structures of these new compounds were elucidated by elemental analysis and IR, UV, ^{1}H-NMR and ^{13}C-NMR spectroscopy. The newly synthesized products were tested using phytobiological tests.[19–21]

The Triticum bioassay (Constantinescu method)[19,21] revealed concentration-dependent mitoinhibitory effects for the investigated substances.

EXPERIMENTAL

Materials, methods and instruments

All chemicals used in this study were supplied by Sigma–Aldrich and Merck.

The melting points were determined using a Böetius apparatus and are uncorrected. Elemental analyses were realized using a Perkin–Elmer CHNS/O Analyzer Series II 2400 instrument and the results were within ±0.4 % of theoretical values. The infrared spectra were recorded on a Vertex 70 Bruker spectrometer using the KBr pellet technique and the results are expressed in wave number (cm^{-1}). The ^{1}H-NMR and ^{13}C-NMR spectra were registered on a Varian Gemini 300 BB spectrometer working at 300 MHz for ^{1}H and 75 MHz for ^{13}C, using DMSO-d_6 as the solvent for hydrazinecarbothioamides and $CDCl_3$ for 1,2,4-triazole compounds. The chemical shifts are expressed in δ (ppm) using TMS as the internal standard. The UV–Vis spectra were recorded on a SPECORD 40 Analytik Jena spectrometer in methanol (2.5×10^{-5} M) in the wavelength range 200–600 nm.

The plant bioassay (Triticum bioassay) used embryonic roots from *Triticum vulgare* Mill. as the biological reagent. A Labophot II Nikon microscope (ob. 10× and 100×) was used.[20,21]

*Procedure for the preparation of 2-(5*H*-dibenzo[*a,d*][7]annulen-5-ylacetyl)hydrazinecarbothioamide **5a***

The mixture of 2-(5*H*-dibenzo[*a*,*d*][7]annulen-5-yl)acetohydrazide (**3**, 0.004 mol), and KSCN (0.008mol) in 40 mL water was refluxed in the presence of 1 mL of concentrated HCl for 10 h. On cooling the reaction mixture to room temperature, a white solid appeared. This was filtered off and recrystallized from methanol–water (1:3, v:v) to obtain the desired compound.

*General procedure for the preparation of 2-(5*H*-dibenzo[*a,d*][7]annulen-5-ylacetyl)-*N*-alkyl-(aryl)hydrazinecarbothioamides **5b–d***

The mixture of 2-(5*H*-dibenzo[*a*,*d*][7]annulen-5-yl)acetohydrazide (**3**, 0.004 mol) and the corresponding isothiocyanate **4b–d** (0.004 mol) in absolute ethanol (30–50 mL) was refluxed for 6–12 h. On cooling the reaction mixture to room temperature, a solid appeared. This was filtered off and recrystallized from ethanol to obtain the desired compound.

*General procedure for the preparation of compounds **6a–d***

A solution of the corresponding carbothioamide **5a–d** (1 mmol) in 8 mL of 8 % NaOH solution was refluxed for 3–9 h and then filtered. After cooling, the filtrate was neutralized

with acetic acid. The obtained white precipitate was filtered and recrystallized from $CHCl_3$:petroleum ether (1:2, v/v).

Triticum bioassay – Constantinescu method

The effects of the title compounds on root growth of wheat were determined according to the bioassay – Triticum test. The method is based on the study of the influence of substances at various dilutions on root elongation and mitotic film, depending on their duration of action on wheat (Triticum sp., Poaceae) caryopses germinated under well-defined laboratory conditions.

All the compounds were tested at 0.5, 0.25 and 0.05 mM concentrations. The solutions were placed in 10 cm diameter Petri dishes and then the wheat caryopses with a main root of 1 cm were introduced.

The dishes were covered with their lids and the caryopses were left in contact with the solutions for 5 days. In parallel, a control sample was prepared, in which the test solutions were replaced by distilled water. Root elongation was evaluated at the same time for 5 days. Observations were made on the morphological changes, as well as on the aspect, the number of radicles and the length of the main radicle.

For the microscopic study, after 24 h, the embryonic root of two caryopses from each Petri dish was sectioned at a distance of 5 mm from the tip and stained with dilute acetic orcein, a dye with a great affinity for chromatin in acetic medium (an acid pH is required for the hydrolysis of the chromatin) which will be stained red. The stained sections were microscopically examined using a LaboPhot II Nikon microscope (ocular 10×, object-glass 100×) by immersion in cedar oil.

The data represent the average values from two independent experiments and the results were processed statistically by the Student's *t*-test (Table I).

TABLE I. Plant growth regulation activities of compounds **5a**–**d** and **6a**–**d** (the root length is the mean value of measurements made on day five of the treatment)

Compd.	Concentration, mM	Root length±SD[a], mm	*p*-Value[b]	Effect, %
M	–	108.4±3.3	–	–
5a	0.5	33.2±3.0	<0.00001	76.42[c]
5a	0.25	42.0±4.1	<0.00001	67.48
5a	0.05	64.0±6.0	<0.00001	45.12
5b	0.5	68.7±5.8	<0.0001	40.34
5b	0.25	85.5±7.0	<0.001	23.27
5b	0.05	92.0±8.7	<0.001	16.66
5c	0.5	52.0±5.2	<0.00001	57.31
5c	0.25	75.3±7.0	<0.001	33.63
5c	0.05	82.1±8.7	<0.001	26.72
5d	0.5	102.8±1.9	NS[d]	5.69
5d	0.25	96.5±9.1	<0.001	12.09
5d	0.05	89.6±9.0	<0.001	19.10
6a	0.5	56.5±5.6	<0.00001	52.74
6a	0.25	61.3±4.0	<0.0001	47.86
6a	0.05	103.7±2.1	NS	4.77
6b	0.5	70.7±7.7	0.0001	38.31
6b	0.25	79.1±8.0	0.001	29.77
6b	0.05	92.5±8.2	<0.001	16.15

TABLE I. Continued

Compd.	Concentration, mM	Root length±SD[a], mm	*p*-Value[b]	Effect, %
6c	0.5	63.3±6.1	<0.00001	45.83
6c	0.25	65.3±5.9	<0.0001	40.75
6c	0.05	98.8±3.9	0.004	9.75
6d	0.5	63.0±5.8	<0.00001	46.13
6d	0.25	83.2±7.9	<0.001	25.60
6d	0.05	109.7±3.9	NS	–1.32[e]

[a]standard deviation; [b]significant level (statistical significance in the two-population (independent) Student's *t*--test); [c]positive value of effect = inhibition effect on wheat root growth; [d]the two means are not significantly different; [e]negative value of effect = stimulating effect on wheat root growth

RESULTS AND DISCUSSION

Chemistry

The synthesis pathway used for the preparation of the title compounds is shown in Scheme 1.

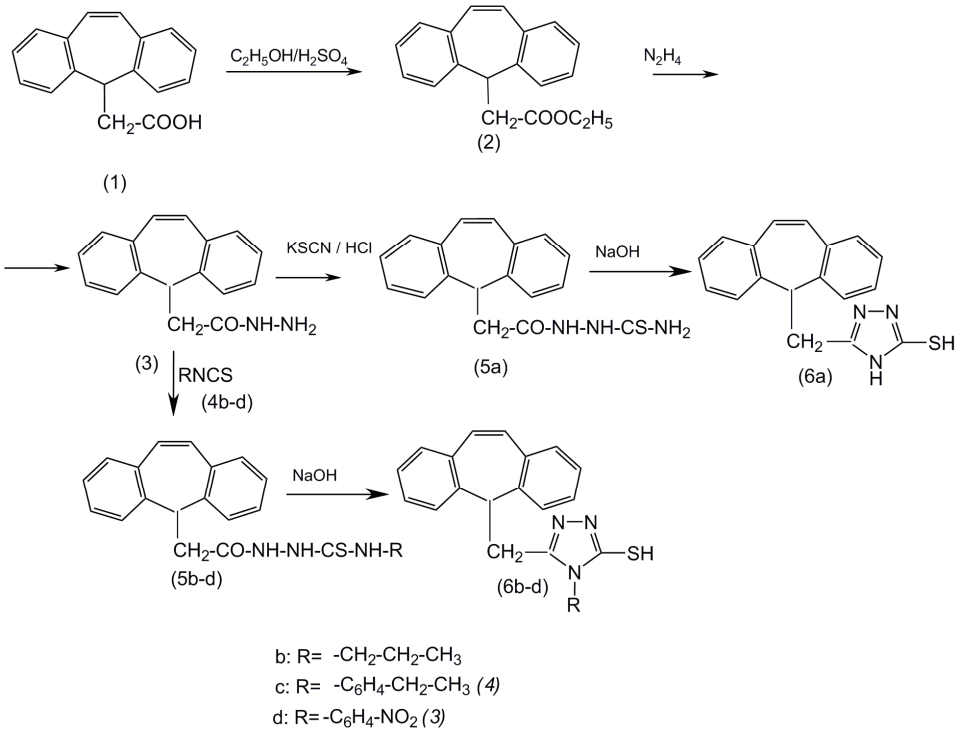

Scheme 1. Reaction pathway to the target compounds **5a**–**d** and **6a**–**d**.

The synthesis of the new compounds was realized in several steps, starting from 5*H*-dibenzo[*a*,*d*][7]annulen-5-ylacetic acid (**1**) that was transformed into the

ethyl ester **2**. Ethyl 5*H*-dibenzo[*a*,*d*][7]annulen-5-ylacetate (**2**) was reacted with hydrazine hydrate according to a literature method[14,22,23] affording 2-(5*H*-dibenzo[*a*,*d*][7]annulen-5-yl)acetohydrazide (**3**).

2-(5*H*-Dibenzo[*a*,*d*][7]annulen-5-ylacetyl)hydrazinecarbothioamide (**5a**) was obtained by refluxing **3** with KSCN and concentrated HCl.

The new 2-(5*H*-dibenzo[*a*,*d*][7]annulen-5-ylacetyl)-*N*-alkyl/arylhydrazinecarbothioamides **5b**–**d** were obtained by nucleophilic addition of **3** to different alkyl or aryl isothiocyanates **4b**–**d**.[14,15,24,25]

The new 5-(5*H*-dibenzo[*a*,*d*][7]annulen-5-ylmethyl)-4-alkyl/aryl-4*H*-1,2,4-triazole-3-thiols **6a**–**d** were synthesized by subjecting **5a**–**d** to intramolecular cyclization in 8 % sodium hydroxide solution under reflux.[14–16,26,27]

Analytical and spectral data of the newly prepared compounds

The spectral data of all the newly synthesized hydrazinecarbothioamides and 1,2,4-triazoles are given in the Supplementary Material to this paper. The data are in accordance with the proposed structures. The general structure of **5** with atom numbering is given Fig. 1.

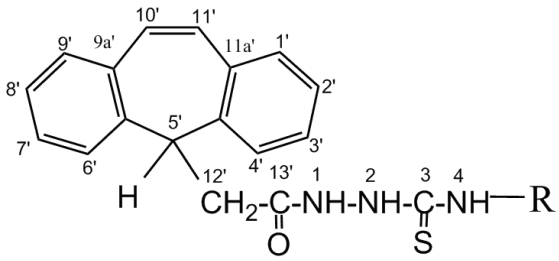

Fig. 1. The general structure of **5** with atom numbering.

The nucleophilic addition of 2-(5*H*-dibenzo[*a*,*d*][7]annulen-5-yl)acetohydrazide to KSCN and various isothiocyanates was confirmed in the infrared spectra of the new acylhydrazinecarbothioamides **5a**–**d** by the appearance of new absorption bands due to the stretching vibration of the C=S group (1256–1259 cm^{-1}), the NO_2 group (1566, 1350 cm^{-1}) and the stretching vibration of the CH_3 group. The C=O and N–H stretching bands were present at 1686–1674 and 3419–3184 cm^{-1}, respectively.

The structures of the 1,2,4-triazole-3-thiols **6a**–**d** were also proved based on their spectral data. The IR spectra confirmed the cyclization of **5a**–**d** to **6a**–**d** by the disappearance of the $\nu_{C=O}$ band. Moreover, instead of two or three NH bands of compound **5,** compound **6** exhibited only one band in KBr at 3419–3092 cm^{-1}, characteristic for the –NH–CS group. It seems that in KBr, the mercaptotriazole **6** existed in the form of their thionic tautomers (Scheme 2).

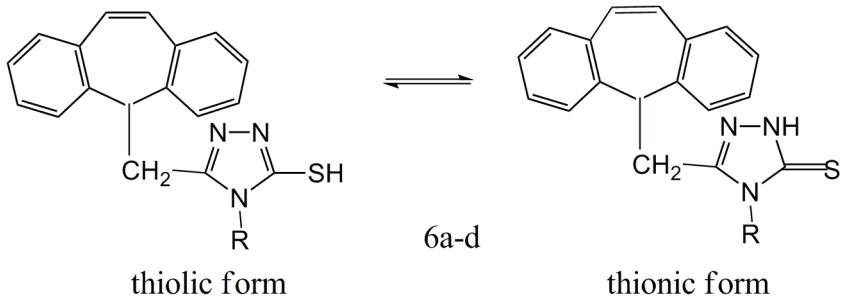

Scheme 2. Tautomeric forms of the mercaptotriazoles **6a**–**d**.

The ^{1}H-NMR spectra of carbothioamides **5a**–**d** indicated the presence of two isomers, 5′-axial and 5′-equatorial in a ratio of about 3:1, interconvertible by middle ring inversion (Scheme 3).

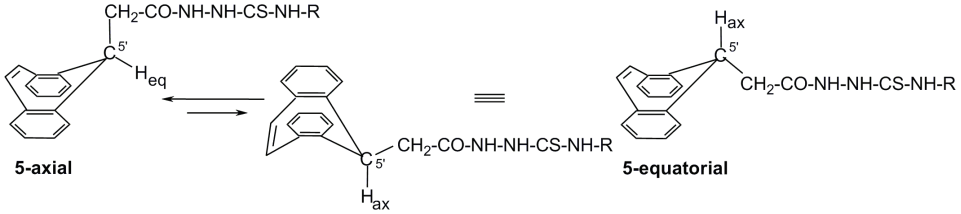

Scheme 3. Interconversion of the acylcarbothioamides **5a**–**d** between the 5′-axial and 5′-equatorial isomers by middle ring inversion.

The NH protons signals appear as singlets between 8.13–10.30 ppm, the double bond protons H$^{10'}$ and H$^{11'}$ appear as singlets at 7.01–7.07 ppm. The aliphatic side chains protons also exhibited normal δ values.

In the ^{13}C-NMR spectra of **5a–d**, the dibenzo[*a*,*d*][7]annulene moiety appears in a narrow δ domain (123–140 ppm), with C$^{10'}$ and C$^{11'}$ easily recognizable at δ 130.9–131.7 ppm. The signal at $\delta \approx 181$ ppm could be attributed to the C=S carbon atom. The remaining carbon atoms afforded signals that partially overlapped with those of the side chains. However, the assignments of these signals could be made using incremental calculations for the substituents and the results were very similar to those of the triazoles **6a**–**d**.

The ^{1}H-NMR spectra of triazoles **6a**–**d** indicated the presence of a single conformational isomer, namely the axial one.

Surprisingly, cyclization of **5** to **6** and the subsequent work-up were accompanied by the loss of the minor equatorial isomer, probably because of its higher solubility in the acidic water.

The H$^{5'}$(eq.) appears at δ 4.35–4.61 ppm (triplet, J = 7.7 Hz) and CH$_2$$^{12'}$ protons as a doublet at 2.89–3.01 ppm in **6a**–**d**. Interestingly, the NH signals of **5b**–**d** totally disappeared being replaced by a singlet at δ 10.85–11.70 ppm, attri-

butable to the SH proton. In the case of triazole **6a**, a singlet appears at 9.04 ppm attributed to the NH group and another one at 10.85 ppm attributed to the SH group.

Thus, in solution, the equilibrium is shifted towards the thiolic form.

Conversion of carbothioamides **5** to triazoles **6** is also nicely supported by ^{13}C-NMR spectra in which a new quaternary carbon signal (for C_3) appears at δ 165.69–168.37 ppm simultaneously with the disappearance of the C=S signal from **5** (δ 181 ppm). Moreover, instead of C=O signal from **5** at 169–170 ppm, a new signal appears for C_5 of **6** at about 150–151 ppm.

Triticum bioassay

The effects of the title compounds **5a**–**d** and **6a**–**d** on the sprouting of wheat were investigated. After treating with solutions of 0.5, 0.25 and 0.05 mM concentrations of compounds **5a**–**d** and **6a**–**d** for 5 days, from the difference in length between the main root of caryopses treated with the title compounds and those treated with distilled water (last day), the plant growth regulating activities of the compounds were determined from the formula:

$$\text{Effect (\%)} = 100 - \frac{\text{length of sample radicle} - 10\text{ mm}}{\text{length of reference radicle} - 10\text{ mm}} \times 100$$

where 10 mm represents the initial length of the main root. A positive result represents inhibition, whereas a negative result implies growth stimulation.

The results of the *Triticum* bioassay – the Constantinescu method (the root elongation values for each sample tested in the day) are presented in Table I.

The compounds **5a**–**d** and **6a**–**c** inhibited root growth at all concentrations, without cytotoxicity (Table I). The inhibitory activity declined with decreasing applied concentration.

The microscopic examination of the wheat embryonic roots showed mitodepressive and mitostatic effects for 0.50 and 0.25 mM concentrations: the shape of the cell was irregular and nuclei with a hypertrophied nucleolus were observed. At 0.05 mM concentration (except for compound **5a**), phases of normal division were noticed, the aspect being generally similar to that observed for the control.

CONCLUSIONS

In this paper, the synthesis and characterization of four new acetylhydrazinecarbothioamides and four 4*H*-1,2,4-triazole-3-thiol derivatives containing 5*H*-dibenzo[*a*,*d*][7]annulene moiety were presented. The structures of new compounds were confirmed by spectral data (IR-, UV-, ^{1}H-NMR and ^{13}C-NMR).

All the compounds were investigated for their biological activities concerning regulation of the growth of wheat using the phytobiological method – the Triticum test. A microscopic study demonstrated mitosis inhibition activity for compounds **5a**–**d** and **6a**–**d**, without cytotoxicity.

SUPPLEMENTARY MATERIAL

Analytical and spectral data of the synthesized compounds are available electronically from http://www.shd.org.rs/JSCS/, or from the corresponding author on request.

Acknowledgements. This paper is supported by the Sectoral Operational Programme Human Resources Development, financed from the European Social Fund and by the Romanian Government under the contract number POSDRU/89/1.5/S/64109.

И З В О Д

СИНТЕЗА И БИОЛОШКА АКТИВНОСТ НОВИХ АЦЕТИЛХИДРАЗИН-КАРБОТИОАМИДА И 1,2,4-ТРИАЗОЛА СУПСТИТУИСАНИХ 5*H*-ДИБЕНЗО[*a*,*d*][7]АНУЛЕНИМА

LAURA I. SOCEA[1], THEODORA V. APOSTOL[1], GABRIEL ŞARAMET[1], ŞTEFANIA F. BĂRBUCEANU[1], CONSTANTIN DRAGHICI[2] и MIHAELA DINU[1]

[1]*Carol Davila University of Medicine and Pharmacy, Faculty of Pharmacy, Organic Chemistry Department, Traian Vuia Street 6, 020956, Bucharest, Romania и* [2]*C. D. Neniţescu Institute of Organic Chemistry, Romanian Academy, Splaiul Independenţei 202B, 060023, Bucharest, Romania*

Описана је синтеза нових деривата **5a**–**d** 5*H*-дибензо[*a*,*d*][7]анулена. Анализа ^{1}H-NMR спектара указује на присуство два конформациона изомера, доминантниог (око 75%) аксијалног и споредног екваторијалног (око 25 %), који подлежу конформационој измени инверзијом средњег прстена. Циклизацијом деривата **5a**–**d** у раствору натријум-хидроксида добијају се одговарајући деривати **6a**–**d**, 4*H*-1,2,4-триазол-3-тиоли, који су добијени као чисти аксијални изомери. Сва нова једињења окарактерисана су елементалном анализом, IR, UV, ^{1}H-NMR и ^{13}C-NMR спектроскопијом и испитана им је биолошка активност фитобиолошким тестом.

(Примљено 20. фебруара, ревидирано 20. јуна 2012)

REFERENCES

1. M. Ilies, M. D. Banciu, A. Scozzafava, M. A. Ilies, M. T. Caproiu, C. T. Supuran, *Bioorg. Med. Chem.* **11** (2003) 2227
2. L. I. Socea, G. Saramet, B. Socea, C. Draghici, *Rev. Chim*. **57** (2006) 1242
3. M. Martindale, *The Extra Pharmacopoeia*, 30th ed., Pharmaceutical Press, London, 1993, pp. 932, 935
4. J. L. Munoz-Bellido, S. Munoz-Crido, J. A. Garcia Rodriguez, *Int. J. Antimicrob. Agents* **14** (2000) 177
5. A. Qandil, H. N. Tuma, M. A. Hassan, *Acta Pharm. Sci*. **48** (2006) 95
6. N. Siddiqui, S. Alam, W. Ahsan, *Acta Pharm*. **58** (2008) 445
7. P. Yogeeswari, D. Srirama, V. Saraswata, J. Vaigunda Ragavendrana, M. Mohan Kumara, S. Murugesana, R. Thirumurugana, J. P. Stablesb, *Eur. J. Pharm. Sci.* **20** (2003) 341
8. G. Küçükgüzel, A. Kocatepe, E. De Clercq, F. Şahin, S. Güllüce, *Eur. J. Med. Chem.* **41** (2006) 353
9. G. L. Almajan, S. F. Barbuceanu, E. R. Almajan, C. Draghici, G. Saramet, *Eur. J. Med. Chem.* **44** (2009) 3083
10. S. F. Barbuceanu, G. L. Almajan, I. Saramet, C. Draghici, A. I. Tarcomnicu, G. Bancescu, *Eur. J. Med. Chem.* **44** (2009) 4752

11. S. F. Barbuceanu, G. L. Almajan, I. Saramet, C. Draghici, R. Socoteanu, F. Barbuceanu, *J. Serb. Chem. Soc*. **74** (2009) 1041
12. J. Jin, L. Zhang, A. Zhang, X. X. Lei, J. H. Zhu, *Molecules* **12** (2007) 1596
13. S. Monazza, A. Tashfeen, S. Hameed, K. M. Khan, *ARKIVOC* **2009** (2009) 210
14. I. Saramet, A. Banciu, L. Socea, C. Drăghici, M. Banciu, *Heterocycl. Comm.* **9** (2003) 653
15. L. I. Socea, I. Saramet, S. Barbuceanu, B. Draghici, *Rev. Chim*. **56** (2005) 1154
16. L. I. Socea, I. Saramet, C. Gard, B. Draghici, *Rev. Chim.* **57** (2006) 75
17. L. I. Socea, I. Saramet, B. Socea, B. Draghici, *Rev. Chim.* **57** (2006) 1123
18. L. I. Socea, I. Saramet, B. Socea, C. Draghici, *Rev. Chim.*, **58** (2007), 328
19. D. G. Constantinescu, G. Retezeanu, R. Oţeleanu, M. Constantinescu, *Pharmazie* **18** (1963) 699
20. S. F. Barbuceanu, L. G. Almajan, E. R. Almajan, M. Dinu, C. Draghici, C. Gard, G. Saramet, *Rev. Chim*. **60** (2009) 810
21. D. G. Constantinescu, E. Haţieganu, *Biologia moleculară a celulei vegetale*, Editura Medicală, Bucureşti, 1983, 67 (in Romanian)
22. N. Nossek, *Bull. Stiintific Stud., IPB Ser. Chem.-Metallurgy* **I** (1977) 80
23. J. Burbiel, *ARKIVOC* **2006** (2006) 16
24. M. Wujec, J. Stefaska, A. Siwek, M. Tatarczak, *Acta Pol. Pharm.* **66** (2009) 73
25. E. Tatar, I. Küçükgüzel, E. De Clercq, F. Şahin, M. Güllücec, *ARKIVOC* **2008** (2008) 191
26. M. Rasir, A. L. Rauf, *Indian J. Chem., B* **48** (2009) 97
27. S. Shelke, G. Mhaske, S. Gadakh, C. Gill, *Bioorg. Med. Chem. Lett.* **20** (2010) 7200.

Journal of the Serbian Chemical Society
JSCS@tmf.bg.ac.rs • www.shd.org.rs/JSCS
J. Serb. Chem. Soc. 77 (11) S209–S212 (2012) *Supplementary material*

SUPPLEMENTARY MATERIAL TO

Synthesis and root growth activity of some new acetylhydrazinecarbothioamides and 1,2,4-triazoles substituted with the 5*H*-dibenzo[*a*,*d*][7]annulene moiety

LAURA I. SOCEA[1]*, THEODORA V. APOSTOL[1], GABRIEL ŞARAMET[1], ŞTEFANIA F. BĂRBUCEANU[1], CONSTANTIN DRAGHICI[2] and MIHAELA DINU[1]

[1]*Carol Davila University of Medicine and Pharmacy, Faculty of Pharmacy, Organic Chemistry Department, Traian Vuia Street 6, 020956, Bucharest, Romania and* [2]*C. D. Nenițescu Institute of Organic Chemistry, Romanian Academy, Splaiul Independenței 202B, 060023, Bucharest, Romania*

J. Serb. Chem. Soc. 77 (11) (2012) 1541–1549

ANALYTICAL AND SPECTRAL DATA FOR THE SYNTHESIZED COMPOUNDS

*2-(5*H*-Dibenzo[*a,d*][7]annulen-5-ylacetyl)hydrazinecarbothioamide* (***5a***). Yield: 87.0 %; m.p.: 146–148 °C; Anal. Calcd. for Anal. Calcd. for $C_{18}H_{17}N_3OS$ (FW: 323.24): C, 66.87; H, 5.26; N, 12.99; S, 9.92 %. Found: C, 66.83; H, 5.30; N, 12.98; S, 9.95 %; IR (KBr, cm^{-1}): 3419, 3214, 3184 (N–H stretching), 3068, 3018 (C–H stretching of aromatic ring), 2967, 2859 (CH_2 stretching), 1686 (C=O stretching), 1611, 1532, 1491 (C=C stretching), 1259 (C=S stretching); ^{1}H-NMR (300 MHz, DMSO-d_6, δ / ppm): 10.11, 9.53, 9.06, 8.13 (*s*, NH), 7.87 (2H, *bs*, NH_2), 7.42–7.20 (8H, *m*, aromatic), 7.01 (2H, *s*, CH=CH), 4.60 (1H, *t*, *J* = 7.4 Hz, CH axial isomer), 3.70 (1H, *t*, *J* = 7.4 Hz, CH equatorial isomer), 3.32 (2H, *d*, *J* = 7.4 Hz, CH_2–CO equatorial isomer), 2.52 (2H, *d*, *J* = 7.4 Hz, **C**H_2–CO axial isomer); ^{13}C-NMR (75 MHz, DMSO-d_6, δ / ppm): 181.56 (C=S), 169.63 (C=O), 131.19 (CH=CH equatorial isomer), 130.70 (CH=CH axial isomer), 139.79, 139.46, 133.7, 129.54, 129.46, 128.73, 128.71, 127.50, 126.50, 125.78, 125.43 (aromatic ring), 48.85 (CH), 34.29 (CH_2); UV–Vis (CH_3OH) (λ_{max} / nm (log ε)): 210.6 (4.34), 227.8 (4.25), 239.2 (4.13), 291.2 (4.04).

*2-(5*H*-Dibenzo[*a,d*][7]annulen-5-ylacetyl)*-N*-propylhydrazinecarbothioamide* (***5b***). Yield: 81.1 %; m.p.: 172–173 °C; Anal. Calcd. for $C_{21}H_{23}N_3OS$ (FW: 365.27): C, 69.04; H, 6.30; N, 11.50; S, 8.78 %. Found: C, 69.01; H, 6.34; N, 11.48; S, 8.75 %. IR (KBr, cm^{-1}): 3370, 3201 (N–H stretching), 3070, 3017 (C–H stretching of aromatic ring), 2961, 2867 (CH_3 stretching), 2933, 2847 (CH_2 stretching), 1688 (C=O stretching), 1534 (C=C stretching), 1256 (C=S stretch-

* Corresponding author. E-mail: laurasocea@gmail.com

ing); ^{1}H-NMR (300 MHz, DMSO-d_6, δ / ppm): 10.05, 9.46, 9.22, 8.97 (*s*, NH), 7.40–7.18 (8H, *m*, aromatic), 7.07 (2H, *s*, CH=CH), 4.61 (1H, *t*, *J* = 7.3 Hz, CH), 3.30 (2H, *t*, *J* = 7.3 Hz, N–CH_2), 2.54 (2H, *d*, *J* = 7.3 Hz, CH_2–CO), 1.40 (2H, *sx*, *J* = 7.3 Hz, C**H**$_2$–CH_3), 0.78 (3H, *t*, *J* = 7.3 Hz, CH_3); ^{13}C–NMR (75 MHz, DMSO-d_6, δ / ppm): 181.84 (C=S), 169.73 (C=O), 131.14 (CH=CH equatorial isomer), 130.70 (CH=CH axial isomer), 139.92, 133.76, 129.46, 129.45, 128.61, 128.35, 127.50, 126.40 (aromatic ring), 48.96 (CH), 45.22 (N–CH_2), 34.76 (**C**H_2–CO), 21.81 **C**H_2–CH_3), 10.92 (CH_3); UV–Vis (CH_3OH) (λ_{max} / nm (log ε)): 226.4 (4.42), 239.2 (4.39), 291.2 (4.24).

*2-(5*H*-Dibenzo[*a,d*)[7]annulen-5-ylacetyl)*-N*-(4-ethylphenyl)hydrazinecarbothioamide (**5c**)*. Yield: 66.6 %; m.p.: 102–104 °C; Anal. Calcd. for $C_{26}H_{25}N_3OS$ (FW: 427.32): C, 73.07; H, 5.85; N, 9.83; S, 7.50 %. Found: C, 73.03; H, 5.84; N, 9.82; S, 7.52 %; IR (KBr, cm^{-1}): 3335, 3226 (N–H stretching), 3043, 3019 (C–H stretching of aromatic ring), 2963, 2871 (CH_3 stretching), 2930, 2828 (CH_2 stretching), 1678 (C=O stretching), 1595, 1526 (C=C stretching), 1259 (C=S stretching); ^{1}H-NMR (300 MHz, DMSO-d_6, δ / ppm): 10.30, 9.70, 9.60, 9.37 (1H, *s*, NH), 7.45–7.10 (12H, *m*, aromatic), 7.02 (2H, *s*, CH=CH), 4.63 (1H, *t*, *J* = 7.3 Hz, CH axial isomer), 3.75 (1H, *t*, *J* = 7.3 Hz, CH equatorial isomer), 3.42 (2H, *d*, *J* = 7.3 Hz, CH_2–CO equatorial isomer), 2.61 (2H, *d*, *J* = 7.3 Hz, CH_2–CO axial isomer), 2.58 (2H, *q*, *J* = 7.3 Hz, C**H**$_2$–CH_3), 1.48 (3H, *t*, *J* = 7.3 Hz, CH_3); ^{13}C-NMR (75 MHz, DMSO-d_6, δ / ppm): 180.95 (C=S), 170.34 (C=O), 131.37 (CH=CH equatorial isomer), 130.90 (CH=CH axial isomer), 140.03, 139.61, 134.95, 133.83, 129.69, 128.89, 128.62, 127.47, 127.25, 126.65 (aromatic ring), 48.81 (CH), 34.65 (**C**H_2–CO), 27.78 (**C**H_2–CH_3), 15.74 (CH_3); UV–Vis (CH_3OH) (λ_{max} / nm (log ε)): 221.6 (4.45), 280.6 (4.27).

*2-(5*H*-Dibenzo[*a,d*)[7]annulen-5-ylacetyl)*-N*-(3-nitrophenyl)hydrazinecarbothioamide (**5d**)*. Yield: 71.6 %; m.p.: 202–203 °C; Anal. Calcd. for $C_{24}H_{20}N_4O_3S$ (FW: 444.27): C, 64.88; H, 4.50; N, 12.60; S, 7.22 %. Found: C, 64.89; H, 4.52; N, 12.59; S, 7.23 %; IR (KBr, cm^{-1}): 3334, 3287, 3188 (N–H stretching), 3063, 3021 (C–H stretching of aromatic ring), 2960, 2864 (CH_2 stretching), 1674 (C=O stretching), 1599, 1531, 1494 (C=C stretching), 1599, 1345 (NO_2 stretching), 1258 (C=S stretching); ^{1}H-NMR (300 MHz, DMSO-d_6, δ / ppm): 9.81, 9.78, 9.70 (*s*, NH), 7.98 (1H, *d*, *J* = 8.0 Hz, CH–nitrophenyl), 7.82 (1H, *dd*, *J* = 8.0, 1.7 Hz, CH–nitrophenyl), 7.59 (1H, *t*, *J* = 8.0, CH–nitrophenyl), 7.50–7.18 (9H, *m*, aromatic), 7.03 (2H, *s*, CH=CH), 4.64 (1H, *t*, *J* = 7.3 Hz, CH), 2.62 (2H, *d*, *J* = 7.3 Hz, CH_2–CO); ^{13}C–NMR (75 MHz, DMSO-d_6, δ / ppm): 181.02 (C=S), 170.47 (C=O), 131.37 (CH=CH equatorial isomer) 130.91 (CH=CH axial isomers), 140.34, 140.04, 139.57, 134.94, 133.83, 129.72, 129.63, 128.90, 128.63, 126.66, 125.66, 123.06 (aromatic ring), 48.68 (CH), 34.64 (**C**H_2–CO); UV–Vis (CH_3OH) (λ_{max} / nm (log ε)): 227.8 (4.56), 274.9 (4.34).

*5-(5*H*-Dibenzo[*a,d*][7]annulen-5-ylmethyl)-4*H*-1,2,4-triazole-3-thiol* (***6a***). Yield: 71.5 %; m.p.: 251–253 °C; Anal. Calcd. for $C_{18}H_{15}N_3S$ (FW: 305.24): C, 70.82; H, 4.94; N, 13.78; S, 10.50 %. Found: C, 70.79; H, 4.95; N, 13.76; S, 10.51 %; IR (KBr, cm^{-1}): 3414 (N–H stretching), 3089, 3019 (C–H stretching of aromatic ring), 2848, 2925 (CH_2 stretching), 1592 (C=N stretching of triazole ring), 1492 (C=C stretching), 1213 (C=S stretching); ^{1}H-NMR (300 MHz, $CDCl_3$, δ / ppm): 10.85 (1H, *s*, SH), 9.04 (1H, *s*, NH), 7.42–7.23 (8H, *m*, aromatic), 7.03 (2H, *s*, CH=CH), 4.61 (1H, *t*, *J* = 8.0 Hz, CH), 2.89 (2H, *d*, *J* = = 8.0 Hz, CH_2–C_5-triazole); ^{13}C-NMR (75 MHz, $CDCl_3$, δ / ppm): 165.69 (triazole-C_3), 150.30 (triazole-C_5), 131.16 (CH=CH), 138.78, 133.65, 130.59, 129.73, 129.28, 127.53 (aromatic ring), 50.69 (CH), 25.98 (**C**H_2–C_5-triazole); UV––Vis (CH_3OH) (λ_{max} / nm (log ε)): 225.5 (4.01), 292.1 (3.90).

*5-(5*H*-Dibenzo[*a,d*][7]annulen-5-ylmethyl)-4-propyl-4*H*-1,2,4-triazole-3-thiol* (***6b***). Yield: 62.5 %; m.p.: 153–155 °C, Anal. Calcd. for $C_{21}H_{21}N_3S$ (FW: 347.27): C, 72.63; H, 6.05; N, 12.09; S, 9.23 %. Found: C, 72.59; H, 6.09; N, 12.06; S, 9.20 %; IR (KBr, cm^{-1}): 3119 (N–H stretching), 3093, 3021 (C–H stretching of aromatic ring), 2970, 2875 (CH_3 stretching), 2938 (CH_2 stretching), 1562 (C=N stretching of triazole ring), 1499, 1480 (C=C stretching), 1245 (C=S stretching); ^{1}H-NMR (300 MHz, $CDCl_3$, δ / ppm): 11.70 (1H, *s*, SH), 7.32–7.18 (8H, *m*, aromatic), 7.01 (2H, *s*, CH=CH), 4.69 (1H, *t*, *J* = 7.7 Hz, CH), 3.52 (2H, *t*, *J* = 7.6 Hz, N–CH_2), 3.09 (2H, *d*, *J* = 7.7 Hz, CH_2–C_5-triazole), 1.49 (2H, *sx*, *J* = 7.6 Hz, C**H**$_2$–CH_3), 0.82 (3H, *t*, *J* = 7.6 Hz, CH_3); ^{13}C-NMR (75 MHz, $CDCl_3$, δ / ppm): 166.49 (triazole-C_3), 151.03 (triazole-C_5), 130.88 (CH=CH), 138.60, 133.67, 129.87, 129.77, 129.17, 127.14 (aromatic ring), 52.40 (CH), 44.89 (N–CH_2), 26.11 (CH_2–C_5-triazole), 21.51(**C**H_2–CH_3), 10.93 (CH_3); UV–Vis (CH_3OH) (λ_{max} / nm (log ε)): 227.3 (4.23), 256.4 (4.16), 290.3 (3.99).

*5-(5*H*-Dibenzo[*a,d*][7]annulen-5-ylmethyl)-4-(4-ethylphenyl)-4*H*-1,2,4-triazole-3-thiol* (***6c***). Yield: 68.4 %; m.p.: 219–221 °C; Anal. Calcd. for $C_{26}H_{23}N_3S$ (FW: 409.32): C, 76.28; H, 5.62; N, 10.26; S, 7.83 %. Found: C, 76.31 ;H, 5.61; N, 10.22; S, 7.87 %; IR (KBr, cm^{-1}): 3410 (N–H stretching), 3069, 3020 (C–H stretching of aromatic ring), 2964, 2873 (CH_3 stretching), 2929 (CH_2 stretching), 1567 (C=N stretching of triazole ring), 1514, 1490 (C=C stretching), 1234 (C=S stretching); ^{1}H-NMR (300 MHz, $CDCl_3$, δ / ppm): 10.98 (1H, *s*, SH), 7.43–7.15 (10H, *m*, aromatic), 6.81 (2H, *d*, *J* = 8.0 Hz, aromatic), 6.62 (2H, s, CH=CH), 4.35 (1H, *t*, *J* = 8.0 Hz, CH), 2.98 (2H, *d*, *J* = 8.0 Hz, CH_2–C_5-triazole), 2.76 (2H, *q*, *J* = 7.8 Hz, C**H**$_2$–CH_3), 1.34 (3H, *t*, *J* = 7.8 Hz, CH_3); ^{13}C-NMR (75 MHz, $CDCl_3$, δ / ppm): 167.39 (triazole-C_3), 151.57 (triazole-C_5), 130.60 (CH=CH), 146.92, 138.48, 133.79, 130.60, 129.93, 129.41, 128.98, 127.76, 126.98, 125.75 (aromatic ring), 52.58 (CH), 28.64 (**C**H_2–CH_3), 26.00 (**C**H_2–C_5-triazole), 15.45 (CH_3); UV–Vis (CH_3OH) (λ_{max} / nm (log ε)): 214.1 (4.40), 266.5 (4.12).

*5-(5*H*-Dibenzo[*a,d*][7]annulen-5-ylmethyl)-4-(3-nitrophenyl)-4*H*-1,2,4-triazole-3-thiol* (***6d***). Yield: 86.5 %; m.p.: 134–136 °C; Anal. Calcd. for $C_{24}H_{18}N_4O_2S$ (FW: 426.28): C, 67.62; H, 4.22; N, 13.14; S, 7.52 %. Found: C, 67.58; H, 4.25; N, 13.16; S, 7.49 %; IR (KBr, cm^{-1}): 3092 (N–H stretching), 3071, 3022 (C–H stretching of aromatic ring), 2932, 2845 (CH_2 stretching), 1566 (C=N stretching of triazole ring), 1534, 1491 (C=C stretching), 1526, 1350 (NO_2 stretching), 1229 (C=S stretching); ^{1}H-NMR (300 MHz, $CDCl_3$, δ / ppm): 11.34 (1H, *s*, SH), 7.67 (1H, *t*, *J* = 2.1 Hz, CH-nitrophenyl), 7.64 (1H, *t*, *J* = 8.3 Hz, CH–nitrophenyl); 7.39 (1H, *ddd*, *J* = 1.0, 2.1, 8.3 Hz, CH-nitrophenyl), 7.32––7.15 (9H, *m*, aromatic), 6.51 (2H, *s*, CH=CH), 4.45 (1H, *t*, *J* = 7.7 Hz, CH), 3.01 (2H, *d*, *J* = 7.7 Hz, CH_2–C_5-triazole); ^{13}C-NMR (75 MHz, $CDCl_3$, δ / ppm): 168.37 (triazole-C_3), 151.23 (triazole-C_5), 130.54 (CH=CH), 148.80, 138.20, 134.18, 133.72, 130.54, 130.25, 129.99, 129.50, 129.27, 127.27, 124.34, 123.81, (aromatic ring), 52.63 (CH), 26.27 (CH_2–C_5-triazole); UV–Vis (CH_3OH) (λ_{max} / / nm (log ε)): 215.0 (4.41), 285.0 (4.18).

Journal of the Serbian Chemical Society
JSCS-info@shd.org.rs • www.shd.org.rs/JSCS
J. Serb. Chem. Soc. 77 (11) 1551–1560 (2012)
JSCS–4370
UDC 677.027.423.1/.2:677.027.625.122
Original scientific paper

Synthesis, characterization and dyeing behaviour of heterocyclic acid dyes and mordant acid dyes on wool and silk fabrics

HITENDRA M. PATEL*

Department of Chemistry, V. P. & R. P .T. P Science College, Vallabh Vidyanagar-388 120, Gujarat State, India

(Received 10 January, revised 3 May 2012)

Abstract: Novel heterocyclic acid and mordant acid dyes were synthesised by the coupling of a diazonium salt solution of different aromatic amines with 2-butyl-3-(4-hydroxybenzoyl)benzofuran. The resulting heterocyclic acid dyes were characterized by elemental analysis, IR, ^{1}H-NMR and ^{13}C-NMR spectral studies and UV–Vis spectroscopy. The dyeing performances of all the heterocyclic acid dyes were evaluated on wool and silk fabrics. The dyeing of chrome pre-treated wool and silk fabrics showed better hues on mordanted fabrics. The dyeing of wool and silk fabrics resulted in pinkish blue to red shades with very good depth and levelness. The dyed fabrics showed excellent to very good light, washing, perspiration, sublimation and rubbing fastness.

Keywords: heterocyclic acid dye; mordant acid dye; light fastness; washing fastness and rubbing fastness.

INTRODUCTION

Traditionally, heterocyclic acid dyes are the most important class of commercial dyes that contain phenols as intermediates and occupying more than half of the dye chemistry.[1–7] If they contain sodium salts of a sulphonic acid group in addition to a phenolic group, they are referred to as an acid azo dye. All such dyes having phenolic and sulphonic acid moieties contain hydroxyl (–OH) and sulphonic (–SO_3H) groups as auxochromic groups. One such auxochromic (–OH) and chromophoric (C=O) groups containing compound, *i.e.*, 2-butyl-3-(4-hydroxybenzoyl)benzofuran, has shown wide applications as a polymer additive. It is also known for its excellent UV absorbing capacity,[8,9] as it prevents the photodegradation of most vinyl polymers.[10–13] The formation of heterocyclic acid dyes and mordant acid dyes based on this compound has not been developed, except in a few patents.[14–16] Considering the above-mentioned importance of 2-butyl-3-(4-hydroxybenzoyl)benzofuran, it was planned to explore the field of

* Correspondence E-mail: shreeniketan71@yahoo.in
doi: 10.2298/JSC120110047P

acid azo dyes based on this compound, which may yield dyes with good hue properties. Hence, in continuation of earlier work,[17–21] the present communication comprises the synthesis, characterization and dyeing assessment of novel heterocyclic acid dyes and mordent acid dyes based on 2-butyl-3-(4-hydroxybenzoyl)benzofuran. The proposed synthetic route is shown in Scheme 1.

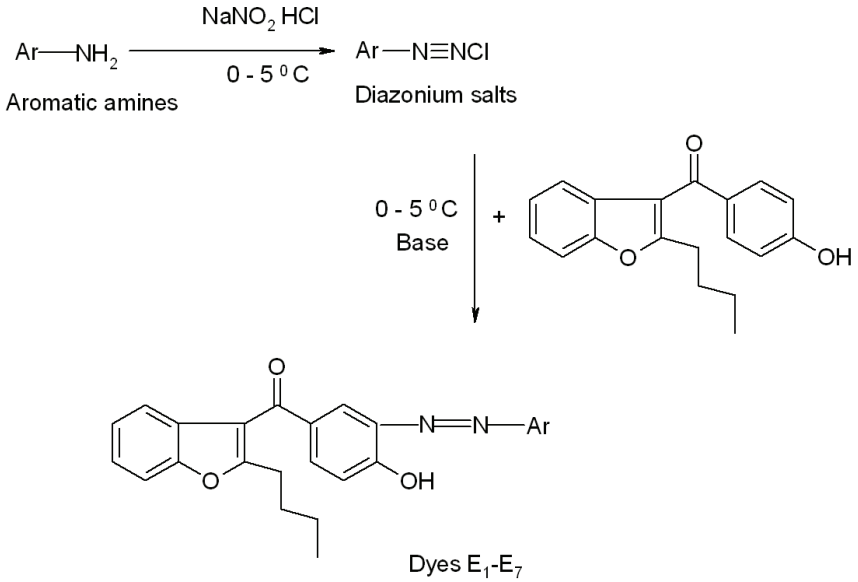

Scheme 1. Proposed synthetic route for the 2-butyl-3-(4-hydroxybenzoyl)benzofuran-based dyes **E_1–E_7**.

EXPERIMENTAL

All the employed chemicals were of analytical reagent grade. The aromatic amines shown in Table I were used for diazotization. The wool and silk fabrics were gifted by Color Tax (Pvt) Ltd., Surat, India. Melting points were determined by the open capillary method and are given uncorrected.

The UV–Vis absorption spectra were measured on a Carl Zeiss UV/Vis Specord spectrometer, and the elemental analyses were realized using a Perkin Elmer CHNS/O analyzer 2400 Series II. The infrared spectra were recorded in KBr pellets on a Perkin–Elmer Spectrum GX FT-IR model. The ^{1}H-NMR spectra were recorded on a Hitachi R-1500 (400 MHz) in DMSO-d_6 solvent, the ^{13}C-NMR spectra (75 MHz) were recorded on a Bruker Avance DPX 100 spectrometer. The purity of the dyes was checked by thin layer chromatography (TLC) on aluminium sheets pre-coated with silica gel 60 F_{254} (Merck, Germany) using a methanol–water–
–acetic acid (12:3:7) solvent system. The colour spots were visualized by a UV cabinet. An HTHP dyeing machine (model LL) was used for dyeing.

Synthesis of heterocyclic acid dyes

Diazotization. Diazotization of various aromatic amines was performed by a reported method.[22,23] Accordingly, each of the aromatic amines (0.0100 mol) was mixed with HCl (25 mL, 37 %) in a mortar, transferred to a 3-neck round bottom flask, and additional HCl (20 mL, 37 %) was added. To the resultant suspension, crushed ice (25 g) and $NaNO_2$ (2.5 mL, 4 M) were added. Diazotization was realized over 0.5 h at 0–5 °C under continuous stirring. The complete synthetic route is shown in Scheme 1 and the structures of the various aromatic amines and the corresponding heterocyclic acid dyes are shown in Table I.

Coupling procedure. The coupling of above mentioned diazotized aromatic amines (as shown in Table I) was performed by a method reported in the literature.[22,23] Thus, 2-butyl-3--(4-hydroxybenzoyl)benzofuran (2.15 g, 0.010 mol) was dissolved in an aqueous sodium hydroxide (100 mL, 0.10 M) solution. The clear solution was cooled in an ice–salt bath and the diazonium salt solution of an aromatic amine was added dropwise over a period of 30 min under vigorous stirring. The pH was maintained between 2.0 and 3.0 by the simultaneous addition of 10 % w/v sodium carbonate solution. Stirring was continued for 2 h, allowing the temperature to rise to ambient. The dye was then filtered off and dissolved in distilled water. Then the heterocyclic acid dye was obtained by evaporation and subsequently dried at room temperature. The dyes were designated as heterocyclic acid dyes $\mathbf{E_1}$–$\mathbf{E_7}$.

Acid mono azo dyeing method

Wool and silk fabrics are conveniently dyed in the laboratory at 90–130 °C and at a high pressure (166–207 kPa). A model glycerine bath, high temperature beaker and a HTHP (model LL) dyeing machine were used. For this purpose, a paste of finely powdered heterocyclic acid dyes (0.060 g) was prepared with the dispersing agent dodamol (0.090 g), the wetting agent Tween-80 (0.0060 g) and water (2.0 mL) in a ball mill. Water (10 mL) was added to this paste under stirring and the pH was adjusted to 2.0–4.0 using acetic acid. This dye suspension (100 mL) was added to a container provided with a lid and a screw cap. A wetted pattern of wool or silk fabric was rolled into the beaker and the lid was placed on the beaker and the metal cap tightened.

The beaker was then placed vertically on the rotatory carrier inside the tank and the clamp plate was firmly tightened. The rotatory carrier was then allowed to rotate in the glycerine bath and the temperature was raised to 90 °C at a rate of 2 °C min^{-1}. The dyeing was continued for 1 h under pressure. After cooling for 1 h, the beaker was removed from the bath and washed with distilled water. The dyed pattern was thoroughly washed with cold water and dried at room temperature.

Mordant dyeing method

A wool or silk fabric dye pattern obtained from the above-mentioned process was treated with 2% potassium dichromate solution equal to half of the weight of the heterocyclic acid dye. The fabric dye pattern was rolled into the container and the container was again placed vertically on the rotator carrier inside the tank and the dyeing was continued for 1 h under pres-sure. After cooling for 1 h, the container was removed from the bath and the fabric was washed with cold distilled water. Finally, the dyed pattern was thoroughly washed with warm water and air dried at room temperature.

Determination of the percentage exhaustion and fixation

The percentage exhaustion and fixation of the dyed fabrics were determined according to reported methods.[24]

Fastness property

All the fastness properties of the synthesized heterocyclic acid dyes and mordanted acid dyes were assessed, *i.e.*, the light, sublimation and perspiration fastnesses according to the British standard 1006-1978, the wash fastness according to the Indian standard IS: 765-1979 and the rubbing fastness using a Crock meter (Atlas) AATCC-1961.

RESULTS AND DISCUSSION

Physical properties of dyes

All the heterocyclic acid dyes obtained upon recrystallization from acetone were crystalline powders ranging in colour from pinkish blue to red. The purity of the dyes was checked by TLC using methanol–water–acetic acid (12:3:7) solvent system. A single spot was observed for each dye.

The analytical and spectral data of all the synthesized dyes are given in the Supplementary material to this paper.

The results of elemental analyses of each heterocyclic acid dyes were consistent with the predicted structure, given in Table I. The number of azo groups was almost one for each dye. The nitrogen content and number of azo groups for each dye were correlated with each other. The IR spectrum of each dye comprised the important features of aromatic, azo, hydroxyl, keto, sulphonic acid and carboxylic acid groups.

TABLE I. Structure of the aromatic amines and their corresponding heterocyclic acid dyes

Dye	Aromatic amines	Acid azo dye structure
E_1	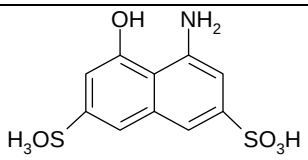	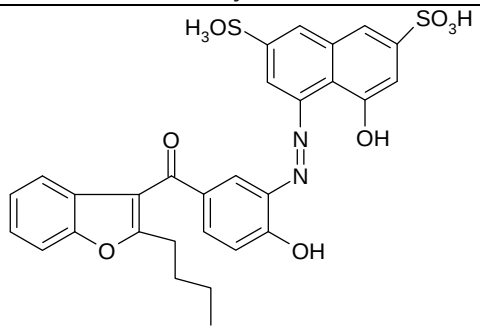
E_2	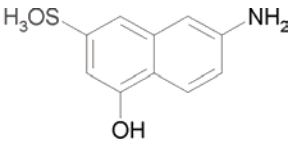	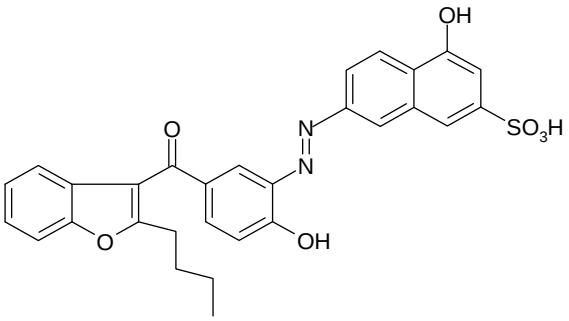

TABLE I. Continued

Dye	Aromatic amines	Acid azo dye structure
E$_3$	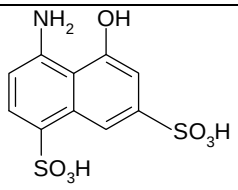	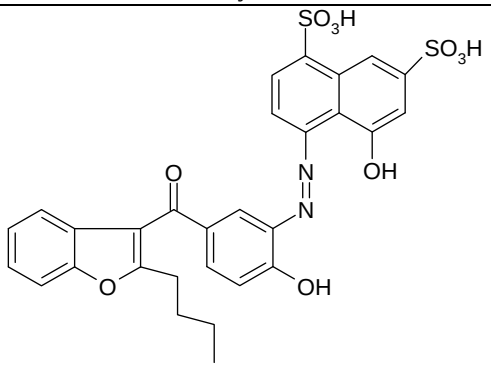
E$_4$	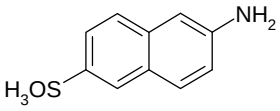	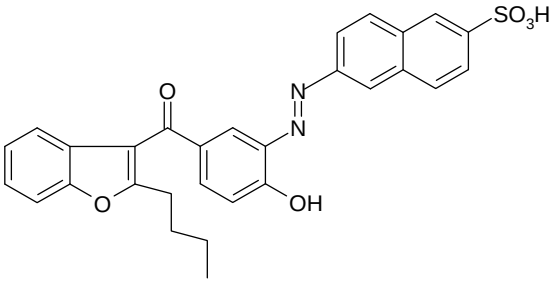
E$_5$	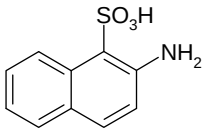	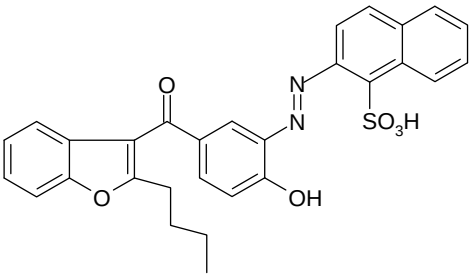
E$_6$	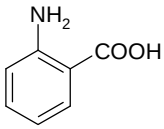	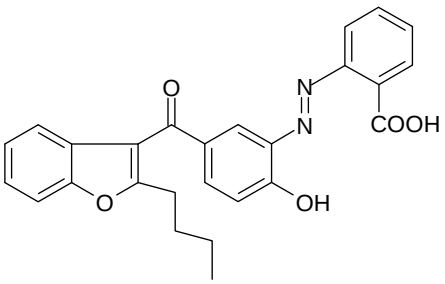

TABLE I. Continued

Dye	Aromatic amines	Acid azo dye structure
E$_7$	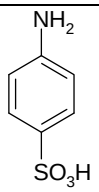	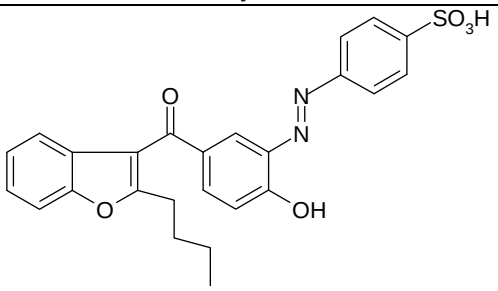

The ^{1}H-NMR spectra of all the heterocyclic acid dye compounds based on 2-butyl-3-(4-hydroxybenzoyl)benzofuran show important signals at their respective positions, confirming the structures of various heterocyclic acid dyes, as shown in Table I. The two OH protons in **E$_1$**, **E$_2$** and **E$_3$** resonated as a singlet at δ 5.35 ppm. In **E$_6$**, the –COOH proton gave a singlet at δ 11.0 ppm. The singlet of the –SO_3H proton resonated between δ 8.0 to 8.2 ppm in some of the heterocyclic acid dyes.

The visible absorption spectroscopic properties of the heterocyclic acid dyes were recorded in DMF. The absorption maxima (λ_{max}) of all the heterocyclic acid dyes fell in the range 428–472 nm in DMF and the values are given in Table II. The values of the logarithm of molar extinction coefficient (log ε) of all the dyes were in the range of 4.30–4.72, consistent with their high absorption intensity. Moreover, the presence of electron donating or electron withdrawing groups did not bring about any marked increase or decrease in λ_{max} in the visible region and the log ε value remained nearly constant.

TABLE II. Absorption maxima in DMF (λ_{max}), intensities (log ε), exhaustion (*E*) and fixation (*F*) of the heterocyclic acid dyes on wool and silk fabrics

Dye	λ_{max} / nm	log ε	Acid azo dyeing on wool		Acid azo dyeing on silk	
			E / %	*F* / %	*E* / %	*F* / %
E$_1$	472	4.73	73	86	70	87
E$_2$	450	4.54	70	80	72	84
E$_3$	443	4.45	74	84	83	92
E$_4$	446	4.47	82	81	76	84
E$_5$	432	4.34	74	78	88	90
E$_6$	428	4.30	80	82	76	85
E$_7$	438	4.36	83	88	74	91

However, an electron withdrawing substituent, such as –SO_3H and –COOH, in the structure of the dyes increases the polarizability and results in bathochromic shifts. This leads to a decrease in the energy between the highest

occupied molecular orbital and lowest unoccupied molecular orbital and thus the $\pi \rightarrow \pi^*$ electronic transition occurs at a lower frequency photon, resulting in a bathochromic shift of the visible absorption band.

Percentage exhaustion and fixation of the dyes

The results of the exhaustion and fixation of the dyes are given in Table II. Acid azo dyeing on wool and silk shows very good shades and if acid azo dyeing is compared with mordent azo dyeing then it clearly indicates that, due to chrome complex of dye, mordent dyeing shows better shades than acid dyeing.

Dyeing properties of dyes

The heterocyclic acid dyes were applied at a 2 % depth on wool and silk fabrics. Their dyeing properties are given in Tables III–VI. These dyes gave a wide range of colours varying from pinkish blue to red shades with good levelness, brightness and depth on the fabrics. The variation in the shades of the dye fabric results from both the nature and position of the substituent present on the diazotized compound. The dyeing showed excellent fastness to light, with very good to excellent washing, perspiration, rubbing and sublimation fastnesses.

TABLE III. Results of heterocyclic acid dyeing and their various fastness properties on wool fabrics; grading: 5 – excellent, 4 – very good, 3 – good, 2 – fair, 1 – poor

Dye	Colour shade on wool	Light fastness	Washing fastness	Perspiration fastness		Sublimation fastness	Rubbing fastness	
				Acid	Alkaline		Dry	Wet
E_1	Pinkish blue	5	4	4	5	5	4	3
E_2	Pinkish blue	5	4	4	4	4	3	4
E_3	Reddish brown	4	5	5	4	4	4	4
E_4	Yellowish pink	5	4	4	4	5	3	3
E_5	Chocolate brown	4	4	4	5	4	4	4
E_6	Red	5	5	5	4	4	3	3
E_7	Red	5	4	4	5	4	4	3

TABLE IV. Results of heterocyclic acid dyeing and their various fastness properties on silk fabrics; grading: 5 – excellent, 4 – very good, 3 – good, 2 – fair, 1 – poor

Dye	Colour shade on silk	Light fastness	Wash fastness	Perspiration fastness		Sublimation fastness	Rubbing fastness	
				Acid	Alkaline		Dry	Wet
E_1	Pinkish blue	4	4	4	4	4	4	3
E_2	Pinkish blue	5	5	4	4	4	3	3
E_3	Reddish brown	4	4	4	5	5	4	4
E_4	Yellowish pink	4	4	4	4	4	3	3
E_5	Chocolate brown	4	5	4	4	4	4	4
E_6	Red	4	5	4	5	4	4	4
E_7	Red	5	4	5	4	5	3	3

A remarkable degree of smoothness after washing was observed. This may be attributed to the good penetration into and affinity of the dye molecule for the structure of the fabrics. The most prominent feature of these dyes is that the dye patterns treated with Cr(III) salt solution afforded an excellent shining shade of dyes. This might be due to chrome complex formation on the fabric matrix.

TABLE V. Results of mordant heterocyclic acid dyeing and their various fastness properties on wool fabrics; grading: 5 – excellent, 4 – very good, 3 – good, 2 – fair, 1 – poor

Dye	Colour shade on wool	Light fastness	Washing fastness	Perspiration fastness		Sublimation fastness	Rubbing fastness	
				Acid	Alkaline		Dry	Wet
E_1	Pinkish blue	4	4	5	4	5	4	3
E_2	Pinkish blue	5	5	4	4	4	4	4
E_3	Reddish brown	4	4	5	5	5	4	4
E_4	Yellowish pink	5	4	4	4	4	4	4
E_5	Chocolate brown	4	4	4	4	4	3	4
E_6	Red	4	4	5	4	4	4	4
E_7	Red	4	4	4	5	5	4	3

TABLE VI. Results of mordant heterocyclic acid dyeing and their various fastness properties on silk fabrics; grading: 5 – excellent, 4 – very good, 3 – good, 2 – fair, 1 – poor

Dye	Colour shade on silk	Light fastness	Wash fastness	Perspiration fastness		Sublimation fastness	Rubbing fastness	
				Acid	Alkaline		Dry	Wet
E_1	Pinkish blue	4	4	4	4	5	4	4
E_2	Pinkish blue	4	5	4	4	4	3	3
E_3	Reddish brown	4	4	5	4	5	4	4
E_4	Yellowish pink	5	4	4	4	4	4	3
E_5	Chocolate brown	4	4	5	5	4	3	4
E_6	Red	5	5	4	4	4	4	5
E_7	Red	4	4	5	4	5	3	4

CONCLUSIONS

All newly synthesized heterocyclic acid dyes and mordant acid dyes exhibited very good to excellent fastness to light, sublimation, perspiration and rubbing. The remarkable degree of levelness after dyeing indicates good penetration into, and affinity of these dyes for the fabric matrix. They gave deep and bright hues with levelling dyeing. The nature of the substituent in the coupling component has little influence on the UV–visible absorption and shade of the dyeing. A comparison of the heterocyclic acid dyes and the mordant acid dyes revealed that the mordant acid dyes had better shades than the heterocyclic acid dyes.

SUPPLEMENTARY MATERIAL

Analytical and spectral data of the synthesized compounds are available electronically from http://www.shd.org.rs/JSCS/, or from the corresponding author on request.

Acknowledgments. The author is thankful to the Principal, V. P. & R. P. T. P. Science College and C. V. M. for providing the necessary research facilities. The author is also thankful to Mr. Ashok C. Kapadia and Mr. Pradeep N. Mistry of the Color Tax (Pvt) Ltd., Surat, India, for characterization of the azo groups and giving the standard of fastness properties and to Raju Mehta of G.P.C.B., Surat, India, for providing useful chemicals.

И З В О Д

СИНТЕЗА И КАРАКТЕРИЗАЦИЈА ХЕТЕРОЦИКЛИЧНИХ КИСЕЛИНА И МОЧИЛСКИХ БОЈА И ЊИХОВЕ СПОСОБНОСТИ БОЈЕЊА ВУНЕНИХ И СВИЛЕНИХ ТКАНИНА

HITENDRA M. PATEL

Department of Chemistry, V. P. & R. P .T. P Science College, Vallabh Vidyanagar-388 120, Gujarat State, India

Синтетисане су нове хетероцикличне киселине и мочилске боје купловањем диазонијум соли различитих ароматичних амина и 2-бутил-3-(4-хидроксибензоил)бензофурана. Добијене хетероцикличне киселине карактерисане су елементалном анализом, IC, ^{1}H-NMR, ^{13}C-NMR и UV–Vis спектроскопијом. Способност бојења испитана је на вуненим и свиленим тканинама. Боље нијансе приликом бојења постижу се на вуни и свили које су претходно третирана хромом. Добијене су роза–плаве до црвене нијансе добре дубине и уједначености. Бојене тканине су постојане према светлу, прању и хабању.

(Примљено 10. јануара, ревидирано 3. маја 2012)

REFERENCES

1. W. M. Cumming, G. J. Howie, *J. Chem. Soc*. (1933) 133
2. A. T. Peters, D. Walker, *J. Chem. Soc*. (1956) 429
3. A. I. Vogel, *A Textbook of Practical Organic Chemistry*, 3rd ed., Longman, London, 1961, p. 620
4. P. F. Gordon, P. Gregory, *Organic Chemistry in Colour*, 1st ed., Springer, Berlin, 1983, p. 60
5. S. K. Mohamed, A. M. Nour El-Din, *J. Chem. Res*. **8** (1999) 508
6. R. D. Naik, C. K. Desai, K. R. Desai, *Orient. J. Chem*. **16** (2000) 159
7. B. S. Dawane, S. S. Chobe, G. G. Mandawad, B. M. Shaikh, S. G. Konda, S. D. Patil, *Der Pharmacia Sinica* **1** (2010) 140
8. T. Bentin, R. Hamzavi, J. Salomonsson, H. Roy, M. Ibba, P. E. Nielsen, *J. Biol. Chem*. **279** (2004) 19839
9. M. Tamura, T. Ohishi, H. Sakurai, US Patent 4,298,522, 1981
10. F. I. Farouqui, I. Hossain, *Text. Dyer Printer* **23** (1990) 15
11. M. Johnson, R. G. Hauserman, *J. Appl. Polym. Sci*. **21** (1977) 3457
12. H. Kamogawa, M. Nanasawa, Y. Uehara, *J. Polym. Sci., A* **15** (1977) 675
13. K. Allmer, A. Hult, B. Ranby, *J. Polym. Sci. Polym. Chem. Ed.* **27** (1989) 3419
14. R. W. Layer, US Patent 4,133,799, 1979
15. N. Seto, M. Morigaki, US Patent 4,864,039, 1989
16. V. Frantisek, N. Hana, *Czech patent* 176, 377 (1979) [*CA* 91:P58685x]
17. B. C. Dixit, H. M. Patel, D. J. Desai, *J. Serb. Chem. Soc*. **72** (2007) 119

18. B. C. Dixit, H. M. Patel, D. J. Desai, R. B. Dixit, *E-J. Chem.* **6** (2009) 315
19. H. M. Patel, *Der Chemica Sinica* **2** (2011) 89
20. H. M. Patel, *Der Chemica Sinica* **3** (2012) 175
21. H. M. Patel, *Adv. Appl. Sci. Res*. **3** (2012) 235
22. H. E. Frirz-David, L. Blengy, *Fundamental Process of Dye Chemistry*, 3rd ed., Wiley, New York, 1949, p. 241
23. M. Szymczyk, A. E. Shafei, H. S. Freeman, *Dyes Pigm.* **72** (2007) 8
24. R. M. E. Shishtawy, Y. A. Youssef, N. S. E. Ahmed, A. A. Mousa, *Dyes Pigm.* **72** (2007) 57.

Journal of the Serbian Chemical Society
JSCS@tmf.bg.ac.rs • www.shd.org.rs/JSCS
J. Serb. Chem. Soc. 77 (11) S213–S216 (2012) *Supplementary material*

SUPPLEMENTARY MATERIAL TO

Synthesis, characterization and dyeing behaviour of heterocyclic acid dyes and mordant acid dyes on wool and silk fabrics

HITENDRA M. PATEL*

Department of Chemistry, V. P. & R. P .T. P Science College, Vallabh Vidyanagar-388 120, Gujarat State, India

J. Serb. Chem. Soc. 77 (11) (2012) 1551–1560

ANALYTIC AND SPECTRAL DATA OF THE HETEROCYCLIC ACID DYES

*4-((5-(2-Butylbenzofuran-3-yl-carbonyl)-2-hydroxyphenyl)diazenyl)-5-hydroxynaphthalene-2,7-disulphonic acid (**E1**)*. Pinkish blue colour; Yield: 74 %; m.p.: 166–169 °C; *Rf* value: 0.72; Anal. Calcd. for $C_{29}H_{24}N_2O_{10}S_2$ (FW: 625): C, 55.76; H, 3.87; N, 4.48; S, 10.27 %. Found: C, 55.72; H, 3.84; N, 4.41; S, 10.24 %; IR (KBr, cm^{-1}): 3463 (–OH), 3072 (=CH, aromatic), 1628 (C=O, diaryl), 1521 (N=N), 1520 (naphthalene substitution), 1481 (C=C, aromatic), 1333 (C–N), 1101 (C–O), 1030, 650 (sulphonic acid), 732, 584, 481 (substituted benzene); ^{1}H-NMR (400 MHz, DMSO-d_6, δ / ppm): 0.90 (3H, *t*, $J_{H–H}$ = 8.0 Hz, $–CH_3$), 1.31–2.40 (6H, *m*, $–CH_2–$), 5.35 (2H, *s*, Ar–OH), 7.31–8.72 (4H, *m*, substituted naphthalene), 7.32–7.89 (7H, *m*, substituted benzofuran and benzene), 8.1 (2H, *s*, $–SO_3H$); ^{13}C-NMR (75 MHz, DMSO-d_6, δ / ppm): 120.8 (C_3) (=CH, benzofuran), 168.0 (C_2) (=CH, benzofuran), 31.6 (CH_2, butyl), 26.3 (CH_2, butyl), 19.9 (CH_2, butyl), 13.5 (CH_3, butyl), 190.7 (C_1, methanone), 156.1 (C_4, phenolic-OH), 158.7 (naphthol), 125.2 (C–N=N), 147.3 (N=N–C), C–Ph of benzofuran: 123.2 (C_1), 120.9 (C_2), 123.3 (C_3), 124.7 (C_4), 111.5 (C_5), 156.1 (C_6), O=C–Ph of benzene: 123.9 (C_1), 123.8 (C_2), 125.2 (C_3), 156.1 (C_4), 119.2 (C_5), 133.3 (C_6), –N=N–naphthyl: 147.3 (C_1), 116.0 (C_2), 128.3 (C_3), 141.3 (C_4), 117.4 (C_5), 141.8 (C_6), 106.2 (C_7), 158.7 (C_8), 119.4 (C_9), 129.5 (C_{10}).

*(*E*)-7-((5-(2-Butylbenzofuran-3-yl-carbonyl)-2-hydroxyphenyl)diazenyl)-4--hydroxynaphthalene-2-sulphonic acid (**E2**)*. Pinkish blue colour; Yield: 81 %; m.p.: 148–152 °C; *Rf* value: 0.79. Anal. Calcd. for $C_{29}H_{24}N_2O_7S$ (FW: 545): C, 63.96; H, 4.44; N, 5.14; S, 5.89 %. Found: C, 63.92; H, 4.38; N, 5.10; S, 5.86 %; IR (KBr, cm^{-1}): 3450 (–OH), 3082 (=CH, aromatic), 1624 (C=O, diaryl), 1540 (substituted naphthalene), 1522 (N=N), 1490 (C=C, aromatic), 1345 (C–N), 1101

* Correspondence E-mail: shreeniketan71@yahoo.in

(C–O), 1032, 653 (sulphonic acid), 744, 564, 478 (substituted benzene); ^{1}H-NMR (400 MHz, DMSO-d_6, δ / ppm): 0.90 (3H, *t*, $J_{H–H}$ = 8.0 Hz, –CH_3), 1.31–2.40 (6H, *m*, –CH_2–), 5.35 (2H, *s*, Ar–OH), 7.31–8.72 (5H, *m*, substituted naphthalene), 7.32–7.89 (7H, *m*, substituted benzofuran and benzene), 8.2 (1H, *s*, –SO_3H); ^{13}C-NMR (75 MHz, DMSO-d_6, δ / ppm): 120.8 (C_3) (=CH, benzofuran), 168.0 (C_2) (=CH, benzofuran), 31.6 (CH_2, butyl), 26.3 (CH_2, butyl), 19.9 (CH_2, butyl), 13.4 (CH_3, butyl), 190.7 (C_1, methanone), 156.1 (C_4, phenolic-OH), 153.9 (naphthol), 125.2 (C–N=N), 151.4 (N=N–C), C–Ph of benzofuran: 123.2 (C_1), 120.9 (C_2), 123.3 (C_3), 124.7 (C_4), 111.5 (C_5), 156.1 (C_6), O=C–Ph of benzene: 123.9 (C_1), 123.8 (C_2), 125.2 (C_3), 156.1(C_4), 119.2 (C_5), 133.3 (C_6), –N=N–naphthyl: 151.4 (C_1), 117.6 (C_2), 121.8 (C_3), 153.9 (C_4), 106.1 (C_5), 141.2 (C_6), 118.1 (C_7), 130.9 (C_8), 133.9 (C_9), 128.7 (C_{10}).

*4-((5-(2-Butylbenzofuran-3-yl-carbonyl)-2-hydroxyphenyl)diazenyl)-5-hydroxynaphthalene-1,7-disulphonic acid (**E$_3$**)*. Reddish brown colour; Yield: 76 %; m.p.: 146–150 °C; *Rf* value: 0.79. Anal. Calcd. for $C_{29}H_{24}N_2O_{10}S_2$ (FW: 624): C, 55.76; H, 3.87; N, 4.48; S, 10.27 %. Found: C, 55.74; H, 3.81; N, 4.43; S, 10.24 %; IR (KBr, cm^{-1}): 3481 (–OH), 3070 (=CH, aromatic), 1632 (C=O, diaryl), 1542 (N=N), 1525 (substituted naphthalene), 1483 (C=C, aromatic), 1337 (C–N), 1103 (C–O), 1029, 650 (sulphonic acid), 737, 562, 472 (substituted benzene); ^{1}H-NMR (400 MHz, DMSO-d_6, δ / ppm): 0.90 (3H, *t*, $J_{H–H}$ = 8.0 Hz, –CH_3), 1.31–2.40 (6H, *m*, –CH_2–), 5.35 (2H, *s*, Ar–OH), 7.31–8.72 (4H, *m*, substituted naphthalene), 7.32–7.89 (7H, *m*, substituted benzofuran and benzene), 8.1 (2H, *s*, –SO_3H); ^{13}C-NMR (75 MHz, DMSO-d_6, δ / ppm): 120.8 (C_3) (=CH, benzofuran), 168.0 (C_2) (=CH, benzofuran), 31.6 (CH_2, butyl), 26.3 (CH_2, butyl), 19.9 (CH_2, butyl), 13.5 (CH_3, butyl), 190.7 (C_1, methanone), 156.1 (C_4, phenolic -OH), 158.7 (naphthol), 125.2 (C–N=N), 147.3 (N=N–C), C–Ph of benzofuran: 123.2 (C_1), 120.9 (C_2), 123.3 (C_3), 124.7 (C_4), 111.5 (C_5), 156.1 (C_6), O=C–Ph of benzene: 123.9(C_1), 123.8 (C_2), 125.2 (C_3), 156.1 (C_4), 119.2 (C_5), 133.3 (C_6), –N=N–naphthyl: 147.3 (C_1), 116.0 (C_2), 128.3 (C_3), 141.3 (C_4), 117.4 (C_5), 141.8 (C_6) , 106.2 (C_7), 158.7 (C_8), 119.4 (C_9), 129.5 (C_{10}).

*(*E*)-6-((5-(2-Butylbenzofuran-3-yl-carbonyl)-2-hydroxyphenyl)diazenyl)-naphthalene-2-sulphonic acid (**E$_4$**)*. Yellowish pink colour; Yield: 83 %; m.p.: 136–140 °C; *Rf* value: 0.81; Anal. Calcd. for $C_{29}H_{24}N_2O_6S$ (FW: 529): C, 65.90; H, 4.58; N, 5.30; S, 6.07 %. Found: C, 65.88; H, 4.52; N, 5.27; S, 6.02 %; IR (KBr, cm^{-1}): 3633 (–OH), 3080 (=CH, aromatic), 1652 (C=O, diaryl), 1560 (substituted naphthalene), 1532 (N=N), 1473 (C=C, aromatic), 1338 (C–N), 1104 (C–O), 1032, 653 (sulphonic acid), 782, 741, 583, 485 (substituted benzene); ^{1}H--NMR (400 MHz, DMSO-d_6, δ /ppm): 0.90 (3H, *t*, $J_{H–H}$ = 8.0 Hz, –CH_3), 1.31––2.40 (6H, *m*, –CH_2–), 5.35 (1H, *s*, Ar–OH), 7.31–8.72 (6H, *m*, substituted naphthalene), 7.32–7.89 (7H, *m*, substituted benzofuran and benzene), 8.2 (1H, *s*, –SO_3H); ^{13}C-NMR (75 MHz, DMSO-d_6, δ / ppm): 120.8 (C_3) (=CH, benzofu-

ran), 168 (C_2) (=CH, benzofuran), 31.6 (CH_2, butyl), 26.3 (CH_2, butyl), 19.9 (CH_2, butyl), 13.5 (CH_3, butyl), 190.7 (C_1, methanone), 156.1 (C_4, phenolic-OH), 125.2 (C–N=N), 151.3 (N=N–C), C–Ph of benzofuran: 123.2 (C_1), 120.9 (C_2), 123.3 (C_3), 124.7 (C_4), 111.5 (C_5), 156.1(C_6), O=C–Ph of benzene: 123.9 (C_1), 123.8 (C_2), 125.2 (C_3), 156.1 (C_4), 119.2 (C_5), 133.3 (C_6), –N=N–naphthyl: 151.3 (C_1), 120.8 (C_2), 127.3 (C_3), 125.8(C_4), 140.3 (C_5), 123.4 (C_6) , 129.6 (C_7) , 121.0 (C_8), 133.4 (C_9), 134.9 (C_{10}).

*(*E*)-2-((5-(2-Butylbenzofuran-3-yl-carbonyl)-2-hydroxyphenyl)diazenyl)-naphthalene-1-sulphonic acid (**E**$_5$).* Chocolate brown colour; Yield: 79 %; m.p.: 138–142 °C; *Rf* value: 0.80. Anal. Calcd. for $C_{29}H_{24}N_2O_6S$ (FW: 529): C, 65.90; H, 4.58; N, 5.30; S, 6.07 %. Found: C, 65.86; H, 4.49; N, 5.25; S, 6.01 %; IR (KBr, cm^{-1}): 3580 (–OH, phenolic), 3070 (=CH, aromatic), 1621 (C=O, diaryl), 1575 (substituted naphthalene), 1531 (N=N), 1482 (C=C, aromatic), 1463 (C–N), 1338 (C–O), 1034, 650 (sulphonic acid), 1103, 732, 574, 473 (substituted benzene); ^{1}H-NMR (400 MHz, DMSO-d_6, δ / ppm): 0.90 (3H, *t*, $J_{H–H}$ = 8.0 Hz, –CH_3), 1.31–2.40 (6H, *m*, –CH_2–), 5.35 (1H, *s*, Ar–OH), 7.31–8.72 (*m*, 6H, substituted naphthalene), 7.32–7.89 (7H, *m*, substituted benzofuran and benzene), 8.2 (1H, *s*, –SO_3H). ^{13}C-NMR (75 MHz, DMSO-d_6, δ / ppm): 120.8 (C_3) (=CH, benzofuran), 168 (C_2) (=CH, benzofuran), 31.6 (CH_2, butyl), 26.3 (CH_2, butyl), 19.9 (CH_2, butyl), 13.5 (CH_3, butyl), 190.8 (C_1, methanone), 156.2 (C_4, phenolic-OH), 125.3 (C–N=N), 151.7 (N=N–C), C–Ph of benzofuran: 123.4 (C_1), 120.9 (C_2), 123.6 (C_3), 124.5 (C_4), 111.7 (C_5), 156.3 (C_6), O=C–Ph of benzene: 123.8 (C_1), 123.9 (C_2), 125.4 (C_3), 156.6 (C_4), 119.8 (C_5), 133.3 (C_6), –N=N–naphthyl: 151.3 (C_1), 120.8 (C_2), 127.3 (C_3), 125.8(C_4), 140.3 (C_5), 123.4 (C_6), 129.6 (C_7), 121.2 (C_8), 133.4 (C_9), 134.9 (C_{10}).

*(*E*)-2-((5-(2-Butylbenzofuran-3-yl-carbonyl)-2-hydroxyphenyl)diazenyl)benzoic acid (**E**$_6$).* Red colour; Yield: 76 %; m.p.: 145–148 °C; *Rf* value: 0.83; Anal. Calcd. for $C_{26}H_{22}N_2O_5$ (FW: 442): C, 70.58; H, 5.01; N, 6.33 %. Found: C, 70.52; H, 4.88; N, 6.30 %; IR (KBr, cm^{-1}): 3430 (–OH, phenolic), 3540 (–OH, acidic), 3062 (=CH, aromatic), 1634 (C=O, diaryl), 1678 (C=O, carboxylic acid), 1581 (N=N), 1483 (C=C, aromatic), 1352 (C–N), 1103 (C–O), 1100, 850 (carboxylic acid), 783, 741, 583, 482 (substituted benzene); ^{1}H-NMR (400 MHz, DMSO-d_6, δ / ppm): 0.90 (3H, *t*, $J_{H–H}$ = 8.0 Hz, –CH_3), 1.31–2.40 (6H, *m*, –CH_2–), 5.35 (1H, *s*, Ar–OH), 7.32–8.41 (11H, *m*, substituted benzofuran and benzene), 11.0 (1H, *s*, –COOH); ^{13}C-NMR (75 MHz, DMSO-d_6, δ / ppm): 168.0 (C_2) (=CH, benzofuran), 120.8 (C_3) (=CH, benzofuran), 31.6 (CH_2, butyl), 26.3 (CH_2, butyl), 19.9 (CH_2, butyl), 13.5 (CH_3, butyl), 190.7 (C_1, methanone), 156.1 (C_4, phenolic-OH), 166.5 (–COOH), 125.2 (C–N=N), 154.1 (N=N–C), C–Ph of benzofuran: 123.2 (C_1), 120.9 (C_2), 123.3 (C_3), 124.7(C_4), 111.5 (C_5), 156.1(C_6), O=C–Ph of benzene: 123.9 (C_1), 123.8 (C_2), 125.2 (C_3), 156.1 (C_4), 119.2 (C_5),

133.3 (C_6), –N=N–Ph. of benzene: 154.1 (C_1), 122.9 (C_2), 134.2 (C_3), 127.8 (C_4), 127.2 (C_5), 117.0 (C_6).

*(*E*)-4-((5-(2-Butylbenzofuran-3-yl-carbonyl)-2-hydroxyphenyl)diazenyl)benzenesulphonic acid (**E**$_7$).* Red colour. Yield: 78 %; m.p.: 154–158 °C; *Rf* value: 0.83. Anal. Calcd. for $C_{25}H_{22}N_2O_6S$ (FW: 479): C, 62.75; H, 4.63; N, 5.85; S, 6.70 %. Found: C, 62.70; H, 4.58; N, 5.81; S, 6.67 %; IR (KBr, cm^{-1}): 3590 (–OH), 3063 (=CH, aromatic), 1632 (C=O, diaryl), 1533 (N=N), 1471 (C=C, aromatic), 1324 (C–N), 1103 (C–O), 1031, 652 (sulphonic acid), 780, 744, 586, 475 (substituted benzene); ^{1}H-NMR (400 MHz, DMSO-d_6, δ / ppm): 0.90 (3H, *t*, $J_{H–H}$ = 8.0 Hz, –CH_3), 1.31–2.40 (6H, *m*, –CH_2–), 5.35 (1H, *s*, Ar–OH), 7.32–8.41 (11H, *m*, substituted benzofuran and benzene), 8.2 (1H, *s*, –SO_3H); ^{13}C-NMR (75 MHz, DMSO-d_6, δ / ppm): 120.8 (C_3) (=CH, benzofuran), 168 (C_2) (=CH, benzofuran), 31.6 (CH_2, butyl), 26.3 (CH_2, butyl), 19.9 (CH_2, butyl), 13.5 (CH_3, butyl), 190.7 (C_1, methanone), 156.1 (C_4, phenolic-OH), 125.0 (C–N=N), 156.5 (N=N–C), C–Ph of benzofuran: 123.2 (C_1), 120.9 (C_2), 123.3 (C_3), 124.7 (C_4), 111.5 (C_5), 156.1(C_6), O=C–Ph of benzene: 123.9 (C_1), 123.8 (C_2), 125.2 (C_3), 156.1 (C_4), 119.2 (C_5), 133.3 (C_6), –N=N–Ph. of benzene: 156.5 (C_1), 124.3 (C_2), 123.2 (C_3), 147.7 (C_4), 123.2 (C_5), 124.3 (C_6).

Journal of the Serbian Chemical Society
JSCS-info@shd.org.rs • www.shd.org.rs/JSCS
J. Serb. Chem. Soc. 77 (11) 1561–1570 (2012)
JSCS–4371
UDC 546.654+547.831.7:542.913+544.478:615.28
Original scientific paper

Lanthanum triflate-triggered synthesis of tetrahydroquinazolinone derivatives of *N*-allylquinolone and their biological assessment

HARDIK H. JARDOSH and MANISH P. PATEL*

Department of Chemistry, Sardar Patel University, Vallabh Vidyanagar-388120, Gujarat, India

(Received 21 January, revised 27 March 2012)

Abstract: A series of 24 derivatives of tetrahydroquinazolinone has been synthesized by the one-pot cyclocondensation reaction of *N*-allyl quinolones, cyclic *β*-diketones and (thio)urea/*N*-phenylthiourea in the presence of lanthanum triflate catalyst. This methodology allowed the products to be achieved in excellent yield by stirring at room temperature. All the synthesized compounds were investigated against a representative panel of pathogenic strains using the broth microdilution *MIC* (minimum inhibitory concentration) method for their *in vitro* antimicrobial activity. Amongst these sets of heterocyclic compounds **5h**, **6b**, **6h**, **5f**, **5l**, **5n** and **6g** were found to have admirable activity.

Keywords: quinolone; Biginelli reaction; one-pot synthesis; catalyst; antimicrobial activity.

INTRODUCTION

Quinazolinones possess diverse pharmacological and biological activities associated with the pyrimidine core, such as hypotensive,[1] analgesic and anti-inflammatory,[2] calcium antagonist[3] and central nervous system (CNS) depressant.[4] Furthermore, quinazolinones were found to exhibit antimicrobial activity against *Staphylococcus aureus*, *Escherichia coli* and *Candida albicans*.[5] Therefore, the synthesis of quinazolinone derivatives still attract much attention of modern-day medicinal chemistry research. On other hand, quinolones have maintained their pharmacological importance since their discovery based on nalidixic acid in the early 1960s.[6] Quinolones possess various biological activities, such as anti-HIV,[7] antitumor,[8] anti-anaerobe[9] and antimicrobial.[10] It is well established that hydrophobicity is one of the factors that directly correlates to antimicrobial activity and intensifies the potency of a molecule.[11,12] In view of this, an allyl group was in-

* Corresponding author. E-mail: patelmanish1069@yahoo.com
doi: 10.2298/JSC120121039J

serted at the *N* of quinolone ring to increase the hydrophobicity of the compounds. Thus, based on the above reports, an attempt was undertaken to synthesize *N*-allylquinolone-incorporated quinazolinone derivatives based on the premise that allylic compounds have an additive effect to antimicrobial potency and the amalgamation of two bioactive moieties into a single scaffold may produce novel heterocycles with appealing antimicrobial activities.

Tetrahydroquinazolinone derivatives have been synthesized under Biginelli reaction conditions (protic acid) but these methods suffer from low to moderate yields, lengthy reaction time and harsh reaction conditions.[13] It was found that not only protic, but also Lewis acids could be used as a catalyst for the synthesis of tetrahydroquinazolinone derivatives.[14] More recently, a number of reports expressing the utility of triflates as a Lewis acid catalyst in Biginelli protocols to give excellent yields, shorter reaction time and mild reaction conditions were published.[15]

From the aforementioned facts and as a part of ongoing studies in the development of new antimicrobial agents containing various heterocyclic systems having a quinoline nucleus,[16] *N*-allylquinolone-incorporated tetrahydroquinazolinone derivatives **5a**–**p** and **6a**–**h** were prepared *via* a multiple component condensation (MCC) approach using lanthanum triflate ($La(OTf)_3$) as the catalyst and the results are reported herein. The constitution of all the products was characterized using elemental analysis, and FT-IR, ^{1}H-NMR, ^{13}C-NMR and mass spectrometry. The synthesized compounds were subjected to an *in vitro* antimicrobial study against a representative panel of seven human pathogens using the broth microdilution minimum inhibitory concentration (*MIC*) method.[17]

RESULTS AND DISCUSSION

Chemistry

In this protocol, 1-allyl-2-oxo-1,2-dihydroquinoline-3-carbaldehydes **1a**–**d** were selected as model compounds for the one-pot syntheses to give heterocyclic systems with a quinazolinone core. The key intermediates **1a**–**d** were prepared by electrophile-favored *N*-alkylation of 2-oxo-1,2-dihydroquinoline-3-carbaldehydes in presence of K_2CO_3 in DMF at room temperature.[18]

All the 4-(1-allyl-2-oxo-1,2-dihydroquinolin-3-yl)-4,6,7,8-tetrahydroquinazoline-2,5(1*H*,3*H*)-dione derivatives **5a**–**p** and **6a**–**h** were obtained by $La(OTf)_3$ catalyzed reaction[19–21] of various 1-allyl-2-oxo-1,2-dihydroquinoline-3-carbaldehydes **1a**–**d**, cyclohexane-1,3-dione or dimedones **2a**–**b** and (thio)ureas **3a**–**b** or *N*-phenylthiourea **4** in ethanol at room temperature (Scheme 1). The reaction was examined by taking different mol ratios of catalyst, *i.e.*, 2.5, 5, 7.5, 10 and 12.5 mol %. It was observed that when the amount of $La(OTf)_3$ was increased to 10 mol %, the reaction rate accelerated within 1.5–2 h for **5a**–**p** and 3–3.5 h for **6a**–**h** with high conversion, but the further increase in the amount of $La(OTf)_3$

had no significant outcome on the reaction. The products were obtained in excellent yield at room temperature in ethanol only by use of 10 mol % catalyst; thus, these conditions were considered as the most optimized conditions for the synthesis of the title quinazolinone derivatives **5a**–**p** and **6a**–**h**.

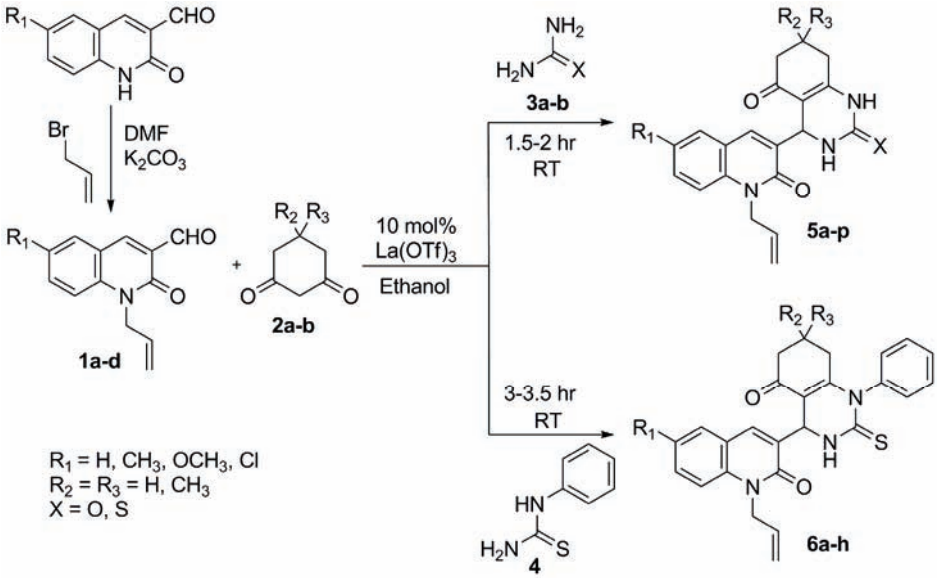

Scheme 1. Synthetic pathway to compounds **1a**–**d**, **5a**–**p** and **6a**–**h**.

The formation of compounds **5a**–**p** and **6a**–**h** may proceed *via* two steps (Scheme 2): *i*) the formation of arylidene(thio)urea **Int-1** and *ii*) interception of the acyliminium ion intermediate by an activated cyclic *β*-diketone to produce an open chain urea **Int-2**, which subsequently undergoes cyclization and dehydration *via* **Int-3** to afford the corresponding quinazolinone. The formation of an acyliminium ion was reported to be the rate-determining step.[20] $La(OTf)_3$ is thought to accelerate the formation of the arylidene(thio)urea **Int-1** and activate the cyclic *β*-diketone **2a**–**b** by forming its metal enolate, thus facilitating the addition reaction with a coordinated acyliminium ion.[21]

The identities of all the synthesized compounds **5a**–**p** and **6a**–**h** were determined from ^{1}H-NMR, ^{13}C-NMR and FT-IR spectral data and elemental analysis. As an example, ^{1}H-NMR (DMSO-d_6) spectrum of **5a**, exhibited singlet peaks at δ 9.52 and 7.80 ppm for the (–NH–) protons of the quinazolinone ring. A doublet was observed at around δ 4.90–5.05 ppm for (N–CH_2–CH=C**H**$_2$). Another doublet appeared at δ 5.18 ppm for (N–C**H**$_2$–CH). Multiplets were observed at δ 5.94 and around 7.08–7.60 ppm for (C**H**=CH_2) and aromatic protons, respectively. The methine proton at C_4 of quinazolinone appeared at δ 5.36 ppm as a singlet. A multiplet appeared at around δ 1.97–2.54 ppm for 3CH_2. The ^{13}C-NMR spec-

trum is in agreement with the assigned structure. Thus, in the ^{13}C-NMR spectrum of compound **5a**, the signals around δ 105.51–152.04 ppm are attributed to aromatic carbons and the allylic C=C. The signals at around δ 21.28–36.80 ppm and at δ 49.39 ppm arise from aliphatic carbons and the allylic methylene carbon, respectively. In addition, the signal observed at δ 49.31 ppm is due to C_4 of quinazolinone. The signals due to carbonyl carbons appeared at δ 156.69, 160.72 and 193.67. The IR spectrum of **5a** exhibited absorption bands at 3435 and 3352 cm^{-1} for N–H str. and at 1711, 1639, and 1593 cm^{-1} for C=O str. The structure of compound **5a** was also confirmed by mass spectral studies. It gave a molecular ion peak at *m*/*z* 350.2 $[M+1]^+$, corresponding to the molecular formula $C_{20}H_{19}N_3O_3$. The obtained elemental analysis data are in consonance with the theoretical values.

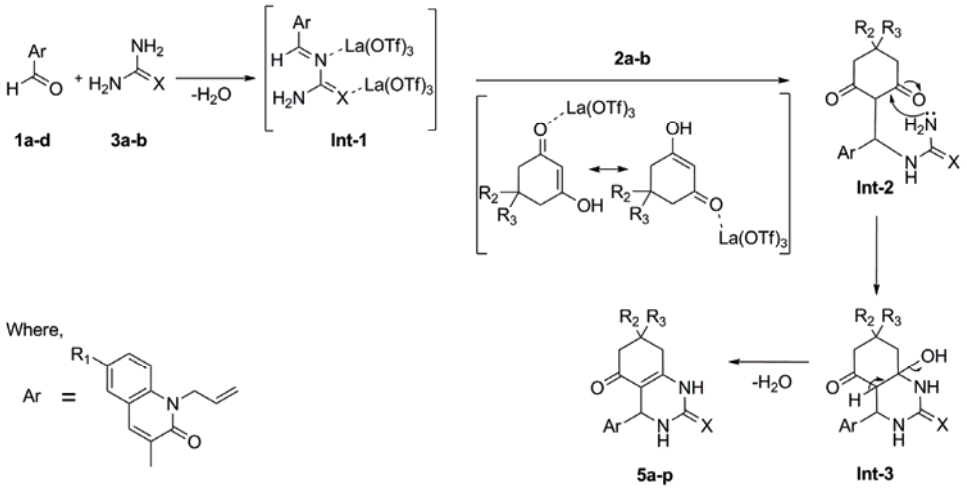

Scheme 2. Believable mechanistic pathway for the formation of compounds **5a**–**p** and **6a**–**h** by La(OTf)$_3$ catalysis.

The analytical and spectroscopic characterization data of **5a**–**p** and **6a**–**h** are given in the Supplementary material to this paper.

Antimicrobial evaluation

The antibacterial screening data (Table I) revealed that compound **5h** (*MIC* = = 20 μg mL^{-1}) had extraordinary antibacterial activity against *Pseudomonas aeruginosa* when compared with chloramphenicol and ciprofloxacin. Against *Escherichia coli*, compounds **6b** and **6h** (*MIC* = 50 μg mL^{-1}) were found to have outstanding antibacterial activity when compared with ampicillin and were equipotent to chloramphenicol, while compounds **5l** and **5n** (*MIC* = 62.5 μg mL^{-1}) were found to have better activity than ampicillin. Against *Staphylococcus aureus*, compounds **5f** and **6g** (*MIC* = 62.5 μg mL^{-1}) were found to have excellent activity; compounds **5e** and **5p** (*MIC* = 100 μg mL^{-1}), as well as **5d**, **5g** and **6e**

(*MIC* = 125 μg mL^{-1}) showed remarkable results, while compounds **5i**, **5k**, **5m** and **6h** (*MIC* = 200 μg mL^{-1}) exhibited good activity; compounds **5a**, **5c**, **5h**, **5j** and **6f** (*MIC* = 250 μg mL^{-1}) were found to be equally potent to ampicillin. Against *Streptococcus pyogenes*, compounds **5e**, **5g**, **5m**, **5p** and **6e** (*MIC* = 100 μg mL^{-1}) were found to have comparable activity to that of ampicillin. Against *E. coli*, compounds **5j**, **5k**, **5m** and **6f** (*MIC* = 100 μg mL^{-1}) were equipotent to ampicillin.

TABLE I. Antimicrobial activity (*MIC* / μg mL^{-1}) of compounds **5a**–**p** and **6a**–**h**

Compounds	Gram-positive bacteria		Gram-negative bacteria		Fungi		
	S. aureus MTCC 96	*S. pyogenes* MTCC 442	*E. coli* MTCC 443	*P. aeruginosa* MTCC 1688	*C. albicans* MTCC 227	*A. niger* MTCC 282	*A. clavatus* MTCC 1323
5a (R_1=H, R_2=R_3=H, X=O)	250	250	125	200	500	1000	1000
5b (R_1=H, R_2=R_3=CH_3, X=O)	500	500	200	250	1000	500	500
5c (R_1=H, R_2=R_3=H, X=S)	250	500	250	250	1000	>1000	>1000
5d (R_1=H, R_2=R_3=CH_3, X=S)	125	200	200	200	>1000	>1000	>1000
5e (R_1=CH_3, R_2=R_3=H, X=O)	100	100	125	125	500	250	500
5f (R_1=CH_3, R_2=R_3=CH_3, X=O)	62.5	125	500	250	500	1000	1000
5g (R_1=CH_3, R_2=R_3=H, X=S)	125	100	250	250	250	500	1000
5h (R_1=CH_3, R_2=R_3=CH_3, X=S)	250	250	250	20	250	1000	500
5i (R_1=OCH_3, R_2=R_3=H, X=O)	200	250	125	200	1000	500	500
5j (R_1=OCH_3, R_2=R_3=CH_3, X=O)	250	250	100	125	>1000	>1000	>1000
5k (R_1=OCH_3, R_2=R_3=H, X=S)	200	200	100	200	>1000	>1000	>1000
5l (R_1=OCH_3, R_2=R_3=CH_3, X=S)	500	500	62.5	100	500	250	500
5m (R_1=Cl, R_2=R_3=H, X=O)	200	100	100	200	1000	>1000	>1000
5n (R_1=Cl, R_2=R_3=CH_3, X=O)	500	200	62.5	125	>1000	>1000	>1000
5o (R_1=Cl, R_2=R_3=H, X=S)	500	250	250	250	>1000	>1000	>1000
5p (R_1=Cl, R_2=R_3=CH_3, X=S)	100	100	200	200	500	250	500
6a (R_1=H, R_2=R_3=H)	500	250	125	100	1000	>1000	>1000
6b (R_1=H, R_2=R_3=CH_3)	500	500	50	125	200	500	500
6c (R_1=CH_3, R_2=R_3=H)	500	500	200	250	500	1000	1000

TABLE I. Continued

Compounds	Gram-positive bacteria		Gram-negative bacteria		Fungi		
	S. aureus MTCC 96	*S. pyogenes* MTCC 442	*E. coli* MTCC 443	*P. aeruginosa* MTCC 1688	*C. albicans* MTCC 227	*A. niger* MTCC 282	*A. clavatus* MTCC 1323
6d (R_1=CH_3, R_2=R_3=CH_3)	500	500	200	250	1000	500	500
6e (R_1=OCH_3, R_2=R_3=H)	125	100	250	250	1000	500	500
6f (R_1=OCH_3, R_2=R_3=CH_3)	250	200	100	100	500	1000	1000
6g (R_1=Cl, R_2=R_3=H)	62.5	200	500	250	500	500	100
6h (R_1=Cl, R_2=R_3=CH_3)	200	250	50	100	250	100	250
Ampicillin	250	100	100	–	–	–	–
Chloramphenicol	50	50	50	50	–	–	–
Ciprofloxacin	50	50	25	25	–	–	–
Nystatin	–	–	–	–	100	100	100
Griseofulvin	–	–	–	–	500	100	100

The antifungal screening data (Table I) revealed that compounds **6b** (*MIC* = = 200 μg mL^{-1}), **5g**, **5h** and **6h** (*MIC* = 100 μg mL^{-1}) were found to have excellent activity against *Candida albicans*, while compounds **5a**, **5e**, **5f**, **5l**, **5p**, **6c**, **6f** and **6g** (MIC = 500 μg mL^{-1}) had comparable activity to that of griseofulvin. Compounds **6h** and **6g** (*MIC* = 100 μg mL^{-1}) were found to be equally potent against *Aspergillus niger* and *A. clavatus*, respectively.

The newly synthesized compounds **5a**–**p** and **6a**–**h** exerted significant inhibitory activity against the growth of the tested bacterial and fungal strains. The data also revealed that insertion of an allyl chain at the ***N*** of the quinolone moiety and derivatization at positions R_1, R_2, R_3, X and *N*-1 of tetrahydroquinazolinone produced marked changes in the potency of the synthesized analogues as antimicrobial agents and demonstrated the following assumptions about the structure–activity relationship (SAR):

Compounds having a $–CH_3$ substituent at the R_2 and R_3 positions have intensified antibacterial effectiveness against Gram negative bacteria, *e.g.*, **5h**, **5l**, **5n**, **6b** and **6h**, but not **5f**. Moreover, an S-atom at the C_2 position and a phenyl group at *N*-1 of tetrahydroquinazolinone may play a significant role in enhancing antifungal activity, *e.g.*, **5h**, **5l**, **6b**, **6h** and **6g**. However, only phenyl substituted compounds displayed similar inhibitory action against the *Aspergillus* family when compared with standard drugs. Compounds with electron withdrawing group –Cl at R_1 of the *N*-allylquinolone ring may have improved activity against *E. coli*, *S. aureus* and all fungal species, *e.g.*, **5m**, **5n**, **6g** and **6h**. On the other hand, the electron donating $–OCH_3$ group may increase the activity against *E. coli* and *S. aureus*, *e.g.*, **5j**, **5k**, **5l** and **6f**. A lipophilic $–CH_3$ group at the R_1 position may intensify the potency against *P. aeruginosa*, *S. aureus* and *C. albicans*.

Furthermore, the allyl chain makes the compounds more hydrophobic and may enhance the antimicrobial potency of the title compounds. The study revealed that changes in substitutions have a vast impact on the antimicrobial effectiveness.

Upon comparison with a previous report,[16b] it could be stated that *i*) insertion of an allyl group at *N* of the quinolone ring increases the antimicrobial properties of the title compounds; *ii*) both electron withdrawing and donating constituents at the R_1 position contribute to enhancement of the antimicrobial effectiveness; *iii*) a phenyl group at *N*-1 of the tetrahydroquinazolinone ring influences the microbial inhibitory action and *iv*) the lipophilic $–CH_3$ group at the R_1 position has an additive effect on the inhibition of microbial pathogens.

EXPERIMENTAL

Materials, instruments and methods

All the reagents were commercially available and used without further purification. Solvents of analytical grade were used. Melting points were determined by the open tube capillary method (using silicon oil 350 cSt) and are uncorrected. Thin-layer chromatography (TLC, on aluminum plates pre-coated with silica gel, $^{60}F_{254}$, 0.25mm thickness) (Merck, Darmstadt, Germany) was used for monitoring the progress of all reactions, as well as the purity and homogeneity of the synthesized compounds; eluent *n*-hexane:ethyl acetate 1:1. UV radiation and/or iodine were used as the visualizing agents. Elemental analysis (% C, H, N) was realized using a Perkin-Elmer 2400 series-II elemental analyzer (Perkin-Elmer, USA) and the results for all compounds were within ±0.4 % of the theoretical value. The IR spectra were recorded in KBr on a Perkin-Elmer Spectrum GX FT-IR Spectrophotometer (Perkin-Elmer, USA) and only the characteristic peaks are reported in cm^{-1}. ^{1}H-NMR and ^{13}C-NMR spectra were recorded in DMSO-d_6 on a Bruker Avance 400F (MHz) spectrometer (Bruker Scientific Corporation Ltd., Switzerland) at 400 and 100 MHz, respectively, using the solvent peak as an internal standard. Chemical shifts are reported in parts per million (ppm). Mass spectra were scanned on a Shimadzu LCMS 2010 spectrometer (Shimadzu, Tokyo, Japan).

*General procedure for the synthesis of 4-(1-allyl-2-oxo-1,2-dihydroquinolin-3-yl)-4,6,7,8-tetrahydroquinazolin-2,5(1*H*,3H)-diones **5a**–**p** and **6a**–**h***

A 100 mL round bottomed flask, was charged with a mixture of 1-allyl-6-(un)substituted-2-oxo-1,2-dihydroquinoline-3-carbaldehydes **1a–d** (3 mmol), cyclohexane-1,3-dione or dimedone **2a**–**b** (3 mmol) and (thio)urea **3a**–**b**/*N*-phenylthiourea **4** (3 mmol) in ethanol (15 mL) containing $La(OTf)_3$ (10 mol %). The mixture was allowed to stir at rt for 1.5–3.5 hr and the progress of the reaction was monitored by TLC. After the completion of reaction (as evidenced by TLC), the solid mass separated was collected by filtration, washed well with ethanol (15 mL) and purified by leaching in equal volume ratio of chloroform and methanol (20 mL) to obtain pure solid sample.

Methodology for screening the antimicrobial activity

All the glass apparatus were sterilized before use. The antimicrobial activity of all the synthesized compounds was screened by the broth microdilution method.[17] Mueller–Hinton broth was used as the nutrient medium to grow and dilute the compound suspension for the test bacteria and Sabouraud dextrose broth was used for fungal nutrition. Inoculum size for test strain was adjusted to 10^8 CFU ml^{-1} (colony forming unit per milliliter) by comparing the turbidity (turbidimetric method). The strains used for the activity were obtained from Mic-

robial Type Culture Collection (MTCC) of the Institute of Microbial Technology, Chandigarh, India. Each synthesized compound was diluted to a concentration of 2000 μg mL^{-1}, as a stock solution. DMSO was used as the vehicle to obtain the desired concentrations of the compounds to test upon microbial strains. The results were recorded in the form of primary and secondary screenings. The compounds **5a**–**p** and **6a**–**h** were screened for their antibacterial activity against the Gram-positive bacteria: *S. aureus* (MTCC 96) and *S pyogenes* (MTCC 442), and Gram-negative bacteria: *E. coli* (MTCC 443) and *P. aeruginosa* (MTCC 1688), and antifungal activity against the fungi: *C. albicans* (MTCC 227), *A. niger* (MTCC 282) and *A. clavatus* (MTCC 1323) at concentrations of 1000, 500, and 250 μg mL^{-1} as primary screening. Compounds that were found to be active in the primary screening were further screened in a second set of dilution at concentrations of 200, 100, 62.5, 50, 25, 12.5, and 6.25 μg mL^{-1}. Ten microliters suspension from each well was further inoculated and growth of the bacteria and fungi was noted after 24 and 48 h, respectively. The lowest concentration which resulted in no visible growth (turbidity) after spot subculture was considered as the *MIC* for each compound. The standard drugs used for comparison in this study were ampicillin, chloramphenicol and ciprofloxacin for evaluating the antibacterial activity and griseofulvin and nystatin for the antifungal activity.

CONCLUSIONS

In present protocol, the synthesis and antimicrobial evaluation of 24 new derivatives **5a**–**p** and **6a**–**h** of tetrahydroquinazolinone possessing an *N*-allylquinolone nucleus at C_4 of quinazolinone were presented. $La(OTf)_3$ as catalyst allowed the smooth synthesis of the title derivatives at room temperature in excellent yield. It could be concluded from the antimicrobial screening data that many of the compounds were more or equipotent against a panel of human pathogens when compared with the standard drugs. It is noteworthy that derivatization of the title compounds alter their antimicrobial activity. Further synthetic work to intensify the potency of these derivatives by changing their molecular configuration is in progress. The present study highlights the identification of this new structural class of compounds as antimicrobials, which could be of interest for further detailed pre-clinical investigations.

SUPPLEMENTARY MATERIAL

Analytical and spectroscopic characterization data of the compounds **5a**–**p** and **6a**–**h** are available electronically from http://www.shd.org.rs/JSCS/, or from the corresponding author on request.

Acknowledgements. The authors are thankful to the Head of the Department of Chemistry, Sardar Patel University, for providing the ^{1}H-NMR and ^{13}C-NMR data and research facilities. We are also thankful to SICART, Vallabh Vidyanagar, for the FT-IR and elemental analysis, Oxygen Health Care Pvt. Ltd., Ahmedabad for the mass spectra and Dhanji P. Rajani, Microcare Laboratory, Surat, for the antimicrobial screening of the compounds reported herein.

И З В О Д

СИНТЕЗА ТЕТРАХИДРОХИНАЗОЛИНОНСКИХ ДЕРИВАТА *N*-АЛИЛХИНОЛОНА ПОМОЋУ ЛАНТАН-ТРИФЛАТА И ОДРЕЂИВАЊЕ ЊИХОВЕ БИОЛОШКЕ АКТИВНОСТИ

HARDIK H. JARDOSH и MANISH P. PATEL

Department of Chemistry, Sardar Patel University, Vallabh Vidyanagar-388120, Gujarat, India

Синтетисана је серија од 24 деривата тетрахидрохиназолинона циклокондензационом реакцијом *N*-алилхинолона, цикличног *β*-дикетона и (тио)урее/*N*-фенилтиоурее у присуству лантан-трифлата као катализатора. Примењена методологија омогућава добијање производа у високом приносу. Сви добијени производи тестирани су према репрезентативном панелу патогена, а *in vitro* антимикробне активности одређене су применом метода микроразблаживања и изражене као *MIC* (минимална инхибиторна концентрација). Утврђено је да седам деривата, **5h**, **6b**, **6h**, **5f**, **5l**, **5n** и **6g**, има запажене активности.

(Примљен 21. јануара, ревидиран 27. марта 2012)

REFERENCES

1. O. I. El-Sabbagh, M. A. Shabaan, H. H. Kadry, E. S. Al-Din, *Eur. J. Med. Chem.* **45** (2010) 5390
2. a) A. B. A. El-Gazzar, H. N. Hafez, H. S. Abbas, *Eur. J. Med. Chem*. **44** (2009) 4249; b) B. A. Rather, T. Raj, A. Reddy, M. S. Ishar, S. Sivakumar, P. Paneerselvam, *Arch. Pharm. Chem. Life Sci.* **343** (2010) 108
3. M. Yarim, S. Sarac, F. S. Kilic, K. Erol, *Farmaco* **58** (2003) 17
4. V. Jatav, P. Mishra, S. Kashaw, J. P. Stables, *Eur. J. Med. Chem.* **43** (2008) 135
5. M. Minu, A. Thangadurai, S. R. Wakode, S. S. Agrawal, B. Narasimhan, *Arch. Pharm. Chem. Life Sci.* **341** (2008) 231
6. G. Y. Lesher, E. J. Froelich, M. D. Gruett, J. H. Bailey, R. P. Brundage, *J. Med. Pharm. Chem*. **5** (1962) 1063
7. E. Filipponi, G. Cruciani, O. Tabarrini, V. Cecchetti, A. Fravolini, *J. Comput.-Aided Mol. Des.* **15** (2001) 203
8. J. Li, J. Tan, L. Chen, J. Zhang, X. Shen, C. Mei, L. Fu, L. Lin, J. Ding, B. Xiong, X. Xiong, H. Liu, X. Luo, H. Jiang, *Acta Pharmacol. Sin.* **27** (2006) 1259
9. R. Schaumann, A. C. Rodloff, *Anti-Infect. Agents Med. Chem.* **6** (2007) 49
10. F. O'Donnell, T. J. P. Smyth, V. N. Ramachandran, W. F. Smyth, *Int. J. Antimicrob. Agents* **35** (2010) 30
11. V. Alptuzun, H. Tasli, E. Erciyas, *J. Fac. Pharm, Ankara* **35** (2006) 177
12. C. Praveen, A. Ayyanar, P. T. Perumal, *Bioorg. Med. Chem. Lett*. **21** (2011) 4072
13. a) N. N. Tonkikh, A. Strakovs, M. V. Petrova, *Chem. Heterocycl. Compd.* **40** (2004) 43; b) M. M. Candan, E. Kendi, M. Yarim, S. Sarac, M. Ertan, *Anal. Sci*. **17** (2001) 1023
14. S. Kantevari, R. Bantu, L. Nagarapu, *ARKIVOC* **2006** (2006) 136
15. M. A. Kolosov, V. D. Orlov, D. A. Beloborodov, V. V. Dotsenko, *Mol. Divers.* **13** (2009) 5
16. a) N. K. Shah, N. M. Shah, M. P. Patel, R. G. Patel, *J. Serb. Chem. Soc*. (2011), *J. Serb. Chem. Soc*. **77** (2012) 279; b) P. M. Shah, M. P. Patel, *Med. Chem. Res.* (2011), *Med. Chem. Res.* **21** (2012) 1188; c) D. C. Mungra, M. P. Patel, D. P. Rajani, R. G. Patel, *Eur. J. Med. Chem.* **46** (2011) 4192; d) N. J. Thumar, M. P. Patel, *Arch. Pharm. Chem. Life Sci.* **2** (2011)

91; e) H. G. Kathrotiya, R. G. Patel, M. P. Patel, *J. Serb. Chem. Soc*. (2011), *J. Serb. Chem. Soc*. **77** (2012) 983
17. National Committee for Clinical Laboratory Standards (NCCLS), *Performance Standards for Antimicrobial Susceptibility Testing*, Twelfth Informational Supplement (ISBN 1–56238-454-6), 2002, M100-S12 (M7). 940, West Valley Road, Suite 1400, Wayne, PA, 19087–1898, USA.
18. A. Srivastava, R. M. Singh, *Indian J. Chem., B* **44** (2005) 1868
19. a) R.-F. Chen, C.-T. Qian, *Chin. J. Chem.* **20** (2002) 427; b) L. Wang, C. Qian, H. Tian, Y. Ma, *Synth. Commun.* **33** (2003) 1459; c) C. Rui-Fang, Q. Chang-Tao, *Chin. J. Chem.* **20** (2002) 407; d) A. Dondoni, A. Massi, S. Sabatini, *Tetrahedron Lett.* **43** (2002) 5913; e) D. Gong, L. Zhang, C. Yuan, *Heteroatom Chem*. **14** (2003) 13; f) Y. Huang, F. Yang, C. Zhu, *J. Am. Chem. Soc.* **127** (2005) 16386
20. I. Suzuki, Y. Suzumura, K. Takeda, *Tetrahedron Lett.* **47** (2006) 7861
21. Y. Ma, C. Qian, L. Wang, M. Yang, *J. Org. Chem.* **65** (2000) 3864.

Journal of the Serbian Chemical Society
JSCS@tmf.bg.ac.rs • www.shd.org.rs/JSCS
J. Serb. Chem. Soc. 77 (11) S217–S225 (2012) *Supplementary material*

SUPPLEMENTARY MATERIAL TO

Lanthanum triflate-triggered synthesis of tetrahydroquinazolinone derivatives of *N*-allylquinolone and their biological assessment

HARDIK H. JARDOSH and MANISH P. PATEL*

Department of Chemistry, Sardar Patel University, Vallabh Vidyanagar-388120, Gujarat, India

J. Serb. Chem. Soc. 77 (11) (2012) 1561–1570

ANALYTICAL AND SPECTROSCOPIC CHARACTERIZATION DATA OF **5a**–**p** AND **6a**–**h**

*4-(1-Allyl-2-oxo-1,2-dihydroquinolin-3-yl)-4,6,7,8-tetrahydroquinazoline-2,5(1*H,3H*)-dione (**5a**)*. White powder; Yield: 87 %; m.p.: 192–194 °C; Anal. Calcd. for $C_{20}H_{19}N_3O_3$ (FW: 349.38): C, 68.75; H, 5.48; N, 12.03 %. Found: C, 68.52; H, 5.84; N, 12.30 %; IR (KBr, cm^{-1}): 3435, 3352 (N–H str.), 1711, 1639, 1593 (C=O str.); ^{1}H-NMR (400 MHz, DMSO-d_6, δ / ppm): 1.97–2.54 (6H, *m*, $3CH_2$), 4.90–5.05 (2H, *d*, J_{trans} = 17.2 Hz, J_{cis} = 10.8 Hz, N–CH_2–CH=C**H**$_2$), 5.18 (2H, *d*, *J* = 4.8 Hz, N–C**H**$_2$–CH), 5.94 (1H, *m*, C**H**=CH_2), 5.36 (1H, *s*, quinazolinone H_4), 7.08–7.60 (5H, *m*, Ar–H), 7.80 (1H, *s*, NH), 9.52 (1H, *s*, NH); ^{13}C-NMR (100 MHz, DMSO-d_6, δ / ppm): 21.28 (CH_2), 26.54 (CH_2), 36.80 (**C**H_2–CO), 44.39 (allylic N–**C**H_2–CH=C**H**$_2$), 49.31 (quinazolinone C_4), 105.51, 115.30, 117.23, 120.20, 122.54, 129.66, 130.92, 132.26, 133.02, 135.28, 138.67, 152.04 (12C, Ar-C and allylic C=C), 156.69 (C=O), 160.72 (C=O), 193.67 (C=O); MS (*m*/*z*): 350.2 $[M+1]^+$.

*4-(1-Allyl-2-oxo-1,2-dihydroquinolin-3-yl)-7,7-dimethyl-4,6,7,8-tetrahydroquinazoline-2,5(1*H,3H*)-dione (**5b**)*. White powder; Yield: 85 %; m.p.: 282–284 °C; Anal. Calcd. for $C_{22}H_{23}N_3O_3$ (FW: 377.44): C, 70.01; H, 6.14; N, 11.13 %. Found: C, 70.32; H, 6.53; N 10.84 %; IR (KBr, cm^{-1}): 3431, 3346 (N–H str.), 1708, 1634, 1604 (C=O str.); ^{1}H-NMR (400 MHz, DMSO-d_6, δ / ppm): 0.98 (3H, *s*, CH_3), 1.03 (3H, *s*, CH_3), 2.07–2.46 (4H, *m*, $2CH_2$) 4.98–5.09 (2H, *d*, J_{trans} = 17.2 Hz, J_{cis} = 10.8 Hz, N–CH_2–CH=C**H**$_2$), 5.21 (2H, *d*, *J* = 4.8 Hz, N–C**H**$_2$–CH), 5.97 (1H, *m*, C**H**=CH_2), 5.41 (1H, *s*, quinazolinone H_4), 7.11–7.68 (5H, *m*, Ar-H), 9.01 (1H, *s*, NH), 10.43 (1H, *s*, NH); ^{13}C-NMR (100 MHz,

* Corresponding author. E-mail: patelmanish1069@yahoo.com

DMSO-d_6, δ / ppm): 20.28 (CH_3), 20.84 (CH_3), 32.79 (**C**(CH_3)$_2$), 39.12 (CH_2), 48.87 (**C**H_2–CO), 49.94 (allylic N–**C**H_2–CH=C**H**$_2$), 50.14 (quinazolinone C_4), 105.52, 115.76, 118.12, 121.03, 122.87, 130.35, 131.73, 132.91, 133.54, 136.37, 139.24, 152.98 (12C, Ar-C and allylic C=C), 156.60 (C=O), 161.73 (C=O), 193.66 (C=O); MS (*m*/*z*): 378.3 $[M+1]^+$.

*4-(1-Allyl-2-oxo-1,2-dihydroquinolin-3-yl)-2-thioxo-2,3,4,6,7,8-hexahydro-quinazolin-5(1*H*)-one (**5c**)*. White powder; Yield: 85 %; m.p.: 197–199 °C; Anal. Calcd. for $C_{20}H_{19}N_3O_2S$ (FW: 365.45): C, 65.73; H, 5.24; N, 11.50 %. Found: C, 66.05; H, 5.01; N, 11.23 %; IR (KBr, cm^{-1}): 3392, 3240 (N–H str.), 1650, 1606 (C=O str.), 1183 (C=S str.); ^{1}H-NMR (400 MHz, DMSO-d_6, δ / ppm): 1.99–2.64 (6H, *m*, 3CH_2), 4.90–5.05 (2H, *d*, J_{trans} = 17.2 Hz, J_{cis} = 10.8 Hz, N–CH_2–CH=C**H**$_2$), 5.18 (2H, *d*, *J* = 4.8 Hz, N–C**H**$_2$–CH), 5.96 (1H, *m*, C**H**=CH_2), 5.40 (1H, *s*, quinazolinone H_4), 7.16–7.82 (5H, *m*, Ar–H), 8.97 (1H, *s*, NH), 10.61 (1H, *s*, NH); ^{13}C-NMR (100 MHz, DMSO-d_6, δ / ppm): 21.24 (CH_2), 26.43 (CH_2), 36.73 (**C**H_2–CO), 44.32 (allylic N–**C**H_2–CH=C**H**$_2$), 48.56 (quinazolinone C_4), 105.08, 115.12, 117.09, 120.18, 122.47, 129.24, 130.74, 132.10, 133.14, 135.23, 138.45, 153.07 (12C, Ar-C and allylic C=C), 157.87 (C=O), 175.83 (C=S), 194.19 (C=O); MS (*m*/*z*): 366.2 $[M+1]^+$.

*4-(1-Allyl-2-oxo-1,2-dihydroquinolin-3-yl)-7,7-dimethyl-2-thioxo-2,3,4,6,7,8--hexahydroquinazolin-5(1*H*)-one (**5d**)*. White powder; Yield: 78 %; m.p.: 285––287 °C; Anal. Calcd. for $C_{22}H_{23}N_3O_2S$ (FW: 393.50): C, 67.15; H, 5.89; N, 10.68 %. Found: C, 66.89; H, 6.23; N, 10.94 %; IR (KBr, cm^{-1}): 3390, 3227 (N–H str.), 1656, 1634 (C=O str.), 1174 (C=S str.); ^{1}H-NMR (400 MHz, DMSO-d_6, δ / ppm): 1.06 (3H, *s*, CH_3), 1.09 (3H, *s*, CH_3), 2.29–2.56 (4H, *m*, 2CH_2) 4.92––5.01 (2H, *d*, J_{trans} = 17.2 Hz, J_{cis} = 10.8 Hz, N–CH_2–CH=C**H**$_2$), 5.26 (2H, *d*, *J* = = 4.8 Hz, N–C**H**$_2$–CH), 5.87–5.94 (1H, *m*, C**H**=CH_2), 5.38 (1H, *s*, quinazolinone H_4), 7.02–7.63 (5H, *m*, Ar–H), 8.87 (1H, *s*, NH), 9.92 (1H, *s*, NH); ^{13}C-NMR (100 MHz, DMSO-d_6, δ / ppm): 26.29 (CH_3), 28.87 (CH_3), 33.44 (**C**(CH_3)$_2$), 39.35 (CH_2), 49.94 (**C**H_2–CO), 50.02 (allylic N–**C**H_2–CH=C**H**$_2$), 51.29 (quinazolinone C_4), 105.08, 115.71, 118.06, 120.97, 122.78, 130.27, 131.65, 132.88, 133.51, 136.32, 139.19, 152.86 (12C, Ar-C and allylic C=C), 156.76 (C=O), 180.34 (C=S), 194.50 (C=O); MS (*m*/*z*): 394.4 $[M+1]^+$.

*4-(1-Allyl-6-methyl-2-oxo-1,2-dihydroquinolin-3-yl)-4,6,7,8-tetrahydroqui-nazoline-2,5(1*H*,3*H*)-dione (**5e**)*. White powder; Yield: 82 %; m.p.: 210–212 °C; Anal. Calcd. for $C_{21}H_{21}N_3O_3$ (FW: 363.41): C, 69.41; H, 5.82; N, 11.56 %. Found: C, 69.30; H, 5.45; N, 11.39 %; IR (KBr, cm^{-1}): 3437, 3348 (N–H str.), 1701, 1611, 1598 (C=O str.); ^{1}H-NMR (400 MHz, DMSO-d_6, δ / ppm): 1.96––2.51 (6H, *m*, 3CH_2), 2.42 (3H, *s*, CH_3), 4.97–5.08 (2H, *d*, J_{trans} = 17.2 Hz, J_{cis} = = 10.8 Hz, N–CH_2–CH=C**H**$_2$), 5.21 (2H, *d*, *J* = 4.8 Hz, N–C**H**$_2$–CH), 5.97 (1H, *m*, C**H**=CH_2), 5.38 (1H, *s*, quinazolinone H_4), 7.06–7.57 (4H, *m*, Ar–H), 7.82 (1H, *s*, NH), 9.53 (1H, *s*, NH); ^{13}C-NMR (100 MHz, DMSO-d_6, δ / ppm): 20.69

(CH_3), 21.23 (CH_2), 26.52 (CH_2), 36.78 (**C**H_2–CO), 44.36 (allylic N–**C**H_2––CH=C**H**$_2$), 49.33 (quinazolinone C_4), 105.23, 115.17, 117.19, 120.14, 122.49, 129.61, 130.87, 132.11, 132.92, 135.03, 138.39, 151.98 (12C, Ar-C and allylic C=C), 156.23 (C=O), 161.54 (C=O), 193.55 (C=O); MS (*m*/*z*): 364.1 $[M+1]^+$.

*4-(1-Allyl-6-methyl-2-oxo-1,2-dihydroquinolin-3-yl)-7,7-dimethyl-4,6,7,8--tetrahydroquinazoline-2,5(1*H*,3*H*)-dione (**5f**).* White powder; Yield: 79 %; m.p.: 308–310 °C; Anal. Calcd. for $C_{23}H_{25}N_3O_3$ (FW: 391.46): C, 70.57; H, 6.44; N, 10.73 %. Found: C, 70.71; H, 6.69; N, 10.40 %; IR (KBr, cm^{-1}): 3440, 3359 (N–H str.),1680, 1626, 1604 (C=O str.); ^{1}H-NMR (400 MHz, DMSO-d_6, δ / ppm): 0.98 (3H, *s*, CH_3), 1.02 (3H, *s*, CH_3), 2.07–2.46 (4H, *m*, $2CH_2$), 2.28 (3H, *s*, CH_3), 4.97–5.05 (2H, *d*, J_{trans} = 17.2 Hz, J_{cis} = 10.8 Hz, N–CH_2–CH=C**H**$_2$), 5.13 (2H, *d*, *J* = 4.8 Hz, N–C**H**$_2$–CH), 5.92 (1H, *m*, C**H**=CH_2), 5.38 (1H, *s*, quinazolinone H_4), 7.06–7.43 (4H, *m*, Ar–H), 8.87 (1H, *s*, NH), 10.14 (1H, *s*, NH); ^{13}C-NMR (100 MHz, DMSO-d_6, δ / ppm): 20.31 (CH_3), 21.12 (CH_3), 22.70 (CH_3) 32.81 (**C**$(CH_3)_2$), 39.24 (CH_2), 49.03 (**C**H_2–CO), 49.86 (allylic N–**C**H_2–CH=C**H**$_2$), 50.21 (quinazolinone C_4), 105.67, 115.88, 118.17, 121.28, 122.93, 130.42, 131.80, 132.96, 133.67, 136.41, 139.26, 153.01 (12C, Ar-C and allylic C=C), 156.66 (C=O), 161.85 (C=O), 193.74 (C=O); MS (*m*/*z*): 392.6 $[M+1]^+$.

*4-(1-Allyl-6-methyl-2-oxo-1,2-dihydroquinolin-3-yl)-2-thioxo2,3,4,6,7,8--hexahydroquinazolin-5(1*H*)-one (**5g**).* Pale yellow powder; Yield: 82 %; m.p.: 211–213 °C; Anal. Calcd. for $C_{21}H_{21}N_3O_2S$ (FW: 379.48): C, 66.47; H, 5.58; N, 11.07 %. Found: C, 66.48; H, 5.27; N, 11.03 %; IR (KBr, cm^{-1}): 3391, 3230 (N–H str.), 1652, 1611 (C=O str.), 1179 (C=S str.); ^{1}H-NMR (400 MHz, DMSO-d_6, δ / / ppm): 1.86–2.44 (6H, *m*, $3CH_2$), 3.28 (3H, *s*, CH_3) 4.93–5.04, (2H, *d*, J_{trans} = = 17.2 Hz, J_{cis} = 10.8 Hz, N–CH_2–CH=C**H**$_2$), 5.19 (2H, *d*, *J* = 4.8 Hz, N–C**H**$_2$––CH), 5.95 (1H, *m*, C**H**=CH_2), 5.37 (1H, *s*, quinazolinone H_4), 7.12–7.78 (4H, *m*, Ar–H), 8.91 (1H, *s*, NH), 10.83 (1H, *s*, NH); ^{13}C-NMR (100 MHz, DMSO-d_6, δ / ppm): 21.11 (CH_3), 21.35 (CH_2), 26.41 (CH_2), 36.75 (**C**H_2–CO), 44.38 (allylic N–**C**H_2–CH=C**H**$_2$), 48.47 (quinazolinone C_4), 105.19, 115.21, 117.14, 120.24, 122.54, 129.32, 130.79, 132.13, 133.16, 135.39, 138.67, 153.16 (12C, Ar-C and allylic C=C), 156.94 (C=O), 176.34 (C=S), 194.21 (C=O); MS (*m*/*z*): 380.5 $[M+1]^+$.

*4-(1-Allyl-6-methyl-2-oxo-1,2-dihydroquinolin-3-yl)-7,7-dimethyl-2-thioxo--2,3,4,6,7,8-hexahydroquinazolin-5(1*H*)-one (**5h**).* White powder; Yield: 79 %; m.p.: 291–293 °C; Anal. Calcd. for $C_{23}H_{25}N_3O_2S$ (FW: 407.53): C, 67.79; H, 6.18; N, 10.31 %. Found: C, 68.06; H, 6.24; N, 10.67 %; IR (KBr, cm^{-1}): 3394, 3217 (N–H str.), 1657, 1639 (C=O str.), 1173 (C=S str.); ^{1}H-NMR (400 MHz, DMSO-d_6, δ / ppm): 0.98 (3H, *s*, CH_3), 1.02 (3H, *s*, CH_3), 2.35 (3H, *s*, CH_3), 2.07–2.51 (4H, *m*, $2CH_2$), 4.82–4.98 (2H, *d*, J_{trans} = 17.2 Hz, J_{cis} = 10.8 Hz, N–CH_2–CH=C**H**$_2$), 5.13 (2H, *d*, *J* = 4.8 Hz, N–C**H**$_2$–CH), 5.88 (1H, *m*, C**H**=CH_2), 5.35 (1H, *s*, quinazolinone H_4), 7.19–7.60 (4H, *m*, Ar–H), 9.06 (1H,

s, NH), 10.50 (1H, *s*, NH); ^{13}C-NMR (100 MHz, DMSO-d_6, δ / ppm): 20.51 (CH_3), 27.83 (CH_3), 29.16 (CH_3), 32.77 (**C**$(CH_3)_2$), 39.11 (CH_2), 49.07 (**C**H_2––CO), 50.13 (allylic N–**C**H_2–CH=C**H**$_2$), 50.90 (quinazolinone C_4), 105.57, 115.18, 117.02, 121.12, 122.97, 129.19, 131.37, 132.95, 133.77, 136.81, 140.26, 153.93 (12C, Ar-C and allylic C=C), 157.83 (C=O), 175.22 (C=S), 193.90 (C=O); MS (*m*/*z*): 408.3 $[M+1]^+$.

*4-(1-Allyl-6-methoxy-2-oxo-1,2-dihydroquinolin-3-yl)-4,6,7,8-tetrahydroquinazoline-2,5(1*H,3H*)-dione (**5i**)*. Pale yellow powder; Yield: 84 %; m.p.: 217–219 °C; Anal. Calcd. for $C_{21}H_{21}N_3O_4$ (FW: 379.41): C, 66.48; H, 5.58; N, 11.08 %. Found: C, 66.20; H, 5.59; N, 11.30 %; IR (KBr, cm^{-1}): 3402, 3265 (N–H str.), 1695, 1632, 1630 (C=O str.); ^{1}H-NMR (400 MHz, DMSO-d_6, δ / ppm): 1.94––2.53 (6H, *m*, 3CH_2), 3.72 (3H, *s*, OCH_3), 4.96–5.11 (2H, *d*, J_{trans} = 17.2 Hz, J_{cis} = 10.8 Hz, N–CH_2–CH=C**H**$_2$), 5.33 (2H, *d*, *J* = 4.8 Hz, N–C**H**$_2$–CH), 6.02 (1H, m, C**H**=CH_2), 5.63 (1H, *s*, quinazolinone H_4), 7.08–7.68 (4H, *m*, Ar–H), 8.18 (1H, *s*, NH), 10.29 (1H, *s*, NH); ^{13}C-NMR (100 MHz, DMSO-d_6, δ / ppm): 21.28 (CH_2), 26.61 (CH_2), 37.17 (**C**H_2–CO), 44.32 (allylic N–**C**H_2–CH=C**H**$_2$), 48.26 (quinazolinone C_4), 55.62 (OCH_3), 106.18, 116.82, 117.96, 120.55, 123.01, 130.13, 131.26, 132.43, 133.12, 135.27, 138.46, 152.05 (12C, Ar-C and allylic C=C), 157.06 (C=O), 162.28 (C=O), 194.13 (C=O); MS (*m*/*z*): 380.5 $[M+1]^+$.

*4-(1-Allyl-6-methoxy-2-oxo-1,2-dihydroquinolin-3-yl)-7,7-dimethyl-4,6,7,8--tetrahydroquinazoline-2,5(1*H,3H*)-dione (**5j**)*. Pale yellow powder; Yield: 82 %; m.p.: 295–297 °C; Anal. Calcd. for $C_{23}H_{25}N_3O_4$ (FW: 407.46): C, 67.80; H, 6.18; N, 10.31 %. Found: C, 67.45; H, 6.34; N, 10.22 %; IR (KBr, cm^{-1}): 3442, 3356 (N–H str.), 1671, 1626, 1602 (C=O str.); ^{1}H-NMR (400 MHz, DMSO-d_6, δ / ppm): 1.02 (3H, *s*, CH_3), 1.04 (3H, *s*, CH_3), 2.05–2.42 (4H, *m*, 2CH_2), 3.86 (3H, *s*, OCH_3), 4.99–5.08 (2H, *d*, J_{trans} = 17.2 Hz, J_{cis} = 10.8 Hz, N–CH_2––CH=C**H**$_2$), 5.15 (2H, *d*, *J* = 4.8 Hz, N–C**H**$_2$–CH), 5.96 (1H, *m*, C**H**=CH_2), 5.43 (1H, *s*, quinazolinone H_4), 7.07–7.41 (4H, *m*, Ar–H), 8.92 (1H, *s*, NH), 10.10 (1H, *s*, NH); ^{13}C-NMR (100 MHz, DMSO-d_6, δ / ppm): 20.26 (CH_3), 21.09 (CH_3), 32.94 (**C**$(CH_3)_2$), 39.27 (CH_2), 49.12 (**C**H_2–CO), 49.86 (allylic N–**C**H_2––CH=C**H**$_2$), 50.21 (quinazolinone C_4), 55.86 (OCH_3), 105.71, 116.01, 118.25, 121.32, 122.97, 130.46, 131.84, 132.99, 133.70, 136.44, 139.29, 153.10 (12C, Ar-C and allylic C=C), 156.82 (C=O), 161.93 (C=O), 193.81 (C=O); MS (*m*/*z*): 408.7 $[M+1]^+$.

*4-(1-Allyl-6-methoxy-2-oxo-1,2-dihydroquinolin-3-yl)-2-thioxo-2,3,4,6,7,8--hexahydroquinazolin-5(1*H*)-one (**5k**)*. Pale yellow powder; Yield: 87 %; m.p.: 225–227 °C; Anal. Calcd. for $C_{21}H_{21}N_3O_3S$ (FW: 395.47): C, 63.78; H, 5.35; N, 10.63 %. Found: C, 63.91; H, 5.28; N, 10.38 %; IR (KBr, cm^{-1}): 3401, 3241 (N–H str.), 1651, 1609 (C=O str.), 1186 (C=S str.); ^{1}H-NMR (400 MHz, DMSO-d_6, δ / ppm): 1.89–2.48 (6H, *m*, 3CH_2), 3.89 (3H, *s*, OCH_3), 4.96–5.07, (2H, *d*,

J_{trans} = 17.2 Hz, J_{cis} = 10.8 Hz, N–CH_2–CH=C**H**$_2$), 5.26 (2H, *d*, *J* = 4.8 Hz, N–C**H**$_2$–CH), 5.97 (1H, *m*, C**H**=CH_2), 5.38 (1H, *s*, quinazolinone H_4), 7.07–7.64 (4H, *m*, Ar–H), 9.01 (1H, *s*, NH), 10.91 (1H, *s*, NH); ^{13}C-NMR (100 MHz, DMSO-d_6, δ / ppm): 21.39 (CH_2), 26.47 (CH_2), 36.82 (**C**H_2–CO), 44.45 (allylic N–**C**H_2–CH=C**H**$_2$), 48.53 (quinazolinone C_4), 55.58 (OCH_3), 104.98, 115.17, 117.21, 120.22, 122.48, 129.29, 130.81, 132.09, 133.13, 135.32, 138.64, 153.22 (12C, Ar-C and allylic C=C), 155.92 (C=O), 175.21 (C=S), 194.39 (C=O); MS (*m*/*z*): 396.1 $[M+1]^+$.

*4-(1-Allyl-6-methoxy-2-oxo-1,2-dihydroquinolin-3-yl)-7,7-dimethyl-2-thioxo--2,3,4,6,7,8-hexahydroquinazolin-5(1*H*)-one (**5l**)*. Pale yellow powder; Yield: 82 %; m.p.: 296–298 °C; Anal. Calcd. for $C_{23}H_{25}N_3O_3S$ (FW: 423.53): C, 65.23; H 5.95; N, 9.92 %. Found: C, 64.95; H 5.87; N, 9.56 %; IR (KBr, cm^{-1}): 3395, 3220 (N–H str.), 1656, 1634 (C=O str.), 1174 (C=S str.); ^{1}H-NMR (400 MHz, DMSO-d_6, δ / ppm): 1.01 (3H, *s*, CH_3), 1.04 (3H, *s*, CH_3), 2.08–2.49 (4H, *m*, 2CH_2), 3.85 (3H, *s*, OCH_3), 4.96–5.02 (2H, *d*, J_{trans} = 17.2 Hz, J_{cis} = 10.8 Hz, N–CH_2–CH=C**H**$_2$), 5.24 (2H, *d*, *J* = 4.8 Hz, N–C**H**$_2$–CH), 6.02 (1H, *m*, C**H**=CH_2), 5.76 (1H, *s*, quinazolinone H_4), 7.16–7.59 (4H, *m*, Ar–H), 8.42 (1H, *s*, NH), 10.69 (1H, *s*, NH); ^{13}C-NMR (100 MHz, DMSO-d_6, δ / ppm): 27.62 (CH_3), 28.96 (CH_3), 32.82 (**C**$(CH_3)_2$), 40.38 (CH_2), 50.17 (**C**H_2–CO), 51.25 (allylic N–**C**H_2–CH=C**H**$_2$), 51.97 (quinazolinone C_4), 55.14 (OCH_3), 106.26, 115.89, 117.36, 121.18, 123.16, 129.41, 131.42, 133.02, 133.94, 137.13, 140.45, 154.15 (12C, Ar-C and allylic C=C), 159.24 (C=O), 177.10 (C=S), 195.72 (C=O); MS (*m*/*z*): 424.2 $[M+1]^+$.

*4-(1-Allyl-6-chloro-2-oxo-1,2-dihydroquinolin-3-yl)-4,6,7,8-tetrahydroquinazoline-2,5(1*H*,3*H*)-dione (**5m**)*. White powder; Yield: 86 %; m.p.: 230–232 °C; Anal. Calcd. for $C_{20}H_{18}ClN_3O_3$ (FW: 383.83): C, 62.58; H 4.73; N, 10.95 %. Found: C, 62.43; H 5.12; N, 11.03 %; IR (KBr, cm^{-1}): 3440, 3357 (N–H str.), 1703, 1642, 1603 (C=O str.); ^{1}H-NMR (400 MHz, DMSO-d_6, δ / ppm): 1.98––2.59 (6H, *m*, 3CH_2), 4.98–5.14 (2H, *d*, J_{trans} = 17.2 Hz, J_{cis} = 10.8 Hz, N–CH_2––CH=C**H**$_2$), 5.47 (2H, *d*, *J* = 4.8 Hz, N–C**H**$_2$–CH), 5.82 (1H, *m*, C**H**=CH_2), 5.66 (1H, *s*, quinazolinone H_4), 7.05–7.60 (4H, *m*, Ar–H), 7.98 (1H, *s*, NH), 10.11 (1H, *s*, NH); ^{13}C-NMR (100 MHz, DMSO-d_6, δ / ppm): 21.27 (CH_2), 26.38 (CH_2), 36.82 (**C**H_2–CO), 44.41 (allylic N–**C**H_2–CH=C**H**$_2$), 48.15 (quinazolinone C_4), 105.53, 115.18, 117.20, 120.41, 123.23, 129.98, 131.12, 132.36, 133.09, 135.12, 138.19, 152.01. (12C, Ar-C and allylic C=C), 156.96 (C=O), 161.83 (C=O), 194.02 (C=O); MS (*m*/*z*): 384.9 $[M+1]^+$.

*4-(1-Allyl-6-chloro-2-oxo-1,2-dihydroquinolin-3-yl)-7,7-dimethyl-4,6,7,8--tetrahydroquinazoline-2,5(1*H*,3*H*)-dione (**5n**)*. Pale yellow powder; Yield: 84 %; m.p.: 286–288 °C; Anal. Calcd. for $C_{22}H_{22}ClN_3O_3$ (FW: 411.88): C, 64.15; H 5.38; N, 10.20 %. Found: C, 64.41; H 5.43; N, 9.85 %; IR (KBr, cm^{-1}): 3445, 3364 (N–H str.), 1660, 1620, 1600 (C=O str.); ^{1}H-NMR (400 MHz, DMSO-d_6,

δ / ppm): 0.99 (3H, *s*, CH_3), 1.02 (3H, *s*, CH_3), 2.02–2.37 (4H, *m*, $2CH_2$), 4.95––5.01 (2H, *d*, J_{trans} = 17.2 Hz, J_{cis} = 10.8 Hz, N–CH_2–CH=C**H**$_2$), 5.10 (2H, *d*, *J* = = 4.8 Hz, N–C**H**$_2$–CH), 5.92 (1H, *m*, C**H**=CH_2), 5.41 (1H, *s*, quinazolinone H_4), 7.02–7.38 (4H, *m*, Ar–H), 8.89 (1H, *s*, NH), 10.03 (1H, *s*, NH); ^{13}C-NMR (100 MHz, DMSO-d_6, δ / ppm): 27.56 (CH_3), 29.11 (CH_3), 32.45 (**C**(CH_3)$_2$), 39.51 (CH_2), 49.22 (**C**H_2–CO), 49.93 (allylic N–**C**H_2–CH=C**H**$_2$), 50.76 (quinazolinone C_4), 106.04, 116.98, 118.79, 121.55, 123.11, 130.88, 131.99, 133.07, 133.87, 136.91, 139.36, 153.26 (12C, Ar-C and allylic C=C), 157.12 (C=O), 162.05 (C=O), 194.13 (C=O); MS (*m*/*z*): 412.7 $[M+1]^+$.

*4-(1-Allyl-6-chloro-2-oxo-1,2-dihydroquinolin-3-yl)-2-thioxo-2,3,4,6,7,8--hexahydroquinazolin-5(1*H*)-one (**5o**)*. Yellowish-orange powder; Yield: 81 %; m.p.: 234–236 °C; Anal. Calcd. for $C_{20}H_{18}ClN_3O_2S$ (FW: 399.89): C, 60.07; H 4.54; N, 10.51 %. Found: C, 59.90; H 4.45; N, 10.57 %; IR (KBr, cm^{-1}): 3396, 3236 (N–H str.), 1647, 1601 (C=O str.), 1184 (C=S str.); ^{1}H-NMR (400 MHz, DMSO-d_6, δ / ppm): 1.85–2.37 (6H, *m*, $3CH_2$), 4.92–5.01, (2H, *d*, *J* = 4.8 Hz, N–CH_2–CH=C**H**$_2$), 5.20 (2H, *d*, J_{trans} = 17.2 Hz, J_{cis} = 10.8 Hz, N–C**H**$_2$–CH), 5.93 (1H, *m*, C**H**=CH_2), 5.30 (1H, *s*, quinazolinone H_4), 7.11–7.64 (4H, *m*, Ar–H), 8.71 (1H, *s*, NH), 10.75 (1H, *s*, NH); ^{13}C-NMR (100 MHz, DMSO-d_6, δ / ppm): 21.31 (CH_2), 26.44 (CH_2), 36.76 (**C**H_2–CO), 44.41 (allylic N–**C**H_2–CH=C**H**$_2$), 48.49 (quinazolinone C_4), 104.71, 114.98, 117.03, 120.08, 122.28, 129.15, 130.67, 131.97, 133.01, 135.19, 138.43, 153.11 (12C, Ar-C and allylic C=C), 155.42 (C=O), 175.12 (C=S), 194.27 (C=O); MS (*m*/*z*): 400.8 $[M+1]^+$.

*4-(1-Allyl-6-chloro-2-oxo-1,2-dihydroquinolin-3-yl)-7,7-dimethyl-2-thioxo--2,3,4,6,7,8-hexahydroquinazolin-5(1*H*)-one (**5p**)*. Pale yellow powder; Yield: 76 %; m.p.: 302–304 °C; Anal. Calcd. for $C_{22}H_{22}ClN_3O_2S$ (FW: 427.95): C, 61.74; H 5.18; N, 9.82 %. Found: C, 61.55; H 5.50; N, 9.53 %; IR (KBr, cm^{-1}): 3398, 3229 (N–H str.), 1662, 1645 (C=O str.), 1175 (C=S str.); ^{1}H-NMR (400 MHz, DMSO-d_6, δ / ppm): 0.98 (3H, *s*, CH_3), 1.01 (3H, *s*, CH_3), 2.04–2.39 (4H, *m*, $2CH_2$), 4.89–4.96 (2H, *d*, J_{trans} = 17.2 Hz, J_{cis} = 10.8 Hz, N–CH_2–CH=C**H**$_2$), 5.15 (2H, *d*, *J* = 4.8 Hz, N–C**H**$_2$–CH), 5.87 (1H, *m*, C**H**=CH_2), 5.54 (1H, *s*, quinazolinone H_4), 7.02–7.47 (4H, *m*, Ar–H), 7.92 (1H, *s*, NH), 9.87 (1H, *s*, NH); ^{13}C--NMR (100 MHz, DMSO-d_6, δ / ppm): 26.26 (CH_3), 27.01 (CH_3), 32.07 (**C**(CH_3)$_2$), 41.19 (CH_2), 49.03 (**C**H_2–CO), 50.86 (allylic N–**C**H_2–CH=C**H**$_2$), 52.04 (quinazolinone C_4), 105.12, 115.16, 116.45, 121.36, 122.73, 129.17, 131.10, 132.59, 133.47, 136.87, 139.55, 153.37 (12C, Ar-C and allylic C=C), 158.65 (C=O), 176.32 (C=S), 193.33 (C=O); MS (*m*/*z*): 429.1 $[M+1]^+$.

*4-(1-Allyl-2-oxo-1,2-dihydroquinolin-3-yl)-1-phenyl-2-thioxo-2,3,4,6,7,8--hexahydroquinazolin-5(1*H*)-one (**6a**)*. White powder; Yield: 74 %; m.p.: 248––250 °C; Anal. Calcd. for $C_{26}H_{23}N_3O_2S$ (FW: 441.54): C, 70.72; H 5.25; N, 9.52 %. Found: C, 70.88; H 5.63; N, 9.39 %; IR (KBr, cm^{-1}): 3464 (N–H str.), 1670, 1653 (C=O str.), 1182 (C=S str.); ^{1}H-NMR (400 MHz, DMSO-d_6, δ /

/ ppm): 1.76–2.32 (6H, *m*, 3CH_2), 4.82–4.98 (2H, *d*, J_{trans} = 17.6 Hz, J_{cis} = 10.4 Hz, N–CH_2–CH=C**H**$_2$), 5.11 (2H, *d*, *J* = 4.8 Hz, N–C**H**$_2$–CH), 5.82 (1H, *m*, C**H**=CH_2), 5.29 (1H, *s*, quinazolinone H_4), 7.12–7.81 (10H, *m*, Ar–H), 9.76 (1H, *s*, NH); ^{13}C-NMR (100 MHz, DMSO-d_6, δ / ppm): 21.38 (CH_2), 26.51 (CH_2), 36.49 (**C**H_2–CO), 45.13 (allylic N–**C**H_2–CH=C**H**$_2$), 49.25 (quinazolinone C_4), 105.41, 115.03, 116.75, 120.18, 122.47, 127.91, 128.34, 129.16, 130.20, 131.12, 132.26, 133.46, 133.85, 135.87, 138.67, 154.31 (16C, Ar-C and allylic C=C), 161.25 (C=O), 165.18 (C=S), 194.46 (C=O); MS (*m*/*z*): 442.3 $[M+1]^+$.

*4-(1-Allyl-2-oxo-1,2-dihydroquinolin-3-yl)-7,7-dimethyl-1-phenyl-2-thioxo--2,3,4,6,7,8-hexahydroquinazolin-5(1*H*)-one (**6b**)*. Pale yellow powder; Yield: 83 %; m.p.: 234–236 °C; Anal. Calcd. for $C_{28}H_{27}N_3O_2S$ (FW: 469.60): C, 71.61; H 5.80; N, 8.95 %. Found: C, 71.38; H 5.41; N, 9.19 %; IR (KBr, cm^{-1}): 3471, (N–H str.), 1653, 1630 (C=O str.), 1176 (C=S str.); ^{1}H-NMR (400 MHz, DMSO-d_6, δ / ppm): 1.09 (3H, *s*, CH_3), 1.11 (3H, *s*, CH_3), 2.26–2.72 (4H, *m*, 2CH_2), 4.96––5.01 (2H, *d*, J_{trans} = 17.6 Hz, J_{cis} = 10.4 Hz, N–CH_2–CH=C**H**$_2$), 5.17 (2H, *d*, *J* = = 4.8 Hz, N–C**H**$_2$–CH), 5.94 (1H, *m*, C**H**=CH_2), 5.44 (1H, *s*, quinazolinone H_4), 7.25–7.73 (10H, *m*, Ar–H), 10.84 (1H, *s*, NH); ^{13}C-NMR (100 MHz, DMSO-d_6, δ / ppm): 28.03 (CH_3), 28.80 (CH_3), 32.60 (**C**$(CH_3)_2$), 37.58 (CH_2), 41.27 (**C**H_2––CO), 44.69 (allylic N–**C**H_2–CH=C**H**$_2$), 50.42 (quinazolinone C_4), 105.64, 115.50, 117.18, 119.92, 121.27, 122.82, 126.62, 128.64, 129.60, 131.24, 131.75, 132.80, 133.92, 137.02, 138.49, 154.56 (16C, Ar-C and allylic C=C), 160.00 (C=O), 166.78 (C=S), 194.62 (C=O); MS (*m*/*z*): 470.4 $[M+1]^+$.

*4-(1-Allyl-6-methyl-2-oxo-1,2-dihydroquinolin-3-yl)-1-phenyl-2-thioxo--2,3,4,6,7,8-hexahydroquinazolin-5(1*H*)-one (**6c**)*. White powder; Yield: 74 %; m.p.: 262–264 °C; Anal. Calcd. for $C_{27}H_{25}N_3O_2S$ (FW: 455.57): C, 71.18; H 5.53; N, 9.22 %. Found: C, 70.79; H 5.32; N, 9.25 %; IR (KBr, cm^{-1}): 3470 (N–H str.), 1651, 1622 (C=O str.), 1184 (C=S str.); ^{1}H-NMR (400 MHz, DMSO-d_6, δ / / ppm): 1.81–2.42 (6H, *m*, 3CH_2), 2.70 (3H, *s*, CH_3), 4.86–5.01 (2H, *d*, J_{trans} = = 17.6 Hz, J_{cis} = 10.4 Hz, N–CH_2–CH=C**H**$_2$), 5.16 (2H, *d*, *J* = 4.8 Hz, N–C**H**$_2$––CH), 5.88 (1H, *m*, C**H**=CH_2), 5.34 (1H, *s*, quinazolinone H_4), 7.21–8.01 (9H, *m*, Ar–H), 10.03 (1H, *s*, NH); ^{13}C-NMR (100 MHz, DMSO-d_6, δ / ppm): 20.86 (CH_3), 21.94 (CH_2), 27.12 (CH_2), 36.54 (**C**H_2–CO), 45.44 (allylic N–**C**H_2––CH=C**H**$_2$), 49.77 (quinazolinone C_4), 105.22, 115.11, 116.81, 120.22, 122.53, 128.02, 128.67, 129.29, 130.31, 131.14, 132.34, 133.48, 133.89, 136.10, 138.83, 154.51 (16C, Ar-C and allylic C=C), 162.82 (C=O), 166.17 (C=S), 194.69 (C=O); MS (*m*/*z*): 456.3 $[M+1]^+$.

*4-(1-Allyl-6-methyl-2-oxo-1,2-dihydroquinolin-3-yl)-7,7-dimethyl-1-phenyl--2-thioxo-2,3,4,6,7,8-hexahydroquinazolin-5(1*H*)-one (**6d**)*. White powder; Yield: 77 %; m.p.: 251–253 °C; Anal. Calcd. for $C_{29}H_{29}N_3O_2S$ (FW: 483.62): C, 72.02; H 6.04; N, 8.69 %. Found: C, 72.13; H 6.21, N, 8.42 %; IR (KBr, cm^{-1}): 3459, (N–H str.), 1654, 1633 (C=O str.), 1180 (C=S str.); ^{1}H-NMR (400 MHz, DMSO-d_6,

δ / ppm): 0.86 (3H, *s*, CH_3), 0.95 (3H, *s*, CH_3), 1.87–2.32 (4H, *m*, $2CH_2$), 2.29 (3H, *s*, CH_3), 4.85–5.04 (2H, *d*, J_{trans} = 17.6 Hz, J_{cis} = 10.4 Hz, N–CH_2––CH=C**H**$_2$), 5.19 (2H, *d*, *J* = 4.8 Hz, N–C**H**$_2$–CH), 5.91 (1H, *m*, C**H**=CH_2), 5.37 (1H, *s*, quinazolinone H_4), 7.06–7.72 (9H, *m*, Ar–H), 9.98 (1H, *s*, NH); ^{13}C-NMR (100 MHz, DMSO-d_6, δ / ppm): 20.47 (CH_3), 27.85 (CH_3), 29.73 (CH_3), 32.48 (**C**$(CH_3)_2$), 39.59 (CH_2), 49.91 (**C**H_2–CO), 50.28 (allylic N–**C**H_2–CH=C**H**$_2$), 51.40 (quinazolinone C_4), 105.37, 115.44, 117.21, 117.67, 121.41, 123.37, 126.78, 127.22, 129.38, 130.55, 131.62, 133.31, 134.54, 137.23, 140.46, 154.33 (16C, Ar-C and allylic C=C), 158.14 (C=O), 166.52 (C=S), 194.43 (C=O); MS (*m*/*z*): 484.7 $[M+1]^+$.

*4-(1-Allyl-6-methoxy-2-oxo-1,2-dihydroquinolin-3-yl)-1-phenyl-2-thioxo--2,3,4,6,7,8-hexahydroquinazolin-5(1*H*)-one (**6e**)*. Pale yellow powder; Yield: 79 %; m.p.: 276–278 °C; Anal. Calcd. for $C_{27}H_{25}N_3O_3S$ (FW: 471.57): C, 68.77; H 5.34; N, 8.91 %. Found: C, 68.84; H 5.46; N, 8.67 %; IR (KBr, cm^{-1}): 3435 (N–H str.), 1653, 1624 (C=O str.), 1178 (C=S str.); ^{1}H-NMR (400 MHz, DMSO-d_6, δ / / ppm): 1.88–2.27 (6H, *m*, $3CH_2$), 3.81 (3H, *s*, OCH_3), 4.94–4.99 (2H, *d*, J_{trans} = = 17.6 Hz, J_{cis} = 10.4 Hz, N–CH_2–CH=C**H**$_2$), 5.15 (2H, *d*, *J* = 4.8 Hz, N–C**H**$_2$––CH), 5.93 (1H, *m*, C**H**=CH_2), 5.40 (1H, *s*, quinazolinone H_4), 7.17–7.75 (9H, *m*, Ar–H), 9.34 (1H, *s*, NH); ^{13}C-NMR (100 MHz, DMSO-d_6, δ / ppm): 21.21 (CH_2), 28.33 (CH_2), 37.42 (**C**H_2–CO), 45.88 (allylic N–**C**H_2–CH=C**H**$_2$), 49.59 (quinazolinone C_4), 56.02 (OCH_3), 105.66, 109.16, 110.13, 116.59, 119.95, 120.33, 122.82, 127.64, 128.81, 129.45, 131.99, 133.39, 137.08, 140.85, 153.80, 154.72, (16C, Ar-C and allylic C=C), 160.96 (C=O), 178.21 (C=S), 195.04 (C=O); MS (*m*/*z*): 472.3 $[M+1]^+$.

*4-(1-Allyl-6-methoxy-2-oxo-1,2-dihydroquinolin-3-yl)-7,7-dimethyl-1-phenyl-2-thioxo-2,3,4,6,7,8-hexahydroquinazolin-5(1*H*)-one (**6f**)*. Pale yellow powder; Yield: 85 %; m.p.: 289–291 °C; Anal. Calcd. for $C_{29}H_{29}N_3O_3S$ (FW: 499.62): C, 69.71; H 5.85; N, 8.41 %. Found: C, 69.37; H 5.66; N, 8.65 %; IR (KBr, cm^{-1}): 3473, (N–H str.), 1657, 1631 (C=O str.), 1185 (C=S str.); ^{1}H-NMR (400 MHz, DMSO-d_6, δ / ppm): 1.04 (3H, *s*, CH_3), 1.06 (3H, *s*, CH_3), 2.08–2.48 (4H, *m*, $2CH_2$), 3.89 (3H, *s*, OCH_3), 5.01–5.12 (2H, *d*, J_{trans} = 17.6 Hz, J_{cis} = 10.4 Hz, N–CH_2–CH=C**H**$_2$), 5.22 (2H, *d*, *J* = 4.8 Hz, N–C**H**$_2$–CH), 6.05 (1H, *m*, C**H**=CH_2), 5.46 (1H, *s*, quinazolinone H_4), 7.14–8.02 (9H, *m*, Ar–H), 10.06 (1H, *s*, NH); ^{13}C-NMR (100 MHz, DMSO-d_6, δ / ppm): 27.82 (CH_3), 29.75 (CH_3), 32.69 (**C**$(CH_3)_2$), 40.15 (CH_2), 50.13 (**C**H_2–CO), 50.29 (allylic N–**C**H_2––CH=C**H**$_2$), 51.24 (quinazolinone C_4), 55.19 (OCH_3), 105.45, 115.37, 117.38, 118.01, 121.63, 123.51, 126.90, 127.47, 129.50, 130.47, 131.85, 133.49, 134.77, 137.39, 140.62, 154.60 (16C, Ar-C and allylic C=C), 158.48 (C=O), 166.75 (C=S), 194.71 (C=O); MS (*m*/*z*): 500.4 $[M+1]^+$.

*4-(1-Allyl-6-chloro-2-oxo-1,2-dihydroquinolin-3-yl)-1-phenyl-2-thioxo--2,3,4,6,7,8-hexahydroquinazolin-5(1*H*)-one (**6g**)*. Pale yellow powder; Yield: 73

%; m.p.: 285–287 °C; Anal. Calcd. for $C_{26}H_{22}ClN_3O_2S$ (FW: 475.99): C, 65.61; H 4.66, N; 8.83 %. Found: C, 65.84; H 4.58; N, 8.44 %; IR (KBr, cm^{-1}): 3467 (N–H str.), 1673, 1648 (C=O str.), 1178 (C=S str.); ^{1}H-NMR (400 MHz, DMSO-d_6, δ / ppm): 2.06–2.79 (6H, *m*, $3CH_2$), 4.95–5.00 (2H, *d*, J_{trans} = 17.6 Hz, J_{cis} = 10.4 Hz, N–CH_2–CH=C**H**$_2$), 5.18 (2H, *d*, *J* = 4.8 Hz, N–C**H**$_2$–CH), 5.94 (1H, *m*, C**H**=CH_2), 5.40 (1H, *s*, quinazolinone H_4), 7.17–8.01 (9H, *m*, Ar–H), 10.89 (1H, *s*, NH); ^{13}C-NMR (100 MHz, DMSO-d_6, δ / ppm): 20.78 (CH_2), 28.23 (CH_2), 37.13 (**C**H_2–CO), 44.86 (allylic N–**C**H_2–CH=C**H**$_2$), 50.63 (quinazolinone C_4), 106.23, 115.32, 117.25, 117.51, 121.42, 122.58, 126.82, 128.64, 129.57, 130.67, 132.60, 132.71, 133.13, 135.06, 137.21, 157.03 (16C, Ar-C and allylic C=C), 159.87 (C=O), 166.72 (C=S), 194.85 (C=O); MS (*m*/*z*): 476.6 $[M+1]^+$.

*4-(1-Allyl-6-chloro-2-oxo-1,2-dihydroquinolin-3-yl)-7,7-dimethyl-1-phenyl--2-thioxo-2,3,4,6,7,8-hexahydroquinazolin-5(1*H*)-one (**6h**)*. Yellowish-orange powder; Yield: 73 %; m.p.: 301–303 °C; Anal. Calcd. for $C_{28}H_{26}ClN_3O_2S$ (FW: 504.04): C, 66.72; H 5.20; N, 8.34 %. Found: C, 66.63; H 5.04; N, 8.63 %; IR (KBr, cm^{-1}): 3452, (N–H str.), 1670, 1644 (C=O str.), 1182 (C=S str.); ^{1}H-NMR (400 MHz, DMSO-d_6, δ / ppm): 1.01 (3H, *s*, CH_3), 1.04 (3H, *s*, CH_3), 2.01–2.43 (4H, *m*, $2CH_2$), 4.98–5.06 (2H, *d*, J_{trans} = 17.6 Hz, J_{cis} = 10.4 Hz, N–CH_2––CH=C**H**$_2$), 5.19 (2H, *d*, *J* = 4.8 Hz, N–C**H**$_2$–CH), 5.97 (1H, m, C**H**=CH_2), 5.41 (1H, *s*, quinazolinone H_4), 7.08–7.76 (9H, *m*, Ar–H), 9.87 (1H, *s*, NH); ^{13}C-NMR (100 MHz, DMSO-d_6, δ / ppm): 26.89 (CH_3), 29.46 (CH_3), 32.39 (**C**$(CH_3)_2$), 40.01 (CH_2), 49.98 (**C**H_2–CO), 50.09 (allylic N–**C**H_2–CH=C**H**$_2$), 51.19 (quinazolinone C_4), 105.37, 115.22, 117.26, 117.89, 121.47, 123.32, 126.78, 127.34, 129.41, 130.38, 131.81, 133.32, 134.52, 137.23, 140.49, 154.71 (16C, Ar-C and allylic C=C), 160.12 (C=O), 166.81 (C=S), 195.08 (C=O); MS (*m*/*z*): 505.2 $[M+1]^+$.

Journal of the Serbian Chemical Society
JSCS-info@shd.org.rs • www.shd.org.rs/JSCS
J. Serb. Chem. Soc. 77 (11) 1571–1588 (2012)
JSCS–4372
UDC 547.915+547.631.6+544.032.6–31+66.094.3–92:541.459
Original scientific paper

UV-induced change in the antioxidant activity of quercetin toward benzophenone-initiated lipid peroxidation

JELENA B. ZVEZDANOVIĆ, DEJAN Z. MARKOVIĆ*, DRAGAN J. CVETKOVIĆ and JELENA S. STANOJEVIĆ#

University of Niš, Faculty of Technology, Bulevar oslobodjenja 124, 16000 Leskovac, Serbia

(Received 1 February, revised 19 May 2012)

Abstract: The aim of this work was to estimate the degradation and change in the antioxidant activity of quercetin in the presence of two different mixtures of phospholipids in methanolic solution, under continuous UV-irradiation from three different sub-ranges (UV-A, UV-B and UV-C), in the presence and in the absence of the selected UV-absorbing photosensitizer, benzophenone. Quercetin was employed to control the lipid peroxidation process generated by UV-irradiation, by absorbing part of the UV incident light, and/or by scavenging the involved, created free radicals. The results showed that quercetin undergoes irreversible destruction, which was highly dependent on the energy input of the UV-photons, and was more expressed in the presence than in the absence of benzophenone. Simultaneously, quercetin expressed a suppression effect on lipid peroxidation processes in UV-irradiated phospholipid mixtures in both the absence and presence of benzophenone (more or less effective, respectively). In the UV-C-irradiated mixtures, photosensitizing function of benzophenone was significantly reduced due to its strong absorption in the UV-C spectral range, therefore affecting lower antioxidant activity of the remaining quercetin.

Keywords: quercetin; phospholipids; benzophenone; UV-irradiation; lipid peroxidation.

INTRODUCTION

Ultraviolet (UV) radiation is part of the natural sunlight spectrum that reaches the Earth's surface. Most of the solar UV energy incident on human skin derives from the deeply penetrating UV-A region (>95 % from 320 to 400 nm),[1] while the rest belongs to the more energetic UV-B radiation (280–320 nm); UV-C radiation (200–280 nm) is completely absorbed by the atmosphere. In addition to being the obligatory driving force of photosynthesis, light may also be a damaging factor in the biosphere:[2] recent depletion of the stratospheric ozone layer

* Corresponding author. E-mail: dejan_markovic57@yahoo.com
# Serbian Chemical Society member.
doi: 10.2298/JSC120012059Z

has led to an increase of the biologically most damaging UV-B portion at ambient levels. It triggers events that affect many crucial biological processes of global importance, such as DNA replication[3,4] and photosynthesis.[5,6] It has been especially recognized as one of the major agents that initiate many harmful free radical-mediated processes, such as lipid peroxidation (LP).

Lipid peroxidation occurs either by a free radical chain reaction (Type I), or, through a non-radical pathway (Type II), by direct reaction with singlet oxygen, created in the presence of a photosensitizer.[7–10] As for every free radical-mediated process – in the form of a chain reaction – lipid peroxidation consists of an initiation step (formation of lipid radicals – $L^{\bullet}$), a propagation step (in which lipid radicals react with oxygen to form lipid peroxy radicals – $LOO^{\bullet}$), and a termination step (formation of lipid hydroperoxides – LOOH – with a diene type of structure).[10,11] Typical lipid peroxidation initiators are reactive oxygen species (ROS), such as hydroxy radicals ($OH^{\bullet}$) or peroxy radicals ($ROO^{\bullet}$). They can be created through a variety of chemical reactions, some of which include typical lipid radical "producers", such are a variety of external stresses,[10] implying very commonly an external radiation;[11–13] in case of UV-irradiation, LP may include a special type of LP initiators, *e.g.*, photosensitizers such as benzophenone (BZP), in very different media.[14–16]

Benzophenone (Fig. 1) has been long recognized for its most known organic photochemical reaction, *i.e.*, H-abstraction by its long lived triplet state, ^{3}BZP.[14–16] The photochemistry of benzophenone and BZP-related compounds is very complex and depends on the particular solvent in homogeneous solutions,[17–19] or on a particular BZP-interactive compound in a given solvent.[20,21] By absorbing UV-light, benzophenone (photosensitizer) can be promoted into a long-lived triplet state (^{3}BZP) which is very reactive toward its surroundings (*e.g.*, phospholipid mixture and quercetin), including the crucial interaction for this study, the direct reaction with lipids resulting in the production of lipid radicals ($L^{\bullet}$) in the initiation step of the lipid peroxidation (LP) chain reaction:[22]

$$^3\text{BZP} + \text{LH} \rightarrow \text{BZPH}^{\bullet} + \text{L}^{\bullet} \quad (1)$$

where ^{3}BZP is the triplet state of benzophenone, $BZPH^{\bullet}$ is the BZP-ketyl-radical, LH is the unsaturated lipid and $L^{\bullet}$ is the lipid radical.

On the other hand, lipid peroxidation is mostly controlled *in vivo* by the action of the antioxidants. Many biomolecules (and classes of biomolecules) serve as antioxidants, including flavonoids.[23–25] Flavonoids are benzo-γ-pyrone derivatives consisting of pyran and phenolic rings. The most important structural elements related to their functions are: the *o*-dihydroxy group in the B-ring (catechol structure) as a potential radical target, the double bond between positions 2 and 3 of the C-ring conjugated with a keto group in position 4 (because of its capacity to delocalize the unpaired electron of a flavonoid radical), and the C-3,

C-5 and C-7 hydroxyl groups (of the C- and A-rings), as potential scavengers of free radicals (Fig. 1).[26–28] Quercetin (flavonol) is a member the flavonoids family, having the structure shown in Fig. 1. Recent studies connect the high antioxidant activity of flavonols with the presence of the OH-group in position 3 of the C-ring in combination with the catechol structure of the B-ring.[25–29]

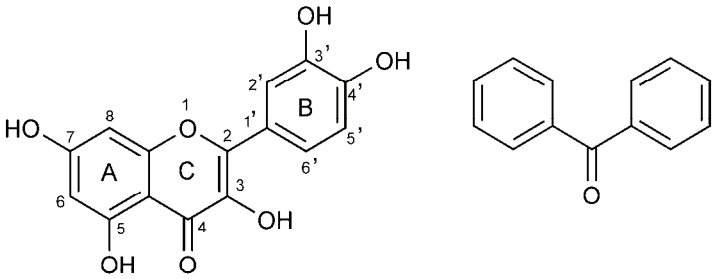

Quercetin Benzophenone

Fig. 1. Structure of quercetin and benzophenone.

Quercetin and its glycosides are reportedly synthesized in plants as a part of their total response toward UV-radiation to prevent extended induced damage.[30,31] Quercetin absorbs UV radiation with absorbance maxima in the UV-A (λ_{max} = 365 nm, ε = 28,400 mol^{-1} dm^3 cm^{-1}) and UV-C range (λ_{max} = 256 nm, ε = 28,300 mol^{-1} dm^3 cm^{-1}). However, flavonoids can also act as free radical scavengers to prevent oxidative skin damage[32–35] and their topical application has met with considerable interest.[36–38] Thus, quercetin may provide protection against UV radiation either through absorption (preventive, inhibition mode) or scavenging activities ("chain-breaking", antioxidant mode). In the former case, the absorbed UV energy may be dissipated as heat[39] or converted into quercetin decomposition products, both *in vitro* and *in vivo*.[29,40,41] In the latter case, quercetin (as well as other flavonoids) scavenges already created free radicals (such as lipid peroxy radicals, LOO$^\bullet$, or some ROS species present), mostly by the hydrogen-atom-transfer mechanism, shown in Eq. (2):[42–44]

$$\text{Fl–OH} + \text{L}^\bullet \rightarrow \text{Fl–O}^\bullet + \text{LH} \qquad (2)$$

The oxidized Fl–O$^\bullet$ radical (which can be stabilized by one intramolecular H-bonding in the B-ring: –O$^\bullet\cdots$H–O–),[44] may react with a second radical (L$^\bullet$), acquiring a quite stable quinone structure.[45]

In a recent publication,[46] the stabilities of two flavonoid components, quercetin and rutin, in solution toward UV-irradiation (from the three sub-ranges, UV-A, UV-B and UV-C), as well as their antioxidant activities in the presence of a lipoidal mixture (*i.e.*, lecithin), as the "protection target", were compared. Despite the lower stability of quercetin against UV-irradiation, its antioxidant ability

to protect the lipid mixture from peroxidation was still found to be higher than that of rutin. In addition, it was recently found that continuous UV-irradiation of quercetin and rutin in solution was followed by the creation of products that absorb in spectral region between 250 and 350 nm.[47]

The system studied in this work was more complex compared to the previous one[46] due to the presence of benzophenone. The investigated system (lipids + BZP + quercetin, in methanol) was planned to provide studies of both protective actions of quercetin during prolonged continuous UV-irradiation: the preventive one (studied through UV-induced degradation), as well as the antioxidant one (studied indirectly, by tracing the proliferation of UV-induced LP process, expressed through creation of diene structures of LP peroxides in the presence and absence of benzophenone. Due to a greater complexity of the studied system, pure phospholipids (of higher "purity", compared to the previous report[46]) and pure BZP were irradiated as blanks (separately and their mixture), in order to estimate in the next step, LP control by quercetin during UV-irradiation, and estimate the differences between the rates of lipid peroxide production (LPP) in the presence and absence of quercetin, as well as in the presence and absence of the photosensitizer (BZP).

The system was studied by using prolonged irradiation from three UV-subranges (UV-A, 320–400 nm; UV-B, 290–320 nm; UV-C, 200–280 nm). The changes of the BZP-initiated lipid peroxidation were estimated in the light of quercetin presence and action in this system, under the same UV-irradiation regime.

EXPERIMENTAL

Phospholipids were gifted by Phospholipid GmbH, Cologne, Germany (Phospholipon® 80 and Phospholipon® 90). According to the Manufacture's declaration, the composition is for Phospholipon® 80 (PL80), phosphatidylcholine 78 %, lyso-phosphatidylcholine 3.3 %; fatty acid composition: palmitic acid 10–15 %, stearic acid 1.5–4 %, oleic acid 6.0–13.0 %, linoleic acid 61–71.0 %, linolenic acid 4.0–7.0 %, peroxide value max. 2.1, and for Phospholipon® 90 (PL90), phosphatidylcholine 98 %, lyso-phosphatidylcholine 2.1 %; fatty acid composition: palmitic acid 12±2 %, stearic acid 3±1 %, oleic acid 10±3 %, linoleic acid 66±5 %, linolenic acid 5±2 %, peroxide value max. 1.3. The phospholipids mixtures were kept in the dark to prevent at least the photooxidation process. Benzophenone (BZP) was obtained from Sigma. (St. Louis, CA, USA). The quercetin standard was purchased from Merck.

UV-irradiation

Continuous irradiation of the samples in methanol were performed in a cylindrical photochemical reactor "Rayonnet", with 10 symmetrically placed lamps with emission maxima in three different ranges: 350 (UV-A), 300 (UV-B) and 254 nm (UV-C). The samples were irradiated in quartz cuvettes (1 cm×1 cm×4.5 cm) placed on the rotating circular holder. The total measured energy flux was about 12.9 W m^{-2} for 350 nm, 15.0 W m^{-2} for 300 nm and 17.9 W m^{-2} for 254 nm at 10 cm distance from the lamps.

UV–Vis spectroscopy

The UV–Vis spectra of the phospholipids dissolved in methanol, and the phospholipids mixed with flavonoids and benzophenone, before and after irradiation with UV-light, were recorded on a Varian Cary-100 spectrophotometer. All spectra were recorded in the spectral range 200 to 600 nm.

Spectrometry for conjugated dienes

The peroxidative dienes structures were determined by measuring the absorbance at 234 nm in methanol solution.[22,48,49] The phospholipids, quercetin and benzophenone were dissolved separately in methanol and then mixed. The final concentrations of phospholipids, quercetin and BZP in mixture were 3.5×10^{-3} g dm^{-3}, 2.5×10^{-5} and 1.1×10^{-5} mol dm^{-3}, respectively. The peroxidation of phospholipids was generated by UV-irradiation at 350 (UV-A), 300 (UV-B) and 254 nm (UV-C). Methanolic solutions of BZP alone and phospholipids (with and without BZP), as kind of blanks, were irradiated simultaneously with the phospholipids/quercetin and phospholipids/quercetin/BZP mixtures. The increase in the absorbance at 234 nm, as an indication of the formation of peroxidative diene structures, was determined by UV–Vis measurements. The maximum quercetin absorbances were recorded as a function of UV-irradiation time to follow the rate of its degradation.

RESULTS

The changes of the absorption spectra of BZP after continuous prolonged irradiation in methanol with UV-B light (300 nm) are shown in Fig. 2A. The analogue spectra obtained for BZP with UV-A (350 nm) and UV-C (254 nm) radiation expressed very similar shapes (data not shown). The corresponding kinetic ln-plots (of BZP absorbance maximum at 253 nm, $A_{253\ nm}$) for increasing irradiation intervals ($t_{irr.}$), for all three UV-subranges (UV-A, -B and -C), are shown in Fig. 2B and the corresponding degradation (*i.e.*, bleaching) rate constants ($k_{BZP\text{-}bleach.}$ in min^{-1}), determined as the slopes of linear plots shown in Fig. 2B are displayed on the corresponding graphs.

The changes in the absorption spectra of the mixture of BZP with quercetin after continuous prolonged irradiation in methanol with UV-B light (300 nm) are shown in Fig. 3A. The analogue spectra obtained for the BZP + quercetin mixture with UV-A (350 nm) and UV-C (254 nm) radiation expressed very similar shapes (not shown). The corresponding kinetic ln-plots (of the mixture absorbance at 372 nm, $A_{372\ nm}$, (the maximum absorbance of quercetin) for increasing irradiation intervals ($t_{irr.}$), for all three UV-sub-ranges (UV-A, -B and -C), are shown in Fig. 3B, and the corresponding degradation rate constants ($k_{(BZP+Querc.)\text{-}bleach.}$ in min^{-1}), determined as the slopes of linear plots shown in Fig. 3B, are displayed on the corresponding graphs.

The changes in the absorption spectra of PL80 and the PL80/BZP mixture in methanol, followed at 234 nm for peroxide formation, during continuous prolonged irradiation with UV-B light are shown in Figs. 4A and 4B, respectively. The corresponding kinetic ln-plots (of absorbance recorded at 234 nm, $A_{234\ nm}$) for increasing UV-B irradiation periods ($t_{irr.}$), with linear fitting (average R va-

lues of about 0.98), are shown in Fig. 4C. The changes in the absorption spectra and corresponding kinetic ln-plots obtained for UV-A and UV-C irradiated PL80 and PL80/BZP, as well as for UV-A, -B and -C irradiated PL90 and PL90/ /BZP mixtures in methanol expressed very similar shapes to the ones presented.

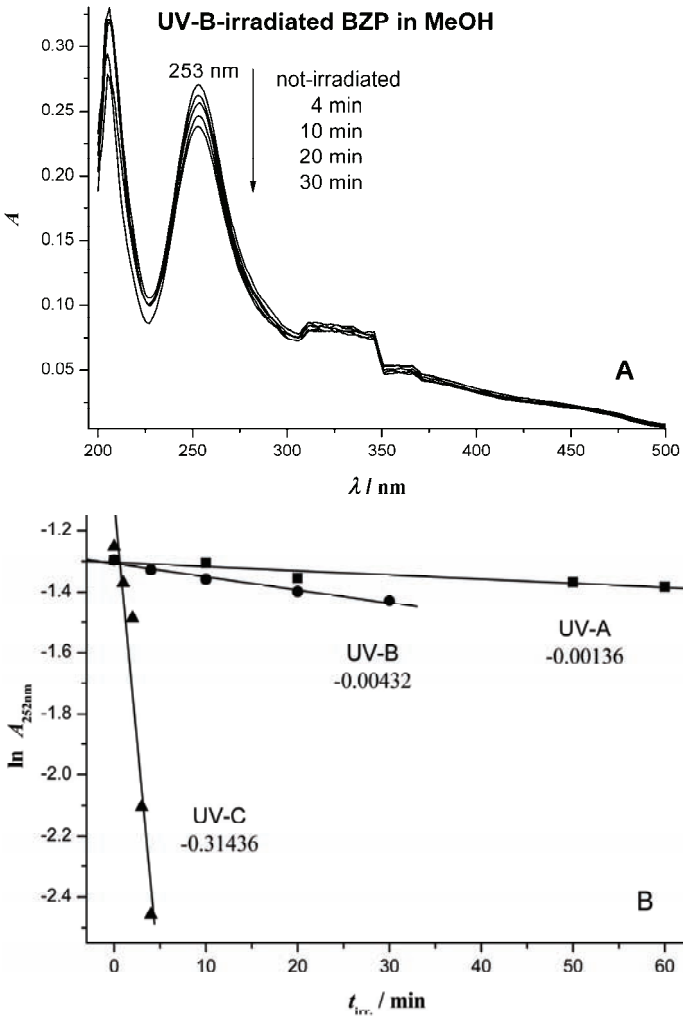

Fig. 2. Changes in the absorption spectrum of benzophenone in methanol during exposure to UV-B radiation at 300 nm. The initial concentration of benzophenone was 1.1×10^{-5} mol dm^{-3} (A). Kinetic ln plot of benzophenone bleaching induced by UV-A, -B and -C irradiation; the absorbance of benzophenone was followed at 253 nm; the corresponding bleaching rate constants ($-k_{\text{BZP-bleach.}}$ in min^{-1}) are displayed for all three UV-irradiation ranges (B).

The changes in absorption spectra of PL90/quercetin and PL90/BZP/quercetin mixtures in methanol, with lipid peroxides production (LPP) followed at

234 nm and quercetin degradation followed at 372 nm after continuous prolonged irradiation with UV-B, are shown in Fig. 5A and 5C, respectively. The augmented parts of the same spectra, focusing only on the quercetin absorption at 372 nm, are shown in the insets in Fig. 5A and 5C, respectively. The corresponding kinetic ln-plots of peroxide production followed at 234 nm ($A_{234\ nm}$) and quercetin degradation followed at 372 nm ($A_{372\ nm}$) showed linear dependences (with average R values of about 0.98), Fig. 5B and 5D, respectively).

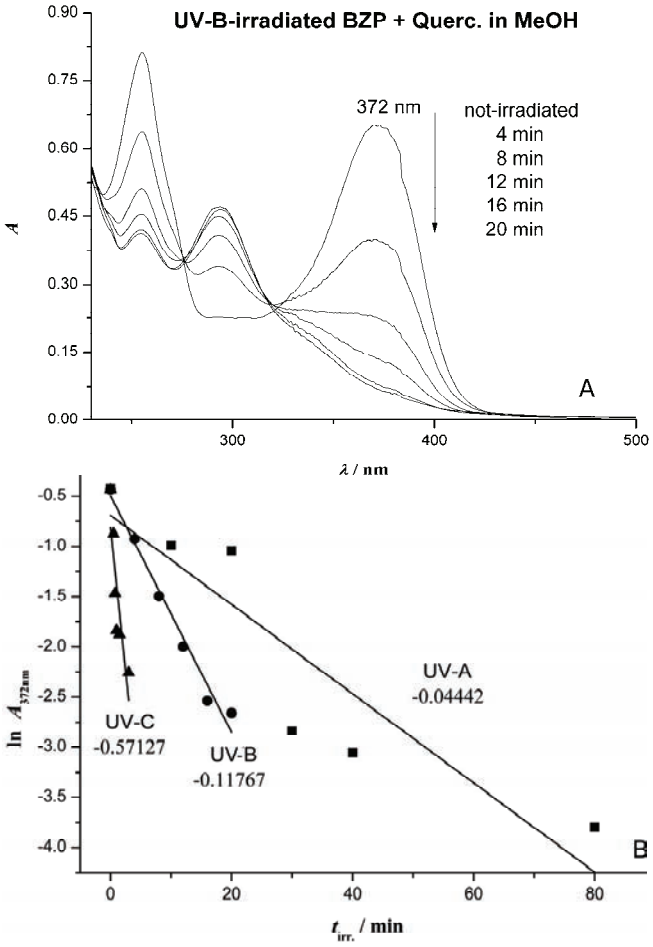

Fig. 3. Changes in the absorption spectrum in the mixture of benzophenone with quercetin in methanol exposed to UV-B radiation at 300 nm. The initial concentration of benzophenone was 1.1×10^{-5} mol dm^{-3} and the quercetin concentration was 2.5×10^{-5} mol dm^{-3} (A). Kinetic ln plot of the (BZP + querc.) mixture bleaching induced by UV-A, -B and -C irradiation; the absorbance of the mixture was followed at 372 nm (the absorbance maximum of quercetin); the corresponding degradation-bleaching rate constants ($-k_{(BZP+Querc.)\text{-}bleach.}$ / min^{-1}) are displayed for all three UV-irradiation ranges (B).

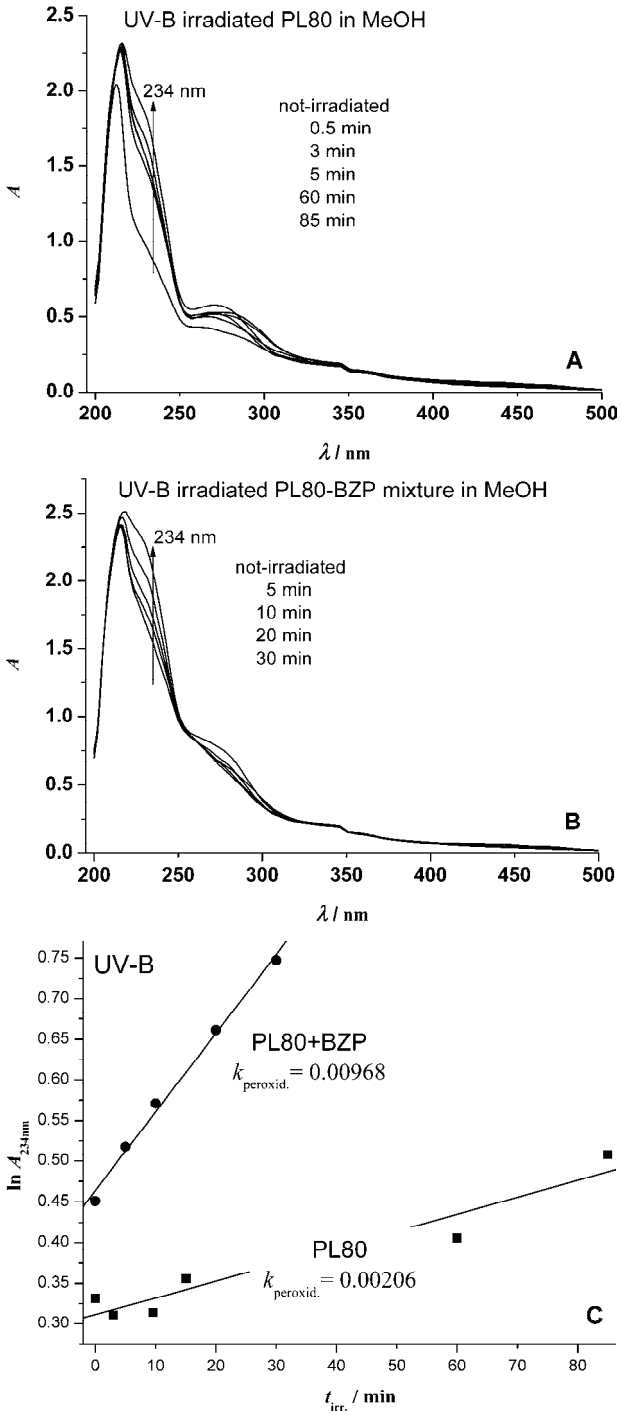

Fig. 4. Changes in the absorption spectrum of PL80 in the phospholipid and phospholipid/ /BZP mixture, respectively, exposed to UV-B radiation (300 nm) in methanol. The initial concentrations of BZP and PL80 phospholipids were 1.1×10^{-5} mol dm^{-3} and 3.5×10^{-3} g dm^{-3}, respectively (A and B); kinetic ln plots for the production of lipid peroxides, obtained by measuring the absorbance of the PL80 and PL80/ /BZP mixture at 234 nm in methanol, following different, increasing periods of UV-B irradiation; the corresponding degradation rate constants ($k_{peroxid.}$ / min^{-1}) are displayed also (C).

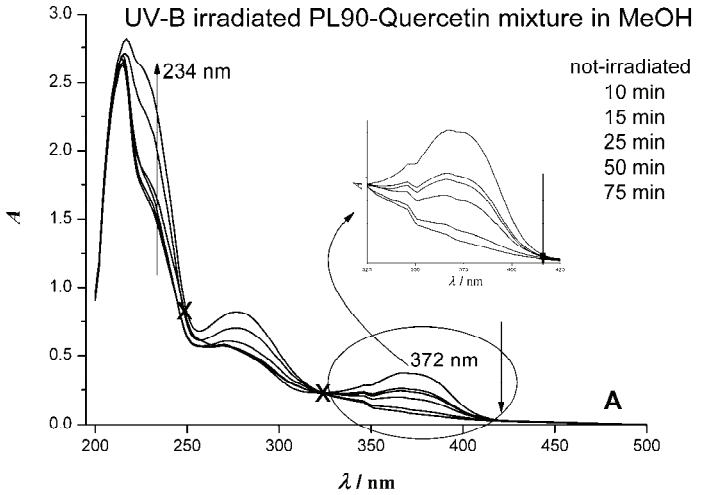

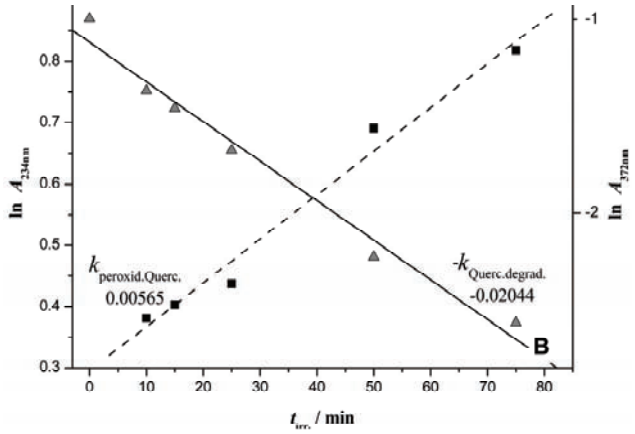

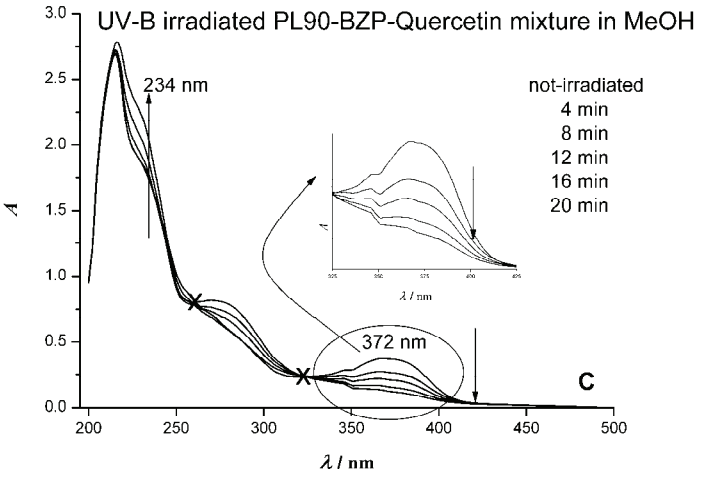

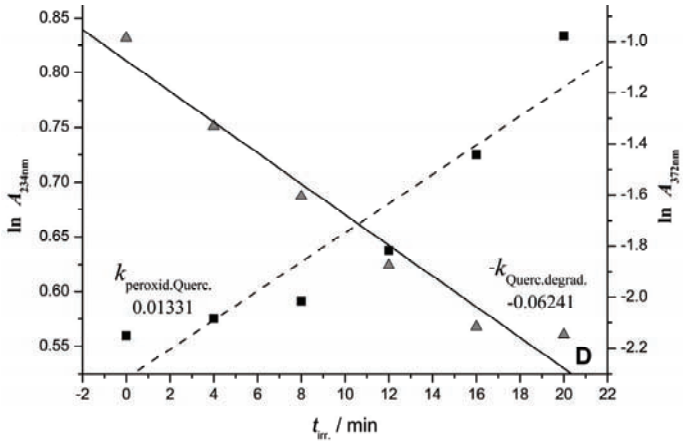

Fig. 5. Changes in the absorption spectrum of PL90 in the phospholipid/quercetin (A) and phospholipid/BZP/quercetin (C) mixtures exposed to UV-B radiation (300 nm) in methanol; the augmented part of the same spectra, focusing only on the quercetin absorption with maximum at 372 nm, is shown as the insets of graphs A and C, respectively. The initial concentrations of BZP, PL90 phospholipids and quercetin were 1.1×10^{-5} mol dm^{-3}, 3.5×10^{-3} g dm^{-3} and 2.5×10^{-5} mol dm^{-3}, respectively. Kinetic logarithmic plots obtained from the lipid peroxides absorbance data at λ_{max} = 234 nm and quercetin degradation data in the same mixture at 372 nm, following increasing periods of UV-B irradiation for phospholipids/quercetin (B) and phospholipids/BZP/quercetin (D) mixtures in methanol; the corresponding LP-production and quercetin UV-induced degradation rate constants ($k_{peroxid.Querc.}$ and $k_{Querc.degrad.}$, respectively, in min^{-1}) are displayed on the graphs B and D.

The changes of the absorption spectra and the kinetic ln-plots obtained with UV-A and -C for these mixtures, as well as for PL80 related mixtures irradiated with UV-A, -B and -C, expressed very similar shapes as the presented ones.

The slopes calculated from kinetic ln-plots shown in Fig. 4, representing the rates of UV-induced production of lipid peroxides (followed at 234 nm, $k_{peroxid.}$) in both investigated mixtures of phospholipids (PL80 and PL90), in the presence and absence of benzophenone, are given in Table I. The $k_{peroxid.}$ rate constants were calculated for all three UV-irradiation ranges. Thus, the $k_{peroxid.}$ rate constants (calculated in min^{-1}) represent some kind of blank indicators for the peroxidation of phospholipids (in absence of quercetin as an antioxidant).

The slopes calculated from kinetic ln-plots shown in Fig. 5, representing the rates of UV-induced lipid peroxides production (followed at 234 nm, $k_{peroxid.Querc.}$) and quercetin degradation (followed at 372 nm, $k_{Querc.degrad.}$) in the investigated phospholipid/quercetin and phospholipid/quercetin/BZP mixtures, are given in Table II for both investigated types of phospholipids (PL80 and PL90). The $k_{peroxid.Querc.}$ and $k_{Querc.degrad.}$ rate constants (in min^{-1}) were calculated for all three UV-irradiation ranges.

TABLE I. Kinetics of phospholipids (PL80 and PL90) peroxidation ($k_{peroxid.}$ / min^{-1}) in the presence or in the absence of BZP in methanol during increasing UV-irradiation intervals ($t_{irr.}$) for the three UV-ranges: 350 (UV-A), 300 (UV-B) and 254 nm (UV-C). The absorbance of phospholipids and phospholipids/BZP mixture were followed at 234 nm. The initial concentrations of BZP and phospholipids were 1.1×10^{-5} mol dm^{-3} and 3.5×10^{-3} g dm^{-3}, respectively

UV-Range	PL80		PL90	
	without BZP	with BZP	without BZP	with BZP
UV-A (350 nm)	0.00156	0.00592	–	0.00590
UV-B (300 nm)	0.00206	0.00968	0.00371	0.01420
UV-C (254 nm)	0.03152	0.00910	–	0.02026

TABLE II. Kinetics of UV-induced quercetin degradation and lipid peroxides production (LPP) in phospholipids (PL80 & PL90)/quercetin and (PL80 and PL90)/BZP/quercetin mixtures in methanol ($k_{Querc.degrad.}$ and $k_{peroxid.Querc.}$ in min^{-1}, respectively) during increasing UV-irradiation intervals for three UV-ranges: 350 (UV-A), 300 (UV-B) and 254 nm (UV-C). Quercetin degradation and phospholipids peroxidation were followed at 372 and 234 nm, respectively. The initial concentrations of BZP, phospholipids, and quercetin were 1.1×10^{-5}, 3.5×10^{-3} and 2.5×10^{-5} mol dm^{-3}, respectively

UV-Range	PL80 + quercetin				PL90 + quercetin			
	without BZP		with BZP		without BZP		with BZP	
	λ / nm							
	372	234	372	234	372	234	372	234
UV-A	–	–	0.01545	0.00244	0.00177	0.00070	0.02554	0.00229
UV-B	0.01804	0.00127	0.05031	0.00742	0.02044	0.00565	0.06241	0.01331
UV-C	0.04796	0.00377	0.07152	0.00515	0.05765	0.02019	0.07439	0.01918

DISCUSSION

Bearing in mind that the all results were obtained by UV spectrophotometry, it is important to define "clarity criteria" for their interpretation, based on the positions of the λ_{max} values. Benzophenone absorbs in the spectral range 225–300 nm, with the absorbance maximum at 253 nm in methanol (Fig. 2). The UV-induced formation of lipid peroxides could be followed at 234 nm (see experimental section and Figs. 4 and 5), while quercetin in methanol has absorption maxima at 256 nm and at 372 nm (at which wavelength the degradation kinetics quercetin was followed) (Fig. 5).

UV-induced bleaching of benzophenone, and the benzophenone + quercetin mixture in methanol

Prolonged continuous irradiation of benzophenone (BZP) in methanol caused a gradual decrease in the absorbance during increasing irradiation periods over the whole spectral range (200–500 nm) for all the three applied UV-sub-ranges (Fig. 2A). These changes measured at 253 nm followed first order kinetics, as shown in Fig. 2B. The BZP bleaching constant, $k_{BZP\text{-}bleach.}$, in methanol in-

creased with increasing UV-irradiation energy input, from UV-A to -C (Fig. 2B); the ratios of the bleaching rates for UV-C and -B and UV-C and -A irradiated BZP in methanol showed differences of two orders of magnitude ($k_{\text{BZP-bleach.(UV-B)}}/k_{\text{BZP-bleach.(UV-A)}}$ = 3.2 and $k_{\text{BZP-bleach.(UV-C)}}/k_{\text{BZP-bleach.(UV-B)}}$ = = 72.8, respectively, and the ratio $k_{\text{BZP-bleach.(UV-C)}}/k_{\text{BZP-bleach.(UV-A)}}$ = 231.2), as shown in Fig. 2B. Thus, the energy input of the UV-incident photons appeared to be the dominant factor governing BZP bleaching.

The same was the case for prolonged continuous irradiation of BZP in the mixture with quercetin in methanol, for both the spectral (Fig. 3A) and kinetic behavior (Fig. 3B) (the absorbance data were in this case obtained at 372 nm, the maximum absorbance of quercetin). The ratios of the bleaching rates $k_{\text{(BZP+Querc.)-bleach.}}$ in min^{-1}, obtained from the slopes from Fig. 3B, reconfirmed the dominant role of the energy input of the UV-incident radiation in the bleaching of the BZP + quercetin mixture, which at 372 nm practically means quercetin degradation (BZP has a negligible absorbance at this wavelength). Compared to BZP (Fig. 2B, UV-B), quercetin undergoes a much faster bleaching in the mixture (Fig. 3B, UV-B), even faster than its own bleaching in methanol (Figs. 6A and 6B): 0.11767 min^{-1}/0.03488 min^{-1} = 3.37. Thus, it seems that BZP contributes to the faster degradation of quercetin (however, the photochemistry of the complete mixture is out of scope of this paper).

The blank experiment: UV-induced peroxide formation in the absence of quercetin – the influence of BZP

The kinetics data corresponding to UV-induced lipid peroxide formation in phospholipid as well as in phospholipid / BZP mixtures in methanol (for both, PL80 and PL90) are listed in Table I. Similar to the UV-induced bleaching of BZP, the results of UV-induced peroxide formation also suggest that the rates of LPP are also highly dependent on the energy of the applied UV radiation since the rate constants increase from UV-A to UV-C irradiation (Table I). Hence, generally, the incident UV-energy also plays a governing role in the production of peroxides. On the other hand, lipid peroxidation in both mixtures of phospholipids was faster in the presence of benzophenone than in its absence, both for UV-A and -B irradiated phospholipid mixtures (Table I). The corresponding rate constant ratios for PL80 in methanol, with and without BZP, $k_{\text{peroxid.BZP-PL80}}/k_{\text{peroxid.PL80}}$, were 3.79 and 4.70 for UV-A and -B, respectively, and for PL90, the ratio $k_{\text{peroxid.BZP-PL90}}/k_{\text{peroxid.PL90}}$ was 3.83 for UV-B. However, the LP rate constant for the UV-C-irradiated PL80/BZP mixture in methanol was smaller than the one for PL80 in methanol without BZP, the corresponding rate constant ratio for the PL80 mixtures in methanol (without and with BZP), $k_{\text{peroxid.PL80}}/k_{\text{peroxid.BZP-PL80}}$, was 1.27 (Table I). In addition, the LP rate constant value for UV-C was similar (even slightly smaller) when compared to the one

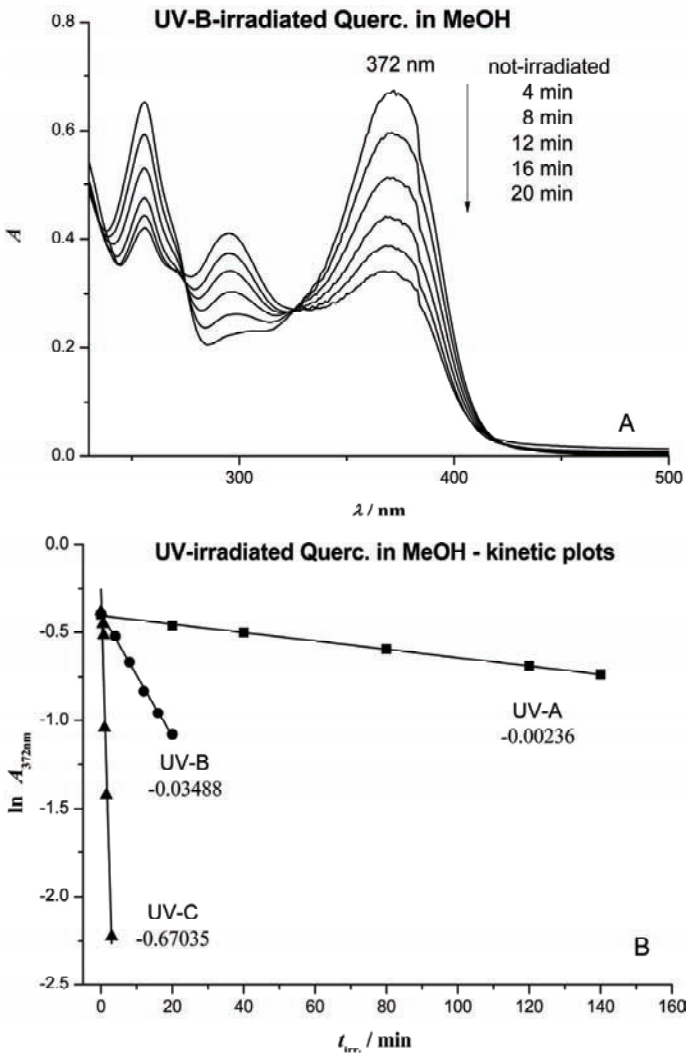

Fig. 6. Changes in the absorption spectrum of quercetin in methanol during exposure to UV-B radiation (300 nm). The initial concentration of quercetin was 2.5×10^{-5} mol dm^{-3} (A). Kinetic ln plot of quercetin degradation induced by UV-A, -B and -C irradiation; the absorbance of quercetin was followed at 372 nm; the corresponding degradation rate constants ($-k_{\text{Querc.degrad.}}$ in min^{-1}) are displayed for all three UV-irradiation ranges (B).

obtained for UV-B irradiated PL80/BZP mixture, $k_{\text{peroxid.BZP-PL80}} = 0.00910$ and 0.00968 min^{-1}, respectively (Table I). Thus, it is obvious that the BZP-initiating role was inefficient when using continuous UV-C irradiation for the PL80/BZP mixture. The BZP-initiating role was the most efficient when using UV-A irradiation: as it was shown that UV-A photons had the smallest impact on benzophenone bleaching (Figs. 2and 3) and thus, the LPP was the highest in the case of

UV-A. The same conclusion was reached in recent publication: BZP-initiating role for LP was the most dominant in the case of UV-A irradiated phospholipid/BZP mixtures in *n*-hexane.[22] However, the LPP kinetic data for PL90 mixtures in methanol were not so consistent although they followed an increasing trend of absorbances at 234 nm (the corresponding UV-spectra are not shown).

UV-induced peroxide formation in the presence of quercetin

A comparative list of the LPP rate constants values, $k_{\text{peroxid.Querc}}$, for both phospholipids mixtures in the presence of quercetin as well as the degradation rates of quercetin itself, $k_{\text{Querc.degrad.}}$, in the absence and in the presence of benzophenone, in methanol, for all three investigated UV sub-ranges are given in Table II. Similar to the UV-induced BZP degradation in methanol (Fig. 3) as well as for UV-induced LPP in PL80 and PL90 mixtures, with and without BZP, in methanol (Table I), the results of UV-induced peroxide formation in phospholipids/quercetin mixtures, with and without BZP, once again suggest that the LP rates were dependent on the applied UV energy, *i.e.*, in general, the rate constants increased from the UV-A to the UV-C irradiation regime (Table II). Hence, the energy input of the incident UV photons plays a major role in the production of peroxides, as well as in the synchronous degradation of quercetin, the $k_{\text{Querc.degrad.}}$ rate constants also increased from UV-A to UV-C, as can be seen in Table II).

Quercetin-BZP competition in the phospholipid mixtures

The effect of BZP on LP production is evident: LP production was more expressed in the presence of BZP than in its absence. For example, the calculated $k_{\text{peroxid.Querc.BZP}}$ (in the presence of BZP)/$k_{\text{peroxid.Querc.}}$ (without BZP) ratios for UV-B-irradiated (PL80 and PL90)/quercetin mixtures in methanol were 5.84 and 2.36, respectively (Table II). This means that BZP-sensitization maintained its important role also in the presence of the quercetin, as it had in the absence of quercetin. Similar to the already cited behavior of UV-C-irradiated (PL80 and PL90)/BZP mixtures in methanol (Table I), BZP was not very efficient for UV-C-irradiated (PL80 and PL90)/quercetin/BZP mixtures in methanol, $k_{\text{peroxid.Querc.BZP}} \approx k_{\text{peroxid.Querc.}}$ (Table II). This could be related to the fact that the rate constant for UV-C-induced BZP bleaching was much higher than in the case of UV-A and -B. Hence, sensitization capacity of benzophenone was significantly reduced under UV-C continuous irradiation (Tables I and II).

On the other hand, the influence of quercetin on LP production in UV-irradiated PL80 and PL90 methanol solutions cannot be neglected. Compared to the "blank-experiments" ($k_{\text{peroxid.BZP}}$ and $k_{\text{peroxid.}}$), LP-production was generally suppressed when quercetin was present. The suppression effect was the most expressed in the case of UV-C-irradiated PL80/quercetin mixture (without BZP): $k_{\text{peroxid.PL80}}/k_{\text{peroxid.Querc.PL80}} = 3.07$ (Tables I and II). The presence of querce-

tin in the phospholipid mixtures both with and without BZP suppressed LP production by a factor between 2.58 and 1.06 for UV-A and -C irradiated PL90/ /quercetin/BZP mixtures, respectively (Tables I and II). The suppression effects of quercetin on LP production were more expressed in the PL80/quercetin than in the PL80/quercetin/BZP mixtures in methanol, which was evidenced by the increasing trend of the corresponding rates ratios with increasing UV-incident energy from UV-B to -C (the $k_{\text{peroxid.PL80}}/k_{\text{peroxid.Querc.PL80}}$ values were 1.62 (UV-B) and 3.07 (UV-C), and the corresponding $k_{\text{peroxid.BZP-PL80}}/k_{\text{peroxid.Querc.BZP-PL80}}$ values were 1.30 (UV-B) and 1.77 (UV-C), Tables I and II).

UV-induced quercetin degradation in methanolic phospholipid and phospholipids/BZP mixtures

The previously published results of UV-induced quercetin degradation in methanol solutions[43] were confirmed by the data presented herein, *i.e.*, quercetin stability against prolonged continuous UV-irradiation decreases with increasing energy input of UV-irradiation, from UV-A to -C (Table II). Thus, in more complex systems such as the ones presented in this work (phospholipid/quercetin and phospholipid/quercetin/BZP in methanol), quercetin still undergoes degradation during continuous UV-irradiation (insets of Fig. 5A and 5C), following first order kinetics (Table II). The sensitizing role of BZP affects quercetin degradation during UV-irradiation in methanolic phospholipid/quercetin/BZP mixtures, *i.e.*, the degradation is faster in the presence than in the absence of BZP (Table II). For example, the calculated $k_{\text{Querc.degrad.BZP-PL90}}$ (with BZP)/ $/k_{\text{Querc.degrad.PL90}}$ (without BZP) ratios for the UV-A, -B and -C irradiated PL90/ /quercetin mixtures were 14.43, 3.05 and 1.29, respectively (Table II). Once again, it could be concluded that BZP had the highest photosensitizing effect with UV-A radiation, since its role in the UV-C-irradiated mixtures appeared to be negligible (Table II). The reason is certainly related to the strong BZP absorption in the UV-C spectral range, having an absorption maximum at 253 nm.

As reported, quercetin has two absorption maximums, in the UV-A (λ_{max} = = 372 nm) and UV-C (λ_{max} = 260 nm) spectral ranges[46] which overlap with the applied UV-irradiation range(s) used in this work. In a recently published investigation, Fahlman and Kroll[50] studied UV-A and -B irradiation of quercetin in BZP-containing methanol solutions, in which irreversible degradation followed by formation of several C-ring-opened photoproducts were registered. They registered BZP-impact on both quercetin degradation and the formation of photoproducts.[50]

On the other hand, in a more complex, organized system, *i.e.*, liposomes, the same authors, Fahlman and Kroll (2009)[40] established quercetin as a strong inhibitor of lipid oxidation induced by UV-A and -B irradiation. However, it was found that the absorption of UV-A and UV-C irradiated quercetin (at the exci-

tation wavelengths of 365 and 255 nm) may lead to greater levels of the excited state species, as reported by Smith and Markham,[51] which may result in an overall decrease in the antioxidant behavior of quercetin toward LP processes. In a recently published paper, suppression effect of quercetin on lipid peroxidation processes (with a lecithin mixture as the "protection target") was clearly registered by the thiobarbituric acid–malon-dialdehyde (TBA–MDA) test.[46]

CONCLUSIONS

To conclude, in the studied complex UV-irradiated system, at least three UV-initiated, more or less synchronous processes occur: BZP bleaching, quercetin degradation and lipid peroxidation. All three processes are highly affected by the incident UV-photons input. A suppression effect of quercetin on the LP process (as a measure of its antioxidant capacity) was proven. The suppression effect is less effective when BZP is present. The reason could lie in more favored degradation of quercetin in the presence of BZP.

Acknowledgements. This work was supported under the Project on Development of Technology No. TR-34012, as well as under Basic Investigations Project No. OI-172044, by the Ministry of Education, Science and Technological Development of the Republic of Serbia.

И З В О Д

УТИЦАЈ КОНТИНУАЛНОГ УЛТРАЉУБИЧАСТОГ ОЗРАЧИВАЊА НА АНТИОКСИДАТИВНУ АКТИВНОСТ КВЕРЦЕТИНА У ОДНОСУ НА ЛИПИДНУ ПЕРОКСИДАЦИЈУ ИНИЦИРАНУ БЕНЗОФЕНОНОМ

ЈЕЛЕНА Б. ЗВЕЗДАНОВИЋ, ДЕЈАН З. МАРКОВИЋ, ДРАГАН Ј. ЦВЕТКОВИЋ и ЈЕЛЕНА С. СТАНОЈЕВИЋ

Универзитет у Нишу, Технолошки факултет, Булевар ослобођења 124, 16000 Лесковац

Циљ овог рада је праћење деградације као и промена антиоксидативне активности кверцетина у присуству две различите смеше фосфолипида у метанолу, у условима континуалног ултраљубичастог (UV) озрачивања из три различита под-опсега, UV-A, UV-B и UV-C, и то, у присуству и одсуству изабраног UV–апсорбујућег фотосензора, бензофенона. Кверцетин служи да контролише процес липидне пероксидације инициране UV-зрачењем, апсорпцијом дела упадне UV светлости, и/или „скупљањем" том приликом створених слободних радикала. Резултати показују да кверцетин подлеже иреверзибилној деструкцији индукованој UV-зрачењем која веома зависи од енергије упадних UV-фотона, при чему је више изражена у присуству бензофенона. Истовремено, кверцетин показује ефекат сузбијања процеса липидне пероксидације у UV-озраченим смешама фосфолипида у оба случаја – у одсуству или присуству бензофенона (више или мање ефикасно, редом). У смешама фосфолипида озрачиваних UV-C зрачењем, фотосензитивна функција бензофенона је знатно редукована као последица његове снажне апсорпције у истом UV-C опсегу спектра, утичући тако на мању антиоксидативну активност преосталог кверцетина.

(Примљено 1. фебруара, ревидирано 19. маја 2012)

REFERENCES

1. G. T. Wondrak, M. K. Jacobson , E. L. Jacobson, *Photochem. Photobiol. Sci*. **5** (2006) 215
2. F. Hollósy, *Micron* **33** (2002) 179
3. M. Ichihashi, M. Ueda, A. Budiyannto, T. Bito, M. Oka, M. Fukunaga, K. Tsuru, T. Horikawa, *Toxicol*ogy **189** (2003) 21
4. G. Pfeifer, Y. You, A. Besaratinia, *Mutat. Res*. **571** (2005) 19
5. A. Teramura, L. Ziska, in *Photosynthesis and the Environment*, N. R. Baker, Ed., Kluwer, Dordrecht, The Netherlands, 1996, p. 435
6. A. Strid, W. Chow, J. Anderson, *Biochim. Biophys. Acta* **1020** (1990) 260
7. D. Markovic, L. Patterson, *Photochem. Photobiol*. **58** (1993) 329
8. N. Paillous, S. Fery-Forgues, *Biochimil*. **76** (1994) 355
9. R. Wheatley, *Trends Anal. Chem*. **19** (2000) 617
10. A. Girotti, J. Photochem. Photobiol., B **63** (2001) 103
11. J. Aikens, T. Dix, *Arch. Biochem. Biophys*. **305** (1993) 516
12. L. Ross, C. Barclay, M. Vinqvist, *Free Radical Biol. Med*. **16** (1994) 779
13. Q.-T. Li, M. H. Yeo, B. K. Tan, *Biochem. Biophys. Res. Commun*. **273** (2000) 72
14. D. Markovic, L. Patterson, *Photochem. Photobiol*. **49** (1989) 531
15. D. Markovic, T. Durand, L. Patterson, *Photochem. Photobiol*. **51** (1990) 389
16. D. Markovic, *Collect. Czech. Chem. Commun*. **66** (2001) 1603
17. C. Viltres Costa, M. A. Grela, M. S. Chorio, *J. Photochem. Photobiol., A* **99** (1996) 51
18. M. von Raumer, P. Suppan, P. Jacques, *J. Photochem. Photobiol., A* **105** (1997) 21
19. P. McGarry, C. Heitner, J. Schmidt, A. Rodenhiser, R. S. J. Manley, G. Cunkle, T. Thompson, *J. Photochem. Photobiol., A* **151** (2002) 145
20. M. Dossot, X. Allonas, P. Jacques, *J. Photochem. Photobiol., A* **128** (1999) 47
21. Q. Q. Zhu, W. Schnabel, *J. Photochem. Photobiol., A* **130** (2000) 119
22. D. Cvetkovic, D. Markovic, *Radiat. Phys. Chem*. **80** (2011) 76
23. A. Saija, M. Scalese, M. Lanza, D. Marzzullo, F. Bonina, F. Castelli, *Free Radical Biol. Med.* **19** (1995) 481
24. C. Choi, S. Kim, S. Hwang, B. Choi, H. Ahn, M. Lee, S. Park, S. Kim, *Plant Sci*. **163** (2002) 1161
25. K. Heim, A. Tagliaferro, D. Bobilya, *J. Nutr. Biochem*. **13** (2002) 572
26. D. Amić, D. Davidović-Amić, D. Bešlo, N. Trinajstić, *Croat. Chem. Acta* **76** (2003) 55
27. D. P. Makris, J. T. Rossiter, *Food Chem*. **77** (2002) 177
28. S. Erkoc, F. Erkoc, N. Keskin, *J. Mol. Struct. (Theochem.)* **631** (2003) 141
29. G. J. Smith, S. J. Thomsen, K. R. Markham, C. Andary, D. Cardon, *J. Photochem. Photobiol., A* **136** (2000) 87
30. A. Strid, R. J. Porra, *Plant Cell Physiol.* **33** (1992) 1015
31. A. Strid, W. S. Chow, J. M. Anderson, *Photosynth. Res*. **39** (1994) 475
32. J. H. Schoemaker, M. T. Schoemaker, H. Zijlstra, F. A. van der Horst, *Dermatol*ogy **191** (1995) 36
33. P. S. Mortimer, *Angiology* **48** (1997) 87
34. B. Choquenet, C. Couteau, E. Paparis, L. J. M. Coiffard, *J. Nat. Prod*. **71** (2008) 1117
35. R. Casagrande, S. R. Georgetti, W. A. Verri Jr., D. J. Dorta, A. C. dos Santos, M. J. Fonseca, *J. Photochem. Photobiol., B* **84** (2006) 21

36. R. Della Loggia, A. Tubaro, P. Dri, C. Zilli, P. Del Negro, in Proceedings of *Plant Flavonoids in Biology and Medicine: Biochemical, Pharmacological and Structure-Activity Relationships*, (1985), Buffalo, NY, USA, 1985, p. 481
37. B. Li, D. F. Birt, *Pharm. Res*. **13** (1996) 1710
38. A. Saija, A. Tomaino, D. Trombetta, M. Giacchi, A. De Pasquale, F. Bonina, *Int. J. Pharm*. **175** (1998) 85
39. E. Falkovskaia, P. K. Sengupta, M. Kasha, *Chem. Phys. Lett.* **297** (1998) 109
40. B. M. Fahlman, E. S. Krol, *J. Agric. Food Chem.* **57** (2009) 5301
41. E. S. B. Ferreira, A. Quye, H. McNab, A. N. Hulme, *Dyes History Archaeol*. **18** (2002) 63
42. S. G. Chiodo, M. Leopoldini, N. Russo, M. Toscano, *Phys. Chem. Chem. Phys*. **12** (2010) 7662
43. D. Procházková, I. Boušová, N. Wilhelmová, *Fitoterapia* **82** (2011) 513
44. P. Pedrielli, G. F. Pedulli, L. H. Skibsted, *J. Agric. Food Chem*. **49** (2001) 3034
45. P. G. Pietta, *J. Nat. Prod*. **63** (2000) 1035
46. D. Cvetković, D. Marković, D. Cvetković, B. Radovanović, *J. Serb. Chem. Soc*. **76** (2011) 973
47. J. B. Zvezdanović, J. S. Stanojević, D. Z. Marković, D. J. Cvetković, *J. Serb. Chem. Soc*. **77** (2012) 297
48. R. C. R. M. Vossen, M. C. E. van Dam-Mieras, G. Hornstra, R. F. A. Zwaal, *Lipids* **28** (1993) 857
49. H. Esterbauer, G. Striegl, H. Puhl, M. Rotheneder, *Free Radical Res.* **6** (1989) 67
50. B. M. Fahlman, E. S. Krol, *J. Photochem. Photobiol., B* **97** (2009) 123
51. G. J. Smith, K. R. Markham, *J. Photochem. Photobiol., A* **118** (1998) 99.

Journal of the Serbian Chemical Society
JSCS-info@shd.org.rs • www.shd.org.rs/JSCS
J. Serb. Chem. Soc. 77 (11) 1589–1597 (2012)
JSCS–4373
UDC 66.094.941+542.9+547.571+547.551:541.8:542.913:535.371
Original scientific paper

Solvent-dependent synthesis and mono-hydrolysis of the di-Schiff base of (±)*trans*-1,2-cyclohexanediamine and 2-pyridinecarboxaldehyde in Cu(II), Co(II) and Zn(II) complexes

MARYAM LASHANIZADEGAN* and MARZIEH SARKHEIL

Department of Chemistry, Faculty of Sciences, Alzahra University, P. O. Box 1993893973, Tehran, Iran

(Received 3 December 2011, revised 24 March 2012)

Abstract: The Schiff base ligand *trans*-*N*,*N*′-bis(2-pyridinylmethylene)-1,2-cyclohexanediamine (L) was synthesized. This ligand when stirred with 1 equivalent of $MCl_2 \cdot xH_2O$ (M = Cu, Co or Zn) in ethanol, undergoes partial hydrolysis of the imino bond and the resultant tridentate ligand (L′) immediately forms complexes with an N_3 coordination sphere. The reactions of L with $MCl_2 \cdot xH_2O$ (M = Cu, Co or Zn) in THF gave the complexes $[ML]Cl_2$. The ligand (L) and the complexes [M(L′)Cl]Cl and $[ML]Cl_2$ were characterized by elemental analysis, UV–Vis, FT-IR, ^{1}H-NMR spectroscopy, GC/MS and their luminescence properties. The ^{1}H-NMR spectra of the ligand and its diamagnetic complexes were recorded in $CDCl_3$ and DMSO solvents, respectively. The obtained data confirmed that the donor N atoms in the ligand coordinated to the metal ions. The luminescence studies show ligands and their complexes display intraligand (π–π*) fluorescence in MeOH solution and the solid state at room temperature.

Keywords: mono-hydrolysis; Schiff base; solvent effect; fluorescence.

INTRODUCTION

Schiff base ligands have been in the chemistry catalogues for decades and have played a key role as chelating ligands in main group and transition metal co-ordination chemistry. This is due to their ease of synthesis and stability under a variety of oxidative and reductive conditions.[1–5] Not only have they played an influential role in the development of modern co-ordination chemistry,[6] but they can also be found at key points in the development of inorganic biochemistry,[7] catalysis,[8,9] medical imaging,[10] optical materials[11] and thin films.[12,13] The formation of a Schiff base by condensation of diamine and carbonyl compounds is

* Corresponding author. E-mail: m_lashani@alzahra.ac.ir
doi: 10.2298/JSC111203035L

well known.[14–17] The reverse process, *i.e.*, the hydrolysis of Schiff bases in the presence of a metal ion was observed by Ghosh and coworkers.[18] It was observed that the hydrolysis is dependent on several factors, such as the pH of the reaction medium,[19] the size of the chelate rings formed by the diamine fragment of the Schiff base,[20,21] the coordinating ability of the counter anions,[22,23] the nature of the metal ions,[20,21] the effect of carbonyl compounds,[24] *etc*. In order to investigate this type of reaction, the Schiff base *trans*-*N*,*N*′-bis(2-pyridinylmethylene)-1,2-cyclohexanediamine was synthesized by condensation of (±)*trans*-1,2-cyclohexanediamine with 2-pyridinecarboxaldehyde in a 1:2 mole ratio, respectively. The reaction of this ligand with a metal chloride in ethanol resulted in the hydrolysis of one of the imine bonds. On the other hand, reaction of this ligand with a metal chloride in THF solvent resulted in the coordination of two imino bonds to the metal. The details of the synthesis, structure, mass spectrum and luminescence behaviours are described herein.

EXPERIMENTAL

Materials

All starting materials and solvents except (±)*trans*-1,2-cyclohexanediamine (Alfa Aesar), were purchased from Merck and were used without further purification. The synthetic reactions and work-up were realized in open air.

Physical measurements

The IR spectra (KBr discs, 500–4000 cm^{-1}) were recorded using a Bruker FTIR model Tensor 27 spectrometer. The elemental analysis was performed in a 2400 Series II CHN analyzer, Perkin-Elmer, USA. The UV–Vis absorption spectra and fluorescence measurements were recorded on a Perkin-Elmer Lambda 35 spectrophotometer and a Varian Cary Eclipse 1.1 spectrofluorometer, respectively. The ^{1}H-NMR spectra were recorded on a Bruker 500 MHz model DRX spectrometer in $CDCl_3$ and DMSO-d_6 with TMS as the internal reference. The mass spectrum of the ligand (**L**) was studied with a GC/MS Quadrupole Agilent 5973 MSD spectrometer.

Preparation of ligand (L)

A diethyl ether solution (5 ml) of 2-pyridinecarboxaldehyde (0.214 g, 2.00 mmol) was added to diethyl ether solution (5 ml) of (±)*trans*-1,2-cyclohexanediamine (0.114 g, 1.00 mmol). The mixture was stirred for 10 min and then kept in air to allow the solvent to evaporate, whereby yellowish crystals of the ligand L were obtained in 90% yield.

*Preparation of [M(L′)Cl]Cl (**1**–**3**)*

[Cu(L′)Cl]Cl (**1**) was prepared by adding an ethanolic solution (10 ml) of $CuCl_2 \cdot 2H_2O$ (0.170 g, 1.00 mmol) to an ethanolic solution (10 ml) of L (0.292 g, 1.00 mmol). The resulting mixture was stirred around 1 h. Finally, the precipitate of complex **1** was recovered by filtration, and washed several times with absolute ethanol and dried under vacuum at 65 °C for 1 h. Yield: 44 %.

[Co(L′)Cl]Cl (**2**) was prepared in a similar manner to **1** but using $CoCl_2 \cdot 6H_2O$ (0.237 g, 1.00 mmol). Yield: 31 %.

[Zn(L′)Cl]Cl (**3**) was prepared in a similar manner to **1** but using $ZnCl_2$ (0.136 g, 1.00 mmol). Yield: 60 %.

*Preparation of [ML]Cl_2 (**4**–**6**)*

[CuL]Cl_2 (**4**) was prepared by adding a THF solution (20 ml) of L (0.292 g, 1 mmol) to a THF solution (10 ml) of $CuCl_2 \cdot 2H_2O$ (0.170 g, 1.00 mmol). After stirring the resulting mixture for around 1 h, the precipitated complex was recovered by filtration, washed with THF and Et_2O and finally dried under vacuum at 65 °C for 1 h. Yield: 41 %.

[CoL]Cl_2 (**5**) was prepared in a similar manner to **4** but using $CoCl_2 \cdot 6H_2O$ (0.237 g, 1.00 mmol). Yield: 78 %.

[ZnL]Cl_2 (**6**) was prepared in a similar manner to **4** but using $ZnCl_2$ (0.136 g, 1.00 mmol). Yield 53 %.

RESULTS AND DISCUSSION

Synthesis and formulation

The ligand L (Scheme 1) was synthesized by condensation of a 1:2 mole ratio of (±)*trans*-1,2-cyclohexanediamine with 2-pyridinecarboxaldehyde. When L reacts with $MCl_2 \cdot H_2O$ (M = Cu, Co or Zn) in ethanol, it undergoes partial hydrolytic cleavage to form an N_3 coordination sphere of copper(II) (**1**), cobalt(II) (**2**) and zinc(II) (**3**) complexes. When L reacts with $MCl_2 \cdot H_2O$ in THF, [ML]Cl_2 (M = Cu (**4**), Co (**5**) or Zn (**6**)) complexes with N_4 coordination sphere are formed.

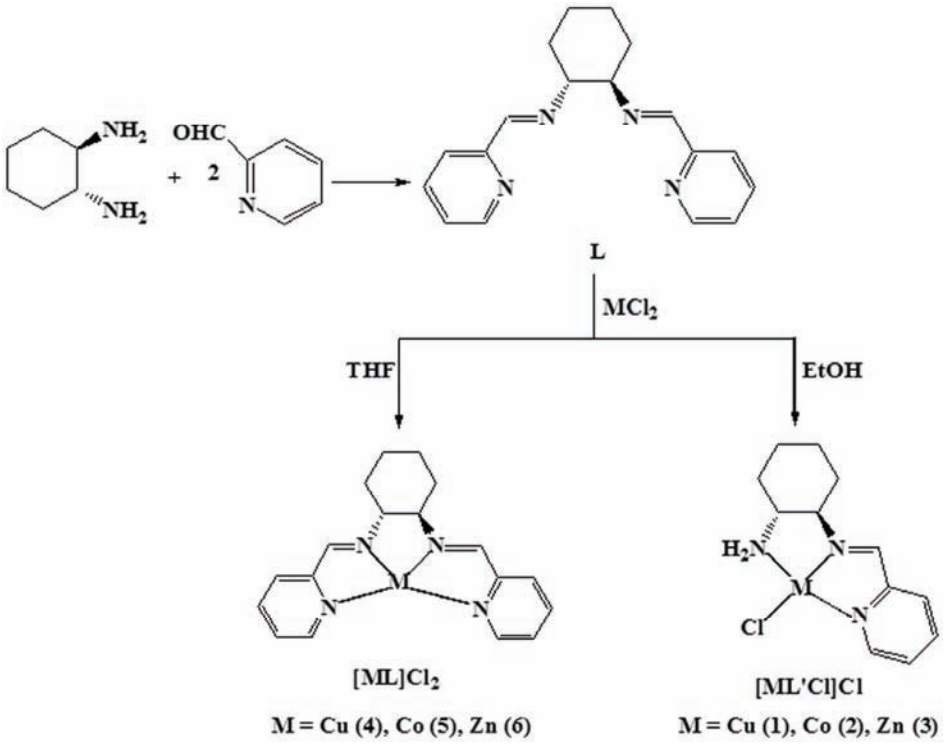

Scheme 1. Synthetic routes to the ligand (L) and complexes **1**–**6**.

*Some analytic and spectral data of the ligand and complexes **1**–**6***

Ligand (L). Yield: 90 %; m.p.: 126 °C; IR (KBr, cm^{-1}): 2931, 2853 (CH_2/CH stretching of cyclohexane ring), 1643 (C=N stretching of azomethine group) , 772 (out-of-plane C–H deformation); ^{1}H-NMR (500 MHz, $CDCl_3$, δ / ppm): 1.51–1.91 (8H, *m*, CH_2), 3.55–3.57 (2H, *m*, CH), 7.22–7.91 (8H, *m*, aromatic), 8.55–8.57 (2H, *d*, J = 7.1 Hz ,CH=N); MS (*m*/*z*, (relative abundance, %)): 292 (M^+, 100); UV–Vis (MeOH) (λ_{max} / nm (ε / L mol^{-1} cm^{-1})): 203 (16595), 236 (20417), 274 (11481).

[Cu(L')Cl]Cl ***(1)***. Yield: 44 %; m.p.: 230 °C; IR (KBr, cm^{-1}): 3267, 3217 (–NH stretching of primary amine), 2862, 2929 (CH_2/CH stretching of cyclohexane ring), 1655 (C=N stretching of azomethine group), 776 (out-of-plane C–H deformation); UV–Vis (MeOH) (λ_{max} / nm (ε / L mol^{-1} cm^{-1})): 203 (12589), 235 (*sh*), 293 (6456), 304 (*sh*), 693 (*b*).

[Co(L')Cl]Cl ***(2)***. Yield: 31 %; m.p.: 190 °C; IR (KBr, cm^{-1}): 3289, 3240 (–NH stretching of primary amine), 2862, 2929 (CH_2/CH stretching of cyclohexane ring), 1634 (C=N stretching of azomethine group), 777 (out-of-plane C–H deformation); UV–Vis (MeOH) (λ_{max} / nm (ε / L mol^{-1} cm^{-1})): 206 (24547), 283 (*sh*), 451 (*sh*), 537 (*sh*).

[Zn(L')Cl]Cl ***(3)***. Yield: 60 %; m.p.: 270 °C; Anal. Calcd. for: $C_{12}H_{17}N_3ZnCl_2$: C, 42.44; H, 5.05; N, 12.37 %. Found: C, 42.54; H, 5.06; N, 12.24 %; IR (KBr, cm^{-1}): 3293, 3248 (–NH stretching of primary amine), 2929, 2859 (CH_2/CH stretching of cyclohexane ring), 1663 (C=N stretching of azomethine group), 776 (out-of-plane C–H deformation); ^{1}H-NMR (500 MHz, DMSO-d_6, δ / ppm): 1.05–1.96 (8H, *m*, CH_2), 3.32–3.62 (2H, *m*, CH), 7.48–8.83 (5H, *m*, aromatic, HC=N); UV–Vis (MeOH) (λ_{max} / nm (ε / L mol^{-1} cm^{-1})): 204 (13803), 240 (7413), 283 (7585), 392 (*sh*).

[CuL]Cl_2 ***(4)***. Yield: 41 %; m.p.: 220 °C; IR (KBr, cm^{-1}): 2926, 2867 (CH_2/CH stretching of cyclohexane ring), 1653 (C=N stretching of azomethine group), 782 (out-of-plane C–H deformation); UV–Vis (MeOH) (λ_{max} / nm (ε / L mol^{-1} cm^{-1})): 208 (17782), 234 (*sh*), 290 (9332), 469 (323), 683 (*b*).

[CoL]Cl_2 ***(5)***. Yield: 78 %; m.p.: 330 °C; IR (KBr, cm^{-1}): 2931, 2868 (CH_2/CH stretching of cyclohexane ring), 1635 (C=N stretching of azomethine group), 775 (out-of-plane C–H deformation); UV–Vis (MeOH) (λ_{max} / nm (ε / L mol^{-1} cm^{-1})): 205 (22908), 264 *(sh)*, 566 (457).

[ZnL]Cl_2 ***(6)***. Yield: 53 %; m.p.: 290 °C; IR (KBr, cm^{-1}): 2932, 2862 (CH_2/ /CH stretching of cyclohexane ring), 1639 (C=N stretching of azomethine group), 768 (out-of-plane C–H deformation); ^{1}H-NMR (500 MHz, DMSO-d_6, δ / ppm): 1.42–1.89 (8H, *m*, CH_2), 3.32–3.69 (2H, *m*, CH), 7.56–8.66 (10H, *m*, aromatic, HC=N); UV–Vis (MeOH) (λ_{max} / nm (ε / L mol^{-1} cm^{-1})): 249 (7079), 258 (*sh*).

IR and UV–Vis spectra of the ligand and complexes

In the IR spectrum of ligand L, a strong and sharp band due to the azomethine ν(C=N) appears at 1643 cm^{-1}. The bands at 2853 and 2931 cm^{-1} are indicative of the presence of 1,2-cyclohexanediamine.

In the IR spectra of **1**–**3**, the two primary NH_2 stretching modes are seen at around 3267–3293 and 3217–3248 cm^{-1} as sharp bands (doublet) for the asymmetric and symmetric vibrations, respectively (Fig. 1). A strong absorption band at 2929–2862 cm^{-1} corroborates the presence of the 1,2-cyclohexanediamine group in the complexes.[25] The band due to azomethine ν(C=N) appears at 1655, 1634 and 1663 cm^{-1} for complexes **1**–**3**, respectively. In the IR spectra of complexes **4**–**6**, the strong absorption bands at 2932–2857 cm^{-1} corroborate the presence of the 1,2-cyclohexanediamine group in the complexes. The band due to azomethine ν(C=N) appears at 1653, 1635 and 1639 cm^{-1}, respectively. A comparison of the IR spectra of **1**–**3** with **4**–**6** provides clear evidence of the hydrolytic cleavage that had occurred in one imine bond of L. The IR spectra of complexes **4**–**6** exhibit bands typical of 2-substituted pyridines.[26] These pyridine bands are the four rings stretching vibrations (1604–1445 cm^{-1}), the ring breathing vibration at around 1026–1024 cm^{-1} and the out-of-plane C–H deformation

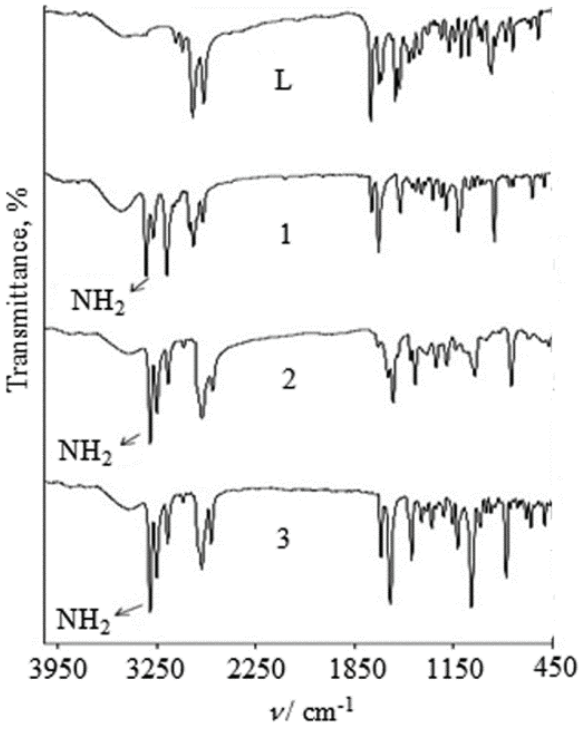

Fig. 1. IR spectra of ligand (L) and complexes **1**–**3**.

at around 782–768 cm^{-1}. These compounds also show a strong band at around 1653–1635 cm^{-1}, assigned[27] to the azomethine stretching vibration, which confirms the Schiff base nature of the coordinated L molecule.

The electronic spectra of complex **1** consist of one broad d–d transition band at 693 nm, as is usual for four coordinated Cu(II).[28,29] The higher energy bands are due to π–π* or n–π* transition. Complex **2** shows one band at 531 nm and the other at 451 nm indicating four coordinated geometry of the Co(II) complexes.[30] The electronic absorption spectra of **4** and **5** show absorption band at 683 and 566 nm, respectively. The bands are typical of d–d transition in a four coordinated environment around Cu(II) and Co(II).[31] The electronic absorption spectra of **3** and **6** show absorption bands at 204, 240, 283 and 392 nm and 249 and 258 nm, respectively. The bands are typical of intraligand transition.

*^{1}H-NMR spectra of the ligand and complexes **3** and **6***

The ^{1}H-NMR spectra of the ligand (L) and complexes **3** and **6** were recorded using $CDCl_3$ and DMSO-d_6 as solvent, respectively. Hydrogen atoms of the azomethine groups of L appeared at δ 8.55–8.57 ppm as a doublet. The aromatic protons are found in the range δ 7.22–7.91 ppm as a multiplet. The hydrogen atoms of the CH_2/CH groups in the cyclohexane ring are observed in the δ 1.51––3.57 ppm range.[12] In **3** and **6**, a slight downfield shift of 0.2–0.3 ppm in the resonance peaks corresponding to the aromatic and the azomethine protons is noticeable. This fact confirms that the nitrogen atoms were coordinated to the Zn(II) ion.[32–34]

Luminescence studies

The photophysical data for the ligand and complexes **1**–**6** are listed in Table I. The luminescence studies showed that complexes **1–3** exhibited an emission band at 413, 426 and 411 nm, respectively, in methanol solution and in the solid an emission band at 397, 385 and 387 nm, respectively, which may be assigned to an intraligand π–π* transition (Fig. 2). The fluorescence spectra of complexes **4**–**6** and the free ligand in the solid state at room temperature are presented in Fig. 3. The free ligand (L) showed an intensive emission band at 440 nm when excited

TABLE I. Photophysical data for L and complexes **1**–**6**

Sample	Absorption λ / nm	Fluorescence at room temperature, λ / nm	
		Solution in MeOH	Solid state
L	274	–	440
1	292	413	397
2	283	426	385
3	283	411	387
4	290	–	395
5	264	–	440
6	249	–	442

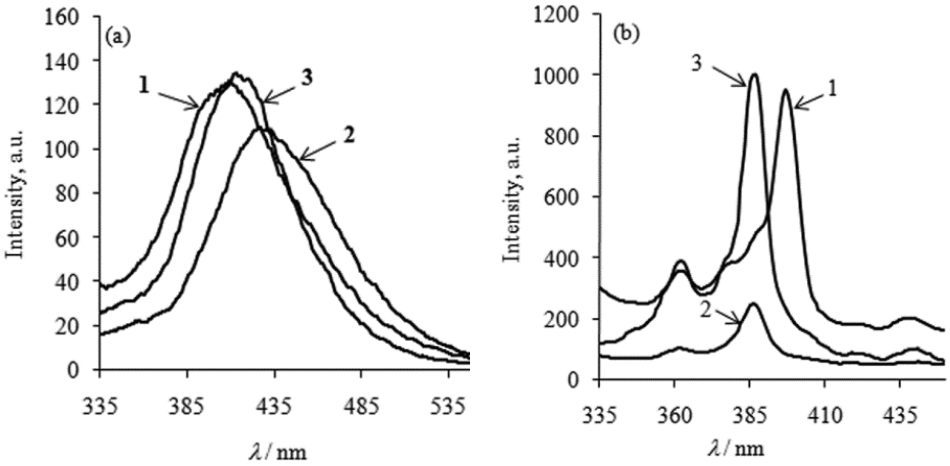

Fig. 2. Emission spectra of complexes **1**–**3**: a) MeOH solution; b) solid state.

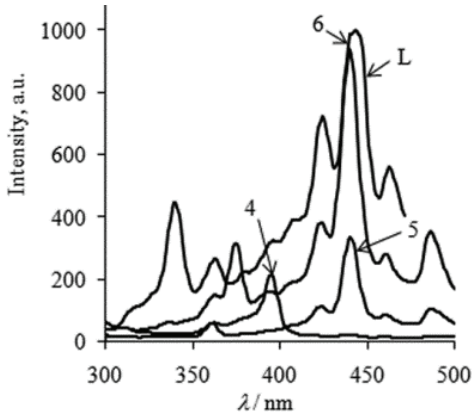

Fig. 3. Solid state emission spectra of ligand (L) and complexes **4**–**6**.

with light of 274 nm which might be assigned to intraligand (π–π*) transition or (n–π*) charge transfer. It is interesting that the Zn(II) complex (**6**) exhibited a higher intensity than that of the free ligand L. In this case the coordination of the ligand to the zinc ion increased the rigidity of the molecular complex and reduced the loss of energy by radiationless thermal vibrations and hence the emission intensity of the complex was increased. However, the emission intensities for complex **4** at 395 nm and complex **5** at 440 nm were reduced, which, according to previous studies, could be assigned to the emission of ligand to metal charge transfer.[35,36] The quenching of fluorescence of a ligand by transition metal ions upon complexation, a rather common phenomenon, can be explained by processes such as magnetic perturbation, redox activity, and electrons.[37,38] The emission bands of the free ligand showed a reduction in intensity upon complexation and the phenomenon could be attributed to (n–π*) transitions

rather than (π–π*) transitions.[39] This is due to the pairs of electrons on the free ligand that are donated to the metal centre in the complex. The (n–π*) emission intensities were therefore reduced in complexes **4** and **5**.

CONCLUSIONS

When the reaction between $MCl_2 \cdot H_2O$ (M = Zn, Cu or Co) and L was performed in THF, complexes $[ML]Cl_2$ (**4**–**6**) were obtained. In these complexes, L acts as a tetradentate ligand leading most probably to tetrahedral stereochemistry. In contrast to the complexes of L obtained in THF, the investigation of the reactions between $MCl_2 \cdot xH_2O$ and L in ethanol led to the novel complexes [M(L′)Cl]Cl (**1**–**3**). In each of these three complexes, one of the two imine bands in the parent ligand was hydrolysed on reaction with $MCl_2 \cdot xH_2O$ (M = Zn, Cu or Co) and the resultant primary amine nitrogen coordinated to the metal ions in a (possibly) pseudo-tetrahedral geometry. Work is also in progress in which this behaviour for other similar ligands is being investigated.

Acknowledgement. Financial assistance from Alzahra University is acknowledged.

ИЗВОД

СИНТЕЗА И МОНО-ХИДРОЛИЗА ДИШИФОВЕ БАЗЕ (±)*trans*-1,2-ЦИКЛОХЕКСАНДИАМИНА И 2-ПИРИДИНКАРБОКСАЛДЕХИДА У Cu(II), Co(II) И Zn(II) КОМПЛЕКСИМА ИНДУКОВАНА РАСТВАРАЧЕМ

MARYAM LASHANIZADEGAN и MARZIEH SARKHEIL

Department of Chemistry, Faculty of Sciences, Alzahra University, P. O. Box 1993893973, Tehran, Iran

Синтетисана је Шифова база *trans*-*N*,*N*′-бис(2-пиридинилметилен)-1,2-циклохександиамин (L). Еквимоларна смеша овог лиганда и одговарајуће $MCl_2 \cdot xH_2O$ соли (M = = Cu, Co или Zn) у етанолу као растварачу уз мешање подлеже парцијалној хидролози имино везе, при чему настаје тридентатни лиганд L′ који истовремено гради комплексе N_3 координационе сфере. У реакцијама лиганда L са $MCl_2 \cdot xH_2O$ (M = Cu, Co или Zn) у THF настају $[ML]Cl_2$ комплекси. Лиганд L и комплекси [M(L′)Cl]Cl и $[ML]Cl_2$ су окарактерисани помоћу елементалне анализе, UV–Vis, FT-IR и ^{1}H-NMR спектроскопије и GC/MS луминисцентних својстава. ^{1}H-NMR спектри лиганда су снимани у $CDCl_3$, а спектри одговарајућих дијамагнетичних комплекса у DMSO растварачима. На основу ових спектроскопских података потврђено је да је лиганд преко донорских атома азота координован за јон метала. На основу луминисцентних испитивања лиганда и одговарајућих комплекса утврђено је да ова једињења показују интралигандну (π–π*) флуоресценцију у метанолу као растварачу, као и у чврстом стању на собној температури.

(Примљено 3. децембра 2011, прихваћено 24. марта 2012)

REFRENCES

1. H. Schiff, *Ann. Suppl*. **3** (1864) 343
2. R. Ziessel, *Coord. Chem. Rev*. **195** (2001) 216
3. P. G. Cozzi, *Chem. Soc. Rev*. **33** (2004) 410
4. K. C. Gupta, A. K. Sutar, *Coord. Chem. Rev*. **252** (2008) 1420.
5. J. P. Costes, S. Shova, W. Wernsdorfer, *J. Chem. Soc., Dalton Trans.* (2008) 1843

6. R. H. Holm, *J. Am. Chem. Soc*. **82** (1960) 5632
7. E. C. Niederhoffer, J. H. Timmons, A. E. Martell, *Chem. Rev*. **84** (1984) 137
8. K. Srinivasan, P. Michaud, J. K. Kochi, *J. Am. Chem. Soc*. **108** (1986) 2309
9. W. Zhang, J. L. Loebach, S. R. Wilson, E. N. Jacobsen, *J. Am. Chem. Soc.* **112** (1990) 2801
10. J. Tisato, F. Refosco, F. Bandoli, *Coord. Chem. Rev*. **135** (1994) 325
11. J. Lacroix, *Eur. J. Inorg. Chem.* **2** (2001) 339
12. J. Nagel, U. Oertel, P. Friedel, H. Komber, D. Mobius, *Langmuir* **13** (1997) 4698
13. S. S. Sundari, A. Dhathathreyan, M. Kanthimathi, U. N. Balachandran, *Langmuir* **13** (1997) 4923
14. M. Kojima, H. Taguchi, M. Tsuchimoto, K. Nakajima, *Coord. Chem. Rev*. **237** (2003) 183
15. N. S. Venkataramanan, G. Kuppuraj, S. Rajagopal, *Coord. Chem. Rev*. **249** (2005) 1249
16. M. Vázquez, M. R. Bermejo, J. Sanmartín, A. M. García-Deibe, C. Lodeiro, J. Mahía, *J. Chem. Soc., Dalton Trans*. (2002) 870
17. E. Kwiatkowski, G. Romanowski, W. Nowicki, M. Kwiatkowski, K. Suwińska, *Polyhedron* **26** (2007) 2559
18. P. Mukherjee, M. G. B. Drew, A. Ghosh, *Eur. J. Inorg. Chem.* (2008) 3372
19. Y.-B. Dong, X. Zhao, R.-Q. Hung, *Inorg. Chem.* **43** (2004) 5603
20. D. Mandal, V. Bertolasi, J. Ribas-Ariño, G. Aromí, D. Ray, *Inorg. Chem*. **47** (2008) 4365
21. B. Sarkar, M. S. Ray, M. G. B. Drew, A. Figuerola, C. Diaz, A. Ghosh, *Polyhedron* **25** (2006) 3084
22. S. Chattopadhyay, M. G. B. Drew, A. Ghosh, *Polyhedron* 26 (2007) 3513
23. S. Chattopadhyay, P. Chakraborty, M. G. B. Drew, A. Ghosh, *Inorg. Chim. Acta* **362** (2009) 502
24. S. Naiya, B. Sarkar, Y. Song, S. Ianelli, M. G. B. Drew, A. Ghosh, *Inorg. Chim. Acta* **363** (2010) 2488
25. M. Aslantaş, E. Kendi, N. Demir, A. E. Şabik, M. Tümer, M. Kertmen, *Spectrochim. Acta, A* **74** (2009) 624
26. T. G. Campbell, F. L. Urbach, *Inorg. Chem*. **12** (1973) 1836
27. A. R. Kartritzky, *Quart. Rev.* **13** (1959) 353
28. R. Vafazadeh, V. Hayeri, A. C. Willis, *Polyhedron* **29** (2010) 1810
29. A. Gölcü, M. Tümer, H. Demirelli, R. Alan Wheatly, *Inorg. Chim. Acta* **358** (2005) 1785
30. D. A. Clemente, A. Marzotto, G. Valle, C. J. Visoná, *Polyhedron* **18** (1999) 2749
31. S. Chandra, R. Kumar, *Spectrochim. Acta, A* **62** (2005) 1050
32. M. Mulqi, F. S. Stephens, R .S. Vagg, *Inorg. Chim. Acta* **62** (1982) 221
33. H. A. Nieuwenhuis, J. G. Haasnoot, R. Hage, J. Reedijk, T. L. Snoek, D.J. Stufkens, J. G. Vos, *Inorg. Chem.* **30** (1991) 48
34. A. Prakash, B. K. Singh, N. Bhojak, D. Adhikari, *Spectrochim. Acta, A* **76** (2010) 356
35. J. C. Dai, X. T. Wu, Z. Y. Fu, C. P. Cui, S. M. Wu, W. X. Du, *Inorg. Chem.* **41** (2002) 1391
36. L. Y. Zhang, G. F. Liu, S. L. Zheng, B. H. Ye, X. M. Zhang, X. M. Chen, *Eur. J. Inorg. Chem*. (2003) 2965
37. A. W. Varnes, R. B. Dadson, E. L. Wehry, *J. Am. Chem. Soc*. **94** (1972) 946
38. J. A. Kemlo, T. M. Sheperd, *Chem. Phys. Lett.* **47** (1977) 158
39. A. D. Naik, V. K. Revankar, *Proc. Indian Acad. Sci., Chem. Sci.* **113** (2001) 285.

Journal of the Serbian Chemical Society
JSCS-info@shd.org.rs • www.shd.org.rs/JSCS
J. Serb. Chem. Soc. 77 (11) 1599–1607 (2012)
JSCS–4374
UDC 546.73+546.811+544.478:
547.217.2:546.215
Short communication

SHORT COMMUNICATION

Polyoxometalate catalysts in the oxidation of cyclooctane by hydrogen peroxide

WIMONRAT TRAKARNPRUK*, APIWAT WANNATEM and JUTATIP KONGPETH

Department of Chemistry, Faculty of Science, and Center of Excellence for Petroleum, Petrochemicals, and Advanced Materials, Chulalongkorn University, Bangkok 10330, Thailand

(Received 24 November 2011, revised 20 April 2012)

Abstract: A Keggin-type tungstocobaltate, $[Co(2,2'\text{-bipy})_3]_2H_2[CoW_{12}O_{40}]\cdot 9.5H_2O$ ([Co]CoW) and tetrabutylammonium salt of vanadium-substituted tungstophosphates $[(n\text{-}C_4H_9)_4N]_4[PVW_{11}O_{40}]$, $[(n\text{-}C_4H_9)_4N]_5[PV_2W_{10}O_{40}]$ (PVW, PV_2W) were used as catalysts for the oxidation of cyclooctane with H_2O_2 as the oxidant in acetonitrile. The activity of $[(n\text{-}C_4H_9)_4N_4H[PCo(H_2O)W_{11}O_{39}]\cdot 2H_2O$ (PCoW) was also compared. The products of the reaction were cyclooctanone, cyclooctanol and cyclooctyl hydroperoxide. The experimental results showed that at an H_2O_2/cyclooctane molar ratio of 3 at 80 °C, [Co]CoW yielded a higher conversion and selectivity to cyclooctanone in 9 h. The V-based catalysts were more active than the Co-based tungstophosphate. PV_2W gave rise to high selectivity to cyclooctyl hydroperoxide. Cyclooctane conversion was increased by increasing the reaction time or H_2O_2/cyclooctane molar ratio. In the presence of tungstocobaltate catalyst, 88 % cyclooctane conversion and 82 % selectivity of cyclooctanone were obtained after 12 h using an H_2O_2/cyclooctane molar ratio of 9. This catalyst is stable upon treatment with H_2O_2. Experiments with radical traps suggested the involvement of a free-radical mechanism.

Keywords: Keggin-type polyoxometalates; cyclooctane; oxidation; hydrogen peroxide; cobalt; vanadium.

INTRODUCTION

The transformation of hydrocarbons into oxygenated derivatives has been extensively investigated because such products are valuable intermediates for industrial organic synthesis. Oxidation of cyclooctane with air was catalyzed by metalloporphyrins and metallophthalocyanines.[1,2] Cr-MCM-41 materials showed high activity and selectivity for the oxidation of cyclooctane to cyclooctanone,

* Corresponding author. E-mail: wimonrat.t@chula.ac.th
doi: 10.2298/JSC111124040T

using H_2O_2 or *tert*-butyl hydroperoxide.[3] A possible way to improve the selectivity is through the selective decomposition of alkyl hydroperoxides formed during the oxidation reactions. Polyoxometalates afford good selectivity towards the formation of alkyl hydroperoxides in the catalytic oxidation of cycloalkanes.[4]

Polyoxometalates are metal–oxygen anionic clusters of early transition metals. They bear many similarities to metal complexes of macrocyclic ligands such as, for example, to metalloporphyrins and related species, because they possess rigid co-ordination sites surrounding a metal centre.[5] The robust nature of polyoxometalate ligands and their resistance to oxidation lead to their valuable applications in catalysis. Their activities can be controlled by changes in the metal center and the counter cation.[6] Reports on oxidation using polyoxometalates include $[SiW_{10}Fe_2(H_2O)_2O_{38}]^{6-}$ and $[M_4(H_2O)_2(PW_9O_{34})_2]^{10-}$, M(II) = Co or Mn and $[Fe_4(H_2O)_2(PW_9O_{34})_2]^{6-}$.[7,8] A few reports have been published concerning the oxidation of cyclooctane in the presence of polyoxometalates, $[(n\text{-}C_4H_9)_4N]_7H_3[Co_4(H_2O)_2(PW_9O_{34})_2]$[9] and $[XW_{11}MO_{39}]^{p-}$, X = P or Si and M = Fe or Mn, as well as $[XW_{11}VO_{40}]^{m-}$.[10] Some vanadium-substituted polyoxometalates have been used as selective oxidation catalysts for a variety of organic reactions,[11,12] *e.g.*, the oxidation of cyclic and linear alkanes by H_2O_2 over $[(n\text{-}C_4H_9)_4N]_4[PVMo_{11}O_{40}]$.[13] In these catalysts, the presence of a vanadium(V) center in the polyoxometalates is a key factor.

Polyoxometalates can form compounds with a number of organic and complex cations containing N, S, O atoms, *e.g.*, diethylamine and bipyridine.[14–16] New properties can be obtained from the interplay of the two components, which can be used as effective catalysts. One example is $[H_5PCo(4,4'\text{-bipy})Mo_{11}O_{39}][H_3PMo_{12}O_{40}]\cdot 3.75(4,4'\text{-bipy})\cdot 1.5H_2O$ for the oxidation of benzaldehyde to benzoic acid using H_2O_2 as the oxidant.[17]

In continuation of research on the utilization of polyoxometalates as catalysts for the oxidation of sulfur compounds,[18] cyclohexane and ethylbenzene,[19] polyoxometalates in the oxidation of cyclooctane by H_2O_2 in acetonitrile as solvent were studied. H_2O_2 is regarded as one of the "greenest" oxidants because of its high content of active oxygen species (47 wt. %), high atom efficiency and co-production of only water. The key for the development of efficient H_2O_2-based oxidation systems is the design of catalysts that can effectively activate H_2O_2 and transfer the active oxygen species to substrates with high efficiencies and selectivities. The results of catalytic activities of the Keggin-type tungstocobaltate, tetrabutylammonium salts of V- and Co-substituted tungstophosphates, the effect of the H_2O_2/cyclooctane molar ratio and reaction time on cyclooctane conversion and product selectivity are presented herein.

EXPERIMENTAL

All reagents and solvents used in this work were commercially available (Fluka Chemika or Merck) and were used as received. The polyoxometalates were prepared according to

published methods[4,20,21] with modifications and were identified by elemental analysis using a CHN analyzer (Perkin Elmer PE2400 Series II) and inductively coupled plasma emission ICP spectroscopy (Perkin Elmer Plasma 1000 Emission Spectrometer) and by infrared spectroscopy using a Nicolet FT-IR Impact 410 spectrophotometer. The analytical and spectroscopic data were in agreement with the published values.

$[(n\text{-}C_4H_9)_4N]_4H[PCo(H_2O)W_{11}O_{39}]\cdot 2H_2O$ (PCoW)[4]

Anal. Calcd. for $C_{64}H_{151}N_4O_{42}PW_{11}Co$: C, 20.44: H, 4.05; Co, 1.57; P, 0.82; W, 53.10; N, 1.49 %; Found: C, 20.20; H, 3.89; Co, 1.54; P, 0.79; W, 53.28; N, 1.38 %. IR (KBr, cm^{-1}): 1060, 963, 886, 810, 760.

$[Co(C_{10}H_8N_2)_3]_2H_2[CoW_{12}O_{40}]\cdot 9.5H_2O$ ([Co]CoW)[20]

Anal. Calcd. for $C_{60}H_{67}N_{12}O_{49:5}W_{12}Co_3$: C, 17.42; H, 1.62; N, 4.06; W, 53.22 %; Found: C, 17.29; H, 1.68; N, 3.93; W, 53.38 %. IR (KBr, cm^{-1}): 935, 870, 760, 457 (from anion) and 1631, 1446, 1168, 1106 (from cation).

$[(n\text{-}C_4H_9)_4N]_4[PVW_{11}O_{40}]$ (PVW)[21]

Anal. Calcd. for $C_{64}H_{144}N_4O_{40}PVW_{11}$: V, 1.37 %. Found: V, 1.29 %; IR (cm^{-1}): 1095, 1064, 965, 888, 809.

$[(n\text{-}C_4H_9)_4N]_5[PV_2W_{10}O_{40}]$ (PV_2W)[21]

Anal. Calcd for $C_{80}H_{180}N_5O_{40}PV_2W_{10}$: V, 2.84 %; Found: V, 2.76 %. IR (cm^{-1}): 1093, 1064, 962, 888, 808.

Oxidation reactions

The reactions were realized in a Parr reactor. Cyclooctane 1 ml (7.6 mmol) and catalyst (11.5 μmol) were added in 10 ml acetonitrile followed by 30 % H_2O_2 (in different H_2O_2/ /cyclooctane ratios). The reactions were usually performed under air. When a reaction was performed in an inert atmosphere, N_2 was bubbled through the reaction mixture before the addition of H_2O_2 and a rubber balloon with N_2 was maintained at the top of the condenser during the reaction. After stirring at the required reaction temperature for the required time, 25 % H_2SO_4 was added to the reaction mixture and the reaction products were extracted with diethyl ether. The organic layer was neutralized with saturated $NaHCO_3$ and dried over anhydrous Na_2SO_4. The products were analyzed by gas chromatography using a Shimadzu model CG-17A instrument equipped with a flame ionization detector and OV-1701 0.50 μm capillary column (30 m, 0.25 mm). *n*-Octane was used as an internal standard. The chromatographic conditions for cyclooctane were initial temperature: 80 °C (2 min), a temperature ramp at 20 °C min^{-1} to the final temperature of 220 °C (1 min); injector temperature: 250 °C and detector temperature: 250 °C. Cyclooctanone and cyclooctanol were identified unambiguously by comparison with authentic standards. The percentage of each compound in the reaction mixture was estimated directly from the corresponding chromatographic peak areas. Blank experiments were also conducted in the absence of catalyst or oxidant. At the end of the oxidation reaction, cyclooctyl hydroperoxide was determined by treating the final reaction solution with an excess of PPh_3 before the GC analysis. PPh_3 reduces the cyclooctyl hydroperoxide quantitatively to the corresponding cyclooctanol, giving triphenylphosphine oxide. The amount of cyclooctyl hydroperoxide was determined by comparing the concentrations of the cyclooctanone and of the cyclooctanol, measured before and after the treatment of the sample with PPh_3.[22] A few experiments were performed in the presence of a radical scavenger (2,6-di-*tert*-butyl-4-methylphenol). To test stability of the [Co]CoW catalyst in the presence

of H_2O_2, infrared and UV spectra were recorded using a Nicolet FT-IR Impact 410 spectrophotometer and a Shimadzu UV-250 spectrometer, respectively.

RESULTS AND DISCUSSION

Oxidation of cyclooctane

The oxidation of cyclooctane over polyoxometalates catalysts were performed in acetonitrile solvent using H_2O_2 as the oxidant. All the catalysts were soluble in hot acetonitrile. The results are summarized in Table I. No oxidized products were detected in the absence of catalyst (entry 1) or H_2O_2 (entry 2). For all the catalyzed reactions, cyclooctanone and cyclooctanol were detected as the oxidized products together with cyclooctyl hydroperoxide. The performances of the different catalysts in the oxidation of cyclooctane with H_2O_2 as oxidant were compared under the same reaction conditions: cyclooctane 1 ml (7.6 mmol), catalyst 11.5 μmol, H_2O_2/cyclooctane molar ratio = 3, CH_3CN 10 ml at 80 °C for 9 h. It was found that [Co]CoW showed the highest activity (50 % conversion) with cyclohexanone as the main product (80 % selectivity) while PCoW showed the lowest activity (34 % conversion and 58% selectivity to cyclooctanone). PV_2W showed a slightly higher activity than PVW (42 and 39 % in entries 7 and 6, respectively) with a similar product selectivity. This activity order is in agreement with the result reported in a previous study using these vanadium catalysts for the oxidation of sulfur compounds[18] and also in the oxidation of aldehydes over $H_4PVMo_{11}O_{40}$ and $H_5PV_2Mo_{10}O_{40}$ with H_2O_2.[23] When the oxidation over the [Co]CoW and PV_2W catalysts was performed in the presence of a radical scavenger (2,6-di-*tert*-butyl-4-methylphenol), no oxidized products were found (entries 5 and 8).

TABLE I. Oxidation of cyclooctane by H_2O_2 using various catalysts; reaction conditions: cyclooctane, 1 ml (7.6 mmol), catalyst, 11.5 μmol, H_2O_2/cyclooctane molar ratio, 3, CH_3CN, 10 ml, temperature 80 °C, time 9 h

Entry	Catalyst	Conversion[a], %	Selectivity[b], %		
			CyONE	CyOH	CyOOH
1	No catalyst	0	0	0	0
2	No H_2O_2	0	0	0	0
3	PCoW	34	58	42	0
4	[Co]CoW	50	80	19	1
5	[Co]CoW[c]	0	0	0	0
6	PVW	39	65	20	15
7	PV_2W	42	63	17	20
8	PV_2W[c]	0	0	0	0

[a]Based on gas chromatographic peak areas; [b]expressed as percentages of total products formed, CyONE = cyclooctanone, CyOH = cyclooctanol, CyOOH = cyclooctyl hydroperoxide; [c]in the presence of the radical scavenger 2,6-di-*tert*-butyl-4-methylphenol, 3 equivalents

Vanadium substituted tungstophosphates catalysts

The catalytic activity of PV_2W was further studied by varying the reaction condition. The results are given in Table II. Increasing the H_2O_2/cyclooctane molar ratio resulted in an increasing conversion of cyclooctane. At a molar ratio H_2O_2/cyclooctane of 9, an 84 % conversion was obtained with selectivities to cyclooctanone:cyclooctanol:cyclooctyl hydroperoxide of 24:7:69. When the reaction time was increased from 9 h to 12 h, the conversion increased to 89 % and the selectivity to cyclooctyl hydroperoxide was further increased (cyclooctanone:cyclooctanol:cyclooctyl hydroperoxide = 23:2:75). At longer times, 18 h, the conversion remained constant. A decomposition of cyclooctyl hydroperoxide produced additional amount of cyclooctanone (entry 5). Under the same reaction condition, the activity of the PVW catalyst was lower (entry 2 *vs*. 6). The activity of the PVW catalyst was previously reported by Balula *et al.* (entries 7–9).[9] They also observed that the activity of $[(n\text{-}C_4H_9)_4N]_4[PVW_{11}O_{40}]$ was higher than that of $[(n\text{-}C_4H_9)_4N]_3[PW_{12}O_{40}]$. When W(VI) in a polyoxometalate was substituted by V(V), the substitution resulted in the generation of a more reactive oxygen associated to the W–O–V species.[24] In this work, the tetrabutylammonium salt dissolved well in acetonitrile. Compared to the sodium salt catalyst: $Na_5PV_2Mo_{10}O_{40}$, it was reported to yield 10 % conversion with a 70 % selectivity to cyclooctanone (reaction conditions: cyclooctane 0.8 mmol, catalyst 2.8 μmol, H_2O_2 1 ml, in 1,2-dichloroethane at refluxing temperature).[25]

TABLE II. Oxidation of cyclooctane over the PV_2W and PVW catalysts; reaction conditions: cyclooctane, 1 ml (7.6 mmol), catalyst, 11.5 μmol, CH_3CN, 10 ml, temperature 80 °C

Entry	Catalyst	H_2O_2/cyclooctane mole ratio	Time, h	Conversion, %	Selectivity, %		
					CyONE	CyOH	CyOOH
1	PV_2W	3	9	42	63	17	20
2		6	9	66	43	12	45
3		9	9	84	24	7	69
4		9	12	89	23	2	75
5		9	18	89	29	2	69
6	PVW	6	9	60	33	10	57
7	PVW[a]	2	9	26	46	13	41
8		9.8	9	87	23	0	77
9		9.8	12	94	23	0	77

[a]Cyclooctane, 1 mmol, catalyst, 1.5 μmol, CH_3CN, 1.5 ml, temperature 80 °C[9]

The [Co]CoW catalyst

The oxidation of cyclooctane over the [Co]CoW catalyst was performed by varying the H_2O_2/cyclooctane molar ratio and the reaction time. The reactions were also performed in the absence of air (under a N_2 atmosphere) or oxidant, and at room temperature. The results are shown in Table III.

When the reaction was conducted under an atmosphere of nitrogen, a similar result to that in air was obtained (compare entry 2 with entry 1). Therefore, the possibility of auto-oxidation may be excluded. In addition, an experiment performed under open air without H_2O_2 (entry 3) did not afford any noticeable amount of product, indicating that oxygen plays no role in this oxidation reaction under the employed experimental conditions. In entry 4, using an H_2O_2/cyclooctane molar ratio of 3 and a reaction time of 12 h, the conversion of cyclooctane was increased to 71 % and the product selectivity cyclooctanone:cyclooctanol:cyclooctyl hydroperoxide was 70:14:16. In entry 5, a higher conversion (77 %) was obtained by increasing the molar ratio to 6, cyclooctyl hydroperoxide decomposed to form more cyclohexanol and cyclohexanone (cyclooctanone:cyclooctanol:cyclooctyl hydroperoxide was 76:20:4). The reaction time could be shortened by increasing the H_2O_2/cyclooctane molar ratio to 9 (entry 6). No cyclooctyl hydroperoxide was detected. The maximum conversion (88 %) was obtained after 12 h reaction time (entry 7) giving 82 % cyclooctanone and remained unchanged after that (entry 8). There was no reaction at room temperature (entry 9).

Table III. Oxidation of cyclooctane over the [Co]CoW catalyst; reaction conditions: cyclooctane, 1 ml (7.6 mmol), catalyst, 11.5 μmol, CH_3CN, 10 ml, temperature 80 °C

Entry	H_2O_2/cyclooctane mole ratio	Time, h	Conversion, %	Selectivity, %		
				CyONE	CyOH	CyOOH
1	3	9	50	80	19	1
2[a]	3	9	49	78	22	0
3[b]	3	9	0	0	0	0
4	3	12	71	70	14	16
5	6	12	77	76	20	4
6	9	9	79	80	20	0
7	9	12	88	82	18	0
8	9	15	88	83	17	0
9[c]	9	12	0	–	–	–

[a]Under an N_2 atmosphere; [b]without H_2O_2; [c]experiment performed at room temperature

The high activity of the [Co]CoW catalyst might result from many factors: solubility, redox property or cation. [Co]CoW consists of two discrete $[Co(2,2'-bipy)_3]^{2+}$ held weakly with a $[CoW_{12}O_{40}]^{6-}$. It was dissolved in hot CH_3CN. The metal active centers are W(VI) and Co(II). An electrochemical study of a related anion, $[CoMo_{12}O_{40}]^{6-}$ showed a one-electron redox Co(III)/Co(II) couple and reversible redox processes ascribed to Mo centers. This was ascribed to the distribution of the charge on Co^{2+} over the whole polyoxometalate cluster.[26] In addition, it was reported that in the presence of an oxidant, the $[CoW_{12}O_{40}]^{6-}$ could be oxidized to give $[CoW_{12}O_{40}]^{5-}$, which is a very strong oxidizing agent.[27,28]

$[Co(2,2'-bipy)_3]^{2+}$ might contribute to the activity, similar to $[Cu(bipy)_3]^{2+}$, which catalyzed the oxidation of cyclohexane by H_2O_2.[29] In addition, this same

tungstocobaltate with $[Co(phen)_2]^{2+}$ as a cation was reported to show that the electrochemical behavior of Co(II) differ from those of $[(n\text{-}C_4H_9)_4N]_5[HCoW_{12}O_{40}]$. This arose from the different coordinated environments of the Co atoms.[30]

It is known that Keggin polyoxometalates degrade in the presence of excess H_2O_2 to form peroxo species $\{(PO_4)[MO(O_2)_2]_4\}^{3-}$ or $[M_2O_3(O_2)_4]^{2-}$ (M = W or Mo), which are the catalytically active intermediate in the oxidation of organic compounds by H_2O_2.[31] Santos *et al*. reported that $(THA)_2[W_2O_3(O_2)_4]$ (THA = = tetrahexylammonium) catalyzed the oxidation of cyclooctane with 83 % conversion and 59:12:29 selectivity to cyclooctanone:cyclooctanol:cyclooctyl hydroperoxide at 80 °C in 12 h. A stoichiometric amount of catalyst was used (catalyst/cyclooctane molar ratio = 1.5:1). They reported that in solution, the $[W_2O_3(O_2)_4]^{2-}$ complex may be involved in a dissociative process, peroxide occupying the empty sites of the W coordination sphere that result from the breakage of the oxygen bridges in solution.[32]

In order to check the stability of [Co]CoW upon reaction with H_2O_2, FTIR and UV spectra were taken of the H_2O_2-treated sample. In the FTIR spectrum of the H_2O_2-treated sample, bands attributed to the Keggin anion were almost preserved, although the band shapes were more or less deformed. The UV spectrum of the H_2O_2-treated sample in CH_3CN exhibited two absorption peaks at 196 and 300 nm ascribed to the charge-transition absorption of O–W. These results indicate that [Co]CoW was stable.

Proposed mechanism

As shown in Table I, the oxidation reaction over the [Co]CoW and PV_2W catalysts in the presence of a radical scavenger (2,6-di-*tert*-butyl-4-methylphenol) yielded no oxidized products, suggesting the involvement of a free-radical mechanism. This is similar to the previously proposed mechanism for the $[PVM_{11}O_{40}]^{4-}$ (M = Mo or W) and $[PMW_{11}O_{39}]^{4-}$ (M = Fe or Mn).[10,13] Thus for PV_2W, H_2O_2 was coordinated to V(V), followed by the formation of V(IV) and peroxyl radicals. Hydroxyl radicals were formed upon interaction of a V(IV) species with H_2O_2.

In the case of the [Co]CoW, it is thought that the same mechanism could be applied. The activation of H_2O_2 may occur simultaneously at W and Co.[10] The difference in product selectivity of these two catalysts, lower selectivity to cyclooctyl hydroperoxide for the [Co]CoW might be due to Co(II) compared to V(VI). The generation of molecular oxygen, *in situ* from H_2O_2, may not be as extensive as proposed for PV_2W.

CONCLUSIONS

The $[Co(2,2'\text{-bipy})_3]_2H_2[CoW_{12}O_{40}]\cdot 9.5H_2O$ and $[(n\text{-}C_4H_9)_4N]_5[PV_2W_{10}O_{40}]$ were shown to be efficient catalysts for the selective oxidation of cyclooctane

using the environmental friendly oxidant, H_2O_2. The vanadium-substituted tungstophosphate gave high selectivity to cyclooctyl hydroperoxide. With the Keggin-type tungstocobaltate, oxidation of cyclooctane could be obtained with high selectivity to cyclooctanone (82 %) with a conversion of 88% at 80 °C in 12 h. The oxidation catalyzed by these catalysts appeared to be a radical process.

ИЗВОД

ПОЛИОКСОМЕТАЛАТИ КАО КАТАЛИЗАТОРИ ОКСИДАЦИЈЕ ЦИКЛООКТАНА ПОМОЋУ ВОДОНИК-ПЕРОКСИДА

WIMONRAT TRAKARNPRUK, APIWAT WANNATEM и JUTATIP KONGPETH

Department of Chemistry, Faculty of Science, and Center of Excellence for Petroleum, Petrochemicals, and Advanced Materials, Chulalongkorn University, Bangkok 10330, Thailand

Keggin-тип волфрам-кобалтата, $[Co(2,2\text{-bipy})_3]_2H_2[CoW_{12}O_{40}]\cdot 9{,}5H_2O$ ([Co]CoW) и тетрабутиламонијум соли ванадијумом супституисаних волфрамфосфата, $[(n\text{-}C_4H_9)_4N]_4[PVW_{11}O_{40}]$, $[(n\text{-}C_4H_9)_4N]_5[PV_2W_{10}O_{40}]$ (PVW, PV_2W) су употребљени као катализатори за оксидацију циклооктана помоћу H_2O_2 у ацетонитрилу као растварачу. Поред тога, одређена је каталитичка активност за $[(n\text{-}C_4H_9)_4N_4H[PCo(H_2O)W_{11}O_{39}]\cdot 2H_2O$ (PCoW) и добијени резултати у овом случају су поређени са претходним. Нађено је да су производи у овим реакцијама циклооктанон, циклооктанол и циклооктил-хидропероксид. Добијени експериментални резултати су показали да [Co]CoW, када је вредност молског односа H_2O_2/циклооктан = 3 и на температури од 80 °C за време од 9 h, даје високу конверзију и селективност у циклооктанон као производ реакције. Катализатори који садрже ванадијум су показали већу активност у односу на катализаторе који садрже кобалт-волфрам-фосфате. Катализатор типа PV_2W даје високу селективност у циклооктил-хидропероксид. Конверзија циклооктана се повећавала са повећањем рекационог времена, или молског односа за систем H_2O_2/циклооктан. У присуству волфрамо-кобалтата као катализатора за време од 12 сати и при молском односу H_2O_2/циклооктан = 9, конверзија циклооктана је износила 88 %, док је селективност била 82 %. Поред тога, овај катализатор је показао велику стабилност након третмана са H_2O_2.

(Примљено 24. новембра 2011, ревидирано 20. априла 2012)

REFERENCES

1. J. Połtowicz, E. Tabor, K. Pamin, J. Haber, *Inorg. Chem. Commun*. **8** (2005) 1125
2. J. Haber, K. Pamin, J. Połtowicz, *J. Mol. Catal. A: Chem.* **224** (2004) 153
3. S. Samanta, N. K. Mal, A. Bhaumik, *J. Mol. Catal., A* **236** (2005) 7
4. M. M. Q. Simoes, I. C. M. S. Santos, M. S. S. Balula, J. A. F. Gamelas, A. M. V. Cavaleiro, M. G. P. M. S. Neves, J. A. S. Cavaleiro, *Catal. Today* **91–92** (2004) 211
5. C. L. Hill, G. S. Kim, C. M. Prosser-McCartha, D. Judd, in: *Polyoxometallates: From Platonic Solids to Anti-retroviral Activity*, M. T. Pope, A. Muller, Eds., Kluwer, Dordrecht, 1994, p. 307
6. I. V. Kozhevnikov, *Catalysis for Fine Chemical Synthesis, Catalysis by Polyoxometalates*, Wiley, New York, 2002, p. 2
7. N. Mizuno, C. Nozaki, I. Kiyoto, M. Misono, *J. Am. Chem. Soc*. **120** (1998) 9267
8. I. C. M. S. Santos, M. S. S. Balula, M. M. Q. Simoes, M. G. P. M. S. Neves, J. A. S. Cavaleiro, A. M. V. Cavaleiro, *Synlett* (2003) 1643

9. I. C. M. S. Santos, J. A. F. Gamelas, M. S. S. Balula, M. M. Q. Simoes, M. G. P. M. S. Neves, J. A. S. Cavaleiro, A. M. V. Cavaleiro, *J. Mol. Catal., A* **262** (2007) 41
10. M. S. S. Balula, I. C. M. S. Santos, M. M. Q. Simoes, M. G. P. M. S. Neves, J. A. S. Cavaleiro, A. M. V. Cavaleiro, *J. Mol. Catal., A* **222** (2004) 159
11. J. T. Rhule, W. A. Neiwert, K. I. Hardcastle, B. T. Do, C. L. Hill, *J. Am. Chem. Soc.* **123** (2001) 12101
12. K. Nomiya, K. Hashino, Y. Nemoto, M. Watanabe, *J. Mol. Catal., A* **176** (2001) 79
13. G. Suss-Fink, L. Gonzalez, G. B. Shul'pin, *Appl. Catal., A* **217** (2001) 111
14. C. L. Hill, C. M. Prosser-McCartha, *Coord. Chem. Rev*. **143** (1995) 407
15. J. Y. Niu, J. P. Wang, B. Yan, D. B. Dong, Z. Y. Zhou, *J. Chem. Crystallogr*. **30** (2000) 43
16. Y. Lu, Y. G. Li, E. B. Wang, J. Lu, L. Xu, R. Clerac, *Eur. J. Inorg. Chem.*(2005) 1239
17. Y.-B. Huang, J.-X. Chen , T.-Y. Lan, X.-Q. Lu, C.-X. Wei, Z.-S. Li, Z.-C. Zhang, *J. Mol. Struct.* **783** (2006) 168
18. W. Trakarnpruk, K. Rujiraworawut, *Fuel Processing Technol.* **90** (2009) 411
19. W. Kanjina, W. Trakarnpruk, *J. Metals Mater. Miner. Res.* **20** (2010) 29
20. J. Y. Niu, Z. L. Wang, J. P. Wang, *Polyhedron* **23** (2004) 773
21. T. Ueda, M. Komatsu, M. Hojo, *Inorg. Chim. Acta* **344** (2003) 77
22. G. B. Shul'pin, *J. Mol. Catal. A: Chem.* **189** (2002) 39
23. A. F. Shojaei, M. A. Rezvani, M. Heravi, *J. Serb. Chem. Soc.* **76** (2011) 1513
24. M. Akimoto, H. Ikeda, A. Okabe, E. Echigoya, *J. Catal*. **89** (1984) 196
25. S. Tangestaninejad, V. Mirkhani, M. Moghadam, I. Mohammadpoor-Baltork, E. Shams, H. Salavati, *Ultrasonics Sonochem.***15** (2008) 438
26. G.-G. Gao, L. Xu, W.-J. Wang, X.-S. Qu, H. Liu, Y.-Y. Yang, *Inorg. Chem.* **47** (2008) 2325
27. J. S. Maestre, X. Lopez, C. Bo, J.-M. Poblet, N. Casan-Pastor, *J. Am. Chem. Soc*. **123** (2001) 3749
28. M. Mehrotra, R. N. Mehrotra, *Polyhedron* **27** (2008) 1989
29. F. P. Canhota, G. C. Salomão, N. M. F. Carvalho, O. A. C. Antunes, *Cat. Commun*. **9** (2008) 182
30. J. Sha, J. Peng, J. Chen, H. Liu, A. Tian, P. Zhang, *Solid State Sci*. **9** (2007)1012
31. C. Venturello, R. D'Aloisio, *J. Org. Chem*. **53** (1988) 1553
32. I. C. M. S. Santos, F. A. A. Paz, M. M. Q. Simoes, M. G. P. M. S. Neves, J. A. S. Cavaleiro, J. Klinowski, A. M. V. Cavaleiro, *Appl. Catal., A* **351** (2008) 166.

Journal of the Serbian Chemical Society
JSCS-info@shd.org.rs • www.shd.org.rs/JSCS
J. Serb. Chem. Soc. 77 (11) 1609–1623 (2012)
JSCS–4375
UDC 546.57+549.753.11–36:621.793:620.193:66.022.362
Original scientific paper

Electrochemical impedance spectroscopy of a silver-doped hydroxyapatite coating in simulated body fluid used as a corrosive agent

ANA JANKOVIĆ[1#], SANJA ERAKOVIĆ[1#], ANTONIJA DINDUNE[2], DJORDJE VELJOVIĆ[1#], TATJANA STEVANOVIĆ[3], DJORDJE JANAĆKOVIĆ[1#] and VESNA MIŠKOVIĆ-STANKOVIĆ[1#*]

[1]Faculty of Technology and Metallurgy, University of Belgrade, Karnegijeva 4, 11000 Belgrade, Serbia, [2]Institute of Inorganic Chemistry, Riga Technical University, 34 Miera Street, Salaspils, LV-2169, Latvia and [3]Département des sciences du bois et de la forêt, Université Laval, 2425 rue de la Terrasse, Québec, Canada

(Received 12 July, revised 27 August 2012)

Abstract: Titanium is a key biomedical material due to its good biocompatibility, mechanical properties and corrosion stability, but infections at the implantation site still pose a serious threat. One approach to prevent infection is to improve the antimicrobial ability of the coating material. Silver-doped hydroxyapatite (Ag/HAP) nanoparticles were synthesized by a new modified precipitation method. The synthesized powder was used for the preparation of Ag/HAP coating on titanium by electrophoretic deposition. The coating was characterized in terms of phase composition and structure by attenuated total reflection Fourier transform infrared spectroscopy (ATR–FTIR) and X-ray diffraction (XRD); the surface morphology and chemical composition was assessed using scanning electron microscopy (SEM) and energy dispersive spectroscopy (EDS). The research focused on an evaluation of the corrosion behaviour of Ag/HAP coating in simulated body fluid (SBF) at 37 °C during prolonged immersion time by electrochemical impedance spectroscopy (EIS). The silver-doped HAP coating provided good corrosion protection in SBF solution.

Keywords: electrochemical impedance; hydroxyapatite; silver; electrophoretic deposition; simulated body fluid.

INTRODUCTION

Titanium still holds a pivotal role for most biomedical applications, primarily as orthopaedic and dental implant material, thanks to its excellent biocompatibility and mechanical properties.[1] The key feature that enables such a wide-

* Corresponding author. E-mail: vesna@tmf.bg.ac.rs
# Serbian Chemical Society member.
doi: 10.2298/JSC120712086J

spread implementation is its excellent corrosion stability. A stable oxide layer that forms spontaneously upon exposure to oxygen is believed to be 3–10 nm thick, thus providing low electronic conductivity and high corrosion resistance.[2,3] The same oxide layer provides a good substrate for adhesion of proteins and cells, precursors for osteogenesis in the vicinity of an implant. Nevertheless, the same property is to blame for biofilm formation on the implant/tissue interface, which usually consists of various microorganisms, such as pathogenic bacteria. Bacterial infection of the implantation site inevitably leads to post-op complications, revision surgeries, implant failure and finally complete removal.

Antibacterial coatings on titanium can be divided into several groups based on their most prominent feature: coatings loaded with antibiotics, coatings containing non-antibiotic antimicrobial agents, coatings containing inorganic antimicrobial agents, adhesion resistant coatings, *etc*.[4] Recently, due to their excellent biocompatibility and stability, attention has been drawn to inorganic antimicrobial agents, silver in particular. The advantages of silver and the silver ion as doping agents are that they inhibit initial bacterial attachment onto biomaterials; the effect is long lasting, and they have a broad antibacterial spectrum at low concentrations. Studies have shown that Ag has excellent biocompatibility without genotoxicity or cytotoxicity, although its mechanism of action is still not completely revealed. Due to its stability, it can be introduced by various techniques (physical vapour deposition, magnetron sputtering, electrophoretic deposition, to name a few). Lastly, silver can be used for doping a variety of biomaterials (ceramics, metals, polymers) and especially Ag has generated great interest in the development of silver-doped hydroxyapatite coatings.

Hydroxyapatite (HAP) [$Ca_{10}(PO_4)_6(OH)_2$] represents a crystallo-chemical analogue of the mineral bone component and has been long used as part of the synthetic materials for orthopaedic implants.[5–9] The titanium implant fixation properties are dramatically enhanced when coated with HAP.[7–9] The release of metal ions into the body can be reduced by suitable biocompatible inorganic coatings, such as hydroxyapatite (HAP), and this can lead to a delay in corrosion, and wear, and also minimize the loosening of implants from the bone. HAP is not only bioactive, but also osteoconductive, non-toxic and non-immunogenic. However, the most striking property of inorganic HAP is its ability to form an apatite layer, similar to bone apatite, on the surface of implants. The coating surface that aids the process of HAP precipitation by firmly anchoring hydroxyapatite on the surface, thus accelerating and securing a direct bond of the implant with bone is known as bioactive.

Among different methods of ceramic coating deposition on a metal surface, such as plasma spraying, sputtering, pulsed laser-deposition, sol–gel, electrophoresis and electrodeposition, electrophoretic deposition (EPD) has emerged as the most suitable one.[10] EPD provides for uniform coatings, even on substrates

of complex shape. Other advantages are that this is an inexpensive electrochemical technique that can be performed at room temperature with a relatively simple set-up. Coating thickness and morphology are well controlled by adjusting the deposition parameters.[11,12]

This paper reports on an investigation of the *in vitro* biological compatibility and corrosion stability of a non-sintered Ag/HAP coating on titanium obtained by electrophoretic deposition, after immersion in SBF solution at 37 °C, with the aim of mimicking human body conditions.

EXPERIMENTAL

Synthesis of hydroxyapatite powder doped with silver

A modified chemical precipitation method was employed for the preparation of a silver/hydroxyapatite powder. Calcium oxide, obtained by aerobic calcination of $CaCO_3$ for 5 h at 1000 °C, was subsequently placed in a reaction vessel with silver nitrate and phosphoric acid. The reaction was conducted in a stepwise manner. The stoichiometric amount of the resulting calcium oxide was mixed and stirred in distilled water for 10 min. In the second step $AgNO_3$ solution, up to 0.4±0.1 wt. % final concentration, was added to the suspension. Lastly, phosphoric acid was added drop-wise to the suspension in order to obtain silver-doped hydroxyapatite, $Ca_{9.95}Ag_{0.05}(PO_4)_6(OH)_2$. Upon addition of the total stoichiometric volume of phosphoric acid, the pH reached a value of 7.4–7.6. The final suspension was heated for 30 min at 94±1 °C and stirred for another 30 min. After sedimentation, the upper clear solution layer was separated from the precipitate by decanting. In the final step, the suspension was spray-dried at 120±5 °C into a granulated powder.

Surface preparation of titanium

Two different dimensions of titanium plates were used, (25 mm×10 mm×0.89 mm) for surface analysis and (40 mm×20 mm×0.25 mm) for impedance measurements, both from Aldrich (purity 99.7 %). The pure Ti foils represented substrates for the cathodic deposition of the Ag/HAP coatings. Before deposition, standard mechanical pre-treatment of metal plates was employed. Grit emery paper was used to polish the Ti plates, followed by wet polishing with 0.3 μm alumina. After polishing, the plates were degreased, first in acetone and then in ethanol for 15 min, both in an ultrasonic bath.

Electrophoretic deposition of Ag/HAP coating

Electrophoretic deposition was performed from 100 ml of absolute ethanol suspension containing 1.0034 g of nano-sized Ag/HAP powder. Homogeneous and stable suspension was obtained by ultrasonic pre-treatment for 15 min. To increase the suspension stability, hydrochloric acid (HCl) was added dropwise until a pH value of 2.00 was attained. Low pH values of the suspension are necessary to keep the colloidal particles positively charged.[13] The effective pH value of 2 was chosen based on optimization of the experimental conditions to obtain the most stable suspension. Prior to electrodeposition, the ethanol Ag/HAP suspension was ultrasonicated for 30 min to obtain a homogeneous suspension.

A three-electrode cell arrangement was used for the cathodic electrodeposition. The working electrode (pre-treated titanium plate) was used as a substrate for the deposition of an Ag/HAP coating. The counter electrodes were two pure platinum panels, placed parallel to the Ti plate at a distance of 1.5 cm.

The coatings were acquired on the titanium from ethanolic Ag/HAP suspension, using the constant voltage method. The experiments were performed at a constant voltage of 60 V for a deposition time of 45 s, at room temperature. Electrodeposited Ag/HAP coatings were air dried for 24 h at room temperature.

Methods for structural and electrochemical analysis

X-Ray diffraction. A Philips PW 1051 powder diffractometer with Ni-filtered Cu K_α radiation (λ = 1.5418 Å) was employed for X-ray diffraction (XRD) assessment of the phase composition of the electrodeposited coatings. The diffraction intensity was measured using the scan-step technique in the 2θ range of 8–80° with a scanning step width of 0.05° and exposition time of 50 s per step. The phase analysis was realised using the PDF-2 database with a commercially available computer program, EVA V.9.0.

Scanning electron microscopy with energy dispersive spectroscopy. A JEOL JSM-5800 scanning electron microscope (SEM), operated at 20 keV, equipped for energy dispersive spectroscopy (EDS) measurements, was used to analyze the morphology of the electrodeposited coatings.

Attenuated total reflection Fourier transform infrared spectroscopy. A Spectrum^{TM} 400 Perkin Elmer infrared spectrometer (USA) instrument was used to perform the attenuated total reflection Fourier transforms infrared spectroscopy (ATR–FTIR) measurements. Scanning was performed in the 600–4000 cm^{-1} wavelength range in order to investigate the functional groups present in the electrodeposited coatings.

Thermogravimetric analysis. The thermal behaviour of the electrodeposited coatings, dried at room temperature and then scraped from the titanium substrate, was examined by the thermogravimetric analysis (TGA) on a Mettler Toledo instrument (TGA/SDTA851e). Scans were recorded in the dynamic mode from 25 to 1000 °C at a heating rate of 20 °C min^{-1}, under a nitrogen atmosphere (flow rate 50 ml min^{-1}). For each experiment, about 5 mg of oven-dried sample were used.

Electrochemical impedance spectroscopy. For the electrochemical impedance spectroscopy (EIS) measurements, an electrodeposited Ag/HAP coating and bare titanium, as a control, were exposed to SBF solution at 37 °C for 72 h. A standard three-electrode cell arrangement was used in the experiments. The SBF solution (Table I) was prepared by dissolving reagent-grade salts in deionised water followed by buffering with tris-hydroxymethyl aminomethane. The final pH value was adjusted to 7.40 (at 37 °C) using 1 M hydrochloric acid. The working electrode was coated titanium or thermally untreated bare titanium (tested surface area of 1 cm^2). The counter electrode was a platinum mesh and the reference electrode was a saturated calomel electrode (SCE). The impedance data were obtained at the open-circuit po-

TABLE I. Composition of the SBF solution similar to human blood plasma

Reagent	c / g dm^{-3}
NaCl	7.996
$NaHCO_3$	0.350
KCl	0.224
$K_2HPO_4 \cdot 3H_2O$	0.228
$MgCl_2 \cdot 2H_2O$	0.305
$CaCl_2$	0.278
Na_2SO_4	0.071
$(CH_2OH)_3CNH_2$	6.057
1 M HCl	40 ml

tential using a Reference 600^{TM} potentiostat/galvanostat/ZRA (Gamry Instruments, Inc., Warminister, PA, USA), over a frequency range of 300 kHz to 10 mHz using 5 mV amplitude of the sinusoidal voltage. The impedance spectra were analyzed using Gamry Instruments Echem Analyst fitting program, version 5.50.

RESULTS AND DISCUSSION

XRD Analysis

XRD analysis of electrodeposited Ag/HAP coating on titanium was performed in order to determine the phase composition and structural changes of silver/hydroxyapatite. HAP high intensity peaks are dominant in the spectrum (Fig. 1) and perfectly match the hydroxyapatite pattern (JCPDS 86–1199). The incorporation of silver ions in the hydroxyapatite crystal lattice caused a shift of specific HAP peaks to the left (towards smaller angles), confirming it substitutes calcium. The HAP peaks on the XRD pattern were broad, indicating the smaller particle size of the Ag/HAP powder compared to pure HAP powder.

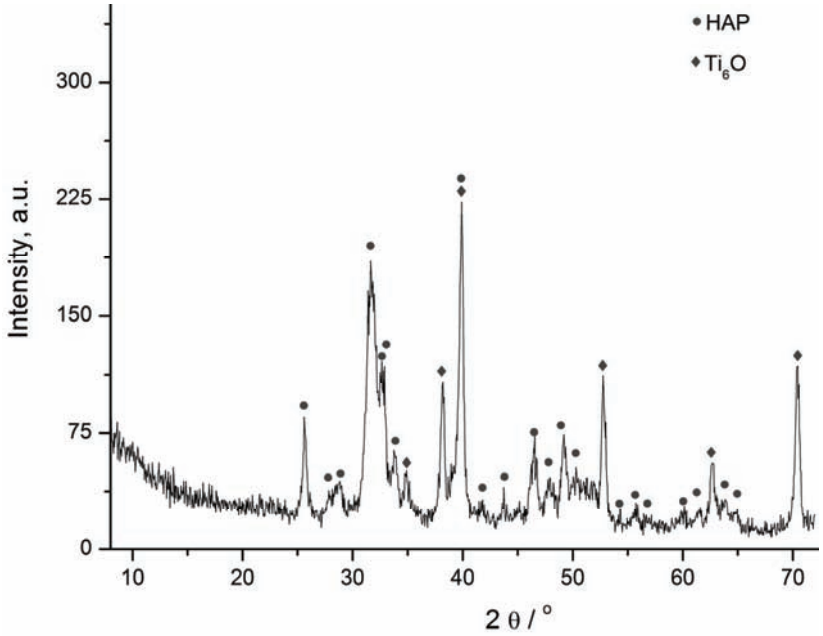

Fig. 1. XRD Pattern of an Ag/HAP coating electrodeposited on titanium.

Other specific peaks, matching titanium suboxide (JCPDS 72-1807), dominated the XRD spectrum instead of Ti peaks. This indicates that Ti was mainly present as Ti_6O on the coating surface. According to Chavan *et al.*,[14] the complex valence status of Ti is the result of oxygen diffusion from the exterior surface to the inside during air drying. Ti suboxides on the Ag/HAP surface are believed to be more active than TiO_2 in a physiological environment and can acti-

vate chemical bonding between the implant surface and adjacent biomolecules.[14] Therefore, the bioactivity of the material is more pronounced within the outermost surface, which not only has reactive functional groups of Ag/HAP, consisting of Ca^{+}, PO_4^{3-} and OH^{-}, but also of Ti suboxide to induce apatite nucleation in SBF.

SEM and EDS analysis

The surface morphology of the electrodeposited Ag/HAP coating on titanium and its EDS analysis are shown in Figs. 2a and 2b, respectively. The SEM microphotograph of the coating revealed the appearance of micro-cracks on the surface and also many agglomerates. The fractured surfaces were most probably formed due to shrinkage during the air drying. Although a cracked Ag/HAP layer would not protect the surface of an implant and thus allowing the possible release of titanium ions from the implant inside the body, the high magnification SEM micrograph (Fig. 2a) revealed that the width and depth of the cracks were in the nano range. Therefore, it is safe to assume that an Ag/HAP coating thus prepared would provide sufficient corrosion protection. On the other hand, the agglomerates on the coating surface would benefit the overall porosity.

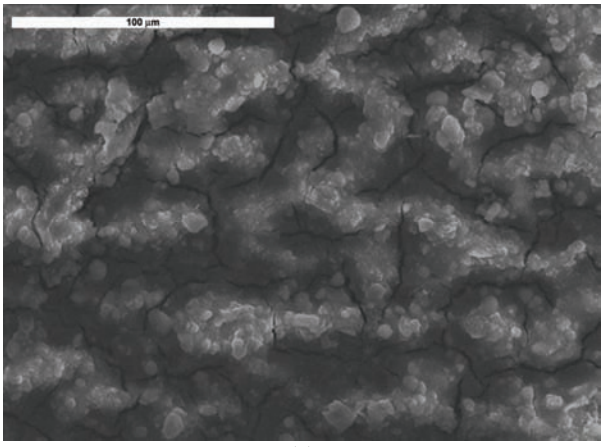

(a)

(b)

Fig. 2. a) SEM Microphotograph and b) EDS profile of the surface of an Ag/HAP coating electrodeposited on titanium.

Chavan *et al.*[14] reported that porous apatite layers could enhance the osteointegration and osteoconduction properties. In addition, it was reported that an open interconnected porous structure is advantageous as it enables penetration of the surrounding bone tissue and hence leads to better biointegration and mechanical stability at the interface of the surrounding bone and coated implants.[15]

The EDS spectra (Fig. 2b) showed two distinct peaks of Ca and P, also the presence of O peak and small peaks of Ti and Ag. The atomic ratio of Ca and P, obtained from the EDS profiling given in Table II was calculated to be 1.64, which is similar to the Ca/P ratio in human bone, known to be 1.67.[16]

TABLE II. The EDS composition of the Ag/HAP coating electrodeposited on titanium

Element	Intensity	Content, at. %
O K	0.662	69.35
P K	1.405	11.53
Ca K	1.024	18.92
Ti K	0.803	0.11
Ag L	0.766	0.08
Ca/P	–	1.64

ATR–FTIR Spectroscopy

The FTIR spectrum of the electrodeposited Ag/HAP coating on titanium and the assigned functional groups are illustrated in Fig. 3. As presented, all characteristic bands correspond to bands typical for hydroxyapatite.

The broad absorption bands at 3000–3500 cm^{-1} and the bending mode at 1613 cm^{-1} were assigned to O–H stretching and bending of H_2O in the spectrum of the Ag/HAP coating.[17] The OH^- stretching vibration was observed at 3572 cm^{-1}.[11] The most intensive band in the region from 1216–920 cm^{-1} was assigned to the P–O asymmetric stretching mode (ν_3) vibration of the PO_4^{3-} group[17–19] Other strong peaks observed as a doublet in the FTIR spectrum, located in 635––500 cm^{-1}, was derived from the triple (ν_4) degenerated bending modes of phosphate O–P–O bonds,[20] except for one of the weak characteristic band at 636 cm^{-1}, which corresponds to the vibration of the structural OH^- groups in the hydroxyapatite.[17]

A small sharp peak at 876 cm^{-1} was attributed to the presence of the HPO_4^{2-} group in the crystal lattice.[18,21] According to the literature, an improvement of the hydroxyapatite crystallinity could be observed by the transformation of the single band in the υ_4 region of the PO_4^{3-} group into a doublet band.[20]

It was reported that nano-sized hydroxyapatite particles, due to their size, have a very large surface area, enabling homogenous resorption by osteoclasts.[17] Therefore these coatings, due to the nano-sized Ag/HAP particles with improved crystallinity[22], as confirmed by the FTIR and XRD results, can present a suitable surface for the proliferation of bone cells.

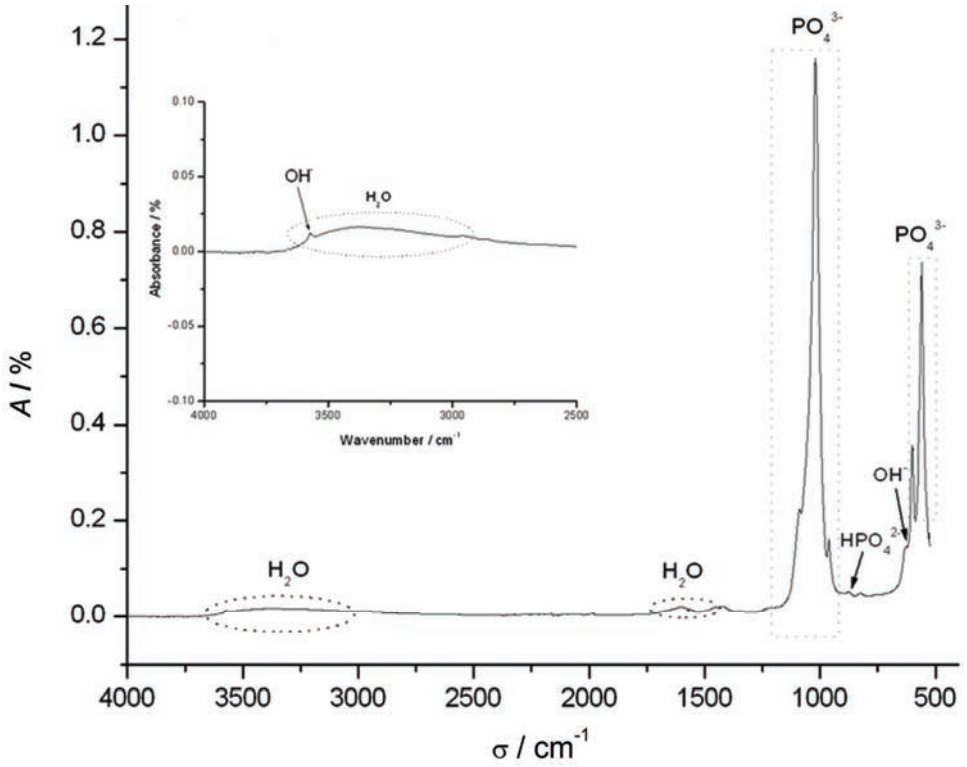

Fig. 3. ATR–FT-IR Spectrum of an Ag/HAP coating electrodeposited on titanium, in the wavenumber range 500–4000 cm^{-1} (inset: in the wavenumber range 2500–4000 cm^{-1}).

Thermogravimetric analysis

Depending on clinical need, nanosized crystalline hydroxyapatite can be used in various forms, including powders or particulate matter for drug delivery, filling bone voids, coatings for metallic prostheses, as scaffolds for bone grafts, drug delivery devices or in the development of composite biomaterials.[23] One of the important factors is the thermal stability of HAP in the temperature range of 400–1200 °C.[23] Therefore, it was necessary to study the thermal behaviour of the electrodeposited Ag/HAP coating scratched from Ti plates. The thermogravimetric (TG) and differential TG (DTG) curve (Fig. 4) revealed the weight loss of Ag/HAP with increasing temperature.

According to the TG and DTG curves, Figs. 4a and 4b, respectively, there are three distinct stages of weight loss. The first stage could be observed from 25 to 150 °C on the TG cure with a sharp peak on the DTG curve at 55 °C. This stage corresponds to desorption of adsorbed water from the surface of the Ag/ /HAP coating.[24]

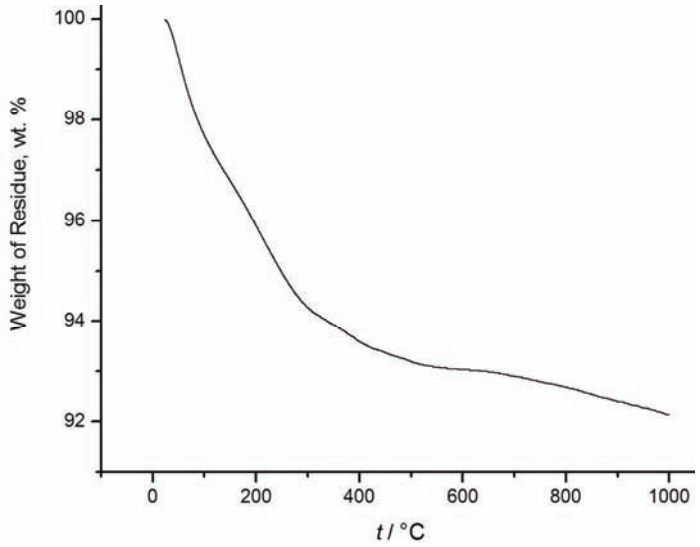

(a)

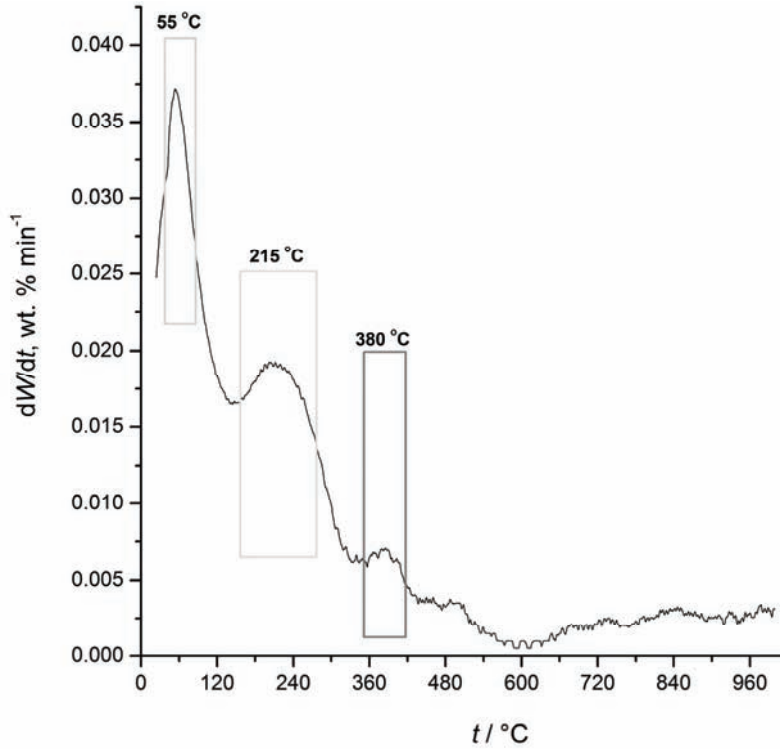

(b)

Fig. 4. a) TG and b) differential TG (DTG) curves of an Ag/HAP coating electrodeposited on titanium.

The second stage of weight loss on the TG curve was observed between 150 and 600 °C (Fig. 4a), with sharp peaks on the DTG curve at 215 and 380 °C (Fig. 4b), which can be attributed to the dehydroxylation of Ag/HAP.[25] As reported by Kalita and Verma,[23] all the endothermic peaks associated with this mass loss below 600 °C can be contributed to desorption of adsorbed water and possible elimination of crystal lattice water.

The third stage of the weight loss was observed between 600 and 1000 °C on the TG curve (Fig. 4a) but without distinguished peaks on the DTG plot. This phase could still be attributed to dehydroxylation or to the early slow decomposition of hydroxyapatite lattice.[26] The total weight loss for the Ag/HAP coating in the temperature range of 25–1000 °C was 7.9 wt. %.

EIS Studies of the corrosion behaviour in SBF solution

EIS measurements were used in order to study the corrosion behaviour of electrodeposited Ag/HAP coating on titanium in a physiological environment (SBF solution). The Nyquist plots of bare titanium and the electrodeposited Ag/HAP coating on titanium after 1 day and 3 days (Fig 5b). Compared to the Nyquist plot for the bare titanium after 1 day of immersion, on the Nyquist plot corresponding to the Ag/HAP coating on titanium after the same time of exposure (Fig. 5a), the semi-circle at the high frequency range (100 kHz–1 Hz) could be attributed to the Ag/HAP layer on the top, while the impedance response at the low frequencies range (1 Hz–10 mHz) showed the characteristics of a passive titanium oxide film beneath the Ag/HAP top layer.

The fitting of the experimental impedance data obtained from the Nyquist plots was accomplished using the equivalent electrical circuits shown in Figs. 6a and 6b and the Gamry Instruments Echem Analyst fitting program. The equivalent circuit in Fig. 6a was used for the fitting of impedance data obtained for the Ag/HAP coating (Fig. 5a). The assumed electrical equivalent circuit (Fig. 6a) consists of the electrolyte resistance, R_s, the coating pore resistance, *i.e.*, the resistance of the electrolyte inside the pores of Ag/HAP coating, R_p, the constant phase elements CPE_c and CPE_{pf}, which include all the frequency dependent electrochemical phenomena: the Ag/HAP coating capacitance, C_c, and the passive titanium oxide film capacitance, C_{pf}, respectively, and diffusion processes. The CPEs are used in this model to compensate non-homogeneity in the system and are defined by two parameters, Y_0 and n. The impedance of a CPE is represented by the following equation:[27–29]

$$Z_{CPE} = Y_0^{-1}(j\omega)^{-n} \quad (1)$$

where $j = (-1)^{1/2}$, $\omega = 2\pi f$ is the frequency in rad s^{-1} and f is the frequency in Hz. If the n value ranges from 0.8–1.0, the impedance of a CPE can be considered to be that of a pure capacitor:

$$Z_{\mathrm{CPE}} = (j\omega C)^{-n} \quad (2)$$

In the present case, the Y_0 value gave a pure capacitance (C). For impedance analysis of bare titanium, the equivalent circuit in Fig. 6b was used, where the electrolyte resistance is represented as R_s, the passive oxide film resistance and capacitance are R_{pf} and CPE_{pf}, respectively. All of the fitting results are listed in Table III.

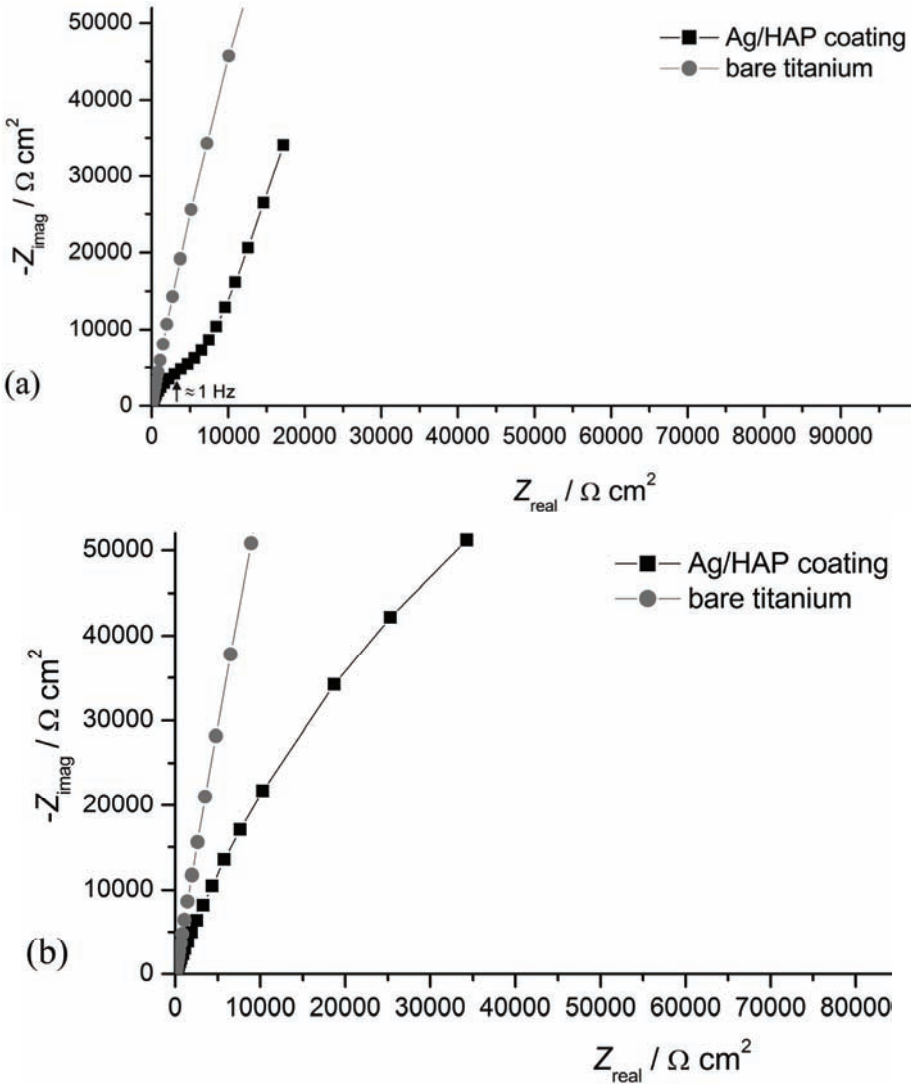

Fig. 5. The Nyquist plots of bare titanium and an Ag/HAP coating electrodeposited on titanium after a) 1 and b) 3 days of exposure to SBF solution at 37 °C.

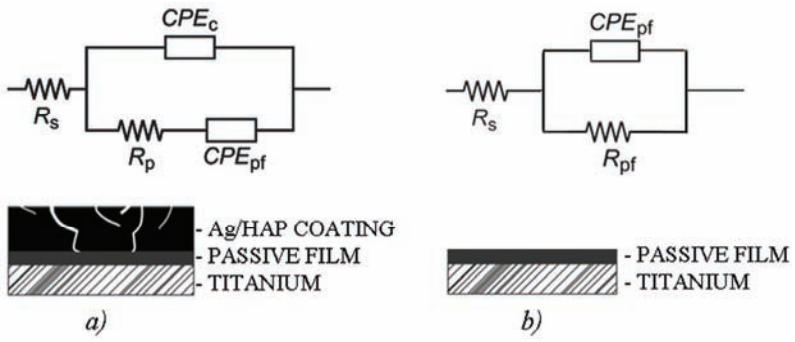

Fig. 6. Equivalent electrical circuits for a) an Ag/HAP coating electrodeposited on titanium and b) bare titanium.

TABLE III. The fitting values of the equivalent electrical circuits parameters

Sample	τ h	R_s Ω cm^2	CPE_{pf} (C_{pf}) μF cm^{-2}	n_{pf}	R_{pf} kΩ cm^2	CPE_C (C_C) μF cm^{-2}	n_C	R_p kΩ cm^2
Ag/HAP	1	31.6	220	0.77	–	89.5	0.83	12.6
	24	31.5	223	0.80	–	88.4	0.83	11.9
	72	51.4	147.2	0.78	240.7	–	–	–
Bare titanium	1	22.6	40.6	0.89	794	–	–	–
	24	22.5	38.8	0.89	1009	–	–	–
	72	67.8	26.6	0.90	3654	–	–	–

From Table III, as the n_c values in the case of Ag/HAP coating are higher than 0.8, CPE_c can be considered as the coating capacitance, C_c. The time dependence of the pore resistance, R_p, and the coating capacitance, C_c, of Ag/HAP coating are presented in Table III. According to the results, R_p and C_c for Ag/HAP coating remained constant during 24 h of exposure to the SBF solution, indicating retention of the good protective properties of the coating. However, after 72 h, the impedance Nyquist plot (Fig. 5b) could not be fitted with equivalent circuit shown in Fig. 6a and instead the equivalent circuit in Fig. 6b was used. The calculated values of R_{pf} (240.7 kΩ cm^2) and C_{pf} (147.2 μF cm^{-2}) after 72 h, given in Table III, could indicate the formation of a new apatite layer on the coating surface in SBF solution.[30] These results suggest that the coating pores filled with the SBF solution were growing into a very resistant passive film and on the other hand, the coating surface represented the site of nucleation and growth of new apatite.

The EIS spectra of the bare titanium exposed to SBF solution (Figs. 5a and 5b) was fitted to the equivalent electrical circuit shown in Fig. 6b. Its impedance plot exhibited behaviour similar to a capacitive response. Furthermore, a slow growth of the titanium oxide film could be traced through a slight decrease in the C_{pf} value and an increase in R_{pf} during 72 h of exposure to the SBF solution (Table III), which is in accordance with previously published data.[31]

In addition, this newly formed apatite that formed during immersion in SBF solution is known to accelerate better bonding between an implant and bone.[32]

CONCLUSIONS

A silver-doped hydroxyapatite Ag/HAP coating was successfully electrophoretically deposited on titanium. The XRD and ATR–FTIR results for the deposited coating showed there was no phase transformation of the hydroxyapatite lattice structure. The Ca/P ratio (from the EDS analysis) was calculated to be 1.64, as in natural bone. The analysis of the thermal behaviour of Ag/HAP coating revealed its stability up to 600 °C. Although SEM micrographs showed microcracks on the coating surface, the Ag/HAP coating provided sufficient corrosion protection during immersion in SBF solution, indicated by increase in pore resistance and decrease in coating capacitance.

Overall, not only did the Ag/HAP coating electrodeposited on titanium retain its protective properties in Kokubo's solution, but also expressed enhanced corrosion resistance due to formation of a bone-like apatite layer.

Acknowledgements. This research was financed by the Ministry of Education, Science and Technological Development of the Republic of Serbia, contract No. III 45019 and by the National Sciences and Engineering Research Council of Canada (NSERC). Dr Ana Jankovic was financed by the FP7 Nanotech FTM Grant Agreement 245916. The authors would like to thank Dr Miodrag Mitrić, Vinča Institute of Nuclear Sciences, University of Belgrade, for his help in the XRD measurements, and also to Mr Yves Bédard, Département des Sciences du bois et de la forêt de l'Université Laval, for technical support and assistance in the laboratory work.

И З В О Д

СПЕКТРОСКОПИЈА ЕЛЕКТРОХЕМИЈСКЕ ИМПЕДАНЦИЈЕ ПРЕВЛАКЕ ХИДРОКСИАПАТИТА ДОПИРАНЕ СРЕБРОМ У СИМУЛИРАНОЈ ТЕЛЕСНОЈ ТЕЧНОСТИ КОРИШЋЕНОЈ КАО КОРОЗИОНИ АГЕНС

АНА ЈАНКОВИЋ[1], САЊА ЕРАКОВИЋ[1], ANTONIJA DINDUNE[2], ЂОРЂЕ ВЕЉОВИЋ[1], ТАТЈАНА СТЕВАНОВИЋ[3], ЂОРЂЕ ЈАНАЋКОВИЋ[1] и ВЕСНА МИШКОВИЋ-СТАНКОВИЋ[1]

[1]Технолошко–металуршки факултет, Универзитет у Београду, Карнегијева 4, Београд, [2]Institute of Inorganic Chemistry, Riga Technical University, 34 Miera Street, Salaspils, LV-2169, Latvia и [3]Département des sciences du bois et de la forêt, Université Laval, 2425 rue de la Terrasse, Québec, Canada

Титан представља кључни биомедицински материјал захваљујући својој доброј биокомпатибилности, механичким својствима и корозионој стабилности, али инфекције на месту имплантирања и даље представљају озбиљан проблем. Један начин да се предупреди инфекција је да се побољша антимикробна активност материјала. Сребром допиране наночестице хидроксиапатита синтетисане су новом модификованом преципитационом методом. Овако синтетисани прах је коришћен за наношење превлаке сребро/хидроксиапатит на титан електофоретским таложењем. Фазни састав и структура превлаке су карактерисани спектроскопијом инфрацрвене светлости са Фуријеовом трансформацијом у моду тоталне рефлексије и дифракцијом X-зрака. Морфологија површине и хемијски састав испитивани су коришћењем скенирајуће електронске микро-

скопије и енергетске дисперзионе спектроскопије. Циљ истраживања је испитивање корозионе стабилности превлаке сребро/хидроксиапатит у симулираној телесној течности користећи спектроскопију електрохемијске импеданције. Превлака сребро/хидроксиапатит обезбеђује добру заштиту од корозије у симулираној телесној течности.

(Примљено 12. јула, ревидирано 27. августа 2012)

REFERENCES

1. C. Moseke, U. Gbureck, P. Elter, P. Drechsler, A. Zoll, R. Thull, A. Ewald, *J. Mater. Sci. - Mater. Med.* **22** (2011) 2711
2. Y.-T. Sul, C. B. Johansson, S. Petronis, A. Krozer, Y. Jeong, A. Wennerberg, T. Albrektsson, *Biomaterials* **23** (2002) 491
3. K. G. Neoh, X. Hu, D. Zheng, E. T. Kang, *Biomaterials* **33** (2012) 2813
4. L. Zhao, P. K. Chu, Y. Zhang, Z. Wu, *J. Biomed. Mater. Res., B* **91** (2009) 470
5. C. Garcia, S. Cere, A. Duran, *J. Non-Cryst. Solids* **352** (2006) 3488
6. K.-C. Kung, T.-M. Lee, T.-S. Lui, *J. Alloys Compd.* **508** (2010) 384
7. P. C. Rath, L. Besra, B. P. Singh, S. Bhattacharjee, *Ceram. Int.* **38** (2012) 3209
8. M. Geetha, A. K. Singh, R. Asokamani, A. K. Gogi, *Prog. Mater. Sci.* **54** (2009) 397
9. M. Swetha, K. Sahithi, A. Moorthi, N. Srinivasan, K. Ramasamy, N. Selvamurugan, *Int. J. Biol. Macromol.* **47** (2010) 1
10. M. S. Djosić, V. B. Mišković-Stanković, V. V. Srdić, *J. Serb. Chem. Soc.* **72** (2007) 275
11. M. S. Lazić, K. Simović, V. B. Mišković-Stanković, P. Jovanić, D. Kićević, *J. Serb. Chem. Soc.* **69** (2004) 239
12. V. B. Mišković-Stanković, *J. Serb. Chem. Soc.* **67** (2002) 305
13. A. A. Abdeltawab, M. A. Shoeib, S. G. Mohamed, *Surf. Coat. Tech.* **206** (2011) 43
14. P. N. Chavan, M. M. Bahir, R. U. Mene, M. P. Mahabole, R. S. Khairnar, *Mater. Sci. Eng., B* **168** (2010) 224
15. M. Javidi, S. Javadpour, M. E. Bahrololoom, J. Ma, *Mater. Sci. Eng., C* **28** (2008) 1509
16. B. Cengiz, Y. Gokce, N. Yildiz, Z. Aktas, A. Calimli, *Colloid. Surf., A* **322** (2008) 29
17. K. P. Sanosh , M.-C. Chu , A. Balakrishnan , Y.-J. Lee, T. N. Kim , S.-J. Cho, *Curr. Appl. Phys.* **9** (2009) 1459
18. L.-N. Wang, J.-L. Luo, *Mater. Sci. Eng., C* **31** (2011) 748
19. D. K. Pattanayak, R. Dash, R. C. Prasad, B. T. Rao, T. R. Rama Mohan, *Mater. Sci. Eng., C* **27** (2007) 684
20. H. Ye, X. Y. Liu, H. Hong, *Mater. Sci. Eng.,C* **29** (2009) 2036
21. E. V. Pecheva, L. D. Pramatarova, M. F. Maitz, M. T. Pham, A. V. Kondyuirin, *Appl. Surf. Sci.* **235** (2004) 176
22. S. Eraković, Đ. Veljović, P. N. Diouf, T. Stevanović, M. Mitrić, S. Milonjić, V. Mišković-Stanković, *Int. J. Chem. React. Eng.* **7** (2009) *Article* A62
23. S. J. Kalita, S. Verma, *Mater. Sci. Eng., C* **30** (2010) 295
24. T. Wang, A. Dorner-Reisel, E. Muller, *J. Eur. Ceram. Soc.* **24** (2004) 693
25. X. Zhang, Y. Li, G. Lv, Y. Zuo, Y. Mu, *Polym. Degrad. Stabil.* **91** (2006) 1202
26. S. Eraković, Dj. Veljović, P. N Diouf, T. Stevanović, M. Mitrić, Dj. Janaćković, I. Z. Matić, Z. D Juranić, V. B. Mišković-Stanković, *Prog. Org. Coat.* **75** (2012) 275
27. M. M. Popović, B. N. Grgur, V. B. Mišković-Stanković, *Prog. Org. Coat.* **52** (2005) 359
28. M. Sluyters-Rehbach, *Pure Appl. Chem.* **66** (1994) 1831
29. V. D. Jović, B. M. Jović, *J. Electroanal. Chem.* **541** (2003) 1

30. S. Eraković, A. Janković, Dj. Veljović, E. Palcevskis, M. Mitrić, T. Stevanović, Dj. Janaćković, V. Mišković-Stanković, *J. Phys. Chem. B*, http://pubs.acs.org/doi/abs/ /10.1021/jp305252a.
31. L. Jonasova, F. A. Muller, A. Helebrant, J. Strnad, P. Greil, *Biomaterials* **25** (2004) 1187
32. G. Manivasagam, D. Dhinasekaran, A. Rajamanickam, *Recent Pat. Corr. Sci.* **2** (2010) 40.

Journal of the Serbian Chemical Society
JSCS-info@shd.org.rs • www.shd.org.rs/JSCS
J. Serb. Chem. Soc. 77 (11) 1625–1640 (2012) UDC 577.164.3+543.426.1:611.018.5+615
JSCS–4376 *Original scientific paper*

Development and validation of a fluorometric method for the determination of hesperidin in human plasma and pharmaceutical forms

LEPOSAVA A. PAVUN[1]*, JASMINA M. DIMITRIĆ MARKOVIĆ[2], PREDRAG T. ĐURĐEVIĆ[3], MILENA D. JELIKIĆ-STANKOV[4], DANIELA B. ĐIKANOVIĆ[5], ANDRIJA R. ĆIRIĆ[3] and DUŠAN L. MALEŠEV[1]

[1]Department of Physical Chemistry, Faculty of Pharmacy, University of Belgrade, Vojvode Stepe 450, 11000 Belgrade, Serbia, [2]Faculty of Physical Chemistry, University of Belgrade, Studentski trg 12, 11000 Belgrade, Serbia, [3]Department of Chemistry, Faculty of Science, University of Kragujevac, Radoja Domanovića 12, 34000 Kragujevac, Serbia, [4]Department of Analytical Chemistry, Faculty of Pharmacy, University of Belgrade, Vojvode Stepe 450, 11000 Belgrade, Serbia and [5]Institute for Multidisciplinary Researches, University of Belgrade, Despota Stefana 142, 11000 Beograd, Serbia

(Received 5 October 2011, revised 17 April 2012)

Abstract: A fluorometric method, based on the fluorescence properties of the aluminium(III)–hesperidin complex, for the determination of hesperidin in human plasma and pharmaceutical forms has been developed and validated. The complex shows a strong emission in the presence of the surfactant betain sulphonate SB 12 at 476 nm with excitation at 390 nm. The linearity range for pharmaceutical forms of hesperidin was 0.06–24.4 μg mL^{-1} with a limit of detection, *LOD*, of 0.016 μg mL^{-1} and a limit of quantification, *LOQ*, of 0.049 μg mL^{-1}. Recovery values in the range 99.3–99.7 % indicate good accuracy of the method. A linear dependence of the intensity of fluorescence of the complex on the concentration of hesperidin in plasma was obtained in concentration range from 0.1–12.2 μg mL^{-1}. The *LOD* was 0.032 μg mL^{-1} while *LOQ* was 0.096 μg mL^{-1}. Recovery values were in the range 98.4–99.8 %. The reliability of the method was checked by an LC–MS/MS method for plasma samples and an HPLC/UV method for tablets with direct determination of hesperidin after separation. Linearity range in determination of hesperidin in pharmaceutical forms was obtained in the range from 0.05 to 10.00 μg mL^{-1}. The *LOD* was 0.01 μg mL^{-1} and the *LOQ* was 0.03 μg mL^{-1}. The linearity range for the determination of hesperidin in plasma was 0.02–10.00 μg mL^{-1} with an *LOD* 0.005 μg mL^{-1} and an *LOQ* of 0.015 μg mL^{-1}. The good agreement between the two methods indicates the usability of the proposed fluorometric method for the simple, precise and accurate determination of hesperidin in clinical and quality control laboratories.

* Corresponding author. E-mail: leposava.pavun@pharmacy.bg.ac.rs
doi: 10.2298/JSC111005060P

Keywords: hesperidin; human plasma; tablets; fluorometry; LC–MS/MS.

INTRODUCTION

Flavonoids constitute a large group of naturally occurring phenolic compounds distributed in the plant kingdom. They are regularly consumed as food (*e.g.*, vegetables and fruits) and beverages such as tea and red wine. According to their chemical structure, they are usually subdivided into flavanols, anthocyanidins, flavones, flavanones and chalcones. These different flavonoids are reported to possess a wide range of biological activities, including anti-inflammatory, anti-oxidant, anti-allergic, hepatoprotective, anti-thrombotic, anti-viral, cardiovascular and anti-carcinogenic effects.[1]

Flavonoids are also effective metal ion chelators and form stable products that in several cases are highly fluorescent, a property which has been used in analytical methods for metal and ligand identification.[2,3] It is well known that they can chelate metallic ions such as beryllium (II),[4] aluminium(III),[5] iron(III),[6] and zinc(II) ion.[7] These complexes shown intense fluorescence signal which increases with metal concentration.

Hesperidin:

(2*S*)-5-hydroxy-2-(3-hydroxy-4-methoxyphenyl)-7-[(2*S*,3*R*,4*S*,5*S*,6*R*)-3,4,5--trihydroxy-6-[[(2*R*,3*R*,4*R*,5*R*,6*S*)-3,4,5-trihydroxy-6-methyloxan-2-yl]oxymethyl]oxan-2-yl]oxy-2,3-dihydrochromen-4-one (Scheme 1),

is a flavanone-type flavonoid that is abundant in citrus fruit[8] and has been reported to exert a wide range of pharmacological effects.[9]

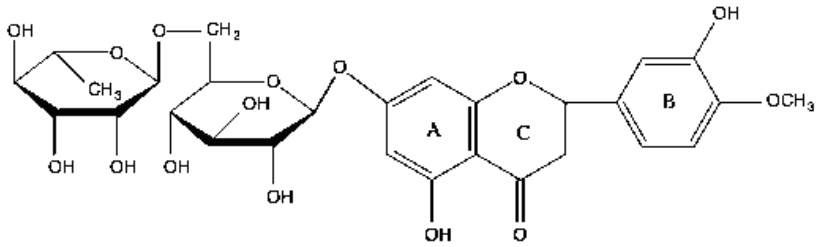

Scheme 1. The molecular structure of hesperidin.

Hesperidin has also been reported to possess anti-inflammatory, anti-allergenic, antihypertensive, antimicrobial, and vasodilatory properties and to decrease bone density loss.[10–12] Taking into account the biological effects of hesperidin, it is of interest to develop simple, accurate and precise methods for its determination in human plasma and pharmaceutical forms.

Various methods have been developed for the determination of hesperidin, such as high-performance liquid chromatography with UV/Vis and electrochemical detection modes,[13,14] liquid chromatography/mass spectrometry (LC–MS),[15] radio-immunoassey,[16] adsorptive-stripping voltammetry,[17] cathodic-stripping vol-

tammetry,[18] spectrophotometry,[19,20] spectrofluorometry with manual and flow injection methods[21] and pulse perturbation of an oscillatory reaction system.[22]

Perez-Ruiz *et al*.[21] developed and validated a spectrofluorimetrc method for the determination of hesperidin in orange peel and orange juice based on complexation between hesperidin and the aluminium(III)-ion in a micellar (sodium dodecylsulphate) medium. Manual and flow injection procedures were used for samples introduction using an excitation wavelength of 391 nm and an emission wavelength of 496 nm. The linear concentration range for hesperidin was between 5×10^{-7} to 2×10^{-5} mol L^{-1}, with a detection limit of 79 μg L^{-1}.

In this work, the same basic chemistry of the fluorescence reaction between aluminium (III)-ion and hesperidin for the determination of hesperidin in human plasma and pharmaceutical forms was employed. The zwiterionic surfactant sulphobetaine SB 12 (3-(*N*-hexadecyl-*N*,*N*-dimethylammonio)propane sulphonate) was used for fluorescence enhancement with an excitation wavelength of 390 nm and an emission wavelength at 476 nm. As comparative methods, an LC-MS/MS determination of hesperidin in human plasma and an HPLC/UV method for its determination in some pharmaceutical formulations were used.

EXPERIMENTAL

Materials and solutions

Aluminium nitrate, hesperidin ($C_{28}H_{34}O_{15}$; M_r = 610.56 g mol^{-1}; CAS number 520-26-3) (Fluka AG), methanol, NaOH, CH_3COOH (Merck), all *p.a*. grade, were used. SB 12 or (*n*-dodecyl sulphobetaine) (Serva, Germany) and sodium dodecylsuphate (SDS, Sigma Aldrich) were used. All reagents were employed without further purification. A stock solution of aluminium nitrate was prepared by dissolving $Al(NO_3)_3$ in doubly distilled water with the addition of an appropriate amount of nitric acid to prevent the initial hydrolysis of the aluminium(III) ion. The content of Al(III) ions was determined gravimetrically by precipitation with ammonia. A solution of hesperidin was prepared by dissolving a precisely measured mass of hesperidin in 70 vol. % methanol. A solution of SB 12 (0.5 mol L^{-1}) was prepared by dissolving a precisely measured mass of SB 12 in deionised water. A solution of SDS (0.5 mol L^{-1}) was prepared by dissolving a precisely measured mass of SDS in deionised water. These solutions were stored in a refrigerator.

Human pool plasma was obtained from the Department of Transfusion of the Clinical Hospital "Dr Dragiša Mišović", Belgrade, Serbia. Helopyrin tablets (nominal composition vitamin C 120 mg, bioflavonoids 20 mg, rutin 15 mg, excipients: microcrystalline cellulose, methylhydroxypropyl cellulose, Mg-stearate, starch hydrolysate) were from Rosch & Handel, (Vienna, Austria) and Vitamin C 1500 tablets with hesperidin were from American Nutrition Products.

Working solutions were prepared by dilution of stock solution and aluminium nitrate (1.00×10^{-3} mol L^{-1} $Al(NO_3)_3$) and hesperidin (1.00×10^{-4} mol L^{-1}).

Instruments

The fluorescence spectra were collected using a Fluorolog-3 spectrofluorimeter (Jobin Yvon Horiba, Paris, France) equipped with a 450 W xenon lamp and a photomultiplier tube. The samples were placed in a 1 cm optical path length quartz cuvette for spectral recording.

The slits on the excitation and emission beams were both set at 5 nm. The spectra were corrected for the dark counts. In each measurement, three scans with a one-second-integration time were averaged. The emission spectrum of the solvent (70 vol. % methanol) was subtracted. All measurements were performed at 25 °C controlled by a Peltier element. The pH measurements of were realised using a Metler Toledo mp 120 pH-meter (precision: ±0.01 pH unit) equipped with a combined glass electrode. All spectrofluorometric measurements were made in acetate buffers at pH 4.58 (in 70 vol. % methanol) which was prepared according to Perrin.[23]

Chromatographic measurements were carried out using the HPLC system Perkin Elmer PE200 (Norwalk, CT, USA), composed of a binary pump, an autosampler (injection volume 20 µL) and equipped with a Gemini C_{18} column (150×4.6 mm, 3 µm, Phenomenex, CA, USA), a column thermostat and variable UV–Vis detector operating at 280 nm. The experimental conditions were as follows: mobile phase A: 2% acetic acid; mobile phase B: acetonitrile, mixed in a linear gradient, 0–5 min: 85 % A, 15 % B; 25–30 min: 10 % A, 90 % B; 35–40 min: 85 % A, 15 % B; flow rate: 0.7 mL min^{-1}; injection volume: 20 µL.

Mass spectrometric conditions

A 3200 QTRAP MS/MS mass spectrometer (Applied Biosystems/MDS Sciex, Foster City, CA, USA) with ESI ionisation (ESI and turbo-ion spray, TIS) was employed. The data were processed using Analyst TM software (PE Sciex). The negative ionization mode of the LC–MS/MS was used for monitoring selected multiple reaction (SRM) analyses with a dwell time 50 ms. The mass spectrometric parameters were optimized to maximize the SRM sensitivity by injecting a 100 µg mL^{-1} standard solution of hesperidin in methanol using a syringe. The optimized instrument conditions were as follows: interface temperature, 500 °C; ion spray voltage, 4500 V; curtain gas He at 10 psi; nebulizing gas N_2 at 40 psi; TIS gas He at 60 psi; declustering potential (DP), 57 V; entrance potential (EP), –5 V; collision energy (CE) –34 eV and collision cell exit potential (CXP), 9 V. The signal used to detect and quantify hesperidin was SRM transition at *m*/*z* 609 → 325. The mass spectrometer was operated at unit mass resolution for both the Q1 and Q3 quadrupoles.

RESULTS AND DISCUSSION

Complex formation between hesperidin and aluminium(III)-ion

Hesperidin and aluminium(III) ions upon reaction in methanolic solution form a complex in the pH range 3.0–7.0. The stoichiometry of the complex was estimated by the Job method[24] and by the mole ratio method.[25]

The reaction of hesperidin and aluminium(III) ions in methanolic solution in the pH range 3.0–7.0 leads to the formation of a complex, as evidenced by the large increase of fluorescence intensity (order of magnitude 10^5) and bathochromic shift (*ca*. 50 nm) of the emission band of hesperidin in the presence of aluminium(III) ions. The fluorescence spectra were recorded using 70 % v/v methanol as a blank. The excitation spectra were followed at λ_{em} = 490 nm and the excitation wavelength used for recording the emission spectra was λ_{ex} = 390 nm. The excitation (1′) and emission (1) spectra of the aluminium(III)–hesperidin solution and the excitation (2′) and emission (2) spectra of hesperidin are shown in Fig. 1.

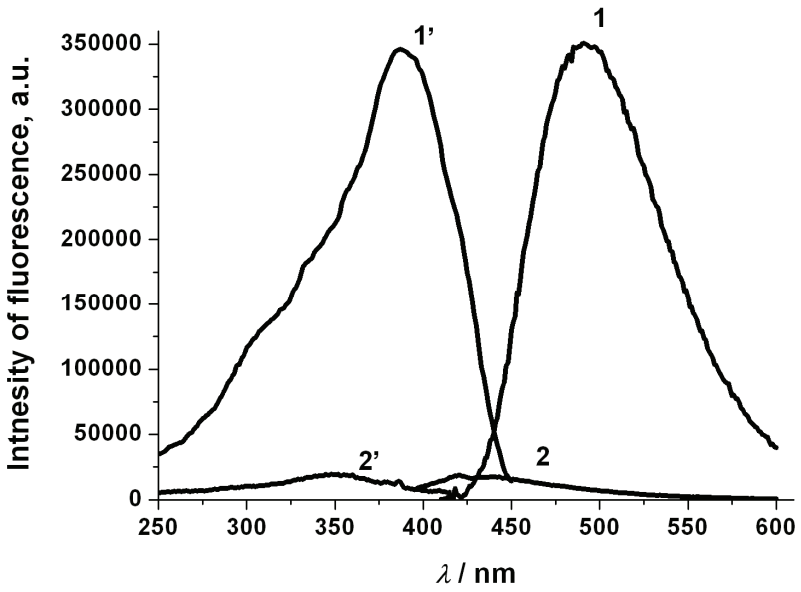

Fig. 1. Exitation (1′) and emission (1) spectra of the aluminium (III)–hesperidin complex and exitation (2′) and emission (2) spectra of hesperidin.

As indicated by the Job[24] method, the most probable stoichiometry of the complex formed at pH 4.58 is aluminium:hesperidin = 1:1. The mole ratio method[25] for the determination of the composition of the aluminium(III)–hesperidin complex formed at pH 4.58 confirmed the 1:1 ratio for the complex (Fig. 2).

Thus, the complexation equilibrium is not stepwise and the complex is formed in a single step.

The stability constant of the complex at pH 4.58 was estimated from the Job plot and the (conditional) stability constant was found to be log K = 8.26±0.02.

The formation of a stable aluminium (III)–hesperidin complex in methanolic solution in presence of SB 12 with enhanced fluorescence could be utilized for the quantitative determination of hesperidin in various matrices in trace amounts. It was decided to develop and validate a method for the determination of hesperidin in human serum and pharmaceutical dosages forms.

Method development

The critical parameters for the development of a fluorometric method involved the composition of the solvent, the concentration of aluminium, the concentration of SB 12, pH and the reaction time between aluminium(III) ion and hesperidin. The optimal values for these parameters were determined in order to attain the maximum fluorescence intensity.

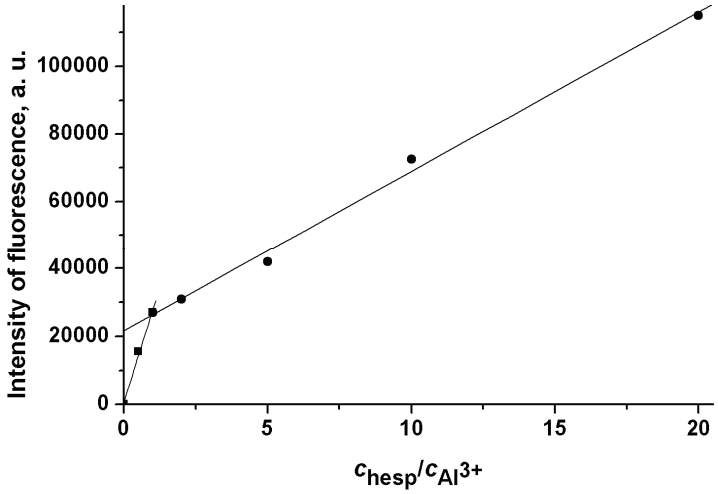

Fig. 2. Method of mole ratios. Dependence of intensity of fluorescence on ratio $c_{hesp}/c_{Al(III)}$.

The composition of the solvent influences the fluorescence intensity and the solubility of the complex. Solvent compositions examined were 30, 50, 70 and 90 vol. % of methanol. The optimal composition of the solvent was methanol:water 70:30 v/v because in this solvent, the maximum intensity of the fluorescence and solubility of the complex was observed.

Concentration of aluminium(III) ions also influences the intensity of fluorescence and for this optimisation, different concentrations of aluminium(III) ions in the range 1×10^{-6}–5×10^{-5} mol L^{-1} (c_{Al}:c_L = 1:1 to 50:1, pH 4.0) were examined. The fluorescence intensity increased with increasing concentration of aluminium(III) ion up to 5×10^{-5} mol L^{-1}.

Influence of pH on the fluorescence intensity of the aluminium(III)–hesperidin complex was examined in the range 3.0–7.0, as shown in Fig. 3. The pH dependence of fluorescence intensity exhibited a complex shape. At low pH values, the intensity decreased because protons tended to displace aluminium(III) ion. At pH values higher than 4.58, the intensity again decreased because more of the aluminium(III) ions were in the form of hydroxide complexes. The optimal pH value was around 4.5, which was used for all further experiments.

According to the work Peres-Ruiz *et al.*,[21] the type of surfactant has a great influence on the fluorescence intensity. They studied the influence of cationic, anionic and non-ionic surfactants on fluorescence intensity, but did not examine the influence of zwiterionic micellar media For this reason, the surfactant SB 12 was used in the present study. The concentration of surfactant was about three times that of the critical micellar concentration and it was shown that this surfactant increase the fluorescence intensity by` about 5 times compared to metha-

nolic solution with no addition of SB 12. With purpose of investigating the influence of surfactants on the fluorescence intensity of the aluminium(III)–hesperidin complex, the emission spectra of aluminium(III)–hesperidin complex without surfactants (Fig. 4, curve 1), and in presence of SDS (Fig. 4, curve 2), and SB 12 (Fig. 4, curve 3) were recorded. Based on the obtained results (Fig. 4), the significant influence of SB 12 on the fluorescence intensity was confirmed.

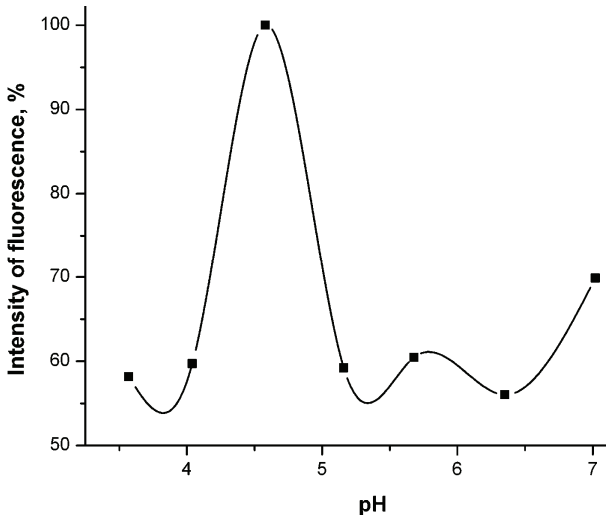

Fig. 3. Effect of pH on the intensity of the fluorescence of the aluminium(III)–hesperidin complex.

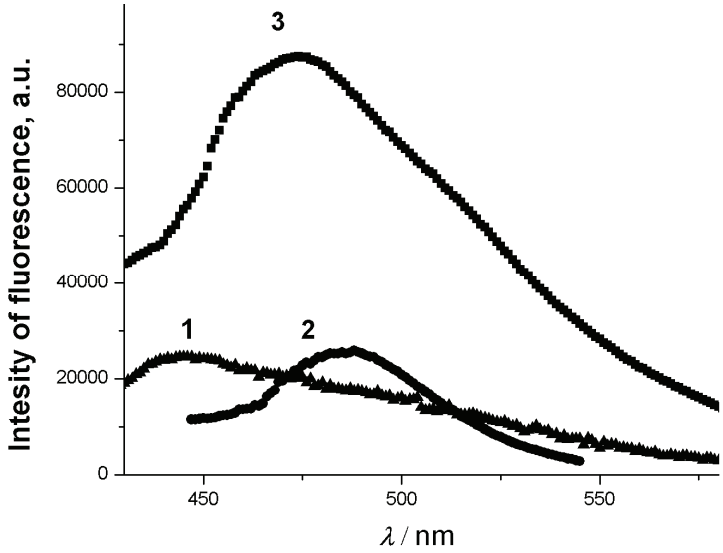

Fig. 4. Influence of surfactants on the intensity of the fluorescence of the aluminium(III)–hesperidin complex: emission spectra of the aluminium(III)–hesperidin complex without surfactants (1), emission spectra of complex in presence of SDS (2) and SB 12 (3).

For the study of the effect of the micelar medium (SB 12) on the excitation and emission spectra of the aluminium(III)–hesperidin complex in 70 % methanol was studied. The zwitterionic surfactant, SB 12 was tested at a concentration of about three times that of the critical micellar concentration. The fluorescence emission spectra shown in Fig. 5 were recorded in 70 vol. % methanol using an excitation wavelength of λ_{ex}= 390 nm. The emission spectra of the aluminium(III)–hesperidin complex (1) and of hesperidin (1′) are illustrated in Fig. 5a, while the corresponding spectra (2 and 2′, respectively) in the presence of SB 12 are presented.

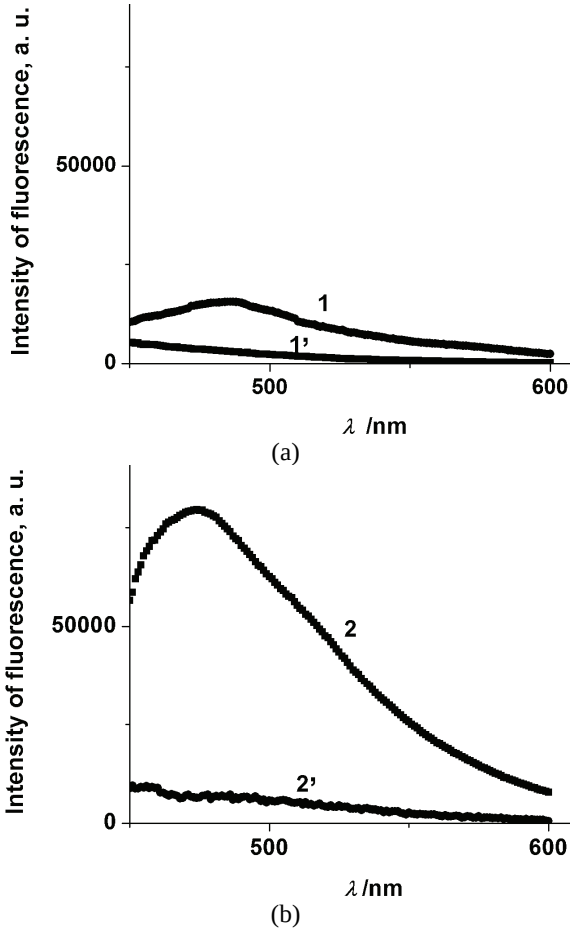

Fig. 5. a) Emission spectra of the aluminium(III)–hesperidin complex (1) and hesperidin(1′); b) emission spectra of the aluminium(III)–hesperidin complex (2) and hesperidin (2′), both in the presence of SB 12.

From Fig. 5, it could be seen that the wavelength of the emission maxima were hypsochromically shifted to λ_{em}= 476 nm and the intensity of the complex fluorescence increased by about four times in presence of SB 12. Due to this, all measurements were performed in the presence of SB 12 at this concentration.

Fluoromeric analysis of hesperidin in pharmaceutical preparations

The calibration curve method was used, requiring solutions containing constant concentrations of SB 12 and $Al(NO_3)_3$ and different concentrations of hesperidin in acetate buffer (using 70 vol. % methanol as the solvent) at pH 4.58. The blank was acetate buffer of pH 4.58.

The regression equation:

$$I_F = (4.06 \pm 0.01)c + (1.27 \pm 0.02) \quad (1)$$

(N = 9) was calculated with the aid of Origin, version 7, software, where I_F is fluorescence intensity in % (λ_{em} = 476 nm) and c is concentration of hesperidin in μg mL^{-1}. The good linearity of the calibration curve and the negligible scatter of experimental points are confirmed by the high correlation coefficient, r = = 0.99999. Linear dependence of the intensity of fluorescence of the complex was obtained in concentration range from 0.06–22.4 μg mL^{-1}.

LOD (limit of detection) and LOQ (limit of quantification). The limit of detection (LOD)[26,27] was calculated by establishing the minimum level at which hesperidin can be detected, according to the formula:

$$LOD = \frac{3.3 s_b}{a} \quad (2)$$

where s_b is the standard deviation of the intercept and a is the slope of the calibration line. It was found that the *LOD* is 0.016 μg mL^{-1}.

The limit of quantification (*LOQ*)[26,27] was determined by using the formula:

$$LOQ = \frac{10 s_b}{a} \quad (3)$$

Thus, hesperidin can be quantified at a concentration of 0.049 μg mL^{-1}.

Precision. The accuracy of the method was determined for four different hesperidin concentrations (Table I). The accuracy and repeatability of the method is fairly high as indicated by good recovery and low values of the *SD*.

TABLE I. The fluorimetric determination of hesperidin in aqueous–methanolic solutions (N = 5)

Added, μg mL^{-1}	Found, μg mL^{-1}	Recovery, %	$SD \times 10^3$	CV / %
0.305	0.303	99.3	2.45	0.81
0.611	0.609	99.7	1.71	0.28
1.222	1.218	99.7	2.92	0.24
6.110	6.085	99.6	7.8	0.13

The results of the obtained analysis are given in Table II.

Procedure for analysis of hesperidin in pharmaceutical preparations

Hesperidin in pharmaceutical forms was analysed by the proposed method. For the analyses of hesperidin in helopyrin tablets, ten tablets were weighed and

powdered using a pestle and mortar. A portion of the powder, equivalent to weight of one tablet, was dissolved in 100 ml 70 vol. % v/v of methanol and the solution was filtered through a Millipore membrane filter with pore size 0.45 μm. 0.25 mL of this solution, 0.35 mL of 0.5 mol L^{-1} SB 12 and 0.5 mL of 1×10^{-3} mol L^{-1} $Al(NO_3)_3$ were mixed in a 10-mL volumetric flask and diluted to the mark with acetate buffer of pH 4.58 (in 70 % v/v methanol). The fluorescence of the prepared solution was taken at λ_{ex} = 390 nm and λ_{em} = 476 nm. The blank was acetate buffer of pH 4.58.

TABLE II. The fluorimetric determination of hesperidin in pharmaceutical preparations

Tablets	Found, mg	Recovery, %	*SD* / %	*CV* / %
Helopyrin, declared 20 mg bioflavonoids	18.06	90.3	0.12	0.66
Vitamin C, content of hesperidin not declared	117.38	–	0.81	0.69

The method suitability was confirmed by taking the fluorescence spectra of the excipient mix (microcrystalline cellulose, methylhydroxypropyl cellulose, Mg-stearate and starch hydrolysate) with the addition of 0.5 mL 1.0×10^{-3} mol L^{-1} of $Al(NO_3)_3$ solution. In Fig. 6 the spectra of aluminium(III) ions + tablet solution and aluminium(III) ion + excipient mix are shown, from which it may be seen that excipients did not interfere with hesperidin determination. Under the chosen experimental conditions, the aluminium complex with rutin (and other citrus flavonoids in the tablets) did not produce measurable fluorescence, and thus, rutin does not interfere with the hesperidin determination.

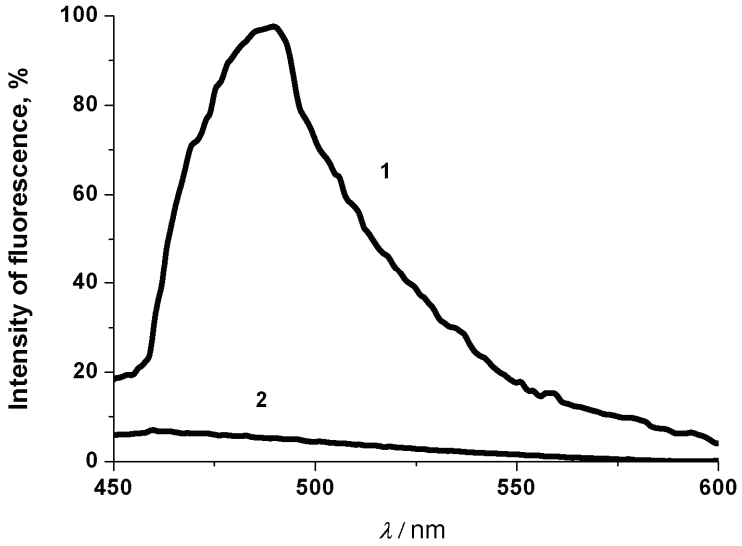

Fig. 6. Emission spectra of the aluminium–hesperidin complex in helopyrin tablets (1) and excipient mix (2). The blank was acetate buffer at pH 4.58.

The content of hesperidin in helopyrin tablets is in good agreement with content that Obendorf *et al*. obtained using the cathodic stripping voltammetry method.[18]

Determination of hesperidin in plasma

0.2 mL human pool plasma, 0.35 mL of 0.5 mol L^{-1} SB 12 and different volumes of hesperidin stock solution to give concentrations of 0.1–12.2 μg mL^{-1} were mixed in a 10-mL volumetric flask and diluted to the mark with pH 4.58 acetate buffer (in 70 vol. % methanol). After incubation (30 min), 0.5 mL of 1×10^{-3} mol L^{-1} $Al(NO_3)_3$ was added. The fluorescence of the prepared solutions were measured at λ_{ex} = 390 nm and λ_{em} = 476 nm. Plasma with SB 12 in acetate buffer (pH 4.58) served as the blank.

Linear dependence of the intensity of fluorescence of the complex on the concentration of hesperidin in diluted plasma samples was obtained in the interval 0.1–12.2 μg mL^{-1}. The regression equation was calculated (I_F is fluorescence intensity in %, and c is the concentration of hesperidin in μg mL^{-1}):

$$I_F = (4.12 \pm 0.02)c + (2.13 \pm 0.04) \quad (4)$$
$$(N = 7, r = 0.99998).$$

The *LOD* of hesperidin in plasma was calculated to be 0.032 μg mL^{-1}. The *LOQ* of hesperidin in plasma showed that it could be quantified at a concentration of 0.096 μg mL^{-1}.

Three different concentrations of hesperidin were added to human plasma in order to obtain concentrations of hesperidin in plasma in the range 0.122–6.110 μg mL^{-1}. These plasma samples were treated in the same way as for the calibration graph. The analytical recovery was 98.4–99.8 %. The low values of relative error (*RE*) and the relative standard deviation of determination (*RSD*) indicate very good reproducibility of the measurements. The results are given in Table III.

TABLE III. The fluorimetric determination of hesperidin in serum samples (N = 5)

Added, μg mL^{-1}	Found, μg mL^{-1}	Recovery, %	$SD\times10^3$	CV / %
0.122	0.120	98.4	1.08	0.86
0.611	0.610	99. 8	1.22	0.20
6.110	6.091	99.7	1.30	0.21

HPLC and mass spectrometric determination of hesperidin

Preparation of solutions for HPLC and mass spectrometric determination of hesperidin. A stock solution of hesperidin (1.0226 mg mL^{-1}) was prepared in methanol. A series of working standard solutions of hesperidin in the concentration range: 0.02–12.2 μg mL^{-1} was prepared by diluting the stock solution with methanol.

Solid phase extraction of plasma samples

Hesperidin was extracted from the plasma samples using LC-18 (500 mg) Supelco cartridges. The cartridges were preconditioned with 5 mL of methanol followed by 5 mL of Milli-Q water. Then 5 mL of sample was forced through the cartridge at a flow rate of about 0.5 mL min^{-1}. After loading, the SPE cartridge was washed with 5 mL of Milli-Q water and then dried under vacuum for 10 min. Finally, the sample was eluted with 2.5 mL of methanol. Human plasma samples were thermostated at 25 °C and after fortification with hesperidin were subjected to protein precipitation and liquid–liquid extraction. To a tube containing 1.0 mL of plasma was added 500 μL methanol or a standard solution of hesperidin. 2-Propanol (1.0 mL) was added to precipitate the proteins. The mixture was then vortex-mixed for 1 min and centrifuged at 10000×*g* for 10 min. The upper clear solution layer was collected and 500 μL water and 500 μL saturated solution of potassium chloride were added. After mixing for 15 s, 5 mL ethyl acetate was added and the sample was vortex-mixed for 1 min and shaken for 10 min. After centrifugation at 3500×*g* for 5 min, the upper organic layer was transferred to another tube and evaporated under nitrogen at 40 °C. The residue was reconstituted in 1 mL methanol and 20 μL was injected into the HPLC and MS system.[28] The extract was first injected onto a Gemini column in the HPLC/UV system with gradient elution and UV detection. The obtained results confirmed the presence of only hesperidin without interfering substances in the extract. The quantification was subsequently performed by injection of 20 μL of the extract into the MS system using the autosampler of the HPLC system but bypassing the chromatographic column.

To check the reliability of fluorescence method the direct HPLC determination of hesperidin in plasma samples LC–MS/MS and HPLC/UV methods in tablets, were developed as modifications of reported methods.[29] Two calibration curves were established for the determination of hesperidin: in methanol medium and in plasma spiked with known quantities of hesperidin.

Analysis of tablets

The helopyrin tablets were analysed for their hesperidin content. The tablets were prepared for analysis according to the procedure given for the fluorometric determination. No extraction procedure was used. Different aliquots of the tablet solutions were subjected to HPLC analysis using a Gemini column and gradient elution with UV detection. The chromatogram of Helopyrin tablets is shown in Fig. 7. The hesperidin peak appeared at a retention time of 13.74 min, as confirmed by comparison with the chromatogram of the standard substance and by checking the UV and mass spectra of the corresponding peak.

The calibration graph was constructed using working standard solutions of hesperidin. The regression equation of the calibration line was:

$$A = (4.83\pm0.05)\times10^4 c + (2.1\pm0.2)\times10^3 \quad (N = 10,\ r^2 = 0.9998) \quad (5)$$

where A is the area of the SRM transition and c is the sample concentration in μg mL^{-1}. The linear range was 0.05–10.0 μg hesperidin mL^{-1}. The *LOD*, calculated from the calibration line, was 0.01 μg mL^{-1} and the *LOQ* was 0.03 μg mL^{-1}. Three aliquots of tablet solution were subjected to chromatographic analysis. The results of the analysis are given in Tables IV and V.

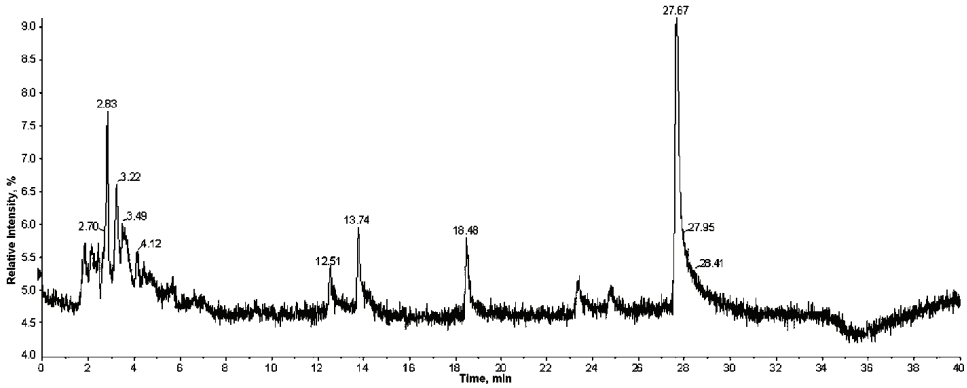

Fig. 7. Chromatogram of the helopyrin tablets.

TABLE IV. HPLC/UV Analysis of helopyrin tablets

Taken, μg mL^{-1}	Found, μg mL^{-1}	Recovery, %	*SD*	*CV* / %
1.5	1.26	84.00	0.25	0.17
3.0	2.84	94.66	0.36	0.12
6.0	5.75	95.83	0.39	0.07

TABLE V. HPLC/UV Analysis of combined Vitamin C tablets for their hesperidin content

Taken, μg mL^{-1}	Found, μg mL^{-1}	Recovery, %	*SD*	*CV* / %
0.1	0.08	75.00	0.3	8.3
0.2	0.2	88.00	0.7	3.65
0.3	0.3	95.33	0.2	0.76

Low recovery of determination of hesperidin in Vitamin C tablets could be explained by absorption of other substances present in tablets that absorb at the same wavelength as hesperidin and could not be removed by the SPE extraction.

Analysis of plasma samples

The mass spectrum consists of six signals of various intensities (Table VI).

Intensity (peak area) of *m/z* 609 → 325 transition was followed. The calculated equation of the calibration line was:

$$A = (4.83\pm0.02)\times10^4 c + (1.75\pm0.09)\times10^3 \quad (6)$$

TABLE VI. Mass spectrum of hesperidin

m/*z*	Abundance, %
609/343	31
609/325	72
609/301	100
609/265	16
609/253	12
609/174	24
609/151	32

where *A* is the area of the SRM transition and *c* is the sample concentration in μg mL^{-1}) for 10 samples. The linearity range was 0.02–10.0 μg mL^{-1}. The *LOD* was estimated from $n = 7$ replicate measurements of the samples in the concentration range 0.002–0.05 μg mL^{-1} and $n = 7$ replicate measurements of the reagent blank (methanol). This procedure provided an *LOD* estimate of 5.0×10^{-3} μg mL^{-1}, *i.e.*, 5.0 ng mL^{-1}. The *LOQ* may then be taken as 15.0 ng mL^{-1}.

The results of analysis of spiked plasma samples are presented in Table VII, from which the excellent recovery can be seen; thus, indicating the good accuracy of the method.

TABLE VII. Accuracy and precision of the HPLC/MS analysis of serum samples spiked with hesperidin ($N = 5$)

Taken, μg mL^{-1}	Found, μg mL^{-1}	Recovery, %	*SD*	*CV* / %
0.5	0.497	99.4	0.006	1.21
1.0	1.02	102.0	0.06	5.88
2.5	2.48	99.2	0.05	2.02
5.0	5.19	102.0	0.03	0.58

The good recovery for the determination hesperidin with the serum sample could be explain by the facts that the LC–MS/MS detection method is much more sensitive and specific compared with the other method and the concentration level was 10 to 100 times higher than in the serum examined by HPLC. This concentration range was used because it is the optimal concentration in human serum after oral dosage of tablets containing hesperidin.[30]

CONCLUSIONS

In this work, a simple, precise and accurate method for the determination of hesperidin in human plasma and tablets based on the fluorescence properties of the aluminium–complex in micellar media was developed. The reliability of the method was confirmed by parallel determination of hesperidin in human plasma using mass spectrometry while the determinations of hesperidin in tablets were compared with an HPLC/UV determination using gradient elution. The fluorometric determination of hesperidin in human plasma, after its complexation with

aluminium(III)-ion, provides good accuracy and precision and may be used for routine clinical analysis, since it is considerably simpler and less time consuming than mass spectrometric determinations. The fluorometric determination in dosage forms may be successful only when no other flavonoids which bind aluminium to adjacent 3-hydroxy and 4-keto groups (stoichiometry 1:1) are present.

Acknowledgements. This work was partly supported by the Ministry of Education, Science and Technological Development of the Republic of Serbia, Project Nos. 172016 and 173017.

ИЗВОД

РАЗВОЈ И ВАЛИДАЦИЈА ФЛУОРИМЕТРИЈСКЕ МЕТОДЕ ЗА ОДРЕЂИВАЊЕ ХЕСПЕРИДИНА У ХУМАНОМ СЕРУМУ И ФАРМАЦЕУТСКИМ ПРЕПАРАТИМА

ЛЕПОСАВА А. ПАВУН[1], ЈАСМИНА М. ДИМИТРИЋ МАРКОВИЋ[2], ПРЕДРАГ Т. ЂУРЂЕВИЋ[3], МИЛЕНА Д. ЈЕЛИКИЋ СТАНКОВ[4], ДАНИЕЛА Б. ЂИКАНОВИЋ[5], АНДРИЈА Р. ЋИРИЋ[3] и ДУШАН Л. МАЛЕШЕВ[1]

[1]Катедра за физичку хемију и инструменталне методе, Фармацеутски факултет, Универзитет у Београду, Војводе Степе 450, 11000 Београд, [2]Факултет за за физичку хемију, Универзитет у Београду, Студентски трг 12, 11000 Београд, [3]Институт за хемију, Природно–математички факултет, Универзитет у Крагујевцу, Радоја Домановића 12, 34000 Крагујевац, [4]Катедра за аналитичку хемију, Фармацеутски факултет, Универзитет у Београду, Војводе Степе 450, 11000 Београд и [5]Институт за мултидисциплинарна истраживања, Универзитет у Београду, Деспота Стефана 142, 11000 Београд

Развијена је флуориметријска метода за одређивање хесперидина у хуманом серуму и фармацеутским препаратима која се заснива на флуоресценцији комплекса алуминијум(III)–хесперидин. Комплекс показује интензивну флуоресценцију у присуству сурфактанта SB 12 на 476 nm приликом ексцитације на 390 nm. Линеарна зависност интензитета флуоресценције од концентрације при одређивању хесперидина у фармацеутским препаратима добијена је у концентрационом опсегу 0,06–24,4 μg mL^{-1} са границом детекције од 0,016 μg mL^{-1} и границом квантификације од 0,049 μg mL^{-1}. Добијене „*recovery*“ вредности у интервалу 99,3–99,7 % показују велику прецизност методе. Линеарна зависност интензитета флуоресценције компекса од концентације хесперидина добијена је у концентрационом опсегу 0,1–12,2 μg mL^{-1} са границом детекције од 0,032 μg mL^{-1} и границом квантификације од 0,096 μg mL^{-1}. „*Recovery*“ вредности су добијене у опсегу 98,4 до 99,8 %. Поузданост методе проверена је LC–MS/MS методом за одређивање хесперидина у серуму, а HPLC/UV методом проверена је поузданост приликом одређивања хесперидина у фармацеутским препаратима. Линеарна зависност при одређивању хесперидина у фармацеутским препаратима добијена је у интервалу 0,05–10,00 μg mL^{-1}. Граница детекције је износила 0,01, а граница квантификације је 0,03 μg mL^{-1}. Линеарна зависност при одређивању хесперидина у хуманом серуму је добијена у интервалу 0,02–10,00 μg mL^{-1} са границом детекције од 0,005 и границом квантификације од 0,015 μg mL^{-1}. Добро слагање између ове две методе показује применљивост флуориметријске методе у клиничким лабораторијама и лабораторијама за контролу квалитета. Предложена флуориметријска метода је једноставна, поуздана и прецизна за одређивање хесперидина у хуманом серуму и фармацеутским препаратима.

(Примљено 5. октобра 2011, ревидирано 17. априла 2012)

REFERENCES

1. E. Middleton Jr., C. Kandaswami, T. C. Theoharides, *Pharmacol. Rev.* **52** (2000) 673
2. K. R. Markham, *Techniques of Flavonoids Identification*, Academic Press, London, 1982
3. G. G. Guilbault, *Practical Fluorescence, Theory, Methods and Techniques*, Marcel Dekker, New York, 1973, p. 221
4. M. H. Fletcher, *Anal. Chem.* **37** (1965) 550
5. S. M. Z. Al-Kindy, F. O. Suliman, S. B. Salama, *Microchem. J.* **74** (2003) 173
6. S. A. B. E. van Acker, G. Plemper van Balen, D. J. van den Berg, A. Bast, W. J. F. van det Vijgh, *Biochem. Pharmacol.* **56** (1998) 935
7. S. M. Z. AL-Kindy, K. H. Al-Hinai, F. E. O. Suliman, H. J. Al-Lawati, A. Pillay, *Arab. J. Chem.* **4** (2011) 147
8. P. K. Wilmsen, D. S. Spada, M. Salvador, *J. Agric. Food Chem.* **53** (2005) 4757
9. S. Tommasini, M. L. Calabro, R. Stancanelli, P. Donato, C. Costa, S. Catania, V. Villari, P. Ficarra, R. Ficarra, *J. Pharm. Biomed. Anal.* **39** (2005) 572
10. J. B. Harborne, C. A. Williams, *Phytochemistry* **55** (2000) 481
11. A. Garg, S. Garg, L. J. Zaneveld, A. K. Singla, *Phytother. Res.* **15** (2001) 655
12. H. Chiba, M. Uehara, J. Wu, X. Wang, R. Masuyama, K. Suzuki, K. Kanazawa, Y. Ishimi, *J. Nutr.* **133** (2003) 1892
13. J. Xia, A. Kotani, H. Hakamata, F. Kusu, *J. Pharm. Biomed. Anal.* **41** (2006) 1401
14. Y. C. Lee, C. Y. Huang, T. T. Wen, K. C. Suen, *J. Chromatogr. A* **692** (1995) 137
15. X. Li, H. Xiao, X. Liang, D. Shi, J. Liu, *J. Pharm. Biomed. Anal.* **34** (2004) 159
16. G. A. Barthe, P. S. Jourdan, C. A. McIntosh, R. L. Mansell, *Phytochemistry* **27** (1988) 249
17. G. J. Volikakis, C. E. Efstathiou, *Talanta* **51** (2000) 775
18. D. Obendorf, E. Reichart, *Electroanalysis* **7 (11)** (1995) 1075
19. D. Malešev, Z. Radović, V. Kuntić, M. Kosanić, *Anal. Lett.* **30** (1997) 917
20. Z. Radović, D. Malešev, M. Jelikic-Stankov, *Pharmazie* **51** (1996) 8
21. T. Perez-Ruiz, C. Martinez-Lozano, V. Tomas, J. Fenoll, *Fresenius J Anal. Chem.* **364** (1999) 279
22. N. Pejić, S. Blagojević, S. Anić, V. Vukojević, Lj. Kolar-Anić, *Anal. Bioanal. Chem.* **381** (2005) 775
23. D. D. Perrin, B. Dempsey, *Buffers for pH and Metal Ion Control*, Chapman and Hall, London, 1974, p. 77–94
24. H. Irving, T. Pierce, *J. Chem. Soc.* (1959) 2565
25. J. Yoe, A. Jones, *Ind. Eng. Chem. Anal. Ed.* **16** (1944) 111
26. J. N. Miller, J. C. Miller, *In Statistics and Chemometrics for Analytical Chemistry*, 5th ed. Pearson Education, London, 2005, p. 121
27. *Validation of analytical procedures: Methodology*, ICH Guideline Q2B. 1997, Federal Register 62, No. 96, p. 27463–27467
28. Y. Yang, H. Li, K Gao, M. Liu, Y. Sun, T. Yan, J. P. Fawcett, Y. Cui, J. Gu, *J. Chromatogr. B* **862** (2008) 119
29. A.Ćirić, H. Prosen, M. Jelikić-Stankov, P. Đurđević *Talanta* **99** (2012) 780
30. V. Kuntić, I. Filipović, Z. Vujić, *Molecules* **16** (2011) 1378.

Journal of the Serbian Chemical Society
JSCS-info@shd.org.rs • www.shd.org.rs/JSCS
J. Serb. Chem. Soc. 77 (11) 1641–1647 (2012) UDC 543.632.4+546.56+543.553:628.1.033
JSCS–4377 *Original scientific paper*

Development of a flow injection method with amperometric detection for the indirect determination of copper in drinking water samples

ALEKSANDAR LOLIĆ[1*#], TATJANA TRIPKOVIĆ[1], RADA BAOŠIĆ[1#], SNEŽANA NIKOLIĆ-MANDIĆ[1#] and BOJANA STANIMIROVIĆ[2]

[1]*Faculty of Chemistry, University of Belgrade, P. O. Box 158, 11001 Belgrade, Serbia and* [2]*Mol a.d., Company for Chemistry, Biotechnology and Consulting, Batajnički drum 2, 11080 Belgrade, Serbia*

(Received 16 June, revised 1 September 2012)

Abstract: A gas-diffusion flow injection method with amperometric detection for the indirect determination of copper on a silver electrode was developed. The flow through system was equipped with two injection valves and a gas-diffusion unit. In the first step, a signal of a cyanide solution was recorded. In the subsequent step, the signal of cyanide in the presence of copper was measured. Interferences (Cd(II), Co(II), Ag(I), Ni(II), Fe(III), Hg(II) and Zn(II)) were investigated and successfully removed. The calibration graph was linear in the range 1–90 μmol dm^{-3} of copper with a correlation coefficient of 0.993. The regression equation is $I = (0.0455\pm0.0015)c + (0.4611\pm0.0671)$, where I is the relative signal decrease in μA and c is concentration in μmol dm^{-3}. Relative standard deviation for six consecutive injections of 30 μmol dm^{-3} copper(II) was 1.47 % and for 1 μmol dm^{-3} copper(II), it was 3.40 %. The detection limit, calculated as 3 s/m (where s is a standard deviation of nine measurement of a reagent blank and m is the slope of the calibration curve), was 0.32 μmol dm^{-3}, which corresponds to 2.44 ng of copper(II) (the loop volume was 0.12 cm^3). The method enables 60 analyses per hour and it was successfully applied for the determination of copper in drinking water samples.

Keywords: copper determination; gas-diffusion; drinking water samples; copper cyano complex.

INTRODUCTION

Copper is essential element with an important role in living organisms. A considerable number of highly sensitive and selective analytical techniques for the determination of copper are based on the use of large and expensive atomic

* Corresponding author. E-mail: lolix@chem.bg.ac.rs
# Serbian Chemical Society member.
doi: 10.2298/JSC120616090L

spectrometric instrumentation (*e.g.*, flame atomic absorption spectrometry,[1–5] electrothermal atomic absorption spectrometry,[6] and inductively coupled plasma spectrometry with optical emission[7]). Less expensive optical[8–14] and electrochemical[15–18] detection techniques, which are amenable to miniaturization, have been successfully used in the development of flow injection (FI) methods for copper. Among electrochemical techniques, amperometry[19–21] has been used in FI systems for the development of biosensors for copper determination. The greatest disadvantages of biosensors are the regeneration of the modified surface of the working electrode and the not very sensitive determinations.

The purpose of this work was to develop a flow injection method for copper determination on a bare silver electrode. It is based on a previously optimized FI system for cyanide determination on a modified silver working electrode.[22] The system described in this paper was equipped with an additional flow stream, carrying copper solutions (samples), containing a single mixing coil and a gas-diffusion unit to increase selectivity. In the mixing coil, two competitive reactions, complex formation and formation of gaseous hydrogen cyanide, occurred. The obtained flow injection signal presents a decreased anodic current for cyanide in the presence of copper(II) ions. The method was successfully applied for copper determination in drinking water samples.

EXPERIMENTAL

Reagents and chemicals

All the chemicals used were of analytic reagent grade. Degassed and filtered water was used throughout. The copper standard solution was CertiPUR (Merck, Germany, $Cu(NO_3)_2$ in 0.5 mol dm^{-3} HNO_3. The stock cyanide solution (KCN, Merck–Alkaloid, Macedonia) was prepared weekly as were other stock reagent solutions, 0.1 mol dm^{-3} HCl solution (J.T. Baker, The Netherlands) and 0.1 mol dm^{-3} sodium hydroxide (Carlo Erba, Italy). Working solutions were prepared daily and the cyanide concentration was determined volumetrically using the Liebig method.

Sample preparation

Drinking water samples were collected from several tap water units within one building. One liter of tap water was collected and acidified at the sampling location with 1 cm^3 of concentrated nitric acid. The samples were filtered. If the pH value was lower than 2, it was adjusted carefully with sodium hydroxide solution (2 mol dm^{-3}) to the desired value (to match 0.01 mol dm^{-3} HCl). Samples were filtered again and injected into a flow injection analysis (FIA) manifold.

Apparatus

The FIA manifold used for copper determination, equipped with a gas-diffusion unit and an amperometric detector, is presented in Fig. 1. Two peristaltic pumps, Model HPB 5400 (Iskra, Slovenia) and Model MS Reglo (Ismatec, Switzerland) with a flow rate control unit were used. Each of two injection valves, Model 5020 (Rheodyne, USA), were equipped with a 0.12 cm^3 sample loop. The gas-diffusion unit was manufactured after a model that was provided by Shenyang Film Projector Factory, China. All connections were made with 0.5 mm

i.d. tubing. Flow went through the amperometric cell, which was equipped with a working silver electrode (BASi, model MF-1008, USA), a reference Ag/AgCl electrode (BASi, model MF-2021, USA) and an auxiliary electrode made of stainless steel. The working electrode was polished with aluminum paste (BASi, 0.5 μm, USA) and well rinsed with distilled water and methanol prior to every recording. The working potential was regulated with a polarograph MA 5450 (Iskra, Slovenia). The obtained FIA signals were recorded on a Servograph Model 61 recorder (Radiometer, Denmark).

Reference results were obtained on an atomic absorption spectrometer, Perkin-Elmer 2380, equipped with a graphite furnace unit. The determinations were performed at 324.8 nm, with slit 0.7 nm and a lamp current of 10 mA. A standard run was 5–150 μg dm^{-3} of copper for the GF-AAS.

Procedure

All experiments were performed at room temperature. Prior to each recording, the silver electrode was optimized by injecting the cyanide solution (1 mmol dm^{-3}) until the system reproducibility was better than 5 %; up to 10 injections were sufficient for this purpose. The system was equipped with two injection valves, one for cyanide solution injection, V_1, and the other for copper solution, V_2, Fig. 1. The anodic current, I_{CN}, was obtained by cyanide solution injection (n = 3). Then, both the cyanide and copper solution were simultaneously injected (n = 3) and current intensity was, I_{CN+Cu}, was measured. The decrease in the current responds to the copper concentration $I_{Cu} = I_{CN} - I_{CN+Cu}$. During system optimization, the relative decrease of the signal intensities were measured, and as optimal conditions were those under which the most prominent decrease was obtained. All waste solutions were collected in a saturated sodium hydroxide solution and disposed of adequately.

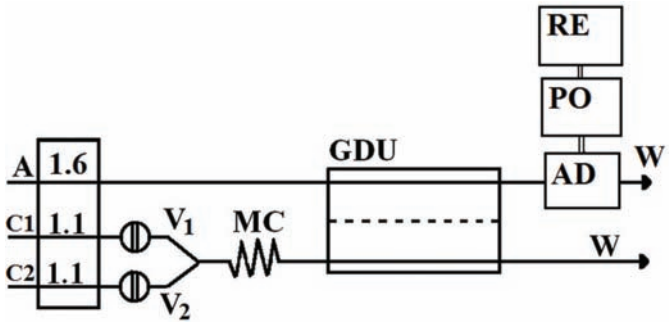

Fig. 1. Schematic presentation of the FIA manifold used for copper determination. C1 – carrier for cyanide solution (0.02 NaOH mol dm^{-3}); C2 – carrier for copper solution (0.01 HCl mol dm^{-3}), A – acceptor (0.1 mol dm^{-3} NaOH), V1 – injection valve, for cyanide solution (0.120 cm^3), V2 – injection valve for copper solution (0.120 cm^3), MC – mixing coil (60 cm × 0.5 mm i.d.), GDU – gas diffusion unit, AD – amperometric detector, PO – potentiostat, RE – recorder, W – waste. Flow rates are given in cm^3 min^{-1}.

RESULTS AND DISCUSSION

Optimization of the flow system

In order to obtain optimal conditions for the copper determination, the effects of several parameters were investigated.

Working potential for all experiments was 0.0 V *vs*. Ag/AgCl, as there are many manuscripts describing cyanide amperometric determination at this potential.[22] This was confirmed by cyclic voltammetry.

Effect of the sample working volume (the gasket thickness effect) was part of a previously published work for the same amperometric flow cell.[23]

There are two competitive reactions occurring in the single mixing coil. One of them is cyano complex formation and the other is the formation of gaseous HCN. Both reactions are very pH sensitive, hence, strict control of the pH value in the mixing coil was mandatory. For the simultaneous injection of 100 μmol dm^{-3} cyanide in 0.02 mol dm^{-3} NaOH and 30 μmol dm^{-3} Cu(II) in 0.01 mol dm^{-3} HCl, a significant signal decrease was noticed.

The next experiment was to determine the optimal sodium hydroxide concentration as acceptor solution. Cyanide signals were recorded for following acceptor solution concentrations: 0.02, 0.05, 0.10 and 0.15 mol dm^{-3} sodium hydroxide. The most intensive decrease was obtained when 0.10 mol dm^{-3} hydroxide was used. With more concentrated hydroxide, an increase of cyanide signal in the presence of copper was noticed.

The length of the mixing coil was the subject of further investigations. Several mixing coils were used: 30, 60, 105 and 210 cm long. The most intensive decrease was obtained when 60 cm long mixing coil was used. Further increase of its length had no effect on the FIA signal.

The last parameter to be investigated was the effect of stream directions and rates. The rate of the donor stream was kept constant (1.1 cm^3 min^{-1}) while the rate of acceptor stream was varied (0.8, 1.6, 2.4 and 3.1 cm^3 min^{-1}). Obtained signals are presented in Fig. 2. All further experiments were performed with parallel streams and with the acceptor rate of 1.6 cm^3 min^{-1}.

Interferences

The interference study was investigated by injection of 100 μmol dm^{-3} cyanide in the presence of 30 μmol dm^{-3} copper, and a mixture of copper and the interferents (Cd(II), Co(II), Ni(II), Fe(III), Ag(I), Hg(II) and Zn(II)) of the same concentration. Silver, zinc and iron did not interfere with the copper signal intensity. When Fe(III) was present in higher concentration (60 μmol dm^{-3}), interference was noticed. Ni(II), Hg(II), Co(II) and Cd(II) also interfered with the copper determination when their concentration was 30 μmol dm^{-3}. However, they did not interfere when their concentration was 3 μmol dm^{-3}. The interferents were removed from the solution by known analytical methods.

Analytical performance

The calibration graph was linear in the range 1–90 μmol dm^{-3} of copper, with a correlation coefficient r^2 of 0.993. The regression equation is I =

(0.0455±0.0015)c + (0.4611±0.0671), where I is relative signal decrease in μA, c is concentration in μmol dm^{-3}. The precision of the method was investigated by six repetitive injections of 30 and 1 μmol dm^{-3} of copper and the relative standard deviations were 1.47 and 3.40 %, respectively. The detection limit, calculated as $LOD = 3\ s/m$ (where s is the standard deviation of nine measurements of a reagent blank, and m is the slope of the calibration curve), was 0.32 μmol dm^{-3}, which corresponds to 2.44 ng of Cu(II) (the loop volume was 0.12 cm^3). The throughput of this method was 60 analyses per hour.

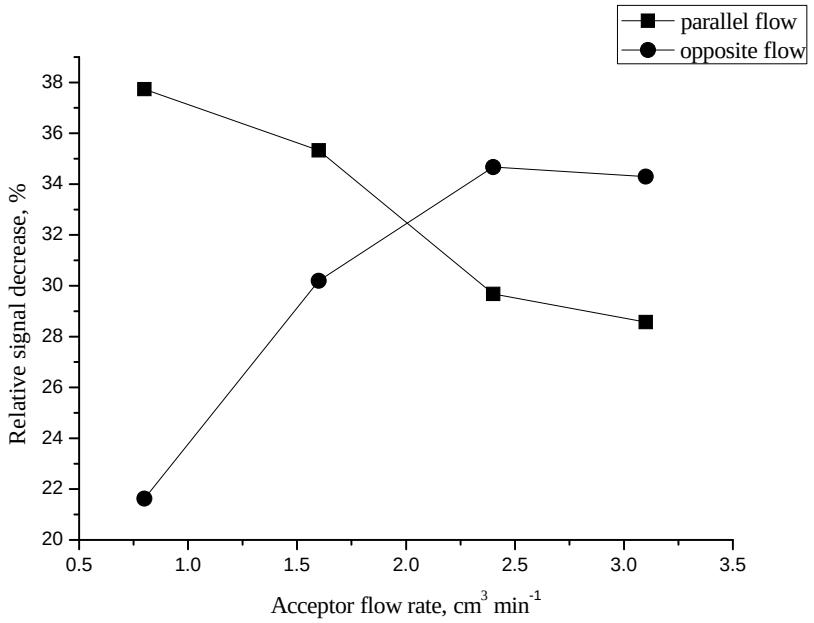

Fig. 2. Effects of parallel and opposite flow rates at different acceptor flow rates (0.8, 1.6, 2.4 and 3.1 cm^3 min^{-1}) for a constant donor flow rate (1.1 cm^3 min^{-1}) on the relative anodic current decrease for a cyanide solution (100 μmol dm^{-3}) in the presence of copper (30 μmol dm^{-3}).

Application

To validate the developed method, it was applied to the determination of copper in drinking water samples (Table I). In order to investigate the recovery of copper(II), known amounts of copper(II) were added to the samples (100 and 150 μmol dm^{-3}). Obtained values were consistent with the values obtained by the reference method (GF-AAS), and the recoveries of about 100 % show that the copper determination was very accurate. The results also showed that interferents were successfully removed.

TABLE I. Determination of copper in drinking water samples. The results are expressed as the average of three replicates (mean value ± *SD*)

Sample No.	Added Cu, μg dm^{-3}	Found Cu, μg dm^{-3}	Recovery, %	GF-AAS, μg dm^{-3}
1	0	103±3	–	105.0±0.6
	100	205±7	102.00	
	150	250±8	98.00	
2	0	107±4	–	106.0±0.6
	100	210±7	103.00	
	150	261±9	102.67	
3	0	73±2	–	74.0±0.3
	100	170±6	97.00	
	150	228±8	103.33	
4	0	127±4	–	132.0±1.0
	100	230±8	103	
	150	275±9	98.67	
5	0	71±2	–	70.0±0.3
	100	169±6	98.00	
	150	223±8	101.33	

CONCLUSIONS

A simple and sensitive flow injection method with amperometric detection for copper determination was optimized. The anodic current *vs*. copper(II) concentration was linear over the concentration range 1–90 μmol dm^{-3}. The precision was 1.47 % for 30 μmol dm^{-3} and 3.40 % for 1 μmol dm^{-3} of copper. The detection limit was 0.32 μmol dm^{-3}, which corresponds to 2.44 ng of copper(II) (for an injection coil volume of 0.12 cm^3). Copper was successfully determined in drinking water samples after a simple preparation procedure. The developed method had a comparable or lower limit of detection compared to other methods for the amperometric determination[19–21] of copper found in the literature.

Acknowledgement. The authors acknowledge the grant from the Ministry of Education, Science and Technological Development of the Republic of Serbia, Project No. 172051.

ИЗВОД

РАЗВОЈ ПРОТОЧНЕ ИНЈЕКЦИОНЕ МЕТОДЕ ЗА ИНДИРЕКТНО ОДРЕЂИВАЊЕ БАКРА СА АМПЕРОМЕТРИЈСКОМ ДЕТЕКЦИЈОМ У ПИЈАЋОЈ ВОДИ

АЛЕКСАНДАР ЛОЛИЋ[1], ТАТЈАНА ТРИПКОВИЋ[1], РАДА БАОШИЋ[1], СНЕЖАНА НИКОЛИЋ-МАНДИЋ[1] и БОЈАНА СТАНИМИРОВИЋ[2]

[1]Хемијски факултет, Универзитет у Београду, п.пр. 158, 11001 Београд и [2] Мол а.д., Акционарско друштво за хемију, биотехнологију и консалтинг, Батајнички друм 2, 11080 Београд

Циљ овог рада био је развој гасно-дифузионе проточно инјекционе методе са амперометријском детекцијом за индиректно одређивање бакра на сребрној електроди. Проточни систем је опремљен са два инјекциона вентила и гасно-дифузионом јединицом. У првом кораку снима се сигнал раствора цијанида, а у другом снима се сигнал при истовременом убризгавању раствора цијанида и раствора бакра. Сметње од Cd(II),

Co(II), Ag(I), Ni(II), Fe(III), Hg(II) и Zn(II) су испитане и успешно уклоњене. Калибрациона крива је линеарна у опсегу 1–90 μmol dm^{-3} бакра, коефицијент корелације је 0,993, а једначина праве $I = (0{,}0455\pm0{,}0015)c + (0{,}4611\pm0{,}0671)$, где је I разлика висине сигнала у μA, а c је концентрација у μmol dm^{-3}. Релативна стандардна девијација за шест узастопних убризгавања раствора бакра концентрације 30 μmol dm^{-3} је 1,47 %, а за 1 μmol dm^{-3} раствор Cu(II) је 3,40 %. Лимит детекције, израчунат као $3s/m$ (где је s стандардна девијација девет мерења слепе пробе и m је нагиб калибрационе праве), је 0,32 μmol dm^{-3}, што одговара 2,44 ng Cu(II) (запремина петље за узорак је 0,12 cm^3). Метода омогућава 60 анализа по једном сату и успешно је примењена за одређивање бакра у пијаћој води.

(Примљено 16. јуна, ревидирано 1. септембар 2012)

REFERENCES

1. C. A. Şahin, I. Tokgöz, *Anal. Chim. Acta* **667** (2010) 83
2. C. A. Şahin, I. Tokgöz, S. Bektaş, *J. Hazard. Mater.* **181** (2010) 359
3. H. Shirkhanloo, H. Z. Mousavi, A. Rouhollahi, *J. Serb. Chem. Soc.* **76** (2011) 1583
4. R. Gong, D. Zhang, K. Zhong, M. Feng, X. Liu, *J. Serb. Chem. Soc.* **72** (2008) 249
5. K. Miranda, A. G. G. Dionisio, E. R. Pereira-Filho, *Microchem. J.* **96** (2010) 99
6. C. Zheng, R. E. Sturgeon, X. Hon, *J. Anal. Atom. Spectrom.* **25** (2010) 1159
7. L. Zhang, Z. Li, X. Du, R. Li, X. Chang, *Spectrochim. Acta A* **86** (2012) 443
8. D. Rekha, K. Suvardhan, K. S. Kumar, P. Peddyprasad, B. Jayaraj, P. Chiranjeevi, *J. Serb. Chem. Soc.* **72** (2007) 299
9. P. Rumori, V. Cerda, *Anal. Chim. Acta* **486** (2003) 227
10. R. J. Cassella, *Microchem. J.* **72** (2002) 17
11. Y. Sekine, I. Shitanda, M. Itagaki, K. Watanabe, S. Nakano, T. Kawashima, *Microchim. Acta* **170** (2010) 113
12. S. Lunvongsa, T. Tsuboi, S. Motomizu, *Anal. Sci.* **22** (2006) 169
13. J. J. Pinto, C. Moreno, M. Garcia-Vargas, *Talanta* **64** (2004) 562
14. T. Leelasattarathkul, S. Liawruangrath, M. Rayanakorn, W. Oungpipat, B. Liawruangrath, *Talanta* **70** (2006) 656
15. R. Chaisuksant, L. Pattanarat, K. Grudpan, *Microchim. Acta* **162** (2008) 181
16. B. C. Janegitz, L. H. Marcolino-Junior, S. P. Campana-Filho, R. C. Faria, O. Fatibello-Filho, *Sensor. Actuat., B* **142** (2009) 260
17. M. Lin, M. Cho, W. S. Choe, Y. Son, Y. Lee, *Electrochim. Acta* **54** (2009) 7012
18. S. Qiu, L. Xie, S. Gao, Q. Liu, Z. Lin, B. Qiu, G. Chen, *Anal. Chim. Acta* **707** (2011) 57
19. M. Lehmann, K. Riedel, K. Adler, G. Kunze, *Biosens. Bioelectron.* **15** (2000) 211
20. K. Tag, K. Riedel, H. J. Bauer, G. Hanke, K. H. R. Baronian, G. Kunze, *Sensor Actuat. B-Chem.* **122** (2007) 403
21. D. Compagnone, A. S. Lupu, A. Ciucu, V. Magearu, C. Cremisini, G. Palleschi, *Anal. Lett.* **34** (2001) 17
22. S. D. Nikolić, E. B. Milosavljević, J. L. Hendrix, J. H. Nelson, *Analyst* **117** (1992) 47
23. A. Lolić, S. Nikolić-Mandić, P. Polić, *J. Serb. Chem. Soc.* **66** (2001) 637.

Journal of the Serbian Chemical Society
JSCS-info@shd.org.rs • www.shd.org.rs/JSCS
J. Serb. Chem. Soc. 77 (11) 1649–1659 (2012) UDC 628.3:547.562.33+543.544.943.3.068.7
JSCS–4378 *Original scientific paper*

Development and validation of a simple thin-layer chromatographic method for the analysis of *p*-chlorophenol in treated wastewater

MAJA NATIĆ[1*#], DRAGANA DABIĆ[2#], DUŠANKA MILOJKOVIĆ-OPSENICA[1#], BILJANA DOJČINOVIĆ[3], GORAN ROGLIĆ[1#], DRAGAN MANOJLOVIĆ[1#] and ŽIVOSLAV TEŠIĆ[1#]

[1]*Faculty of Chemistry, University of Belgrade, P. O. Box 51, 11158 Belgrade, Serbia,* [2]*Innovative Centre, Faculty of Chemistry Ltd., University of Belgrade, Studentski trg 12–16, 11158 Belgrade, Serbia and* [3]*Centre of Chemistry, Institute of Chemistry, Technology and Metallurgy, University of Belgrade, Njegoševa 12, 11000 Belgrade, Serbia*

(Received 9 May, revised 30 August 2012)

Abstract: A thin-layer chromatographic (TLC) method with densitometric detection was established for the quantification of *p*-chlorophenol in wastewater. Degradation efficiency of *p*-chlorophenol was monitored after each treatment of the wastewater samples. Degradation of *p*-chlorophenol was performed by advanced oxidation processes (AOPs), using UV, H_2O_2/UV, O_3/H_2O_2/UV, O_3 and O_3/UV. The developed TLC procedure was found to be simple, rapid and precise. The method is characterized by high sensitivity (the limit of detection was 11 ng per band and limit of quantification 35 ng per band), a linear range from 75 to 500 ng per band, r = 0.9965), and high precision, accuracy (mean percentage recovery 98.6 %), and specificity. Additionally, the efficiency of degradation was monitored using HPLC giving comparable results with the reversed phase TLC measurements.

Keywords: p-chlorophenol; TLC-scanner; HPLC; AOPs; wastewater treatment.

INTRODUCTION

Chlorophenols are considered as one of the major aquatic pollutants with toxicity for humans and animals. Various chlorophenols are intermediates in synthesis of many pesticides and dyes. In the chlorination process of water, they arise as products of phenol chlorination. As they subsequently enter the aquatic environment, chlorophenols are to be found in surface water, groundwater and especially in wastewater.[1]

* Corresponding author. E-mail: mmandic@chem.bg.ac.rs
# Serbian Chemical Society member.
doi: 10.2298/JSC120509087N

Some of the chlorophenols are slightly biodegradable, while others are more persistent and mobile in the aquatic environment. Their bioaccumulation increases with the introduction of substituents into the phenol ring. O*rtho*-substituted chlorophenols are less toxic than *meta*- and *para*-substituted derivatives.[2]

Wastewater treatment is very important to minimize water pollution and prevent waterborne diseases. The search for ways to treat wastewater in a safe manner with low running costs is constant. Many processes, chemical, physical, biological and a combination of them could be used for water treatment.[3] Standard techniques for water treatment, such as coagulation, carbon adsorption, reverse osmosis, and ultrafiltration, are not efficient in the removal of chlorophenols. One of alternatives for the water treatment is processes based on the formation free hydroxy radicals with very strong oxidation potential, known as advanced oxidation processes (AOPs).[4] These processes lead to complete degradation of chlorophenols to carbon(IV) oxide or to biodegradable and less toxic intermediates.

Previously, the experimental results of the efficiency of *p*-chlorophenol degradation using a falling film dielectric barrier discharge (DBD) reactor were published.[5] Different conditions for the degradation of *p*-chlorophenol in aqueous solution were examined. The kinetics of the degradation in several successive passes through the reactor was monitored using high performance liquid chromatography (HPLC).[5]

The efficiency of degradation processes is usually monitored using techniques such as HPLC and gas chromatography (GC). Literature references indicate that these techniques are the most reliable and the most sensitive methods for such evaluations.[6,7] However, some results could be found for phenol and its derivatives on bonded amino, cyano and diol thin-layer stationary phases.[8] Modern thin-layer chromatography (TLC) is an instrumental technique that is comparable by its accuracy and precision with both HPLC and GC. With high efficiency and significant reproducibility, it became applicable for environmental monitoring.[9,10]

In comparison with HPLC, TLC has several advantages: it is a simple, fast technique, requires little or no sample preparation and clean-up, it is easy to perform, saving both time and expense. The major advantage of TLC is that several samples can be run simultaneously using a small quantity of mobile phase, unlike in HPLC, thus reducing analysis time and cost per analysis. Solvent consumption and the amount of waste associated with the sample preparation in TLC are minimal. This is particularly important from the green chemistry point view.[11] Furthermore, even cruder samples can be analyzed by TLC because each plate is used only once, and therefore development is not as critical as in HPLC, where the possibility of destroying the column occurs.

To this end, a TLC procedure for the determination of *p*-chlorophenol in wastewater samples is presented herein. Main goals were to: *i*) use a simple and

cheap technique for monitoring the removal of *p*-chlorophenol from wastewater samples, *ii*) obtain optimal thin-layer efficiency and *iii*) to validate in such way the adopted thin-layer chromatographic method.

EXPERIMENTAL

Reagents and chemicals

All reagents used were of analytical grade purity. *p*-Chlorophenol (*p.a.*) was purchased from Aldrich (USA). Acetonitrile and triethylamine used for the experiments were purchased from Merck (Germany). Ultrapure water was obtained from a Micropure TKA system (Germany) and used for the preparation of the mobile phases for reversed phase (RP) TLC and HPLC. Wastewater samples and a standard stock solution were prepared by dissolving *p*-chlorophenol in ultrapure water to give a concentration 100.0 mg L^{-1}.

Advanced oxidation processes

The starting concentration of *p*-chlorophenol was 100.0 mg L^{-1}. Five different sets of conditions were examined: UV, H_2O_2/UV, O_3/H_2O_2/UV, O_3 and O_3/UV. A UV flow lamp (BULEGO SH-500, Italy) with a maximum at 253.7 nm and 38 W power was used. The UV lamp was included in all systems, except the O_3 system. The flow rate of the solution (210 mL min^{-1}) was set by a peristaltic pump.

The working principle of an ozonizator is based on an electrical discharge through air, whereby the oxygen is converted to ozone. A Lifepool 1.0 ozonizator (Lifetech, (Czech Republic), was used. The flow rate of the air through the ozonizator, measured by rotameter, was adjusted to 10 L min^{-1}. This model generates 1 g h^{-1} of ozone. A schematic representation of the experimental setup is shown in Fig. 1. In all experiments, the reactor was filled with 750 mL of an aqueous solution of *p*-chlorophenol. Ozone was introduced into the bottom of the reactor (round bottom flask, 1 L) through a glass tube (with sintered-glass diffusers at the end) for 30 minutes at a flow rate 2 L min^{-1}.

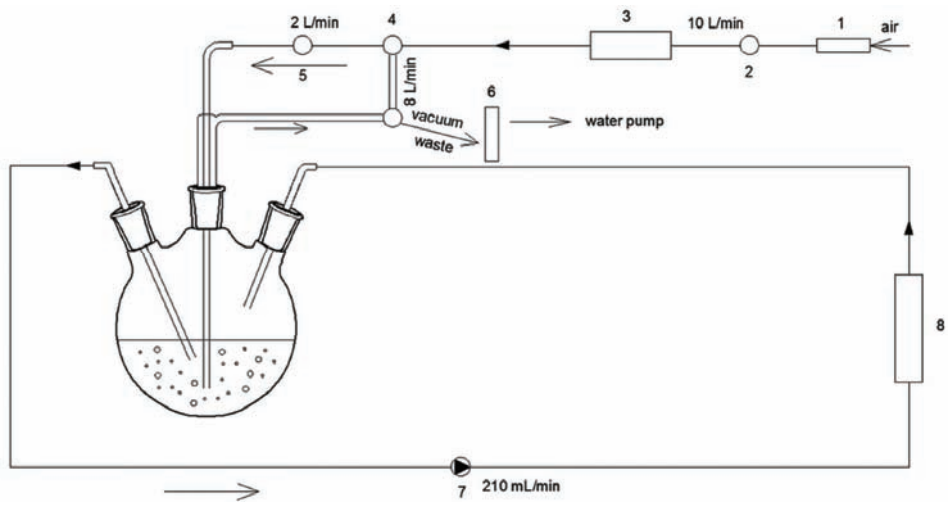

Fig. 1. Schematic diagram of the experimental setup: 1) air drying column, 2) rotameter, 3) ozonizator, 4) three-way valves, 5) rotameter, 6) safety glass vessel, 7) peristaltic pump, and 8) UV lamp.

In the experiments where H_2O_2 was used, the concentration of H_2O_2 was adjusted to 20 mmol L^{-1} and the pH value was set to 9. The removal efficiency was monitored after 5, 10, 20, and 30 minutes from the start of the treatment.

Optimization of the TLC method

To obtain optimal thin-layer efficiency, several parameters were evaluated, including the choice of mobile phase and plate type. Commercially available precoated C 18 plates were chosen as the stationary phase. The applicability of C 18 plates was already suggested in a previous paper when the possibility of separating different mono- and poly-substituted phenols under reversed phase chromatographic conditions was investigated.[10] The reversed phase proved to be good choice for the determination of the partition coefficients of phenols.[10] High performance thin-layer plates (HPTLC C 18 plates) were also investigated, but *p*-chlorophenol eluted with the solvent front and the peak shape was poor. The desired symmetrical and reproducible peak shape was achieved using conventional reversed-phase C 18 plates.

The selection of a suitable mobile phase involved several trials. Different concentrations of standard solution (15–100 ppm) were spotted onto C 18 TLC plates and run in different solvent systems. Different organic modifiers were used in different ratios with water as the mobile phase. Initially, acetonitrile and methanol in different ratios as mobile phase modifiers were selected. Then, mobile phase composition was modified and acetone as solvent modifier gave the optimal chromatogram and a suitable retardation factor, R_F, value. Triethylamine (TEA) and silanol blocking agents were tested as mobile phase additives to reduce zone tailing and improve peak shape, as it was already emphasized in a previous paper.[12] Finally, the optimum mobile phase consisting of acetone:water:TEA in the ratio 60:38:2 (v/v/v) was chosen.

RP TLC densitometric analysis

A standard stock solution containing 100.0 mg L^{-1} of *p*-chlorophenol was freshly prepared in ultrapure water. Five standard solutions (15–100 ppm) were prepared by serial dilution of the standard stock solution. To prepare a calibration curve, aliquots of 5 µl of the standard solutions were applied on the C 18 TLC plate along with the treated water samples (5 µl). Solutions were spotted as bands with a Camag (Muttenz, Switzerland) microlitre syringe onto a RP 18 TLC plates 10 cm×10 cm (1.05559, Merck (Darmstadt, Germany) using a Camag Linomat V sample applicator. A constant application rate (dosage speed 50 nL s^{-1}) was employed.

Linear ascending development was realized in a Camag twin-trough glass development chamber saturated with the mobile phase. The optimum chamber saturation time for the mobile phase was 15 min at room temperature. The plates were developed up to 8 cm. Subsequent to the development TLC plates were dried at room temperature. The plates were scanned with a Camag TLC Scanner 3 with Wincats integration software. Densitometric scanning was performed in the absorbance mode at 240 nm with slit dimensions of 6.00 × 0.30 mm and a scanning speed of 20 mm s^{-1}. A deuterium lamp was used as the radiation source. From the respective calibration curves obtained by plotting the concentrations of standards against the corresponding peak areas, the amounts of *p*-chlorophenol in the water samples were determined.

HPLC Analysis

The HPLC system consisted of a Waters 1525 Binary HPLC pump and a Waters 2487, Dual λ absorbance detector. System management and data acquisition were accomplished with Empower software. The compounds were separated on a Symmetry® 5 µm C 18, Waters column (150 mm× 4.6 mm, 5 µm particle size). Standard solutions of *p*-chlorophenol (5, 10,

25, 50, and 100 ppm) and treated water samples were injected (10 μL) after equilibration of the column. Samples were filtered through 0.45 μm filter prior to analysis. Chromatography was performed at room temperature and the eluate was monitored at 280 nm. A binary mixture of acetonitrile and water was used as the mobile phase at a flow rate of 1 ml min^{-1}. The initial mobile phase was a mixture of acetonitrile and water 30:70 (v/v); then a linear gradient increasing to 80 % acetonitrile in 20 min was applied. For identification and quantitative determination of the *p*-chlorophenol remaining in the water samples, retention time (t_R) and UV spectra were compared with the retention time and UV spectra of the standard solution (t_R = 7.6 min).

Validation procedure of the TLC Method

Validation of the optimized TLC method was performed with respect to the following parameters.

Linearity and range. From the standard stock solution (100.0 mg L^{-1}) of *p*-chlorophenol, standard solutions were prepared, and 5μL of each solution were spotted on a TLC plate to obtain a final concentration of 75–500 ng per band. Each concentration was applied three times on the TLC plate. The plate was then developed using the previously described mobile phase and the peak areas were plotted against the corresponding concentrations to obtain the calibration curves.

Precision. The repeatability of the method was assessed by analysis of the 375 ng per band of standard solution of *p*-chlorophenol (n = 6) and is expressed as the relative standard deviation (*RSD*, %) and standard error (*SE*) of the peak areas. The variability of the method was studied by analyzing standard solutions of *p*-chlorophenol (250, 375, and 500 ng per band) three times on the same day (intra-day precision) and for three times on three different days over a period of one week (inter-day precision); results were again expressed as *RSD*, %. The instrument precision was assessed by scanning the same band of *p*-chlorophenol (375 ng) six times and is expressed as *RSD*, % of the peak area.

Limit of detection and limit of quantification. The limit of detection (*LOD*) and limit of quantification (*LOQ*) represent the concentrations of the analyte that would yield signal-to-noise ratios of 3 for *LOD* and 10 for *LOQ*. To determine the *LOD* and *LOQ*, serial dilutions of standard solutions were made from the standard stock solution in the range of 75–500 ng per band.

Specificity. The specificity of the method was determined by analyzing a standard solution of *p*-chlorophenol and wastewater samples. The R_F values and the obtained spectra of samples and standard solution were compared. The peak purity was accessed by comparing the spectra at peak start, peak apex and peak end positions of band.

Accuracy. The accuracy of the method was studied by performing experiments using the standard addition technique. Varying amount of standard was added to previously analyzed samples and accuracy was determined at three different levels (50, 80 and 100 %). Known amounts of *p*-chlorophenol (100, 150 and 200 ng) were added to a treated wastewater sample. The results of the recovery are expressed as %.

Robustness. The robustness of the method was studied by introducing small changes (± 0.2 mL for each component) in mobile phase composition (acetone:water:TEA 60:40:2, 60:36:2, 58:38:2 and 62:38:2, v/v/v). The time from spotting to chromatography and from chromatography to scanning was varied from ±10 min. The robustness of the method was determined at a concentration level of 375 ng per band.

RESULTS AND DISCUSSION

Wastewater samples were successively treated for the degradation study using five different sets of conditions: UV, H_2O_2/UV, O_3/H_2O_2/UV, O_3 and O_3/UV. Samples were tested at certain time intervals (5, 10, 20 and 30 min). As expected, concentration of *p*-chlorophenol decreased as a function of the length of time during which the degradation was performed. Degradation products, *i.e.* organic acids (formic acid, acetic acid, and oxalic acid) and chloride intermediates were monitored and quantified using ion chromatography.

Quantitative analysis of p-*chlorophenol by TLC*

Different concentrations of *p*-chlorophenol were plotted against peak area to obtain a calibration plot. A 5-μl aliquot of the treated water samples were applied along with standard solution of *p*-chlorophenol. A representative 3D chromatogram of the standard (tracks 1–3, 12, and 13) and wastewater samples treated by usage of O_3 (tracks 4–7) and O_3/UV, (tracks 8–11), pH = 9 is shown in Fig. 2. The application position was Y = 10.0 mm; band length = 6.0 mm.

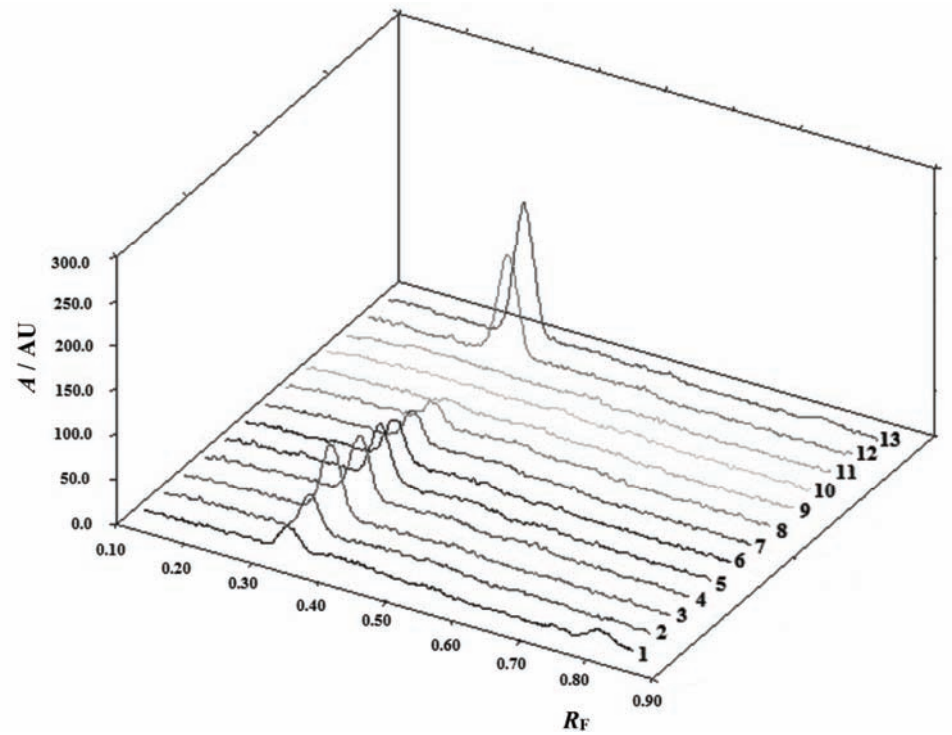

Fig. 2. 3D TLC Densitogram at 240 nm of *p*-chlorophenol standard solutions (tracks 1–3, 12 and 13) and wastewater samples treated with O_3 (tracks 4–7) and O_3/UV (tracks 8–11).

The identity of *p*-chlorophenol in different samples was confirmed by comparing the R_F value and UV spectrum of the peak of the standard with the corresponding peak from the sample. The peaks corresponding to *p*-chlorophenol were on the same R_F value (0.32). The TLC chromatogram of *p*-chlorophenol with the corresponding R_F at 240 nm is depicted in Fig. 3. Comparison of the absorption spectra of *p*-chlorophenol from the standard (250 ng per band) and treated water sample (O_3), measured on the TLC plate (data resolution step = 10 nm) is given in Fig. 4.

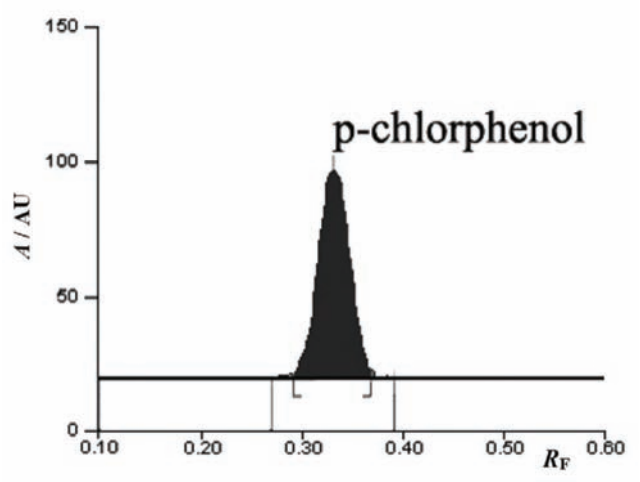

Fig. 3. TLC Densitogram peak display of *p*-chlorophenol standard, 250 ng per band (track 3, R_F 0.32±0.02).

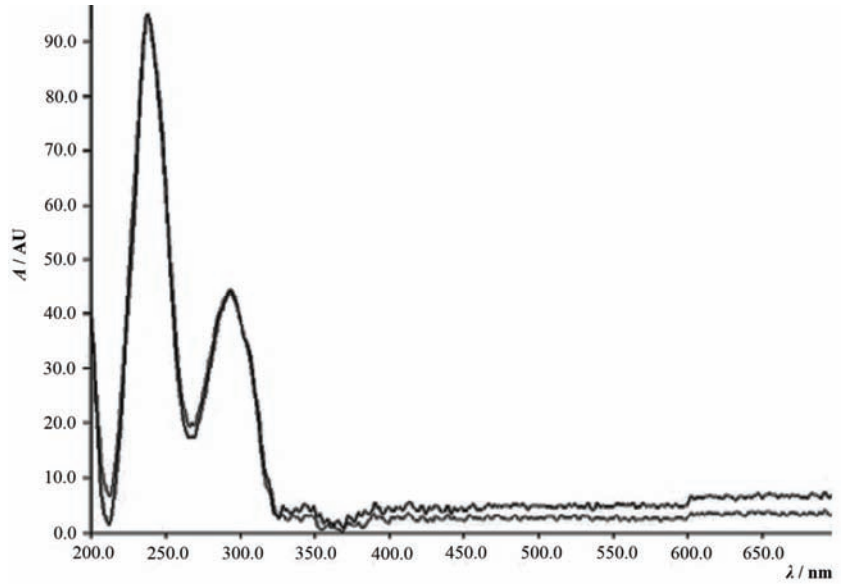

Fig. 4. Overlaid absorption spectrum of *p*-chlorophenol standard and a treated water sample.

Validation of the TLC method

The standard response was linear (r = 0.99986, SD = 1.29) over the concentration range between 75–500 ng per band. The linear regression equation was represented as $Y = 7.63X + 27.39$, where X is concentration of *p*-chlorophenol in ng per band and Y is the peak area.

The results of the repeatability and intermediate precision experiments are given in Table I. The developed method was found to be precise as the *RSD* values for the repeatability and intermediate precision studies were <2 %.

TABLE I. Precision studies for *p*-chlorophenol; instrument precision: 372.2±3.9 (1.0 %)

Taken ng per band	Intra-day (n = 3)		Inter-day (n = 3×3)	
	Measured concentration±*SD* ng	*RSD* / %	Measured concentration±*SD* ng	*RSD* / %
250	252.0±2.1	0.8	251.0±2.9	1.2
375	372.9±2.5	0.7	373.7±2.0	0.5
500	502.0±1.3	0.2	501.2±2.5	0.5

The *LOD* and *LOQ* were calculated from the equations $LOD = 3 \times N/B$ and $LOQ = 10 \times N/B$, where N is the *SD* of the peak area of the standard, taken as a measure of the noise, and B is the slope of the corresponding calibration curve. The *LOD* and *LOQ* were found to be 11 and 35 ng per band, respectively. The method was found to be specific for *p*-chlorophenol.

As shown in Table II, good recoveries of *p*-chlorophenol in the range from 99.2 to 100.5 % were obtained for various added concentrations. The average recovery of three levels (nine determinations) was 98.6 %.

TABLE II. Results of the recovery study (n = 3, ng per band); amount in sample: 182.6 ng per band

Amount in sample	Total amount	Amount detected	Recovery, %
100 (50 % level)	282.6	283.3 ± 1.2	100.2 ± 0.4
150 (80 % level)	332.6	334.4 ± 3.1	100.5 ± 0.9
200 (100 % level)	382.6	379.8 ± 2.2	99.2 ± 0.6

The low values of the *RSD*, given in Table III, indicate the robustness of the method. No significant change in the R_F of *p*-chlorophenol was observed when the composition of the mobile phase was changed slightly. In addition, changing the time interval between chromatography, spotting and scanning had no impact.

TABLE III. Robustness testing (n = 3)

Parameter	*SD* of peak area	*RSD* / %
Mobile phase composition (± 0.2 mL)	2.7	0.7
Time from spotting to chromatography (± 10 min)	3.3	0.9
Time from chromatography to scanning (± 10 min)	3.8	1.0

The standard deviation of the peak areas was calculated for each parameter and the *RSD* was found to be less than 2 %.

Comparison of TLC and HPLC results

The concentration of *p*-chlorophenol remaining in the treated wastewater samples was determined using two different reversed-phase chromatographic methods, TLC densitometry and HPLC with UV detection. The percent degradation of *p*-chlorophenol as a function of the irradiation time, monitored by TLC and HPLC are illustrated in Figs. 5A and 5B, respectively. The results obtained by these two methods were treated as paired data and were compared by the matched pair Student's *t*-test. The calculated *t*-value was 0.40, *i.e.*, below the critical two-tail *t* value of 3.18. Hence, it was concluded that both methods gave comparable results for the analysis of *p*-chlorophenol degradation.

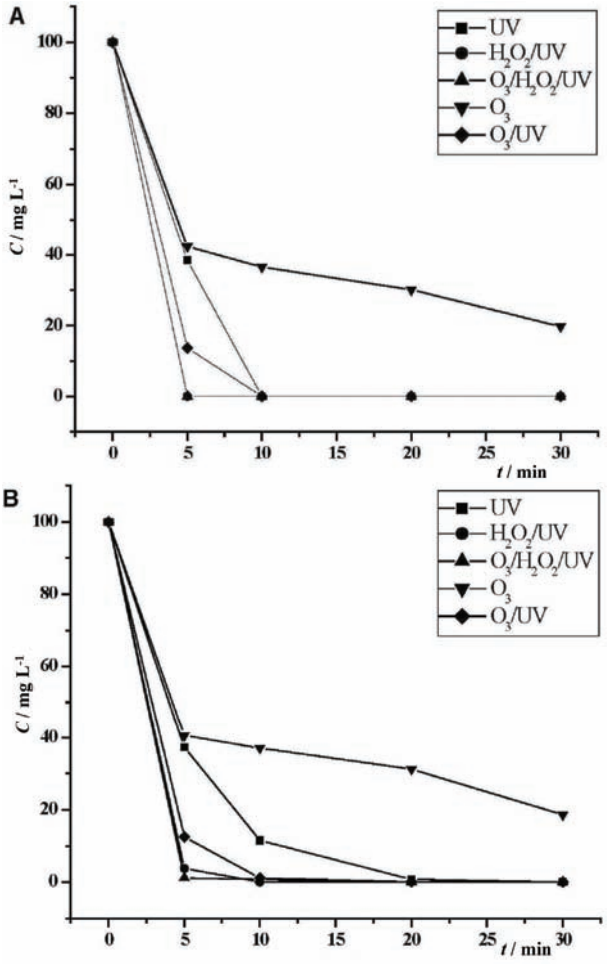

Fig. 5. The change of *p*-chlorophenol concentration as a function of the time using different AOPs, monitored by TLC (A) and HPLC (B).

CONCLUSIONS

The concept of this study was to develop a TLC densitometric method for both qualitative and quantitative determination of *p*-chlorophenol in wastewater samples. The proposed method is cheap and simple, and proved to be suitable for the accurate monitoring of degradation efficiency during the treatment of wastewater samples. The almost identical results obtained using TLC and HPLC, led to the conclusion that both methods could be applied for such investigations. However, the developed TLC method is an attractive alternative to HPLC. The fast analysis time, no sample preparation, low solvent consumption (which in ecological sense makes it more acceptable) and the possibility of analyzing several samples simultaneously, make the TLC the method of choice. In view of the importance of wastewater purification, the proposed method might find many direct applications and could be widely applied for routine analysis of related compounds under environmental control.

Acknowledgement. This work was performed within the framework of the research project No. 172017 supported by the Ministry of Education, Science and Technological Development of the Republic of Serbia.

И З В О Д

ВАЛИДАЦИЈА ТАНКОСЛОЈНЕ ХРОМАТОГРАФИЈЕ КАО МЕТОДЕ ЗА ЈЕДНОСТАВНО ОДРЕЂИВАЊЕ *p*-ХЛОРФЕНОЛА У ТРЕТИРАНОЈ ОТПАДНОЈ ВОДИ

МАЈА НАТИЋ[1], ДРАГАНА ДАБИЋ[2], ДУШАНКА МИЛОЈКОВИЋ-ОПСЕНИЦА[1], БИЉАНА ДОЈЧИНОВИЋ[3], ГОРАН РОГЛИЋ[1], ДРАГАН МАНОЈЛОВИЋ[1] и ЖИВОСЛАВ ТЕШИЋ[1]

[1]Хемијски факултет, Универзитет у Београду, п. пр. 51, 11158 Београд, [2]Иновациони центар Хемијског факултета, Универзитет у Београду, Студентски трг 12–16, 11158 Београд и [3]Институт за хемију, металургију и технологију, Универзитет у Београду, Његошева 12, 11000 Београд

Квантификација *p*-хлорфенола у узорцима отпадних вода урађена је применом танкослојне хроматографије са денситометријском детекцијом. Ефикасност деградације *p*-хлорфенола праћена је након сваког третмана узорка отпадне воде. UV светлост, O_3, као и комбинација H_2O_2/UV, O_3/H_2O_2/UV и O_3/UV су коришћени за деградацију *p*-хлорфенола. Примењен TLC поступак је једноставан, брз и прецизан. Висока осетљивост (лимит детекције је 11 ng по траци и лимит квантификације је 35 ng по траци), опсег линеарности (од 75 до 500 ng по траци, r = 0,9965), висока прецизност и тачност, као и специфичност су карактеристике коришћеног TLC поступка. HPLC метода, као стандардна метода за одређивање *p*-хлорфенола је такође примењена за проучавање ефикасности поступка деградације. Резултати добијени применом TLC методе су упоредиви са HPLC мерењима.

(Примљено 9. маја, ревидирано 30. августа 2012)

REFERENCES

1. P. N. Moza, K. Fytianos, V. Samanidou, F. Korte, *Bull. Environ. Contam. Toxicol.* **41** (1988) 678
2. J. Michałowicz, W. Duda, *Pol. J. Environ. Stud.* **16** (2007) 347

3. R. L. Droste, *Theory and practice of water and wastewater treatment*, Wiley, New York, USA, 1997, p. 219
4. W. Z. Tang, *Physicochemical treatment of hazardous wastes*, Lewis Pub., Boca Raton, FL, USA, 2003
5. D. Manojlovic, D. R. Ostojic, B. M. Obradovic, M. M. Kuraica, V. D. Krsmanovic, J. Puric, *Desalination* **213** (2007) 116
6. I. Oller, S. Malato, J. A. Sánchez-Pérez, *Sci. Total Environ.* **409** (2011) 4141
7. C. A. Somensi, E.L. Simionatto, S. L. Bertoli, A. Wisniewski Jr., C. M. Radetski *J. Hazard. Mater.* **175** (2010) 235
8. I. Baranowska, C. Pieszko, *J. Planar Chromatogr.* **11** (1998) 119
9. S. Babić, M. Petrović, M. Kastelan-Macan, *J. Chromatogr. A* **823** (1998) 3
10. F. Lj. Andrić, J. D. Trifković, A. D. Radoičić, S. B. Šegan, Ž. Lj. Tešić, D. M. Milojković-Opsenica, *Chemosphere* **81** (2010) 299
11. C. J. Welch, N. Wu, M. Biba, R. Hartman, T. Brkovic, X. Gong, R. Helmy, W. Schafer, J. Cuff, Z. Pirzada, L. Zhou, *Trends Anal. Chem.* **29** (2010) 667
12. S. Ilić, M. Natić, D. Dabić, D. Milojković-Opsenica, Ž. Tešić, *J. Planar Chromatogr.* **24** (2011) 93.

Journal of the Serbian Chemical Society
JSCS-info@shd.org.rs • www.shd.org.rs/JSCS
J. Serb. Chem. Soc. 77 (11) 1661–1670 (2012)
JSCS–4379
UDC 628.316.12:546.47+66.067.1
Original scientific paper

Zinc removal from wastewater by a complexation–microfiltration process

KATARINA TRIVUNAC[1]*, ZORAN SEKULIĆ[2] and SLAVICA STEVANOVIĆ[1]

[1]*University of Belgrade, Faculty of Technology and Metallurgy, Department of Analytical Chemistry and Quality Control, Karnegijeva 4, 11120 Belgrade, Serbia and* [2]*Institute of Public Health of Belgrade, Bul. Despota Stefana 54a, 11000 Belgrade, Serbia*

(Received 2 March, revised 19 April 2012)

Abstract: Due to its wide industrial applications, zinc has become an important contaminant in aquatic environments since it is a toxic heavy metal and some of its compounds, such as zinc arsenate and zinc cyanide, may be extremely hazardous. Therefore, there is a growing need to develop simple methods capable of separating and recovering trace zinc from environmental waters. Nowadays, ultra- and microfiltration methods for trace metals removal from waters by the addition of a water-soluble polymer into the aqueous solutions have become a significant area of research. The choice of water-soluble macroligands remains important for the development of this technology. Sodium carboxymethyl cellulose (Na-CMC) was selected as the complexing agent. The microfiltration experiments were performed in a stirred dead-end cell. Versapor membranes were used to separate the formed polymer–metal complex. The concentration of heavy metal ions after microfiltration in aqueous solution was determined using atomic absorption spectroscopy (AAS). The effects of the amount of complexing agent, pH value, type of anion, ionic strength and operating pressure on the flux (J) and rejection coefficient (R) were investigated. Experimental results indicate a considerable influence of the pH, ionic strength and type of anion on the rejection coefficient, while the effect of the amount of the complexing agent was relatively insignificant. The Na-CMC used in the research proved very effective, which is supported by the high rejection coefficients obtained (99 %).

Keywords: microfiltration; complexation; heavy metal ions; wastewater treatment.

INTRODUCTION

Zinc is an essential heavy metal for biological functions; however in high concentrations, it can be harmful to people and animals. The toxicity of heavy metal contamination, however, is highly dependent on the chemical form of the

* Corresponding author. E-mail: trivunac@tmf.bg.ac.rs
doi: 10.2298/JSC120302037T

metal in question. Dissolved free ions are more toxic than metals that are bound in particles or to organic compounds. Zinc is naturally present in water. Industrial wastewaters containing zinc stem from galvanic industries, battery production, *etc*. Zinc compounds are applied for many different purposes. Zinc chloride is applied for parchment production, zinc oxide is a constituent of salves, paints and catalysts, and zinc vitriol is applied as a fertilizer. Zinc leaks from zinc pipes and rain pipes, consequential to the circulation of carbon-rich water. Car tires containing zinc and motor oil from zinc tanks release zinc compounds on roads. Zinc compounds are present in fungicides and insecticides, and consequently end up in water. When inadequate safety measures are taken, zinc may be emitted from chemical waste dumps and landfills, or from dredge mortar.

Zinc may be removed from water by different methods. To achieve a level that meets legal standards, techniques such as coagulation, ion exchange, sand filtration and active carbon may be applied.[1]

The continuous increase of world needs for most of the known metals, the decrease in the grade of the available ores and strict environmental regulations make it of interest to find effective and efficient methods for processing waste solutions containing metal ions, even at very low concentrations. The efficient and selective separation of heavy metal ions can be achieved by using water-soluble macroligands in combination with membrane filtration.[2] The use of membrane separation processes in the treatment of wastewater containing toxic metal ions is today an attractive and suitable technique, and is easily included in the whole process. For this reason, membrane separations are being employed more and more frequently. Moreover, the separation can be performed at room temperature; the modular membrane surface can be easily adjusted to the wastewater flow and various industrial membranes are now available. In order to retain metallic ions, reverse osmosis (or at least nanofiltration) can be used due to the size of the ions in aqueous solutions. However, the usual permeate fluxes of reverse osmosis membranes are limited and require high transmembrane pressure, which makes the process expensive.[3] There are two widely used separation techniques among the membrane methods for the removal of heavy metal ions from aqueous solutions: micellar enhanced ultrafiltration (MEUF) and polyelectrolyte ultrafiltration (PEUF). MEUF[4–7] and PEUF[8–26] combine ultrafiltration with the presence of water-soluble surfactants and polymers, respectively. The enhanced ultrafiltration processes have the advantages of operation at relatively low pressures and temperatures, resulting in excellent rejection of multivalent metals and organics. PEUF is the combination of two phenomena, the binding of metal ions to a water-soluble natural or synthetic polyelectrolyte, and ultrafiltration. Since the pore size of ultrafiltration membranes are not suitable to separate heavy metal ions, water-soluble polymers are used to bind the metals to form macromolecular complexes rejected by ultrafiltration.

THEORY AND EXPERIMENTAL

The removal and rejection of heavy metal ions from aqueous solutions has been traditionally carried out by chemical precipitation, ion exchange, adsorption, *etc*. Nowadays, ultra- and microfiltration methods for trace metals removal from waters by the addition of a water-soluble polymer into the aqueous solutions have become a significant research area. This method is based on the principles that polymers with a large molecular weight could bind heavy metal ions to form macromolecular complexes. Their metal complexes could then be retained and concentrated by a microfiltration membrane, whereas unbound metal ions would pass through the membrane. Up to now, many polymers, such as poly(vinyl alcohol) and sulfonated poly(vinyl alcohol),[8,9] poly(ammonium acrylate),[10] poly(acrylic acid),[11–13] polyethylenimine,[13–17] diethylaminoethyl cellulose,[18] poly(4-vinylpyridine) and poly(diallyl dimethylammonium) chloride,[21] poly(vinyl sulfonic acid),[22] partially ethoxylated polyethylenimine[23,24] and chitosan and pectin[15,25] have been used for metal removal from wastewaters.

Sodium carboxymethyl cellulose (Na-CMC) is a derivative of cellulose that is colorless, odorless and tasteless, physiologically inert, chemically stable, not dangerous for health or the environment and is water-soluble. It also possesses good complexation ability for some metal ions and was chosen as the macromolecular complexing agent for the selective removal and rejection of copper from water in a complexation–microfiltration process.[20]

The aim of the present research was to evaluate the efficiency of Na-CMS in the removal of zinc ions from water. The experiments were conducted on two model solutions, $ZnCl_2$ (solution 1) and $Zn(CH_3COO)_2$ (solution 2) in order that the influence of the anion be investigated. The initial concentration of zinc ions in both solutions was 50.00 mg dm^{-3}. The microfiltration experiments were performed in a stirred dead-end cell Millipore 8050. The influence of different experimental parameters, *i.e*., the amount of complexing agent, ionic strength, pH value and operating pressure, on the flux and rejection coefficient were investigated. Versapor polyacrylic membrane 200 filters (Gelman Sciences Inc., USA) were used to separate the formed polymer–metal complex. A feed volume of 25.0 cm^3 of concentration 50.0 mg Zn dm^{-3} and the desired Na-CMC concentration were prepared and stirred for 1 h at room temperature before filtration. Experiments with longer mixing time demonstrated that 1 h was sufficient to reach the complexation equilibrium. The pH was adjusted with HCl and NaOH solutions. The concentration of heavy metal ions in aqueous solution after microfiltration was determined using atomic absorption spectroscopy (Pye Unicam SP9, Philips) at 213.9 nm.

RESULTS AND DISCUSSION

The effects of the amount of complexing agent, ionic strength, pH value and operating pressure on the flux and rejection coefficient were investigated.

The flux, *J*, of solution containing Zn(II)-ions was calculated from equation:

$$J = \frac{V}{A\tau} \tag{1}$$

where *V* is the volume of the permeate, *A* is the effective membrane area and τ is time.

The rejection, *R*, of Zn-ions was calculated from equation:

$$R = 100\left(1 - \frac{c_p}{c_f}\right) \quad (2)$$

where c_p and c_f are the concentrations of zinc ions in the permeate and feed, respectively.

Effect of pressure

The effect of applied pressure was investigated at a fixed initial concentration of zinc ions of 50.0 mol dm^{-3}, pH 9.0 and pressure of nitrogen in the range 100–400 kPa.

The flux of the solute was lower than that of pure water. From the shape of the curve in Fig. 1, it could be concluded that no sharp change in the curve of flux *vs*. pressure was found, although the flux was still a slight function of pressure at higher pressure. This indicates that a concentration polarization exists but no plateau was reached; hence, the gel-polarization effect was not dominant for the polymer in the pressure range studied.

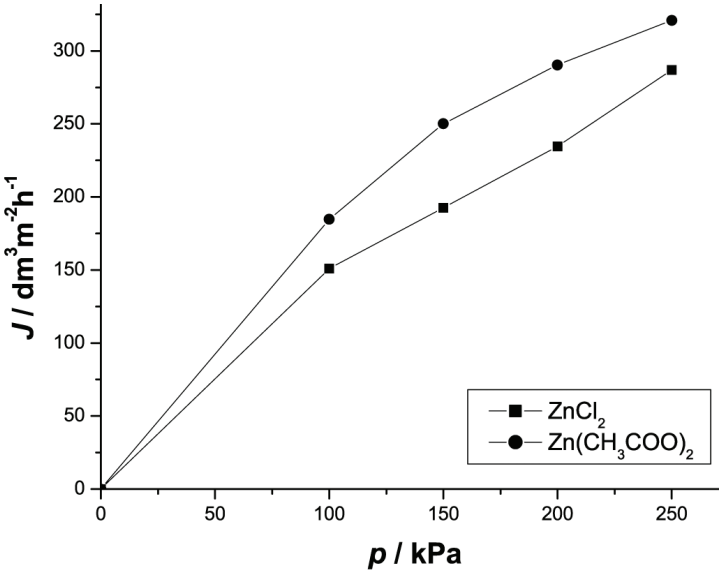

Fig. 1. Effect of pressure on the flux. Versapor membrane, c_{zn} = 50.0 mg dm^{-3}, $c_{Na\text{-}CMC}$ = 75.0 mg dm^{-3}.

Effect of sample pH on the rejection of zinc

The effects of the solution pH in the range 2.0–9.0, at a fixed concentration of zinc ions of 50.0 mg dm^{-3} and pressure of 100 kPa were evaluated.

A strong influence of the pH of the solution on the retention was observed in complexation-microfiltration process. Increasing the pH leads to an increase in

the concentration of deprotoned carboxylic groups, which favors the formation of macromolecular polymer–metal complexes and subsequently increases in the metal rejection coefficients. As can be seen in Fig. 2, the rejection of zinc was increased with increasing pH value until the rejection reached its maximum (99 %) at pH 8.0 and then a flat profile was maintained when the pH was changed to 10.0. With increasing pH, more and more carboxymethyl groups dissociate gradually and complex with zinc ions. At low pH values, a large number of the H_3O^+ groups occupy the positions, which prevent the target zinc ions from form complexes with Na-CMC.

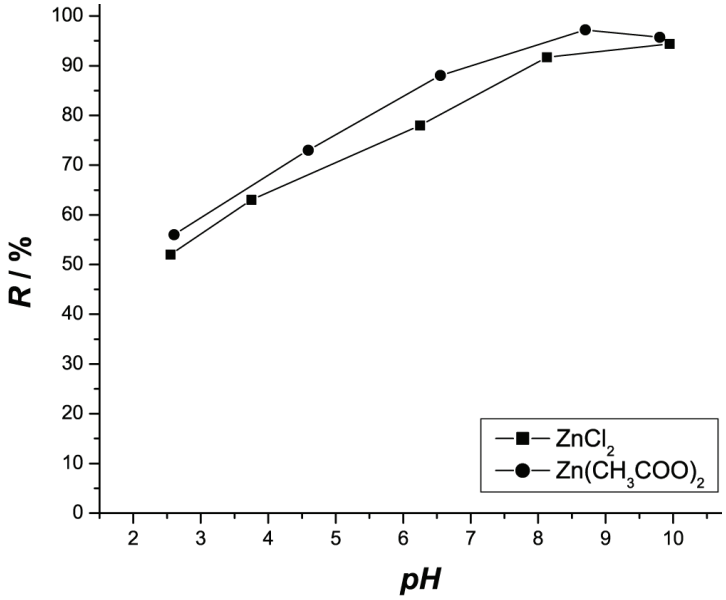

Fig. 2. Effect of pH on the retention. Versapor membrane, c_{zn} = 50.0 mg dm^{-3}, p = 100 kPa, $c_{Na\text{-}CMC}$ = 75.0 mg dm^{-3}.

Effect of polymer concentration on zinc ion retention

The effect of the Na-CMC concentration on zinc removal was studied at pH 6.8 and 8.3 using solutions 1 and 2 containing 50.0 mol dm^{-3} of Zn and the concentration of Na-CMC was varied in range of 35.0–300.0 mg dm^{-3}.

The retention values of Zn(II) at different Na-CMC concentrations at pH 6.3 for both solutions are plotted in Fig. 3, from which it could be seen that the retention of Zn(II) remained almost constant at a value of around 89 % for all employed Na-CMC concentrations. It was also shown that the rejection of Zn(II), was not significantly affected by the Na-CMC concentration. Moreover, it was found that Na-CMC even at a very low concentration has the capability to bind with the metal to form macromolecular complexes as an effective complexing

agent. The explanation of this behavior is that equilibrium existed between free zinc ions, Na-CMC molecules and the formed complexes, and indicates that Na-CMC could be employed as a very effective water-soluble polymer for the removal of zinc(II).

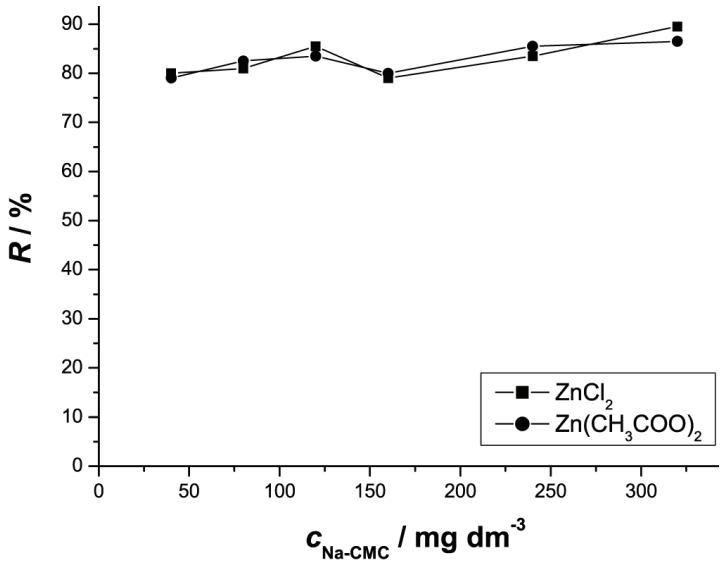

Fig. 3. Effect of different concentrations of Na-CMC on the retention at pH 6.8. Versapor membrane, c_{zn} = 50.0 mg dm^{-3}, p = 100 kPa.

A similar behavior was observed at pH 8.3 (Fig. 4). The retention remained almost constant at a value of around 85 % for solution 1 and 97 % for solution 2. Besides the influence of pH, the presence of the carboxyl anion in solution 2 affects the stability of the formed complexes and thus increases the retention of this solution.

Effects of ionic strength on the retention

The ionic strength of an aqueous stream may greatly affect the effectiveness of polymer-assisted microfiltration processes. Increasing the salt concentration leads to compression of the electrical double layer and thus to a reduction in the electrostatic attraction between ions and charged polymers. As a result, the unbound metals in the solution pass through the membrane leading to lower retention.[25]

The effect of ionic strength on Zn(II) retention was examined at pH 6.8 and 8.3 by adding increasing amount of $NaNO_3$ into the solution. The effect of ionic strength on Zn(II) retention was observed to be more pronounced at pH 6.8 than at pH 8.3, especially at high salt concentrations.

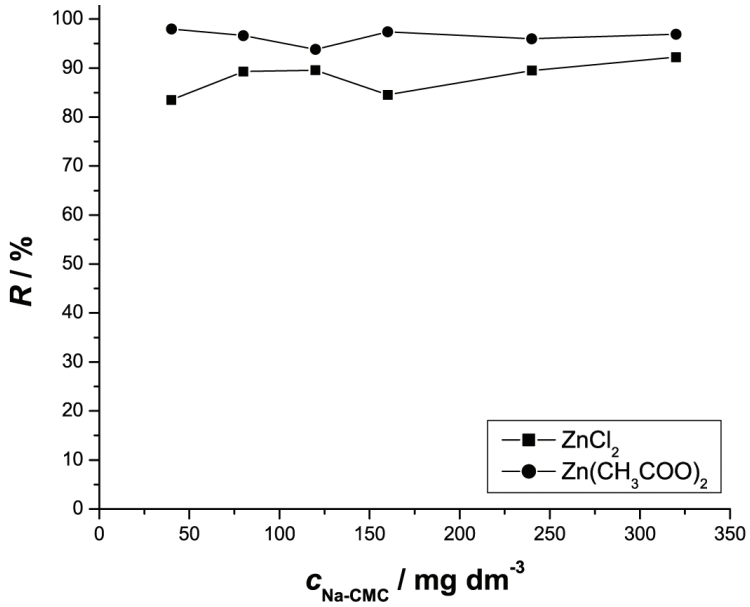

Fig. 4. Effect of different concentrations of Na-CMC on the retention at pH 8.3. Versapor membrane, c_{zn} = 50.0 mg dm^{-3}, p = 100 kPa.

As shown in Fig. 5, at pH 6.8, the rejection decreased sharply in the presence of 0.05 mol dm^{-3} with a reduction of 40 and 50% for solutions 1 and 2, respectively. On increasing the salt concentration (up to 0.5 mol dm^{-3} $NaNO_3$), no further decline of the retention was observed. These results can be explained by a conformational change of the polymer chains, a competitive adsorption between Na and Zn ions on the negatively charged polymer and an attenuation of the electrostatic repulsion. It is well known that negatively charged polyelectrolytes interact with positively charged divalent metal ions stronger than with monovalent ions.[26] Nevertheless, the filtration of metal ions and their subsequent release from the polymer induces an increase of the net negative charge on the polymer surface and then an expansion of the chains in order to increase the total surface, thereby minimizing the electrostatic repulsions. Related with this, the decrease on the surface charge density of the polymer induces a decrease in the strength of the interactions with the metal ions and, consequently, their easier release to the solution from the polymer domain during filtration.

At pH 8.3, the effect of salt addition was observed over a wider concentration range, *i.e.*, between 0.05 and 1.0 mol dm^{-3} $NaNO_3$. As shown in Fig. 6, at pH 8.3, the addition of 0.05–0.1 mol dm^{-3} $NaNO_3$ caused only a 1–3 % decrease in the retention values. Since Zn(II)–Na-CMC complexation is more favorable at pH 8.3 and the bond is probably stronger than the one formed at pH 6.8, it can withstand changes in ionic strength. On increasing the salt concentration to 0.5

mol dm^{-3} $NaNO_3$, the retention dropped by around 28 % for both solutions. On the increasing the salt concentration further to 1.0 mol dm^{-3} $NaNO_3$, the slight increase in the rejection by 2–5 % is relatively insignificant.

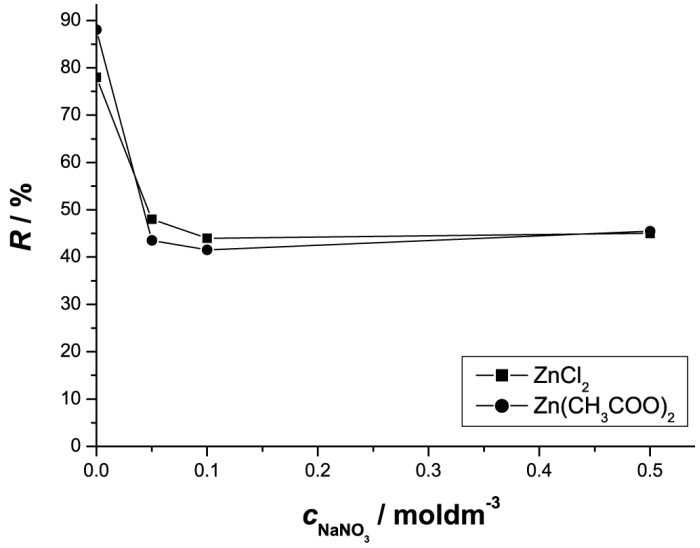

Fig. 5. Effect of ionic strength on the retention at pH 6.8. Versapor membrane, c_{zn} = 50.0 mg dm^{-3}, p = 100 kPa, $c_{Na\text{-}CMC}$ = 75.0 mg dm^{-3}.

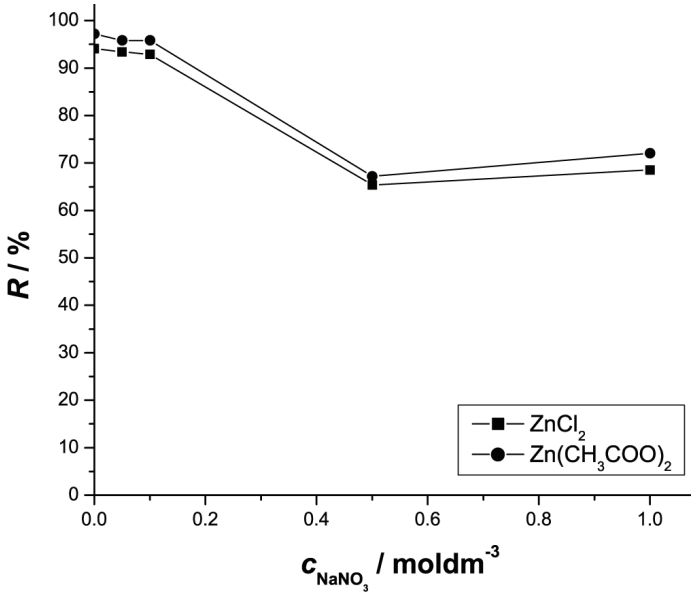

Fig. 6. Effect of ionic strength on the retention at pH 8.3. Versapor membrane, c_{zn} = 50.0 mg dm^{-3}, p = 100 kPa, $c_{Na\text{-}CMC}$ = 75.0 mg dm^{-3}.

CONCLUSIONS

A complexation–microfiltration process was successfully applied for removal of Zn(II) ions from synthetic wastewater solutions. A polyacrylic membrane was used for filtration process, while sodium carboxymethyl cellulose was used as the metal complexing agent. It was shown that the complexation and filtration processes were pH dependent, the metal rejection was more efficient at neutral and alkaline conditions than at acidic ones. The Na-CMC used in the research proved to be very effective, which is evidenced by the high retention coefficients obtained. It was found that even at very low concentrations, Na-CMC has the capability to bind with zinc ions to form macromolecular complexes and is thus an effective complexing agent. The effect of ionic strength on Zn(II) retention was observed to be more pronounced at pH 6.8 than at pH 8.3, especially at high salt concentrations. Influence of anions proved to be very important for complexation process and stability of formed complexes.

The process is characterized by low-energy requirements involved in the microfiltration, very fast reaction kinetics and high selectivity for the metal ion separation. For developing a practical process, other important factors and operational parameters, such as different concentration of metal ions, mixture of metal ions, different anions, other membranes, *etc*., must be studied.

Acknowledgement. This work was financially supported by the Ministry of Education, Science and Technological Development of the Republic of Serbia (Project No. ON 172007).

И З В О Д

УКЛАЊАЊЕ ЦИНКА ИЗ ОТПАДНИХ ВОДА КОМПЛЕКСИРАЈУЋЕ-МИКРОФИЛТРАЦИОНИМ ПРОЦЕСОМ

КАТАРИНА ТРИВУНАЦ[1], ЗОРАН СЕКУЛИЋ[2] и СЛАВИЦА СТЕВАНОВИЋ[1]

[1]Универзитет у Београду, Технолошко–металуршки факултет, Катедра за аналитичку хемију и контролу квалитета, п. пр.494, Карнегијева 4, 11120 Београд и [2]Градски завод за јавно здравље Београд, Бул. Деспота Стефана 54а, 11000 Београд, Србија

Као резултат његове широке индустријске примене, цинк и његова једињења су постали значајне загађујуће материје водених ресурса. Због тога је постало неопходно развијати нове методе за њихово уклањање, које би биле ефикасне, једноставне и нешкодљиве по животну средину. Међу њима, метода мембранске филтрације се показала као веома успешна за уклањање различитих загађујућих материја, посебно у комбинацији са макромолекулима. Велики број истраживања усмерен је на избор селективног и специфичног макромолекула. У раду је проучаван комплексирајуће-филтрациони процес за уклањање јона цинка помоћу натријум-карбоксиметил целулозе. Микрофилтрација је вршена у ћелији са мешањем. Сепарација формираних комплекса је вршена на Версапор микрофилтрационим мембранама. Концентрација јона метала после микрофилтрације је одређена атомском апсорпционом спектроскопијом. Испитани су утицаји количине комплексирајућег средства, pH вредности раствора, радног притиска, јонске јачине и анјона на флукс и коефицијент задржавања. Експериментални резултати су показали значајан утицај pH, јонске јачине и анјона на коефицијент задржавања, док концентра-

ција комплексирајућег средства није имала значајан утицај на процес. Натријум карбоксиметил целулоза се показала као успешно средство за уклањање јона цинка што се може закључити на основу постигнутог веома високог коефицијента задржавања јона цинка од 99 %.

(Примљено 2. марта, ревидирано 19. априла 2012)

REFERENCES

1. F. Fu, Q. Wang, *J. Environ. Manage.* **92** (2011) 407
2. G. M. Geise, H.-S. Lee, D. J. Miller, B. D. Freeman, J. E. McGrath, *J. Polym. Sci. Part B: Polym. Phys.* **48** (2010) 1685
3. L. F. Greenlee, D. F. Lawler, B. D. Freeman, B. Marrrot, P. Moulin, *Water Res.* **43** (2009) 2317
4. E. Samper, M. Rodríguez, M. A. De la Rubia, D. Prats, *Sep. Purif. Technol.* **65** (2009) 337
5. J. Landaburu-Aguirre, V. García, E. Pongracz, R. L. Keiski, *Desalination* **240** (2009) 262
6. R. S. Juang, Y. Y. Xu, C. L. Chen, *J. Membr. Sci.* **218** (2003) 257
7. E. Samper, M. Rodríguez, I. Sentana, D. Prats, *Water Air Soil Pollut.* **208** (2010) 5
8. L. Dambies, A. Jaworska, G. Zakrzewska-Trznadel, B. Sartowska, *J. Hazard. Mater.* **178** (2010) 988
9. N. Uzal, A. Jaworska, A. Miskiewicz, G. Zakrzewska-Trznadel, C. Cojocaru, *J. Colloid Interface Sci.* **362** (2011) 615
10. D. J. Ennigrou, L. Gzara, M. R. B. Romdhane, M. Dhahbi, *Chem. Eng. J.* **155** (2009) 138
11. R. Camarillo, J. Llanos, L. García-Fernández, Á. Pérez, P. Canizares, *Sep. Purif. Technol.* **70** (2010) 320
12. J. Zeng, H. Ye, Z. Hu, *J. Hazard. Mater.* **161** (2009) 1491
13. R. Molinari, P. Argurio, T. Poerio, *Desalination* **162** (2004) 217
14. D. Zamariotto, B. Lakard, P. Fievet, N. Fatin-Rouge, *Desalination* **258** (2010) 87
15. R. Molinari, T. Poerio, P. Argurio, *Chemosphere* **70** (2008) 341
16. S. Islamoglu Kadioglu, L. Yilmaz, N. Aydogan, H. O. Ozbelge, *Sep. Sci. Technol.* **45** (2010) 1363
17. C. W. Li, C. H. Cheng, K. H. Choo, W. S. Yen, *Chemosphere* **72** (2008) 630
18. K. Trivunac, S. Stevanovic, *Desalination* **198** (2006) 282
19. Z. Wang, Z. Fu, C. Ye, *J. Hazard. Mater.* **170** (2009) 705
20. S. Petrov, V. Nenov, *Desalination* **162** (2004) 201
21. J. D. Roach, R. F. Lane, Y. Hussain, *Water Res*. **45** (2011) 1387
22. M. Palencia, B. L. Rivas, E. Pereira, *J. Membr. Sci.* **345** (2009) 191
23. J. Labanda, M. S. Khaidar, J. Sabaté, J. Llorens, *Desalination* **281** (2011) 165
24. J. Llanos, R. Camarillo, Á. Pérez, P. Canizares, *Sep. Purif. Technol.* **73** (2010) 126
25. R. S. Juang, R. C. Shiau, *J. Membr. Sci.* **165** (2000) 159
26. P. Canizares, A. Pèrez, R. Camarillo, J.J. Linares, *J. Membr. Sci.* **240** (2004) 197.

Journal of the Serbian Chemical Society
JSCS-info@shd.org.rs • www.shd.org.rs/JSCS
J. Serb. Chem. Soc. 77 (11) 1671–1685 (2012)
JSCS–4380
UDC 550.8.04:622.276:66–965.00057
Original scientific paper

Characterisation of weathered petroleum hydrocarbons during a landfarming bioremediation study

SNEŽANA MALETIĆ*, SRĐAN RONČEVIĆ#, BOŽO DALMACIJA#, JASMINA AGBABA#, MALCOLM WATSON, ALEKSANDRA TUBIĆ# and SVETLANA UGARČINA PEROVIĆ

University of Novi Sad, Faculty of Sciences, Trg Dositeja Obradovića 3, 21000 Novi Sad, Serbia

(Received 30 April, revised 3 July 2012)

Abstract: Landfarming bioremediation was performed over 2 years on soil heavily polluted with weathered oil and oil derivatives: 23200 mg kg^{-1} of mineral oil, 35300 mg kg^{-1} total hydrocarbons and 8.65 mg kg^{-1} of total polycyclic aromatic hydrocarbons, PAHs. During the experiment, mineral oil, total hydrocarbon and PAH concentrations decreased by approximately 53, 27 and 72 %, respectively. A GC/MS scan was used to identify the crude oil components that persisted after the bioremediation treatment of the contaminated soil and the metabolites generated during this process. The data shows that in soil contaminated with weathered-hydrocarbons, the number of initially detected compounds after the bioremediation process further decreased over a 2-year period and, concurrently, several new compounds were observed at the end of experiment. Higher persistence was shown by heavier *n*-alkanes and branched alkanes, which could be detected over a longer period. The analysis highlighted the importance of *n*-alkanes, their substituted derivatives and PAHs as the most significant pollutants.

Keywords: weathering; bioremediation; crude oil; GC-MS fingerprint; PAH.

INTRODUCTION

Petroleum hydrocarbons contain a complex mixture of compounds that can be categorized into four fractions: saturates, aromatics, resins and asphaltenes. The saturates fraction includes straight chain alkanes, branched alkanes and cycloalkanes. The aromatic fraction contains volatile monoaromatic hydrocarbons, such as benzene, toluene, xylenes *etc*., polyaromatic hydrocarbons, naphthenoaromatics and aromatic sulphur compounds such as thiophenes and dibenzothiophenes. The resin (N, S, O) and asphaltene fractions consist of polar molecules containing nitrogen, sulphur and oxygen. Resins are amorphous solids that are

* Corresponding author. E-mail: snezana.maletic@dh.uns.ac.rs
# Serbian Chemical Society member.
doi: 10.2298/JSC120430072M

truly dissolved in oil, whereas asphaltenes are large molecules colloidally dispersed in oil. The relative proportions of these fractions are dependent on many factors, such as the source, geological history, age, migration and alteration of crude oil.[1–4]

Of the various petroleum fractions, *n*-alkanes of intermediate length (C_{10}–C_{20}) are the preferred substrates for microorganisms and tend to be the most readily degradable, whereas shorter chain compounds are more toxic. Longer chain alkanes (C_{20}–C_{40}) are hydrophobic solids and consequently are difficult to degrade due to their poor water solubility and bioavailability, branched chain alkanes and cycloalkanes are also degraded more slowly than the corresponding normal alkanes. Highly condensed aromatic and cycloparaffinic structures, tars, bitumen and asphaltic materials have the highest boiling points and exhibit the greatest resistance to biodegradation. Asphaltenes are the product of petroleum hydrocarbons in soil that appear to be resistant to microbial degradation. It has been proposed that such residual material from oil degradation is analogous to, and could even be regarded as, humic material. Due to its inert characteristics, insolubility and similarity to humic materials, it is unlikely to be environmentally hazardous.[1,5–7]

The effectiveness of bioremediation is usually evaluated by measurement of the degradation of total oil and a limited number of individual oil compounds.[8,9] This is not always easy to interpret because as well as the concentration of individual contaminants, the composition of the oil changes as the oil degrades.[2,10] GC-MS fingerprinting analysis could be conveniently used to monitor specific classes of organic pollutants in the environment. Fingerprint analysis provides a picture of the overall pollutant composition. This data could serve as a basis for tracing the source and time of pollution, and to detect pollutants not covered by regulations and metabolites derived from pollutants.[11] The purpose of this work was to identify weathered petroleum-hydrocarbons that persisted after the bioremediation process, and metabolites generated during this process, by applying GC/MS analysis at various stages of the biotreatment process.

EXPERIMENTAL

Contaminated soil

The soil for this investigation was contaminated with oil and oil derivatives (gasoline, crude oil, kerosene, diesel and oil combustion products) as a consequence of infrastructure destruction at the Novi Sad Oil Refinery,[12,13] Serbia, and had been exposed to uncontrolled natural processes of weathering and decomposition for the last 8 years in the controlled depot of the Novi Sad Oil Refinery. The soil particle size distribution of the mineral fraction was 94.0 % sand, 4.1 % silt and 0.5 % clay, which is as expected as the area of the Novi Sad Oil Refinery was covered with a sand layer before its construction. The investigated soil had the following characteristics: 22.7 % water holding capacity, 2.6×10^{-4} cm s^{-1} permeability coefficient (k_f), pH 7.30, and 3.6 % humus content.

Landfarming

After 8 years of weathering, part of the contaminated soil (2.7 m^3) was placed in a 3×3 m wide and 0.4 m deep prismatic hole, and covered with resistant polypropylene foil to prevent contamination spreading from the landfarm (Fig. 1). With the aim of facilitating oxygen and water transport through the soil, the contaminated soil was composted with straw. The landfarm was turned twice a month and watered twice a week; moisture was maintained at approximately 50–80 % of the water holding capacity during the experiment. In addition to the stimulation of native microflora by soil aeration and irrigation, bioaugmentation was also performed with microorganisms separated from the contaminated soil and cultivated in a laboratory bioreactor. Approximately 25 L of the inoculated water from the bioreactor was used together with leaching water for weathering the landfarm.

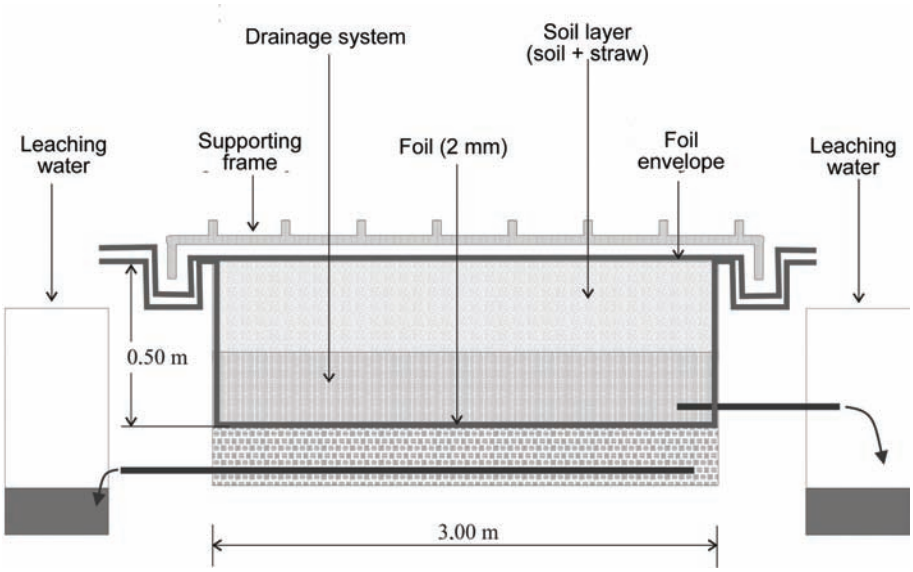

Fig. 1. Landfarm vertical cross-section.

Sampling, and chemical and microbiological analyses

For the chemical and microbiological analyses, approximately 10 soil samples were taken from the experimental field before the start of the experiment (day 0 was taken as a control sample) and after 56, 92, 128, 196, 280, 328, 443, 504, 613 and 710 days. Soil samples were homogenised and mixed, and one composite sample was made. Samples were analysed for moisture content, total hydrocarbons, mineral oil, PAHs and GC-MSD scan organic profile, and a microbiological characterisation was also performed.

Determinations of total hydrocarbons and mineral oils were performed on a Thermo Nicolet Nexus 670 FTIR instrument by standard IR spectrophotometric methods.[14] The analyses were performed by preparing approximately 7g samples according to standard methods.[15] Extraction was realised in a Soxhlet apparatus with carbon tetrachloride (100 mL) for 6 h. All compounds with hydrocarbon functionalities (both adsorbable on Al_2O_3 and mineral oils) were determined by IR spectroscopy before and after filtration of the carbon tetrachloride extract through aluminium oxide. Thus, an indication was obtained of the total hydro-

carbon moieties in the samples, regardless of other functional groups and mineral oil content. The carbon tetrachloride was of Merck grade for IR spectroscopy (≤ 99.9 %). It was checked for possible impurities before analysis by the IR method. Cross contamination of samples during preparation and analysis did not occur as demonstrated by solvent checks. The practical quantification limit (*PQL*) was 15 mg kg^{-1} dry weight for hydrocarbons. Measurements were performed as single probes. For four replicate soil analyses, the relative standard deviation (*RSD*) was 10 %.

To realise the GC/MS analysis, 7 g of soil sample was mixed with a water–methanol mixture (1:3) and extracted with dichloromethane–hexane mixture (1:1). Elemental sulphur was removed with copper powder.[16] Samples were fractionated over silica gel.[17] The GC/MS scan analysis was performed on an HP 5890GC Series II gas chromatograph with a 5971 MSD mass spectrometer in the splitless mode. The chromatographic conditions were: column 25 m×0:2 mm×0:33 μm ULTRA 2; helium flow rate 1 mL min^{-1}, injector temperature 250 °C and detector temperature 280 °C. The temperature programme was set at: 40 °C for 5 min, 4 °C min^{-1} to 130 °C hold for 2:2 min, increase by 12 °C min^{-1} to 180 °C, hold for 2:2 min, increase at 7 °C min^{-1} to 300 °C, hold 11:79 min. Qualitative analysis of the samples was performed by scanning the mass range between 35 and 550 amu, one run per sample. The interpretation of each spectrum was performed by comparison with the commercial Wiley database of spectra, using Hewlett Packard G1035A probability base matching (PBM) software for the mass spectrometric search. The performance of the MSD was evaluated using 2,6,10,15,19,23-hexamethyltetracosane, 0.93 mg mL^{-1}, and *N*-phenylbenzeneamine, 0.97 mg mL^{-1}. The PBM search results were 83 % for the former and 87 % for the latter. Quantitative PAH analyses were performed under the same chromatographic conditions used for the GC/MS scan analysis but in the selected ion monitoring (SIM) mode. Details of the method are given elsewhere.[13] The concentrations of the PAHs were calculated by the internal standard method (target ion peak areas were used for the calculation). The results were not corrected for recoveries. Replicate analyses gave results of relative *SD*s up to ±27 %.

Microbiological characterisation. Bacteria counts in the contaminated soil and the leaching water used for watering the landfarm were determined by the indirect (cultivation) method on solid agar medium.[18] A series of dilutions was made first in 0.1 % sodium pyrophosphate solution with intensive shaking on a Vortex shaker, and the solutions were inoculated on the nutritive medium. After incubation (5 to 7 days at 26–28°C), the colonies were counted. The study encompassed several important groups of bacteria: organotrophs, facultative oligotrophs, lipolytic bacteria, and hydrocarbon-oxidizing bacteria.[19]

RESULTS AND DISCUSSION

Total hydrocarbon and mineral oil degradation

During the 2-year landfarming bioremediation treatment of the soil heavily polluted with weathered oil and oil derivates, the mineral oil and total hydrocarbons content decreased by approximately 53 % (from 23.2 to 10.8 g kg^{-1}) and 27 % (from 35.3 to 25.8 g kg^{-1}), respectively (Fig. 2). The rate limiting step in the biodegradation pathways of alkanes and alkenes and most other hydrocarbons is the initial oxidation. In this case, the higher degradation rate of the mineral oil compared to the total hydrocarbons degradation rate is a consequence of the significant contribution of poorly degradable material (humus material, lignin, as-

phaltenes, *etc*.) to the total hydrocarbon degradation rate. Additionally, the most intensive degradation of mineral oil was observed in the first and in the last six month periods of the landfarming bioremediation process. In between, a long period of stagnation was observed, as a consequence of the degradation of easily degradable short-chain alkanes and alkenes in the initial period of the bioremediation process, and then a long lag period for microbiological adaptation for the oxidation of poorly degradable long chain alkanes, branched alkanes and cyclic alkanes. In the case of the total hydrocarbons, the most rapid degradation was observed in the first six months of the bioremediation process, with the total hydrocarbon content remaining relatively constant after this period. This is also a consequence of the presence of poorly degradable material, such as humus material, lignin, asphaltenes *etc*.

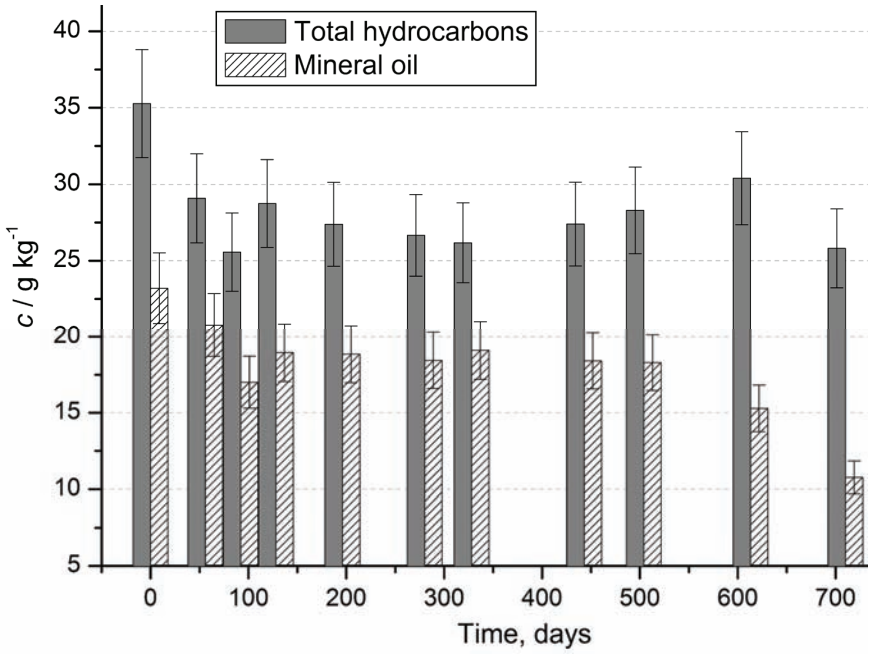

Fig. 2. Concentration change of total hydrocarbons and mineral oil.
Error bars represent a relative *SD* of 10 %.

PAH Degradation

The results for the changing concentrations over time of the total PAHs and the sums of PAHs with three, four, and five–six rings are presented in Fig. 3. During the observation period, the amount of PAHs with 3 rings decreased by 97 % (from 485 to 13 μg kg^{-1}), with 4 rings by 72 % (from 4854 to 1344 μg kg^{-1}) and for the 5–6 rings by 70 % (from 3300 to 998 μg kg^{-1}), with the approximate

total amount of PAHs during this period decreasing by 72 %. The highest degradation of PAHs was obtained for PAHs with a smaller number of rings, as a consequence of their simple structure relative to PAHs with a larger number of rings. This is in agreement with literature findings.[6,20] Additionally, it is important to stress at this point that the concentration of PAHs with 3 rings was approximately ten times lower than the concentration of PAHs with a larger number of rings at the start of the landfarming bioremediation process. This is due to the higher degradation rate of PAHs with a smaller number of rings during the uncontrolled weathering processes which occurred in the 8 previous years.

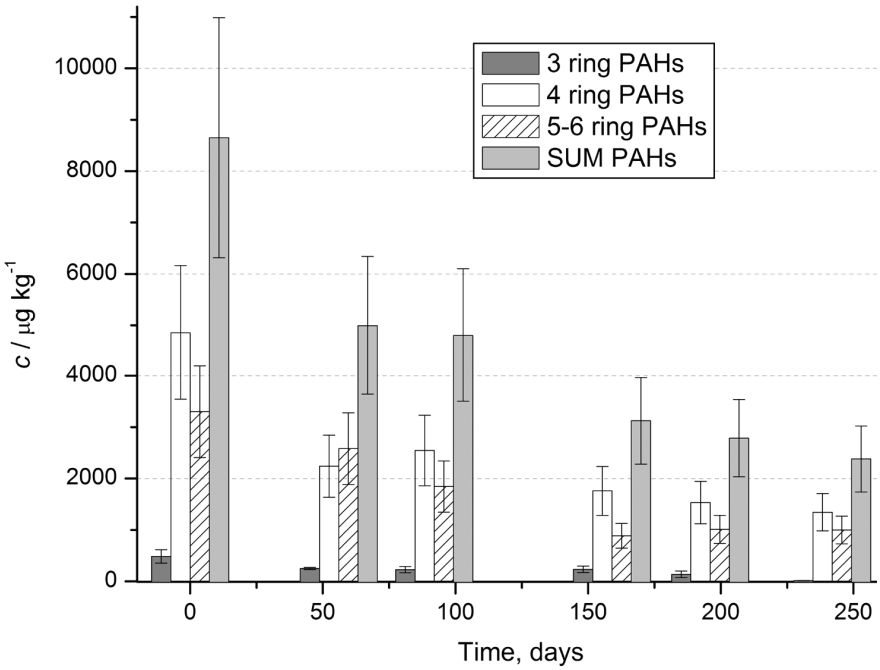

Fig. 3. PAHs in the contaminated soil during the experiment. Error bars represent a relative *SD* of 27 %.

GC/MS Scan qualitative analysis

The compounds detected by GC/MS analysis of the extracts of the various soil samples taken during the landfarming bioremediation process are given in Table I, with only the main compounds from the hit-lists of the PBM search presented. Additionally, the *TIC* and *m/z* 85 SIM ion chromatograms for some representative samples are presented in Fig. 4. The data reflect the fact that the soil used in this investigation was sampled from the dumping area of a refinery where the initial pollutants were of very diverse composition, *i.e.*, a mixture of crude oil, masut, diesel, middle distillates, heavy distillates, kerosene, *etc*.[12] The

TABLE I. Compounds detected in soil samples during the bioremediation process; Quality of the PBM search results quoted as percentages (first compounds from the hit lists)

Detected compound	Time, days						Detected compound	Time, days					
	0	92	280	443	613	710		0	92	280	443	613	710
Tridecane					64		Pentacosane, 13-undecyl-					80	
Tetradecane	93		90		81		5-Undecene, 7-methyl-(*Z*)						35
Pentadecane	96		45		76		2-Undecene, 4,5-dimethyl-						50
Hexadecane	97	60	47	53	72		1,4-Hexadiene, 2,3,4,5-tetra-methyl-				27		
Heptadecane	95						1,6-Decadiene, 2,6,9-trimethyl-(*E*)-				30		27
Octadecane	97	76			62		1,4-Undeca-diene, (*Z*)-				35		47
Nonadecane	95	60			49		Benzene, methyl-				91		
Eicosane	95	59	72				Benzamine, 4-butyl-			27			
Heneicosane	91		78				Benzaldehyde, 4-ethyl-					53	
Docosane	97	64	60		91		1,2-Benzenedi-carboxylic acid			83			
Tricosane	91	93			87		Benzene, 1,1'--methylene-bis(3-methyl)-					35	
Tetracosane	93	84				87	1,3-Benzenedi-amine, 4-methoxy-				38		
Pentacosane	95	96		60		95	Dibenz(*B*,*F*)-azepine	38			64	72	
Hexacosane	89						Phenol, 2,4-bis-(1,1-dimethyl-ethyl)-	38					
Heptacosane	91					49	Anthracene, 1,4-dimethyl-	22					
Octacosane	93						Anthracene, 9-dodecyltetra-decahydro-	27		37			18
Nanocosane	96					87	Phenanthrene, 2,3,5-trimethyl-			40			
Hentriacontane	94				38		2-Methyl-chrysene	59				38	
Tetratriacontane	98				87		Cyclopenta[*cd*]-pyrene	43					

TABLE I. Continued

Detected compound	Time, days						Detected compound	Time, days					
	0	92	280	443	613	710		0	92	280	443	613	710
Hexatriacontane	97			83	58	50	Naphthalene, 2-(1,1-dimethyl-ethyl)-	25					
3-Dodecene, (*Z*)-					64	43	2,6-Naphthalenedione, octahydro-1,1,8-		38				18
7-Tetradecene, (*Z*)-					91		1*H*-Inden-5-ol, 2,2-dihydro-		25		78	59	
1-Octadecene, (*E*)-					35		Cyclopropane, 1-(1,2-dimethyl-propyl)-	25					64
3-Octadecene, (*E*)-					38		Cyclopentane, 1,3-dimethyl-2--8(1-methyl)-	53			38		
9-Eicosene, (*E*)-					74		Cyclopentene, 3,3-Dimethyl-2-isopropyl-			25			
Nonane, 5-butyl-	76					27	Cyclopentane, 1-butyl-2-propyl-			35			
Decane, 2-methyl-					64		Cyclohexene, 3,3,5-trimethyl-				45	64	43
Decane, 3,6-dimethyl-	72						Cyclohexane, pentyl-	50					
Decane, 2,6,8--trimethyl-					90	72	Cyclohexane, octyl-					86	
Undecane, 4,6-dimethyl-	80		78	64	87	47	Cyclohexane, undecyl-	96		43			
Dodecane, 2,6,10-trimethyl-		72				60	Cyclohexane, eicosyl-		43				
Tridecane, 5-propyl-	83				74	22	Cyclohexane, (1,3-dimethyl-butyl)-	42		38			
Pentadecane, 3-methyl-			76				Cyclohexane, (3,3-dimethyl-pentyl)-				53		
Pentadecane, 2,6,10-trimethyl-	94	95			90	72	Cyclohexane, 1,2-diethyl-3--methyl-				58	59	
Pentadecane, 2,6,10,14-tetramethyl-	93	95	93	96	99	95	Cyclohexane, 1-(1,5-dimethyl-hexyl)-4-			47			

TABLE I. Continued

Detected compound	Time, days						Detected compound	Time, days					
	0	92	280	443	613	710		0	92	280	443	613	710
Hexadecane, 3-methyl-	64		46		62	64	Cyclohexane, 1-(cyclohexyl-methyl)-2-e					49	
Hexadecane, 2,6,10,14-tetra-methyl-	99	91	94	94	91	97	Cyclohexane, 1, 1′-(1-methyl-1, 3-propane)-			30		55	49
Heptadecane, 2,6-dimethyl-	94		53			87	Cyclododecane					89	89
Heptadecane, 2,6,10,15-tetra-methyl-	78	90	53	46	90	86	Cycloundecane, (1-methylethyl)-				45		
Heptadecane, 9-octyl-	83	66		80	83		Cyclohexa-decane				43		
Octadecane, 2,6-dimethyl-	38		49				Cycloeicosane					87	87
Nonadecane, 2,6,10,14-tet-ramethyl-	64	81	86	55	83		Androstane, (5*α*, 14*β*)-		50	11			
Nonadecane, 2-methyl-5-pro-pyl-			59				Pregnane	53	43	59	83	64	64
Heneicosane, 3-methyl-		91					Cholestane	59	95	91			
Heneicosane, 11-decyl-	91						2-Pntanone, 4-cyclohexyl-iden-3,3-diene-				32		
Docosane, 11-decyl-	91						Isoquinoline, 1,2,2,4-tetra-hydro-7-methyl-			52			
Tricosane, 2-methyl-			70				Camphor					45	
Tetracosane, 2,6,10,15,19,23--hexamethyl-	94	86	72				1*H*-Pyrazole, 1,3,5-trimethyl-			43	43		
Total (both columns)								49	22	33	25	42	29
In total with qual ≥70 %								34	13	6	7	21	11

untreated weathered soil sample contained a large variety of straight-chain hydrocarbons and their methyl derivatives (both those with even and odd numbers of C atoms), many of which persisted during the treatment. However, many of the aromatic hydrocarbons found in the untreated soil, mainly substituted polycyclic aromatic hydrocarbons, were not detected in the samples of treated soil, thus showing lower persistence than the alkanes. The absence of volatile components may indicate that the contamination was caused by heavier oil fractions, but is

most likely caused by the loss of lighter components by evaporation and biodegradation during the uncontrolled aging process in the dumping area of the refinery. According to a previous investigation, the *n*-alkanes ≤ C20 disappear very quickly, leaving behind isoprenoid structures;[21] this was confirmed by the presented data. At the start of the process, the soil sample contained a large variety of straight-chain hydrocarbons and their methyl derivates. Many of these compounds, in particular branched alkanes, were also detected after the treatment. Several new compounds were found at the end of the experiment, including mainly unsaturated *n*-alkenes and different derivates of cycloalkanes. It was very difficult to establish which compounds originated exclusively from the spilled oil and which were of natural origin, but data clearly showed that the number of organic compounds extracted from the soil decreased during the treatment process.

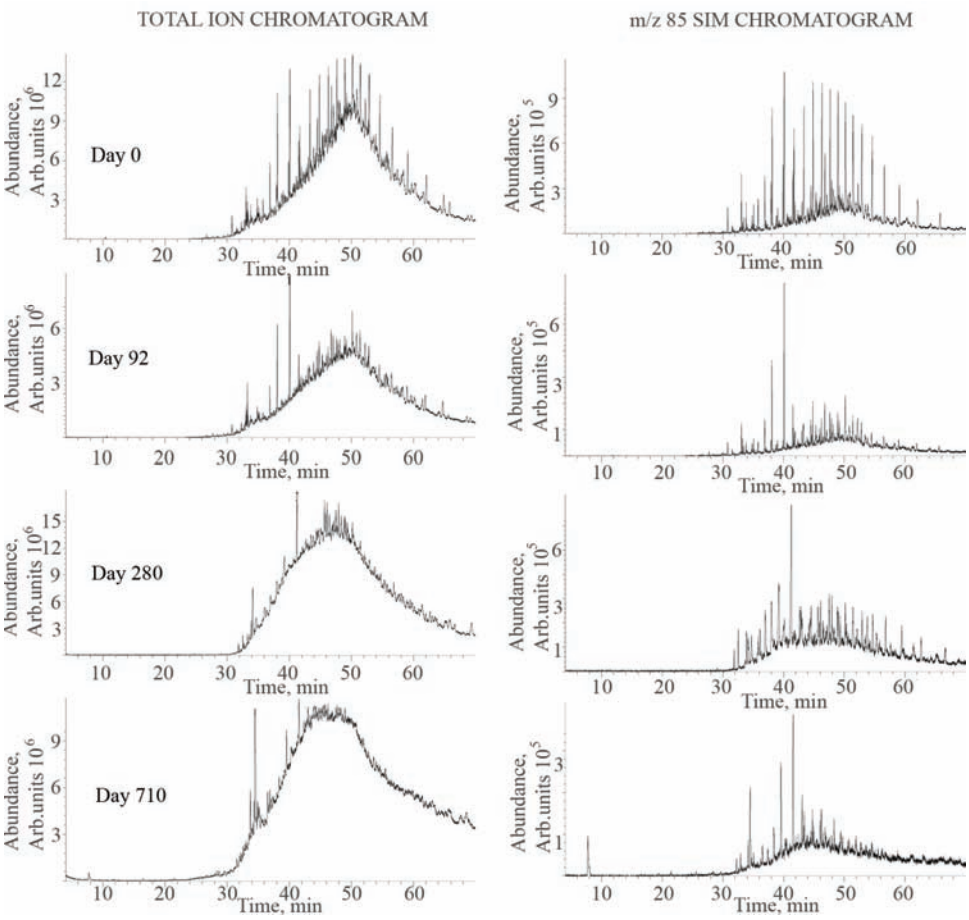

Fig. 4. TIC and *m/z* 85 SIM ion chromatograms for some representative samples.

In the original soil samples, 34 compounds were identified exhibiting a PBM ≥70 %. After the first six months of bioremediation, the number of compounds dropped significantly to 13 (≈ 62 %), after this period the number of detected compounds remained approximately constant. At the end of the treatment, the number of compounds in the treated soil was 11, of which 6 compounds were newly formed. However, a better insight into the bioremediation processes can be obtained by examining changes in the number of compounds in the different groups of compounds (PBM ≥70 %).

The number of the straight chain alkanes (PBM ≥ 70%), 19 at the beginning of the experiment, dropped to 4 (≈ 79 % reduction in the number of compound) in the first six months, and while the number of compounds remained mainly constant to the end of the process. It is important to note that after 710 days in the soil, only heavier straight chain alkanes remained in the soil. With respect to the branched alkanes, the number of detected compounds (PBM ≥ 70 %) in the untreated soil was 12, 8 after the first six months of treatment and remained mainly constant until near the end of the experiment, when the number dropped to 6 compounds, 3 of which were newly formed. Significantly, highly branched alkanes such as 2,6,10-trimethyl-pentadecane, 2,6,10,14-tetramethyl-entadecane, 2,6,10,15-tetramethyl-heptadecane, 2,6,10,15-tetramethyl-heptadecane and 2,6,10,14-tetramethyl-nonadecane were present in the soil sample from the start to the end of the experiment, as a consequence of their poor biodegradation characteristics. This is in accordance with the literature.[1,11,22,23] Additionally, a few unsaturated straight chain and branched alkenes were detected in the last six months of the treatment, in which a significantly higher number of compounds was also detected, indicating the formation of metabolites during the biodegradation processes occurring in the investigated soil.

A certain number of substituted polyaromatic hydrocarbons were detected in the treated and untreated soil, but the search results for all these compounds were mainly below 70 %. Significantly, most of the originally present substituted PAHs were degraded after the first six months. A large number of different cycloalkanes were also detected, but the search results for most of these compounds were below 70%. Most of these compounds were not originally present in the untreated soil; hence, it could be concluded that they were the metabolic products of straight chain and branched hydrocarbon biodegradation.

The lowest concentration of each compound in the soil that is detectable by GC-MS could be estimated based roughly on the following. Assuming that the detection limit for the detector is approximately 500 ng for each compound and knowing that 7 g soil were extracted, that the residues were dissolved in 500 μL, and the volume injected was 2 μL, the lowest concentration of any given pollutant for effective identification should be of the order of 20 mg kg^{-1}. Thus, it is likely that there are many compounds present in oil, such as substituted deriva-

tives of alicyclic and polycyclic aromatic compounds, which are not included in standard mixtures used for routine analyses and thus not detected by GC/MS--SIM analyses, but which were detected by GC/MS scan analysis. This suggests that for bioremediation purposes, it is necessary to also apply this approach for more detailed identification of such components.

Characterization of the microbial population

The change in the counts of bacterial strains in the soil during the bioremediation experiment is presented in Fig. 5. Microbiological analyses confirmed that the bacterial populations in the landfarming were involved in the removal processes of the soil contaminants by degrading them.[19] High counts (10^8–10^9 CFU g^{-1}) of all investigated groups of bacteria were detected in the soil. It is significant that the counts of bacteria during the treatment were considerably greater than at the beginning of the experiment, which indicates that the landfarming treatment contributes to increasing the microbial degradation of hydrocarbons and increases biomass. This was confirmed by the decreasing hydrocarbon concentration during the experiment. At the end of the experiment, the counts of all the investigated groups of bacteria were reduced, and since there was still some available nitrogen and phosphorous for bacterial growth, this is probably a consequence of the changing composition of the mineral oil; after the easily degradable short-chain alkanes and alkenes had been degraded, long chain alkanes

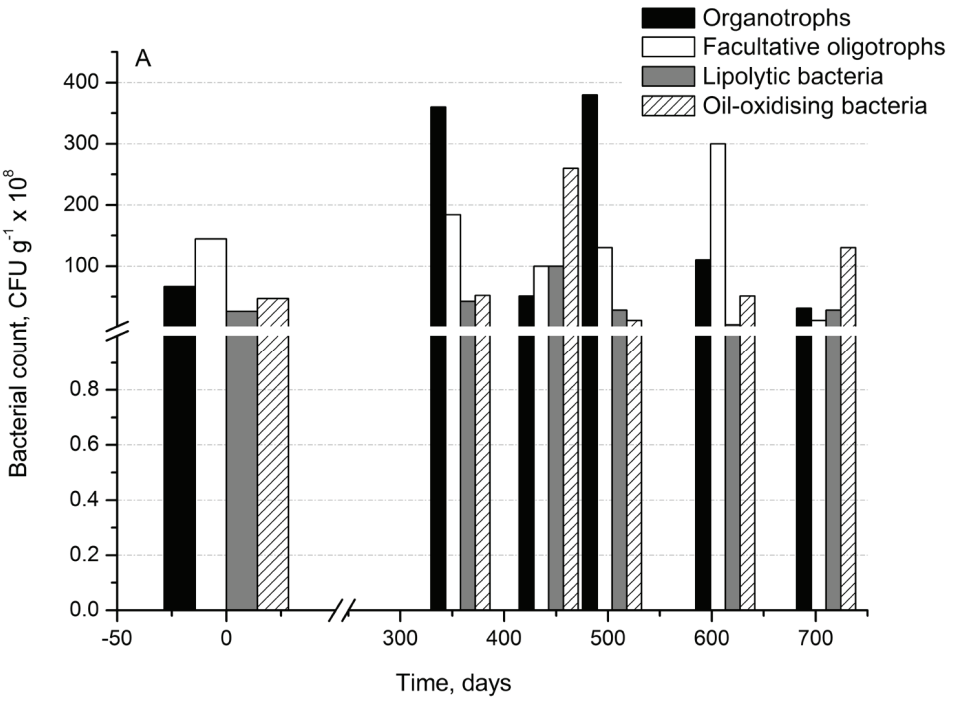

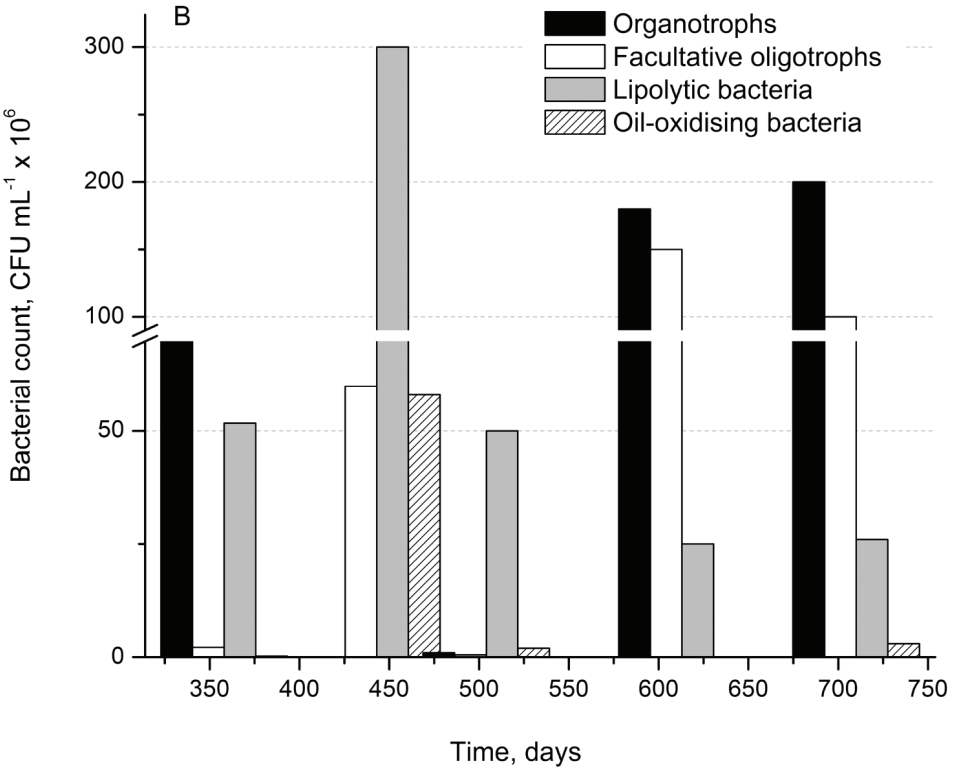

Fig. 5. Bacterial count in the soil (A) and water (B) during the experiment.

and cyclic alkanes remained. The bacteria count in the leaching water was much higher than in the initial period of the experiment, 10^7–10^8 CFU per mL of leaching water. This also confirms the microbiological degradation of hydrocarbons during the landfarming treatment.

CONCLUSIONS

During the observation period of bioremediation in the landfarm, the concentration of hydrocarbons significantly decreased. During the experiment, the contents of mineral oil and total hydrocarbons decreased by approximately 53 and 27 %, respectively, and the concentration of PAHs decreased by about 72 %. Based on GC/MS characterization of aged-hydrocarbons contaminated soil, the number of initially detected compounds after the bioremediation process further decreased during the investigation period: at the start of the experiment, the number of detected compounds was 34 and after 710 days it was 11, about 32 % of the original number, and included 6 that were newly formed. With respect to the nature of the compounds detected, three groups of organic compounds appeared to be most prominent in the contaminated soil, acyclic, substituted polycyclic aro-

matic hydrocarbons and different cycloalkanes derivates. Higher persistence was found for the heavier *n*-alkanes and branched alkanes, which were detectable over a long period.

The dominant microflora was the physiological group facultative oligotrophs, which indicates a satisfactory process of soil self-cleansing. During the experiment, lipolytic and oil-oxidising bacteria significantly increased, indicating that the hydrocarbon biodegradation processes had intensified.

Acknowledgments. This research was financed by the Ministry of Education, Science and Technological Development of the Republic of Serbia (Projects Nos. III43005 and TR37004) and the Novi Sad Oil Refinery.

И З В О Д

КАРАКТЕРИЗАЦИЈА УГЉОВОДОНИКА СТАРОГ НАФТНОГ ЗАГАЂЕЊА ТОКОМ БИОРЕМЕДИЈАЦИОНОГ ТРЕТМАНА ПОВРШИНСКОМ ОБРАДОМ

СНЕЖАНА МАЛЕТИЋ, СРЂАН РОНЧЕВИЋ, БОЖО ДАЛМАЦИЈА, ЈАСМИНА АГБАБА, MALCOLM WATSON, АЛЕКСАНДРА ТУБИЋ и СВЕТЛАНА УГАРЧИНА ПЕРОВИЋ

Универзитет у Новом Саду, Природно–математички факултет, Трг Доситеја Обрадовића 3, 21000 Нови Сад

Биоремедијација површинском обрадом вршена је 2 године на земљишту загађеном изузетно високим концентрацијама старог загађења нафте и њених деривата: 23200 mg kg^{-1} минералних уља, 35300 mg kg^{-1} укупних угљоводоника и 8,65 mg kg^{-1} укупних PAH-ова. Током експеримента концентрација минералних уља, укупних угљоводоника и PAH-ова је опала за око 53, 27 и 72 %, респективно. GC/MS *scan* анализа је коришћена за идентификацију нафтних угљоводоника који заостају након биоремедијационог третмана загађеног земљишта, као и насталих метаболита током овог процеса. Резултати су показали да у земљишту загађеном старим нафтним загађењем, број иницијално детектованих једињења након 2 године биоремедијационог третмана опада, при чему истовремено долази до формирања неколико нових једињења. Показано је да виши угљоводоници имају већу презистентност и могли су бити детектовани током дугог временског периода. GC/MS *scan* анализа је омогућила праћење различите биорезградљивости *n*-алкана и њихових супституисаних деривата, као и полицикличних ароматичних угљоводоника у земљишту загађеном нафтом и њеним дериватима током процеса биоремедијације.

(Примљено 30. априла, ревидирано 3. јула 2012)

REFERENCES

1. M. T. Balba, N. Al-Awadhi, R. Al-Daher, *J. Microbiol. Meth.* **32** (1998) 155
2. S. T. Jensen, E. Arvin, B. Svensmark, P. Wrang, *Soil Sediment Contam.* **9** (2000) 549
3. S. J. T. Pollard, R. L. Hough, K. Kim, J. Bellarby, G. I. Paton, K. T. Semple, F. Coulon, *Chemosphere* **71** (2008) 1432
4. P. V. O. Trinidade, A. C. L. Sobral, S. G. F. Rizzo, *Chemosphere* **58** (2005) 515
5. K. J. Brassington, R. L. Hough, G. I. Paton, K. T. Semple, G. C. Risdon, J. Crossley, I. Hay, K. Askari, S. J. T. Pollard, *Environ. Sci. Technol.* **37** (2007) 199

6. S. Maletić, B. Dalmacija, S. Rončević, J. Agbaba, O. Petrović, *Water Air Soil Pollut.* **202** (2009) 149
7. J. L. Stroud, G. I. Paton, K. T. Semple, *J. Appl. Microbiol.* **102** (2007) 1239
8. K. Müller, M. Deurer, *Agr. Ecosys. Environ.* **144** (2011) 208
9. M. A. Zahed, H. A. Hamidi Aziz, M. H. Isa, L. Mohajeri, S. Mohajeri, S. R. M. Kutty, *J. Hazard. Mater.* **185** (2011) 1027
10. J. R. Gallego, C. Sierra, R. Villa, A. I. Peláez, J. Sánchez, *Org. Geochem.* **41** (2010) 896
11. I. Ivančev-Tumbas, J. Tričković, E. Karlović, Z. Tamaš, S. Rončević, B. Dalmacija, O. Petrović, M. Klašnja, *Int. Biodeter. Biodegr.* **54** (2004) 311
12. B. Dalmacija, I. Ivančev-Tumbas, I. Bikit, M. Vesković, M. Đurendić, M. Miladinov-Mikov, V. V. Baltić, Lj. Čonkić, M. Bečelić, *Arch. Oncol.* **8** (2000) 113
13. B. Dalmacija, I. Ivancev-Tumbas, J. Zejak, M. Djurendic, *Soil Sediment Contam.* **12** (2003) 591
14. USEPA 8440: *Total recoverable petroleum hydrocarbons by Infrared*, US Environmental Protection Agency, http://www.epa.gov/osw/hazard/testmethods/sw846/pdfs/8440.pdf (accessed on December, 2012)
15. USEPA 3560: *Supercritical extraction of total recoverable petroleum hydrocarbons*, US Environmental Protection Agency, http://www.epa.gov/osw/hazard/testmethods/ /sw846/pdfs/3560.pdf (accessed on December, 2012)
16. USEPA 440/4–87–010: *Guidance for sampling of and analyzing for organic contaminants in sediments*, US Environmental Protection Agency http:// nepis.epa.gov/ Exe/tiff2png.cgi/00001J7E.PNG?-i+-r+75+-g+7+D%3A%5CZYFILES%5CINDEX-D%7E1%5C86THRU90%5CTIFF%5C00000113%5C00001J7E.TIF (accessed on December, 2012)
17. USEPA 3630C: *Silica Gel Cleanup, Revision 3. In: Test methods for evaluating solid waste, physical/chemical methods (SW-846)*, US Environmental Protection Agency, http://www.epa.gov/osw/hazard/testmethods/sw846/pdfs/3630c.pdf (accessed on December, 2012)
18. A. G. Rodina, *Methods in Aquatic Microbiology*. University Park Press, Baltimore, MD, USA, 1972
19. O. Petrović, P. Knežević, J. Marković, S. Rončević, *J. Microbiol. Meth.* **74** (2008) 110
20. S. Rončević, B. Dalmacija, I. Ivančev-Tumbas, O. Petrović, M. Klašnja, J. Agbaba, *Arch. Environ. Con. Tox.* **49** (2005) 27
21. T. A. T. Aboul-Kassim, B. R. T. Simoneit, *Handbook of Environmental Chemistry*, Vol. 5, Part E: *Water Pollution*, O. Hutzinger, Ed., Springer, New York, 2001, p. 4
22. S. Maletić, B. Dalmacija, S. Rončević, J. Agbaba, S. Ugarčina Perović, *J. Environ. Sci. Heal., A* **46** (2011) 1042
23. L. T. Nhi-Cong, A. Mikolasch, H. P. Klenk, F. Schaueret, *Int. Biodeterior. Biodegrad.* **63** (2009) 201.